3-17-2020

Hybrid monomers & resins for high-performance thermosetting polymers, thermoplastics, & additive manufacturing

Alexander William Bassett
Rowan University

HYBRID MONOMERS & RESINS FOR HIGH-PERFORMANCE THERMOSETTING POLYMERS, THERMOPLASTICS, & ADDITIVE MANUFACTURING

by

Alexander William Bassett

A Dissertation

Submitted to the
Department of Chemical Engineering
College of Engineering
In partial fulfillment of the requirement
For the degree of
Doctor of Philosophy
at
Rowan University
March 6, 2020

Dissertation Chair: Joseph F. Stanzione, III, Ph.D.

Dedications

For Mom and Dad

Acknowledgments

First and foremost, I'd like to thank Dr. Joseph F. Stanzione, III, my graduate advisor, teacher, mentor, and friend. Since I began working with Dr. Stanzione as an undergraduate student in 2014, he has continuously encouraged me through my research and academic endeavors and, in 2016, gave me the opportunity to pursue a doctorate degree. Dr. Stanzione continuously gave me full creative freedom throughout my doctoral studies and always provided support and expertise, and for that I thank him.

I'd also like to express my sincere gratitude to all the individuals who have worked with me, especially Amy E. Honnig, Claire M. Breyta, Kayla R. Sweet, Julia H. Reilly, and Ian C. Dunn. Words cannot express how much impact these individuals have had on this dissertation and without them, this dissertation would not have been possible. Furthermore, I'd like to thank all my colleagues, especially Elyse A. Baroncini, Ph.D., Joseph R. Mauck, M.S., Silvio Curia, Ph.D., Daniel P. Rogers, M.S., and Eric D. Hernandez, M.S. for sharing their extensive knowledge and providing an overall enjoyable work environment.

Moreover, I'd like to thank Dr. John J. La Scala and Dr. Joshua M. Sadler of the Combat Capabilities Development Command – Army Research Laboratory (CCDC-ARL) for providing me with guidance throughout both my undergraduate and graduate research career. I would also like to express gratitude to CCDC-ARL for their support via Cooperative Agreements W911NF-14-2-0086, W911NF-16-2-0225, and W911NF-17-2-0227 and the Strategic Environmental Research and Development Program (WP-2402).

I'd also like to thank my parents, family, and friends for their encouragement and support throughout my life and academic career.

Abstract

Alexander William Bassett
HYBRID MONOMERS & RESINS FOR HIGH-PERFORMANCE THERMOSETTING POLYMERS, THERMOPLASTICS, & ADDITIVE MANUFACTURING
2019-2020
Joseph F. Stanzione, III, Ph.D.
Doctor of Philosophy in Engineering

Vinyl ester and epoxy resins are used to produce thermosetting polymeric materials for a variety of commercial and military applications due to their relatively high moduli (2-3 GPa at 25 °C), glass transition temperatures (T_gs) (≥120 °C), and adequate fracture toughness ($G_{1C} \approx$ 200-250 J m^{-2}). Most commercially available vinyl ester and epoxy resins are typically cured via traditional manufacturing techniques such as resin transfer molding and thermal curing. However, additive manufacturing (AM) has gained significant traction as a favorable manufacturing technique over traditional methods due to the ability to create customizable parts with complex geometries on-demand.

This work aims to design high-performance materials that display similar thermal properties to conventional vinyl ester and epoxy resins while achieving significant gains in polymer fracture toughness and, in some cases, enable the use of such materials in stereolithography, an AM technique. Studies of the structure-property relationships of prepared, bio-based materials demonstrate that, in general, there are significant tradeoffs between T_g and fracture toughness; therefore, desired properties are not achieved. However, manipulation of polymer network connectivity via sequential formation of interpenetrating polymers allows for not only the use of AM, but also yields polymeric materials with T_gs that exceed 120 °C and fracture toughness values four to five times higher in magnitude than conventional vinyl ester and epoxy resins.

Table of Contents

Abstract v
List of Figures xi
List of Tables xv
Chapter 1: Introduction 1
1.1 Motivation and Background 1
1.2 Polymers 2
1.2.1 Introduction to Polymers 2
1.2.2 Thermosets 2
1.2.3 Thermoplastics 4
1.3 The Hybrid Approach 5
1.3.1 Molecularly Hybrid & Formulation Hybrid. 5
1.3.2 Functionally Hybrid 7
1.4 Dissertation Summary 8
Chapter 2: Characterization Methods 10
2.1 Introduction 10
2.2 Nuclear Magnetic Resonance Spectroscopy (NMR) 10
2.3 Rheology 11
2.4 Fourier Transform Infrared (FTIR) Spectroscopy 11
2.5 Stereolithography (SLA) Working Curve 12
2.6 Density Measurements 14
2.7 Size Exclusion Chromatography (SEC) 14
2.8 Differential Scanning Calorimetry (DSC) 15
2.9 Thermogravimetric Analysis (TGA) 15
2.10 Dynamic Mechanical Analysis (DMA) 16
2.11 Tensile Testing 17
2.12 Fracture Toughness 18
Chapter 3: Molecularly Hybrid Bisphenols Derived From Lignin and Cashew Nutshell Liquid (CNSL) 20
3.1 Introduction 20

Table of Contents (Continued)

3.2 Experimental Methods & Procedures 24

3.2.1 Materials 24

3.2.2 Synthesis of VAC and VAHC 25

3.2.3 Synthesis of VAC and VAHC Dimethacrylate 26

3.2.4 Characterization of Monomers and Resins 27

3.2.5 Resin Cure 28

3.2.6 Extent of Cure 29

3.2.7 Polymer Properties 30

3.3 Results and Discussion 32

3.3.1 Resin Characterization 32

3.3.2 Extent of Cure 35

3.3.3 Polymer Properties 38

3.4 Conclusions 46

Chapter 4: Molecularly Hybrid, Ester-Spaced, Aromatic Diglycidyl Ethers From Bio-Based Feedstocks 48

4.1 Introduction 48

4.2 Experimental Methods & Procedures 50

4.2.1 Materials 50

4.2.2 Synthesis of Ester-Spaced, Aromatic Diglycidyl Ethers 50

4.2.3 Monomer Characterization 52

4.2.4 Resin Cure 52

4.2.5 Polymer Properties 52

4.3 Results and Discussion 53

4.3.1 Synthesis of Ester-Spaced, Aromatic Diglycidyl Ethers 53

4.3.2 Polymer Properties 54

4.4 Conclusions 60

Chapter 5: Functionally Hybrid Monomers From Aromatic, Bio-Based, Asymmetric Diols and Their Respective Epoxy-Functional Homopolymers 62

5.1 Introduction 62

Table of Contents (Continued)

5.2 Experimental Methods & Procedures 65

5.2.1 Materials 65

5.2.2 Synthesis of 3-methoxy-4-(oxiran-2-ylmethoxy)benzyl methacrylate (VAEM) 65

5.2.3 Synthesis of 3,5-dimethoxy-4-(oxiran-2-ylmethoxy)benzyl methacrylate (SAEM) 67

5.2.4 Synthesis of 4-(oxiran-2-ylmethoxy)benzyl methacrylate (GDEM) 68

5.2.5 Synthesis of 4-(oxiran-2-ylmethoxy)phenethyl methacrylate (TEM) 69

5.2.6 Preparation of Homopolymers 70

5.2.7 Characterization of Monomers & Homopolymers 71

5.3 Results and Discussion 73

5.3.1 Monomer Synthesis and Characterization 73

5.3.2 Polymer Characterization 76

5.4 Conclusions 83

Chapter 6: Vanillin-Based Resin for Additive Manufacturing 84

6.1 Introduction 84

6.2 Experimental Methods & Procedures 88

6.2.1 Materials 88

6.2.2 Resin Synthesis 89

6.2.3 Resin Characterization & Photorheology 90

6.2.4 Determination of Working Curve Parameters 91

6.2.5 Resin Additive Manufacturing 91

6.2.6 Extent of Cure 91

6.2.7 Polymer Properties. 92

6.3 Results and Discussion 93

6.3.1 Rheology 93

6.3.2 Working Curve Parameters 95

6.3.3 Extent of Cure 96

6.3.4 Polymer Properties 98

Table of Contents (Continued)

6.4 Conclusions 105
Chapter 7: CNSL-Isosorbide-Lignin Derived (Formulated Hybrid) Resins for Additive Manufacturing 107
7.1 Introduction 107
7.2 Experimental Methods & Procedures 109
7.2.1 Materials 109
7.2.2 Resin Synthesis 110
7.2.3 Resin Characterization & Photorheology 111
7.2.4 Determination of Working Curve Parameters 112
7.2.5 Resin Additive Manufacturing 112
7.2.6 Extent of Cure 113
7.2.7 Polymer Properties 113
7.3 Results and Discussion 114
7.3.1 Rheology 114
7.3.2 Working Curve Parameters 116
7.3.3 Extent of Cure 118
7.3.4 Polymer Properties 119
7.4 Conclusions 127
Chapter 8: Network Toughening of Additively Manufactured, High Glass Transition Temperature Materials via Sequentially Cured, Interpenetrating Polymers 129
8.1 Introduction 129
8.2 Experimental Methods & Procedures 132
8.2.1 Materials 132
8.2.2 Dual-Cure Resin Synthesis 133
8.2.3 Resin Formulation 134
8.2.4 Resin Rheology 136
8.2.5 Resin Additive Manufacturing & Cure 136
8.2.6 Extent of Cure 137
8.2.7 Polymer Properties 137

Table of Contents (Continued)

8.3 Results and Discussion 139

8.3.1 Resin Rheology 139

8.3.2 Extent of Cure 140

8.3.3 Polymer Properties 142

8.4 Conclusions 153

Chapter 9: Conclusions and Recommendations for Future Work 154

9.1 Conclusions 154

9.2 Recommendations for Increased Manufacturing Rate of Sequential Interpenetrating Polymers 157

9.2.1 Photoreactive Extrusion 157

9.2.2 Cold Spray 159

9.3 Recommendations for Bio-Based, Sequential Interpenetrating Polymers 161

References 166

Appendix A: Alternative Monomers to 4,4′-methylenedianiline in Thermosetting Epoxy Resins 193

Appendix B: Supporting Information for Chapter 3 232

Appendix C: Supporting Information for Chapter 4 239

Appendix D: Supporting Information for Chapter 5 242

Appendix E: Supporting Information for Chapter 6 262

Appendix F: Supporting Information for Chapter 7 264

Appendix G: Supporting Information for Chapter 8 268

Appendix H: List of Acronyms, Abbreviations, and Symbols 272

Appendix I: Copyright Permissions 274

List of Figures

Figure Page

Figure 1. Chemical structure of diglycidyl ether of bisphenol A (DGEBA, Epon828)..... 3

Figure 2. Synthesis of bismethacryl glycidyl ether of bisphenol A epoxy, VE828..... 4

Figure 3. a) Lignin derivatives vanillin and vanillyl alcohol and b) CNSL derivative cardanol. 6

Figure 4. Chemical structure of glycidyl methacrylate..... 7

Figure 5. Example preparation of a dual-functional, vinyl ester-epoxy monomer..... 8

Figure 6. 3D model of printed part to determine resin cure characteristics..... 13

Figure 7. Chemical structures of all bisphenolic dimethacrylates. 24

Figure 8. Electrophilic Condensation of Vanillyl Alcohol and Cardanol to Produce Vanillyl Alcohol Cardanol (VAC) 26

Figure 9. Hydrogenation of VAC to produce vanillyl alcohol hydrogenated cardanol (vahc)..... 26

Figure 10. Methacrylation of VAC to produce vanillyl alcohol cardanol dimethacrylate (VACDM) 27

Figure 11. Methacrylation of VAHC to produce vanillyl alcohol hydrogenated cardanol dimethacrylate (VAHCDM)..... 27

Figure 12. The styrene vinyl and methacrylate region of interest of the mid-IR spectra of VAHCDM 35 wt% Styrene as a function of cure time at 90 °C..... 36

Figure 13. Near-IR spectra of VACDM 35 wt% Styrene resin and cured resin. Methacrylate (*) absorption is indicated. Spectra are offset vertically for clarity 37

Figure 14. TGA thermograms and their respective 1st derivatives of VERs cured with 35 wt% Styrene in N_2. 40

Figure 15. DMA thermograms of E' and E'' of the VERs cured with 35 wt% Styrene.... 42

Figure 16. Tan δ thermograms of the VERs cured with 35 wt% Styrene..... 43

Figure 17. Load displacement curves for VERs cured with 35 wt% Styrene..... 46

Figure 18. Ester-spaced, aromatic diglycidyl ethers prepared. 49

Figure 19. Synthetic route to prepare ester-spaced, aromatic diglycidyl ethers 51

Figure 20. ^{1}H-NMR spectrum of DGEBVA-C18 with peak assignments and integrations 54

List of Figures (Continued)

Figure Page

Figure 21. TGA thermograms and the respective first derivatives of the cured epoxy-amine thermosets in N_2 55

Figure 22. DSC traces of the cured epoxy-amine thermosets 56

Figure 23. DMA thermograms of E' and E'' for the epoxy-amine thermosets 58

Figure 24. Tan δ thermograms of the cured epoxy-amine thermosets 58

Figure 25. Structures of dual-functional monomers prepared 64

Figure 26. Representative reaction scheme for homopolymers; solution polymerization of VAEM to prepare poly(VAEM) 71

Figure 27. General synthesis route for the preparation of dual functional monomers. 75

Figure 28. ^{1}H-NMR spectrum for synthesized VAEM molecule with peak assignments and integrations 76

Figure 29. Epoxy-functional thermoplastics prepared 77

Figure 30. Representative ^{1}H-NMR spectrum with partial peak integrations of poly(VAEM) 78

Figure 31. TGA thermograms and the respective first derivatives of the polymers in N_2 80

Figure 32. 1P2S MV-GMA reaction scheme 90

Figure 33. a) Shear storage and loss moduli and the complex viscosity for the 1P2S MV-GMA resin during photorheology and b) Zoomed shear storage and loss moduli and the complex viscosity for the 1P2S MV-GMA resin at modulus crossover. Light turns on at 30 s 94

Figure 34. Comparison of OLS model and observed data points. 95

Figure 35. Near-IR spectra of 1P2S MV-GMA Resin, AM and AM-FC. Methacrylate (*) absorption is indicated. Spectra are offset vertically for clarity. 97

Figure 36. TGA thermograms and their respective 1st derivatives of the 1P2S MV-GMA AM and 1P2S MV-GMA AM-FC cured samples in N_2. 98

Figure 37. DMA thermograms of E' and E'' of 1P2S MV-GMA AM and 1P2S MV-GMA AM-FC. 100

Figure 38. Tan δ thermograms of 1P2S MV-GMA AM and 1P2S MV-GMA AM-FC. 101

Figure 39. Stress-strain curves of 1P2S MV-GMA AM and 1P2S MV-GMA AM-FC. 104

Figure 40. 1P2S PM-NC514sVE reaction scheme 111

List of Figures (Continued)

Figure Page

Figure 41. Structure of isosorbide dimethacrylate 111

Figure 42. Viscosity of 1P2S PM-NC514sVE with varying IM content. 115

Figure 43. Working curve for 1P2S PM-NC514sVE 20% IM. 117

Figure 44. Near-IR spectra for 1P2S PM-NC514sVE Resin, AM and AM-FC for 10% IM. Methacrylate (*) absorption is indicated. Spectra are offset vertically for clarity 118

Figure 45. TGA thermograms and respective 1st derivatives of 1P2S PM-NC514sVE with varying IM weight percent in N_2. 120

Figure 46. DMA thermograms of E' and E'' of 1P2S PM-NC514sVE samples with varying IM weight percent. 121

Figure 47. Tan δ thermograms for 1P2S PM-NC514sVE samples with varying IM weight percent. 122

Figure 48. Stress-strain curves of 1P2S PM-NC514sVE with varying IM weight percent. 124

Figure 49. Load displacement curves for 1P2S PM-NC514sVE with varying IM weight percent. 126

Figure 50. Chemical structures used in this study. 132

Figure 51. PM-EM828 reaction scheme. 134

Figure 52. Visual representations of a) the PM-EM828 network, b) the PM-VE828 – Epon828 Blend network, c) the PM-EM828_025VE828 network, and d) the PM-EM828_05Epon828_025VE828 network. 136

Figure 53. Near-IR spectra of PM-EM828 resin, and the resin at the AM, FC, and PC stages of cure. Spectra are vertically offset for clarity. 140

Figure 54. TGA thermograms and the respective 1st derivatives of all IPNs in N_2. 143

Figure 55. DMA thermograms of E' and E'' of all IPNs. 144

Figure 56. Tan δ thermograms of all IPNs. 145

Figure 57. Stress-strain curves of all IPNs. 148

Figure 58. Load-displacement curves of all IPNs. 151

Figure 59. Summary of the fracture toughness values and glass transition temperatures of all thermosets prepared in this dissertation. 156

List of Figures (Continued)

Figure Page

Figure 60. Visual representation of the photoreactive extrusion (PRE) process. 158

Figure 61. Proposed reactive cold spray (CS) process diagram. 160

Figure 62. Reaction scheme for the preparation of PM-EMNC514s..... 163

Figure 63. Load-displacement curves of IPNs containing bio-based epoxies. 164

Figure 64. Proposed, bio-based IPN components. 165

List of Tables

Table Page

Table 1. Viscosity of monomers and resins at 25 °C 33

Table 2. Extent of cure of resins via mid-IR and near-IR spectroscopy after postcure based on styrenic vinyl and methacrylate vinyl bonds, taken at room temperature. (* Denotes near-IR results) 38

Table 3. Thermogravimetric properties of the cured VERs in N_2 40

Table 4. Thermomechanical properties of VERs cured with 35 wt% Styrene 42

Table 5. Fracture toughness K_{1c} and G_{1c} values of VERs cured with 35 wt% Styrene 46

Table 6. Thermogravimetric properties for all ester-spaced, aromatic diglycidyl ether samples cured with Epikure W in N_2 55

Table 7. DSC results for all ester-spaced, aromatic diglycidyl ether samples cured with Epikure W 57

Table 8. Thermomechanical results for all ester-spaced, aromatic diglycidyl ether samples cured with Epikure W 59

Table 9. Molecular weight and T_gs of prepared homopolymers 79

Table 10. Thermogravimetric properties of the epoxy-functional homopolymers in N_2 . 80

Table 11. Film thicknesses and static contact angles of the flow coated polymer samples 82

Table 12. Surface energies for each film 83

Table 13. Working Curve Parameter Estimates 96

Table 14. Thermogravimetric results for the 1P2S MV-GMA AM and 1P2S MV-GMA AM -FC in N_2 99

Table 15. Viscoelastic properties of 1P2S MV-GMA AM and 1P2S MV-GMA AM-FC 101

Table 16. Tensile testing values of 1P2S MV-GMA AM and 1P2S MV-GMA AM-FC 104

List of Tables (Continued)

Table Page

Table 17. Viscosity at room temperature for 1P2S PM-NC514sVE with varying IM weight percent 116

Table 18. Working curve parameters for 1P2S-PM NC514sVE with varying IM weight percent 117

Table 19. Extent of cure for before and after FC of printed samples for 1P2S PM-NC514sVE with varying IM weight percent 118

Table 20. Thermogravimetric properties for 1P2S PM-NC514sVE samples with varying IM weight percent in N_2 120

Table 21. Thermomechanical results for 1P2S PM-NC514sVE samples with varying IM weight percent 122

Table 22. Tensile testing results for 1P2S PM-NC514sVE with varying IM weight percent 125

Table 23. Fracture toughness K_{1C} and G_{1C} for 1P2S PM-NC514sVE with varying IM weight percent 127

Table 24. Resin formulation composition 135

Table 25. Viscosity of resins at 25 °C 139

Table 26. Extent of cure of resins via near-IR spectroscopy at various stages of cure, taken at room temperature 141

Table 27. Thermogravimetric properties of all IPNs in N_2 143

Table 28. Viscoelastic properties of all IPNs 145

Table 29. Tensile testing values of all IPNs 149

Table 30. Fracture toughness K_{1C} and G_{1C} values of all IPNs 151

Table 31. Fracture toughness K_{1C} and G_{1C} values of IPNs containing bio-based epoxies 164

Chapter 1

Introduction

1.1 Motivation and Background

Polymers encompass an increasingly broad range of materials that are used in applications from consumer goods to paints, finishes, electrical laminates, composites, optical materials, structural materials, and so on [1, 2]. Polymers are so ubiquitous in today's world that most individuals do not realize their importance in everyday life. With continuously evolving technologies in today's world, the demand for polymeric materials for such technologies is steadily growing. While the quantitative demand for polymer production continues to grow, so does the desired properties of which these polymers exhibit. Furthermore, with the advancement of manufacturing sciences for materials in general, the desire for polymers designed for advanced manufacturing techniques is also steadily increasing. While polymeric materials that exist today exhibit good overall properties, the desire to push the limit of performance does, and always will, exist. Therefore, striving for increased polymer performance is a common goal across the globe to improve materials not only in consumer and industrial markets, but also military, to continuously modernize today's society. With this impetus, this dissertation focuses on the development of advanced structural materials via unique methodologies, discussed in Chapter 1.3, which aim to push the envelope of polymer performance and, in some cases, enable modern manufacturing.

The following sections introduce polymers, and the subsequent polymer categories of thermoplastics and thermosets, and define the approaches utilized to further

the development of performance-advantaged, structural polymeric materials which is utilized throughout this dissertation.

1.2 Polymers

1.2.1 Introduction to polymers. Polymers are large macromolecular molecules that are comprised of smaller, individual units called monomers that are linked together chemically. Polymers and polymer science encompass materials that are synthetically prepared such as polyethylene, polystyrene, and nylon, as well as those that are naturally occurring such as proteins, silk, and cellulose [2]. Polymer science can be dated back to the 1830s with the development of the vulcanization process for the preparation of rubber for car tires by Charles Goodyear and was followed by the development of Bakelite by Leo Baekeland in 1907 and the development of nylon and Teflon^{TM} by Dupont in the 1930s [2, 3]. In today's world, polymers are ubiquitous in everything from consumer goods to high-demanding applications such as aerospace and military. Polymers are generally divided into two groups: thermosets and thermoplastics, based on the behavior of the polymer during thermal processing [2].

1.2.2 Thermosets. Thermosets are polymeric materials that contain chemical crosslinks, thus causing the resulting material to be resistant to flow when heated and not exhibit a melting point [2]. Some examples of thermosetting polymers include epoxy, vinyl ester, and unsaturated polyester resins which are utilized in a variety of military and commercial applications such as coatings and composites as they typically impart high thermal stabilities, moduli, strengths, glass transition temperatures (T_gs), and chemical resistances [4-6].

Epoxy resins account for approximately 70% of the overall thermosetting polymers market. Epoxy monomers and oligomers prepared via the reaction of bisphenol A and epichlorohydrin to prepare the diglycidyl ether of bisphenol A (DGEBA, Figure 1) account for over 90% of the worldwide thermosetting epoxy resin market and were first invented in 1934 and subsequently commercialized in 1947 [1, 7].

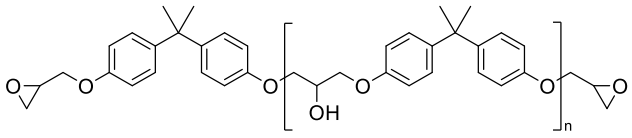

Diglycidyl Ether of Bisphenol A
(DGEBA, Epon828)

Figure 1. Chemical structure of diglycidyl ether of bisphenol A (DGEBA, Epon828).

Epoxy resins are generally cured with hardeners such as amines, anhydrides, or Lewis acids, and are found in a wide variety of applications such as coatings, adhesives, and composites due to their exceptional corrosion resistance, excellent adhesive properties, low shrinkage during cure, as well as high T_gs and moduli [2, 3, 8].

Vinyl ester resins are generally produced via the esterification of epoxy resins and possess terminal reactive double bonds which can be utilized to form crosslinked polymers easily via radical-based polymerization mechanisms [2, 3, 9]. One of the most widely used vinyl ester resins in commercial applications is bismethacryl glycidyl ether of bisphenol A (vinyl ester 828, VE828), which is the product of reacting diglycidyl ether of bisphenol A (DGEBA, Epon828) with methacrylic acid, pictured in Figure 2 [4, 10, 11].

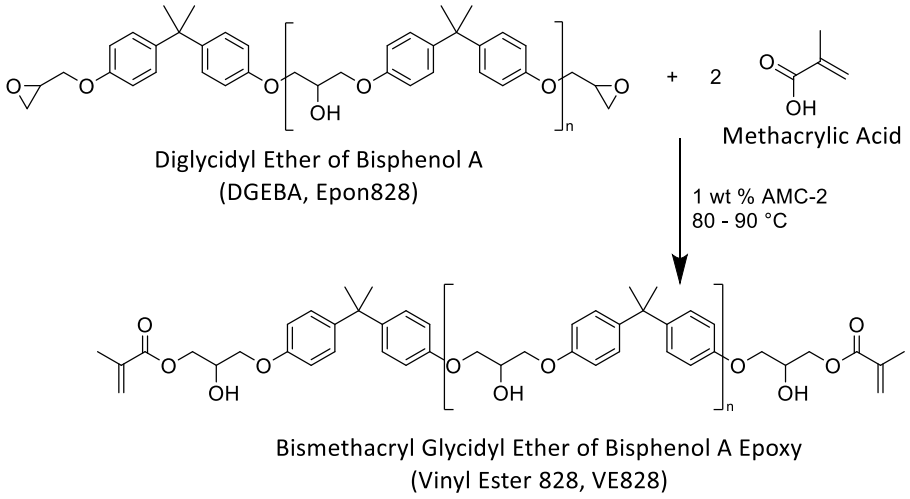

Figure 2. Synthesis of bismethacryl glycidyl ether of bisphenol A epoxy, VE828.

Analogous to epoxy resins, vinyl ester resins exhibit good chemical resistance, low water absorption as well as high T_gs and moduli [4, 12]. Vinyl ester resins were first commercialized in 1965 by the Shell Chemical Company and subsequently commercialized by Dow Chemical [12]. These resins are often used as alternatives to unsaturated polyesters due to their superior properties and are employed in the marine, transportation, and construction industries [4, 13]. While epoxy resins and vinyl ester resins exhibit adequate T_gs (typically higher than 120 °C) for structural use, both are hindered by their relatively low fracture toughness which limits the utility of these materials for more advanced structural applications.

1.2.3 Thermoplastics. Thermoplastics are linear polymers that can be softened upon heating, thus enabling the material to flow at elevated temperatures [2]. Furthermore, thermoplastics can be recycled and refabricated more easily compared to thermosets. Thermoplastics can be utilized in a wide range of applications depending on the monomers that are combined to make the polymer backbone. One of the most

commonly known thermoplastics is polystyrene, first produced by Dow Chemical in 1938 [2]. Polystyrene is commonly utilized in packaging materials such as foams. However, thermoplastics that bear functional handles along the polymer backbone, such as poly(glycidyl methacrylate) which bears a pendant epoxy moiety, are widely utilized in automotive coatings, protective finishes, adhesives, and electrical laminates as the epoxy moiety can be used to facilitate the robust attachment of the polymer to various surfaces [14-16]. Yet, the lack of aromatic character in poly(glycidyl methacrylate) limits the use of the material at elevated temperatures.

1.3 The Hybrid Approach

This dissertation focuses on molecular-level approaches to develop performance-enhanced structural materials, specifically those with both improved glass transition temperatures (T_gs) ($\geq$ 120 °C) and enhanced fracture toughness (G_{1C} > 250 J m^{-2}) while enabling the use of both conventional and/or upcoming manufacturing methodologies, such as additive manufacturing (AM). The following sections detail the approaches investigated to achieve such goals.

1.3.1 Molecularly hybrid & formulation hybrid. Specific monomeric feedstocks for the development of polymers offer unique attributes that can address specific performance needs, depending on the intended application. However, most applications of interest always require that multiple performance characteristics be fulfilled simultaneously. The molecularly hybrid approach proposes the combination of building blocks from different resources at the molecular level to capture a balance of polymer performance characteristics. One specific aspect of this approach is for the development of bio-derived materials with improved performance. Bio-derived resources

such as lignin, a major component of the cell wall of vascular plants, and cashew nutshell liquid (CNSL), an industrially produced byproduct of cashew harvesting, have been proven to be viable building blocks in the development of sustainable materials [8, 11, 17-20]. However, each of these resources provides their own unique properties independent of one another. For example, the aromaticity of lignin-derived molecules such as vanillin and vanillyl alcohol (Figure 3a) provides enhanced structural and thermal stabilities and the phenolic lipid structure of CNSL-derived cardanol (Figure 3b) provides enhanced flexibility and processability.

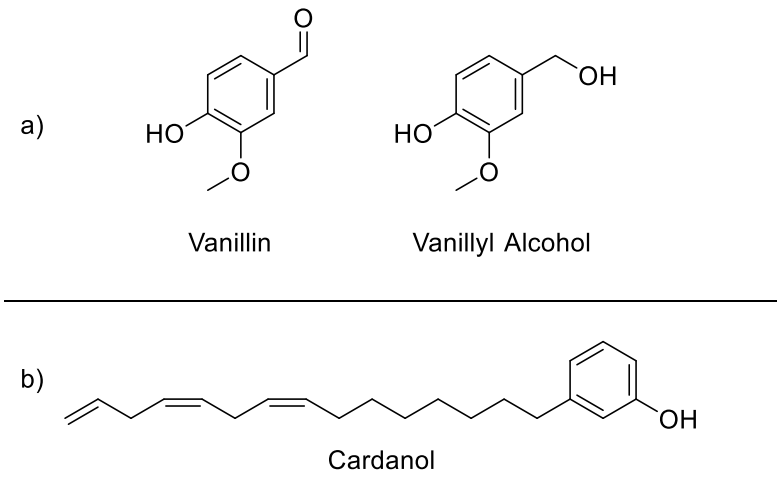

Figure 3. a) Lignin derivatives vanillin and vanillyl alcohol and b) CNSL derivative cardanol.

Naturally, most applications of interest always require that multiple performance characteristics be satisfied simultaneously; therefore, the molecularly hybrid approach aims to combine such bio-based resources at the molecular level to design monomeric structures that target improved performance, most notably the improvement in toughness of traditional vinyl ester and epoxy resins while maintaining adequate thermal properties.

Similarly, the formulation hybrid approach aims toward the goal of developing materials with increased toughness over traditional vinyl ester and epoxy resins via the incorporation of materials derived from biomass; however, while the molecularly hybrid approach focused primarily on the development of unique monomers, the formulation hybrid approach seeks to combine individual monomers derived from different, individual feedstocks that are already known to have specific performance attributes.

1.3.2 Functionally hybrid. Functionally hybrid monomers are characterized as bearing two different reactive substituents that allow for multiple and versatile methods of chemical modification and/or monomer polymerization, permitting customization of linear polymers and polymer networks for a variety of commercial uses [21]. Creating a monomer with both epoxy and (meth)acrylate (vinyl) functionalities specifically can facilitate unique polymer network formation via reactive sites for covalent bonding or inter-connected, interpenetrating polymer network formation [22]. The functionally hybrid approach in this dissertation spans into both thermoplastics and thermosets. The functionally hybrid approach first aims to develop aromatic compliments to glycidyl methacrylate (GMA, Figure 4) and the subsequent preparation of epoxy-functional thermoplastics for improved thermal stability of coatings and adhesives.

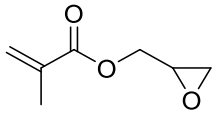

Figure 4. Chemical structure of glycidyl methacrylate.

Furthermore, the functionally hybrid approach expands into thermosets, whereby the reaction of a polyepoxide with a less than stoichiometric amount of methacrylic acid yields dual-functional, vinyl ester-epoxy monomers (shown in Figure 5) to facilitate unique bonding in AM (3D printed), inter-connected, interpenetrating polymer networks for improved performance analogous to that mentioned in Chapter 1.3.1: the improvement in toughness of traditional vinyl ester and epoxy resins while maintaining adequate thermal properties.

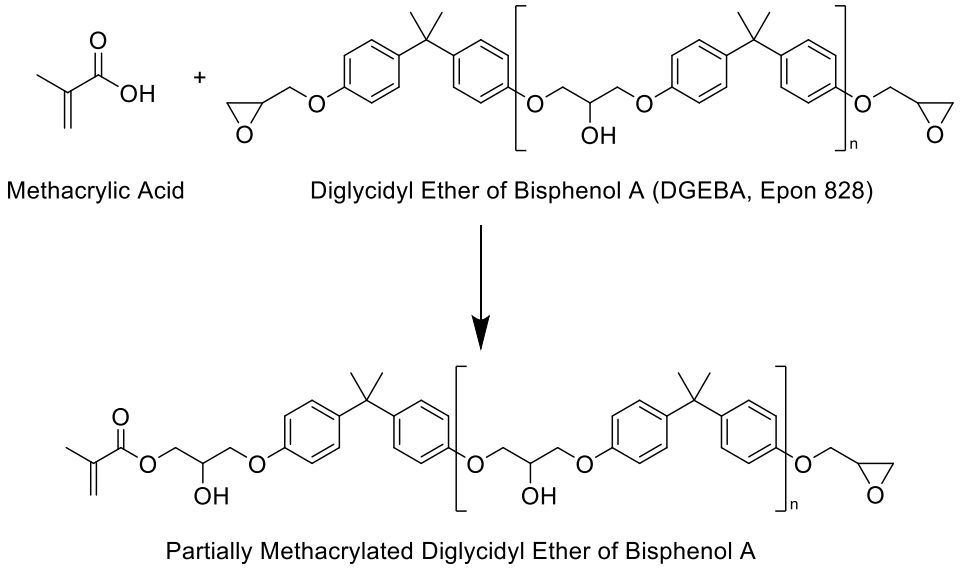

Figure 5. Example preparation of a dual-functional, vinyl ester-epoxy monomer.

1.4 Dissertation Summary

As described in the previous section, this dissertation primarily aims toward developing structural polymeric materials with enhanced performance characteristics, namely improved glass transition temperatures (T_gs) (≥ 120 °C) and enhanced fracture toughness (G_{1C} > 250 J m^{-2}), over that of incumbent materials via molecular, formulation,

and functional hybrid approaches. Chapter 2 provides a brief description of all analytical techniques and instrumentation utilized in this work. Chapter 3 explores the molecular hybrid approach via the molecular-level combination of bio-based building blocks derived from lignin and CNSL to prepare asymmetric bisphenols for incorporation into vinyl ester resins. The molecular hybrid approach is further explored in Chapter 4 via the molecular-level combination of monomers derived from lignin and plant oils to prepare epoxy resins. The application of the functionally hybrid approach begins in Chapter 5, whereby aromatic monomers possessing both methacrylate and epoxy functionalities were prepared and subsequently homopolymerized to produce aromatic compliments to industrially viable poly(glycidyl methacrylate) for applications such as coatings and adhesives. Chapter 6 revisits utilizing bio-based materials in vinyl ester resins; however, these materials are applied towards AM, more commonly known as 3D printing. Chapter 7 continues to focus on AM; though, this chapter implements the formulation hybrid approach towards developing performance-advantaged materials. AM materials prepared via the implementation of the functionally hybrid approach to create interpenetrating polymers is investigated in Chapter 8. This dissertation concludes with Chapter 9, which details the major conclusions of this work as well as recommendations for future endeavors.

Chapter 2

Characterization Methods

2.1 Introduction

Chapter 2 encompasses an overview of the characterization techniques utilized throughout this dissertation. The general principles of the techniques used as well as relevant equations are provided. Specific experimental procedures are discussed within the chapters to which they pertain.

2.2 Nuclear Magnetic Resonance Spectroscopy (NMR)

Nuclear magnetic resonance (NMR) is a spectroscopic method that utilizes the magnetic response of atomic nuclei to subsequently analyze and identify chemical structures of organic compounds. NMR is used for a variety of nuclei; however, proton (^{1}H) and carbon (^{13}C) are the most common nuclei that are analyzed because they are the most abundant in organic compounds [23]. In general, NMR applies a magnetic field to a sample which, in turn, alters the frequencies of the nuclei in the molecule. The nuclei frequencies are then compared to a reference compound, such as tetramethylsilane (TMS), and the difference between the frequencies observed is the chemical shift, δ, in parts per million (ppm) and coincides with a peak in the NMR spectrum [24]. The observed chemical shift is highly dependent on molecular architecture. Furthermore, the intensities and splitting patterns of the signals obtained from NMR can be used to interpret how many nuclei of each type are present and information regarding nearby nuclei [23, 24]. In this dissertation, all molecules were characterized by ^{1}H-NMR (400.15 MHz, 32 scans at 298 K) and/or ^{13}C-NMR (111 MHz, 512 scans at 298 K) using a Varian 400 MHz FT-NMR Spectrometer.

2.3 Rheology

Rheology is defined as the study of material flow and rheological techniques and instruments are often utilized to determine viscosities of liquids, or the resistance of the liquids to flow [25]. Viscosity is highly dependent on internal friction within liquid samples; therefore, materials with high viscosities have higher internal friction and require more applied force to flow. Rheological instruments apply a shear rate to a liquid sample and measure the shear stress response of the sample. When the ratio of shear rate and shear stress is constant, the liquid is determined to be Newtonian. If a liquid material results in varying shear stresses with linear changes in shear rate, the liquid is determined to be non-Newtonian [25]. In this dissertation, rheological analysis was performed on a TA Instruments Discovery HR-2 Rotational Rheometer. Specific operating parameters and equipment setups are described in the chapters to which they apply.

2.4 Fourier Transform Infrared (FTIR) Spectroscopy

Fourier transform infrared (FTIR) spectroscopy is an analytical technique that can be used to analyze materials [25]. An infrared (IR) spectrum of a sample shows peaks which correspond to the vibrational frequency of specific bonds within the overall material. Different materials and molecular bonds will subsequently show different IR spectra, allowing the identification of such materials and bonds based on the collection of observed peaks [25].

In this dissertation, FTIR spectroscopy was performed in both the near-IR (4000 – 8000 cm^{-1}) and mid-IR (650 – 4000 cm^{-1}) regions using a Thermo Scientific Nicolet iS50 FTIR and Thermo Scientific Nicolet 6700 FTIR, respectively. Specific absorbances in the IR spectra were examined and detailed in the following chapters to which they pertain.

2.5 Stereolithography (SLA) Working Curve

Text and figures are reproduced and adapted with permission from A.W. Bassett et al, "Vanillin-based Resin for Additive Manufacturing," *In preparation,* reference [26].

The fundamental working curve model for stereolithography (SLA) is utilized to determine the ability for a material to be printed using SLA techniques and is described by Equation 1. A derivation of the working curve model is provided elsewhere [27]. The model is fundamental for determining SLA operating parameters.

$$C_d = D_p \, ln\left(\frac{E_{max}}{E_c}\right) \qquad \textit{Eq. 1}$$

C_d is the cure depth of a single layer, D_p is the depth at which the irradiance is 13.5% of the irradiance at the interface where the laser contacts the resin, E_c is the exposure per unit area required for the resin to reach its gel point, and E_{max} is the maximum exposure on the surface of the resin. D_p and E_c are considered to be the characteristic parameters of an SLA resin. A square part composed of 25 equal-area square tiles was printed on a Peopoly Moai SLA printer. A model of the part is shown in Figure 6.

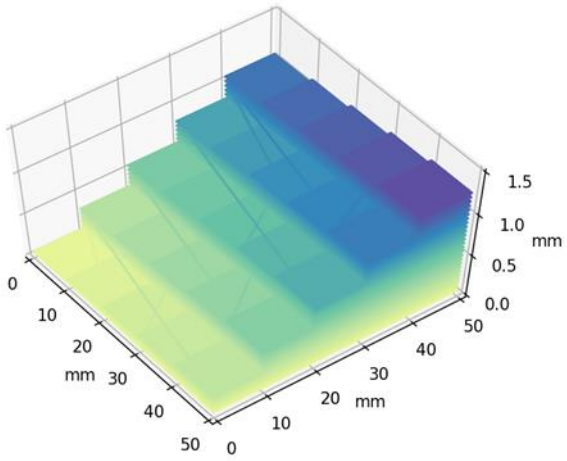

Figure 6. 3D model of printed part to determine resin cure characteristics.

The part was comprised of 25 layers with the first layer covering the area of 25 tiles, the second layer covering 24 tiles, and so on. This structure was created such that there was a tile that received 1 exposure, a tile that received 2 exposures, and so on up to 25 exposures. The part was not printed on a build platform; rather, the laser underneath the resin vat was directed into the vat, curing the part onto the surface of the vat. The height of each tile was measured with calipers and the maximum exposure for a single tile is determined from Equation 2:

$$E_{max} = \sqrt{\frac{2}{\pi}} \frac{nP_L}{W_0 V_s} \qquad \textit{Eq. 2}$$

where P_L is the power of the laser, W_0 is the width of the beam, V_s is the scanning speed, and n is the number of times the laser passed over the tile. P_L and W_0 for the printer were 150 mW and 0.07 mm, respectively.

E_c and D_p were estimated by ordinary least squares (OLS) regression of C_d against $\ln(E_{max})$. For OLS, C_d is the depth of cure measured on the printed part and E_{max} is computed from Equation 2. According to Equation 1, the slope of regression

obtained is D_p and the intercept is $-\ln(E_c)$. Via this technique, D_p is normally distributed and E_c is lognormally distributed. The mean and variance of E_c were estimated from the normally distributed regression intercept as described elsewhere [28].

2.6 Density Measurements

Density of materials is simply the ratio of mass to volume. In this dissertation, density was determined for all samples using Archimedes' Principle [29]. The dry mass of the polymer and mass of the polymer submerged in water were measured and the sample density, ρ, was calculated according to Equation 3:

$$\rho = \left(\frac{W_{dry}}{W_{dry}-W_{wet}}\right)\rho_{water} \qquad Eq.\ 3$$

where the dry sample weight is indicated as W_{dry}, the wet sample weight is indicated as W_{wet}, and ρ_{water} is the density of water at the temperature of which the measurements were performed.

2.7 Size Exclusion Chromatography (SEC)

Size exclusion chromatography (SEC), also known as gel permeation chromatography (GPC), is an analytical technique used to determine the molecular weight distribution of thermoplastic polymers. SEC instrumentation operates by dissolving the polymeric material into a solvent, such as tetrahydrofuran (THF), and injecting the solution into a continuous flow which then carries the materials into columns. The columns, comprised of porous particles, facilitate separation of the polymer injected sample based on the effective size of the molecules, which directly correspond to molecular weight [25]. The separated sample then passes through detectors such as a refractive index detector, and the signals are compared to a calibration sample to determine molecular weight.

In this dissertation, the number-average molecular weight (M_n), weight-average molecular weight (M_w), and dispersity ($Đ$) of all samples were obtained on a Waters Acquity Advanced Polymer Chromatography (APC) instrument with THF as the eluent (0.6 mL min^{-1}) using polystyrene standards with M_n of 537,000 Da ($Đ$=1.03), 59,300 Da ($Đ$=1.05), and 8,650 Da ($Đ$=1.03) as a calibration reference.

2.8 Differential Scanning Calorimetry (DSC)

Differential scanning calorimetry (DSC) is a widely used thermal analysis technique whereby the heat flow in and out of a sample is measured relative to a known reference [25]. DSC is utilized to understand thermal events of materials such as melting, crystallization, glass transition temperature, and so on. In short, the experimental procedure for DSC uses 5 – 10 mg of sample that is loaded into an aluminum pan and placed in a furnace which also contains an empty aluminum pan as a reference. The furnace is then heated at specific ramp rates across varying temperature ranges and the heat flow through both the pan containing the sample and the empty pan is measured via thermocouples to determine the heat flow, in W g^{-1}, through the sample. In this dissertation, a TA Instruments Discovery DSC 2500 was used. Specific temperature ranges and temperature ramp rates were employed and are discussed in the following chapters.

2.9 Thermogravimetric Analysis (TGA)

Thermogravimetric analysis (TGA) is an analytical technique used to measure changes in weight of a material as the sample is heated either at a set rate or stepwise in inert or oxidative atmospheres. TGA measures mass changes via an analytical balance which occur as a result of events such as oxidation, vaporization, and degradation [25]. In

this dissertation, a TA Instruments Discovery TGA 550 was employed. Samples of approximately 10 mg in weight were, in general, loaded onto a platinum pan heated from room temperature to 700 °C in both inert (N_2) and oxidative (air) environments.

2.10 Dynamic Mechanical Analysis (DMA)

Dynamic mechanical analysis (DMA) is a technique used to evaluate the viscoelastic properties of materials [25]. DMA techniques apply an oscillatory strain to a sample and the displacement or response of the sample is measured. The modulus and response delay from the sample, measured via phase angle δ, are calculated for each cycle [30]. The applied strain, ε, and stress response, σ, are shown in Equations 4 and 5.

$$\varepsilon = \varepsilon_0 sin\,(\omega t) \qquad Eq.\ 4$$

$$\sigma = \sigma_0 sin\,(\omega t + \delta) \qquad Eq.\ 5$$

From this information, measurements such as storage and loss moduli, and the damping factor, tan δ, can be determined. Storage modulus, *E′*, represents the elastic portion of the material, and is often referred to as the energy stored in the chemical bonds of the material. The loss modulus, *E″*, represents the viscous response from the material upon deformation and is referred to as the energy dissipated as heat. *E′* and *E″* are calculated as shown in Equations 6 and 7. Tan δ is simply the ratio of *E″* to *E′* as shown in Equation 8.

$$E' = \frac{\sigma_0}{\varepsilon_0} cos\,(\delta) \qquad Eq.\ 6$$

$$E'' = \frac{\sigma_0}{\varepsilon_0} sin\,(\delta) \qquad Eq.\ 7$$

$$tan\,\delta = \frac{E''}{E'} \qquad Eq.\ 8$$

Furthermore, DMA can be utilized to determine the molecular weight between crosslinks, M_c, for polymeric materials. M_c was estimated using the Theory of Rubber Elasticity as seen in Equation 9 [31].

$$E = \frac{3RT\rho}{M_c} \qquad \textit{Eq. 9}$$

where E is the minimum rubbery storage modulus, R is the ideal gas constant, T is the absolute rubbery temperature and ρ is the density.

In this dissertation, a TA Instruments Q800 dynamic mechanical analyzer (DMA) was used to evaluate the viscoelastic properties of all materials. A single cantilever geometry with a frequency of 1.0 Hz, Poisson's ratio of 0.35, and deflection amplitude of oscillation of 7.5 μm was used. The heating ramp was 2 °C per minute and the temperature range of testing varied and is discussed in the following chapters. Samples were prepared with appropriate dimensions (35 x 12 x 2.5 mm^3 and 35 x 12 x 1.5 mm^3) and tested in accordance with McAninch et al [32].

2.11 Tensile Testing

Tensile testing is one of the most fundamental evaluation methods for materials. Tensile testing evaluates the ability of a material to withstand forces that are applied to pull the material apart and to measure the extent to which a material stretches before failure. From this test, material properties such as tensile strength, tensile strain, and Young's modulus can be determined [33]. Data from tensile experiments are often manipulated as to not be geometry specific, therefore a stress-strain curve is usually generated whereby stress, σ, and strain, ε, are calculated at each point of force according to Equations 10 and 11, respectively [25].

$$\sigma = \frac{F}{A} \qquad \textit{Eq. 10}$$

$$\varepsilon = \frac{L - L_0}{L_0} \qquad \textit{Eq. 11}$$

where F is the tensile force, A is the cross-sectional area of the specimen, L_0 is the initial gauge length of the specimen, and L is the final gauge length of the specimen. In this dissertation, tensile testing was conducted using an Instron 5966 mechanical tester. Type IV dogbone specimens were prepared and analyzed according to ASTM D638 [33].

2.12 Fracture Toughness

Fracture toughness is utilized to determine toughness of polymeric materials via the determination of the critical stress intensity factor, K_{1C}, and critical strain energy release rate, G_{1C}, upon fracture [34]. Fracture toughness experiments are performed by placing a pre-notched, pre-cracked specimen into a mechanical tester and applying a load to the material until fracture while displacement is measured. K_{1C} is calculated based on the load applied to the sample and G_{1C} is determined from the integration of the load-displacement curve [34]. K_{1C} and G_{1C} are mathematically related as shown by Equation 12.

$$G_{1C} = \frac{(1 - \nu^2){K_{1C}}^2}{E} \qquad \textit{Eq. 12}$$

where ν is Poisson's ratio and E is the modulus of the material. Fracture properties are used to characterize the resistance to fracture for a material, whereby the higher the K_{1C} and G_{1C} obtained, the tougher the material. In this dissertation, fracture toughness was evaluated according to ASTM D5045 [34]. Three-point, single edge notched bend (SENB) samples of all cured resins were prepared to be 44 x 10 x 4 mm^3 to ensure plane-strain. Using a diamond saw, samples were notched, and a single edged razor blade was used to instantly propagate a crack. Upon cracking the samples, the tip of the crack was marked with ink [35]. Samples were tested on an Instron 5966 mechanical tester

equipped with a 3-point bend flexure fixture. The K_{1C} and G_{1C}, were determined upon fracture.

Chapter 3

Molecularly Hybrid Bisphenols Derived From Lignin and Cashew Nutshell Liquid (CNSL)

Text and figures are reproduced and adapted with permission from A.W. Bassett, C.M. Breyta, A.E. Honnig, J.H. Reilly, K.R. Sweet, J.J. La Scala, and J.F. Stanzione III, "Synthesis and characterization of molecularly hybrid bisphenols derived from lignin and CNSL: Application in thermosetting resins," *European Polymer Journal*, 2019, 111, 95-103, reference [36].

3.1 Introduction

BPA-based methacrylates and vinyl ester resins (VERs) are utilized in a variety of military and commercial applications such as coatings and composites as they typically impart high thermal stabilities, moduli, strengths, glass-transition temperatures (T_gs), and chemical resistance [4-6]. Due to their high-performance characteristics and low processing costs, these materials are regularly used in the construction, marine, and transportation industries for applications such as vehicle components, under-the-hood vehicle parts, and marine hulls [13]. Dimethacrylates form crosslinked network polymers easily via free-radical polymerization due to the two terminal reactive double bonds [9]. One of the most widely used dimethacrylates in commercial applications is bismethacryl glycidyl ether of bisphenol A (vinyl ester 828, VE828), which is the product of reacting diglycidyl ether of bisphenol A (DGEBA, Epon 828) with methacrylic acid [4, 10, 11]. However, the utilization of BPA is particularly unfavorable due to concerns of human endocrine disruption [37-42]. In addition, BPA is derived from petrochemical feedstocks, which are considered unsustainable resources that possess frequent price fluctuations

[43]. As a result, bio-based feedstocks, monomers, and polymers are becoming considerably more attractive as viable alternatives to their petrochemical-based counterparts.

The search for bio-based alternatives to BPA-based methacrylates and vinyl esters is ongoing. Previous studies have identified isosorbide as a potential building block for VERs. Derived from the hydrolysis of glucose, isosorbide's fused bicyclic structure with chiral diols has been shown to provide structural integrity and thermal stability when used in thermosetting resins [44-47]. Isosorbide methacrylate (IM) is a low viscosity resin that could be cured with or without a reactive diluent. The cured resin containing neat IM resulted in a thermoset with a T_g of approximately 245 °C, the highest known T_g for a vinyl ester resin [44]. Soybean oil has also gained interest for thermosetting materials due to its availability and low cost [48, 49]. Previous studies show that functionalized soybean oil, first with epoxy functionality then with acrylate functionality to synthesize acrylated epoxidized soybean oil (AESO), is a capable material for VERs [50, 51]. AESO-based VERs, however, tend to exhibit lower T_gs than that of VE828-based VERs, as AESO contains no aromaticity in its chemical structure [51-53]. Cardanol, a component of cashew nutshell liquid (CNSL) and phenolic lipid, has also shown promise in the development of VERs [11, 54, 55]. Cardanol-based vinyl esters have exhibited reduced viscosities relative to VE828, improving processability; however, depending on formulation, comparable T_gs to commercial VERs have been difficult to obtain from modified cardanols [11, 17, 18].

The polymer properties exhibited by BPA-based VERs are due to the rigidity provided by their aromaticity and bisphenolic structure, therefore it is necessary to utilize

biomass alternatives with aromatic content similar to BPA to provide the highest potential for replacing BPA in polymer applications. In addition, while upholding aromaticity, alternatives are desired to have substituents on the aromatic rings, thus ultimately reducing the toxicity of the resulting compounds [56]. Lignin is an abundant, natural resource with a complex, three dimensional, substituted polyphenol structure [57-59]. Lignin, a waste product of the paper and pulp industry, accounts for up to 18-35% by weight of wood with an annual production of up to 50 million tons [60-62]. Due to the high aromatic content of lignin, lignin depolymerization has gained significant interest. Ongoing research has shown that the strategic depolymerization of lignin can result in a variety of aromatics and methoxy phenols that can be more easily processed [63, 64]. Industrially, vanillin is the most widely produced lignin derivative. Vanillin, a major component of natural vanilla extract, is currently derived from lignin via the paper pulping sulfite process [65-69]. Approximately 15% of vanillin for the flavor and fragrance market is produced from lignin, while the remaining 85% is produced from petrol derived guaiacol [66, 70]. Vanillyl alcohol, the reduced form of vanillin, has been shown to be a platform chemical for the production of polymeric materials, and most notably, bisphenolic analogues, as the hydroxymethyl group provides the necessary reactivity for phenolic coupling and avoids the use of volatile and carcinogenic molecules, such as formaldehyde and acetone [61, 71].

Cardanol, derived from cashew nutshell liquid (CNSL), is a non-edible byproduct of the cashew production industry with a unique phenolic structure bearing a saturated and/or unsaturated carbon chain [55, 72, 73]. CNSL makes up approximately one third of the total cashew nut weight; therefore, CNSL is largely available as a byproduct of the

mechanical process of removing the cashew kernel from the shell [11]. CNSL can be extracted from the largely available, and otherwise unused, shell of the cashew nut at a relatively low cost [54]. Production of crude CNSL approaches 1 million tons annually as a mixture of different unsaturated long-chain phenols with up to three unsaturation points. The aliphatic chain of cardanol can have double bonds in positions (8), (8, 11), or (8, 11, 14) with an average number of two double bonds per molecule [54, 55, 74]. The phenolic lipid structure of cardanol provides the flexibility to create monomers with unique properties to impart both water and thermal resistance into polymeric materials for applications such as coatings, laminates, and thermosetting matrices [9, 18, 75, 76].

In this study, vanillyl alcohol and cardanol were coupled to yield an asymmetric bisphenolic analogue, vanillyl alcohol cardanol (VAC), using similar methods described in Hernandez, et al [77]. Due to the unsaturation points on the C15 chain on VAC, the mechanical properties and toughness on the polymer network can be improved. Additionally, the unsaturation points on the C15 chain of VAC were hydrogenated to create VAHC, and the effects of saturation level on polymer properties were evaluated. VAC and VAHC are structurally similar to BPA, which is a known endocrine disruptor; however, the C15 chain and methoxy moieties present on VAC and VAHC have the potential to reduce the toxicity of these compounds, although this result was not tested in this work [56]. VAC and VAHC were subsequently dimethacrylated to prepare VACDM and VAHCDM, as bio-based alternatives to BPA in thermosetting matrices with comparable mechanical, thermal, and chemical properties. The properties of VACDM and VAHCDM were compared to bisguaiacol dimethacrylate (BGDM), which was prepared from a previously reported bio-based bisphenol, bisguaiacol (BG), as well as to

Vinyl Ester 828 (VE828) and bisphenol A dimethacrylate (BPADM) as commercial comparisons [77]. The chemical structures of all dimethacrylates used in this study are shown in Figure 7. The rheological properties of the resins, and thermogravimetric, thermomechanical, and fracture toughness properties of the cured resins were evaluated to determine the effect of structure on the properties of thermally cured VERs.

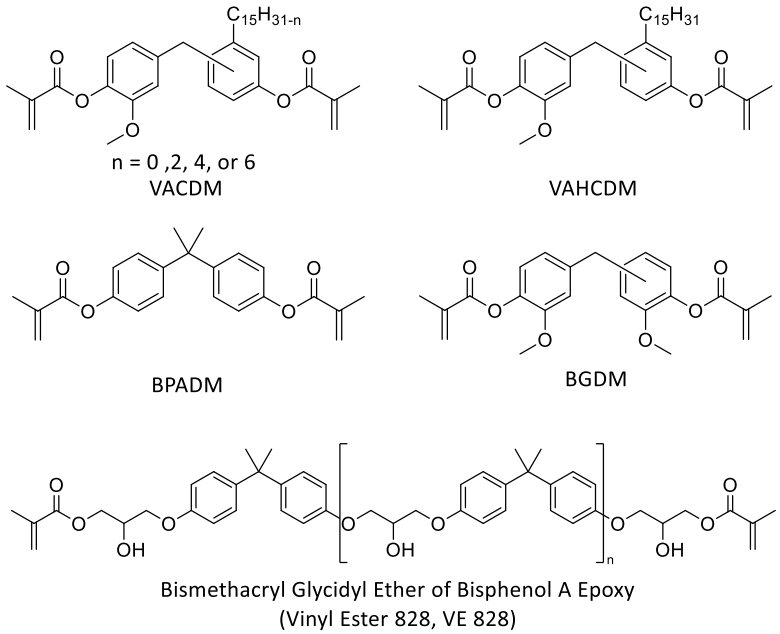

Figure 7. Chemical structures of all bisphenolic dimethacrylates.

3.2 Experimental Methods & Procedures

3.2.1 Materials. Vanillyl alcohol (4-hydroxy-3-methoxybenzyl alcohol, 99%), guaiacol (2-methoxyphenol, 99%), dichloromethane (DCM, 99.6%), and chloroform-*d* ($CDCl_3$, 99.8 atom% *d*) were purchased from Acros Organics. Ethyl acetate (99.9%), hexanes (99.9%), triethylamine (TEA, 99%) and styrene monomer (99.9%) were purchased from Fischer Scientific. Palladium on carbon powder 10 wt% loading (dry

basis), Dowex-DR 2030 hydrogen form, and methacrylic acid (99%) were purchased from Sigma Aldrich. Ethanol (200 proof) was purchased from Pharmco-Aaper. Compressed hydrogen (H_2, 99.999%), compressed nitrogen (N_2, 99.998%), compressed argon (Ar, 99.999%) and liquid nitrogen (N_2) were purchased from Airgas. Bisphenol A dimethacrylate (4,4' -Isopropylidenediphenol dimethacrylate, > 98%) was purchased from Tokyo Chemical Industry, Co. Trigonox® 239, containing 45% cumyl hydroperoxide, was purchased from AkzoNobel Polymer Chemicals. Epon Resin 828 (Diglycidyl Ether of Bisphenol A- DGEBA, Epon828) was obtained from Momentive Specialty Chemicals, Inc. AMC-2 was purchased from AMPAC Fine Chemicals. Epon828 was transformed into bismethacryl glycidyl ether of bisphenol A and is denoted as vinyl ester 828 (VE828). Synthesis and characterization described in literature were performed with similar results [4, 5]. Bisguaiacol (BG) was prepared and characterized as described in literature with similar results [77]. All chemicals mentioned above were used without further purification. Cardanol (NX-2025) was provided by Cardolite Corporation and was purified via flash chromatography (hexanes/ethyl acetate, 70:30).

3.2.2 Synthesis of VAC and VAHC. In a one neck round bottom flask with thermometer, vanillyl alcohol (18.5 g, 0.12 mol) and cardanol (90 g, 0.3 mol) were coupled together in an electrophilic aromatic condensation reaction (Figure 8). Equal amounts of vanillyl alcohol were added over five days to excess cardanol and Dowex DR 2030 (10.8 g, 10 wt% of total reactant mass) with continuous mixing at 64 °C. The reaction was left for an additional 24 hours after the final addition of vanillyl alcohol. The mixture was then cooled to room temperature and dissolved in DCM. The solution was filtered to remove the catalyst and then concentrated via reduced pressure. Purification by

flash chromatography (hexanes/ethyl acetate, 70:30) was utilized to separate excess cardanol and unreacted vanillyl alcohol from the mixed isomer bisphenol product, VAC (pale yellow liquid; viscosity: 989 ± 59 cP; 70% yield).

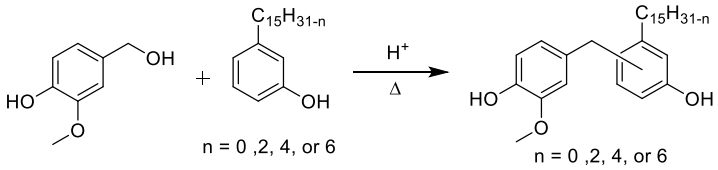

Figure 8. Electrophilic condensation of vanillyl alcohol and cardanol to produce vanillyl alcohol cardanol (VAC).

Using a Parr 3910 Hydrogenation Apparatus, VAC (15 g, 0.04 mol) was combined with ethanol (70 mL) and Pd/C (0.12 g) in a 500 mL reaction bottle (Figure 9). After the desired pressure drop (5.5 psi) occurred, the solution was filtered to remove the catalyst then concentrated under reduced pressure to yield VAHC (white solid; melting point: 50-55 °C; yield 99%).

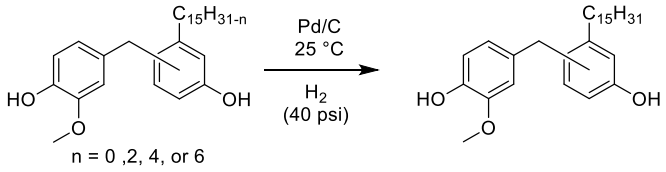

Figure 9. Hydrogenation of VAC to produce vanillyl alcohol hydrogenated cardanol (VAHC).

3.2.3 Synthesis of VAC and VAHC dimethacrylate. The bisphenol (30 g, 0.07 mol), DCM (60 mL), and TEA (19 mL) were added to a three-neck round-bottom flask in an ice bath equipped with a constant pressure dropping funnel and inlet for dry argon gas.

With constant stirring, DCM (125 mL) and methacryloyl chloride (20.9 g, 0.2 mol) solution was added dropwise in an argon atmosphere (Figure 10 & Figure 11). The reaction mixture was slowly warmed to room temperature for 24 hours, dissolved in DCM, and then washed once with DI water in a separatory funnel. Solvent was removed under reduced pressure after the organic phase was isolated. Flash chromatography was used to purify the product (clear liquid; yield 80%) from any unreacted methacryloyl chloride. Similar methods described above were used for the preparation of BGDM (white solid; yield 76%).

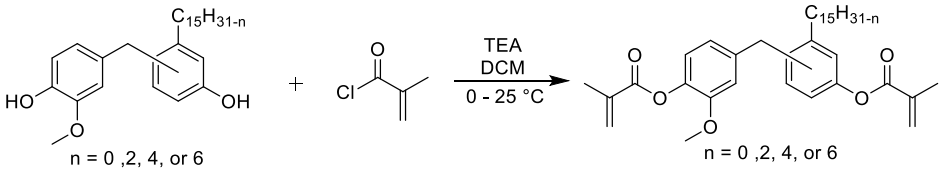

Figure 10. Methacrylation of VAC to produce vanillyl alcohol cardanol dimethacrylate (VACDM).

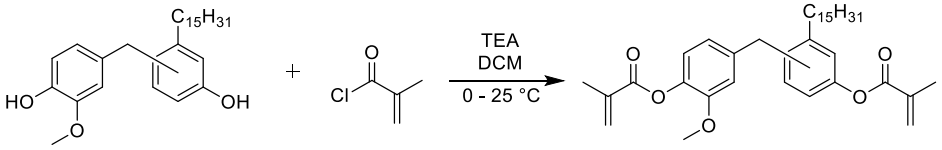

Figure 11. Methacrylation of VAHC to produce vanillyl alcohol hydrogenated cardanol dimethacrylate (VAHCDM).

3.2.4 Characterization of monomers and resins. All molecules synthesized in this work were characterized by ^{1}H-NMR (400.15 MHz, 32 scans at 298 K) using a Varian 400 MHz FT-NMR spectrometer. Relevant ^{1}H-NMR spectra are provided in Appendix B.

The melting points of VAHC and BGDM was measured in triplicate using a TA Instruments Discovery DSC 2500. Approximately 10 mg of sample was placed into a Tzero pan with a Tzero Hermetic lid and heated from 0 °C to 100 °C at a rate of 10 °C min^{-1} in a N_2 atmosphere. The melting point of VAHC was determined to be 50-55 °C and the melting point of BGDM was determined to be 130-132 °C. All other synthesized bisphenols and VE monomers were liquids at room temperature.

The viscosities of the uncured resins and the synthesized monomers were obtained using a TA Instruments Discovery Hybrid Rheometer 2 using a 40 mm parallel plate geometry and a Peltier plate kept at a constant 25 °C. The shear rate was increased logarithmically from 1 s^{-1} to 1000 s^{-1}, and then decreased from 1000 s^{-1} to 1 s^{-1} in a logarithmic progression, collecting 3 measurements per decade to indicate the presence of any non-Newtonian behavior and thixotropic properties [44, 78].

3.2.5 Resin cure. VACDM, VAHCDM, BGDM, VE828, and BPADM were individually blended with 35 wt% styrene, one of the most commonly utilized reactive diluents for VERs, and well mixed by hand. Qualitatively, the resins were clear and homogenous with the exception of resin systems containing BGDM, which was found to be insoluble in styrene at elevated temperatures. Residual BPADM solids were heated at 40 – 50 °C until all solids were dissolved in styrene. All resins were free radically polymerized using Trigonox® 239, 1.5 wt% of the total resin mass, and degassed for approximately 5 minutes to remove any trapped air. Resins were poured into silicon rubber molds of uniform dimensions and cured at 90 °C for 4 hours and post-cured at 160 °C for 2 hours in an argon atmosphere. The cured samples were allowed to cool to room

temperature and then removed from the molds. ^{1}H-NMR spectra are provided in Appendix B.

3.2.6 Extent of cure. To determine the extents of cure of the polymers, a Thermo Scientific Nicolet iS50 FTIR operating in transmission mode was used. The set-up of the FTIR cell is explained elsewhere [79]. A drop of the uncured resin was sandwiched between two 13 mm diameter, 0.6 mm thick KBr disks (International Crystal Labs). The salt plate assembly was placed in a cell holder, which can be controlled to within ± 0.1 °C of the set-point. When the cell holder equilibrated to the reaction temperature, the salt plate assembly was placed in the holder, and the first FTIR scan was taken. All resin mixtures were cured at 90 °C until vitrification and then postcured at 160 °C until ultimate cure was achieved. An FTIR spectrum comprised of 16 scans with 4 cm^{-1} resolution was taken every 60 seconds during the cure reaction.

The conversion, α, of the methacrylates or styrene was calculated by measuring the area of the peak relative to an internal standard (i.e., a group that is not affected by the reaction) (Equation 13):

$$\alpha_{meth/sty} = 1 - \left(\frac{ABS(t)_{\frac{meth}{sty}}}{ABS(t=0)_{\frac{meth}{sty}}} \right) \left(\frac{ABS(t=0)_{std}}{ABS(t)_{std}} \right) \qquad \textit{Eq. 13}$$

The crosslinkers all contained methacrylate groups that appear at 942 cm^{-1}. The methacrylate conversion was calculated by measuring the area of this peak as a function of time, *t*. Changes in thickness were accounted for via the area of an internal standard as a function of time (i.e. the ester stretch at 1740 cm^{-1}) [79, 80]. The vinyl ester aromatic C-H stretch at 828 cm^{-1} [79, 80] was also used as an internal standard in analysis of the vinyl ester resin, but the results were not significantly different. The styrene conversion

was calculated similarly by measuring the styrene carbon-carbon double bond peak area (910 cm^{-1}) as a function of time relative to the styrene aromatic C-H stretch (700 cm^{-1}) internal standard peak area [79, 80]. The overall conversion was calculated as a sum of the relative molar ratios of styrene vinyl to methacrylate peaks.

Due to overlapping of cardanol unsaturations with methacrylate functionalities in mid-IR, a Thermo Scientific Nicolet iS50 FTIR was used to obtain near-infrared (near-IR) spectra of both VACDM 35 wt% Styrene and VAHCDM 35 wt% Styrene uncured and cured resins to elucidate the extent of cure of the VACDM 35 wt% Styrene system relative to the VAHCDM 35 wt% Styrene system. Uncured resins were contained in a glass reservoir with a thickness of 3 mm and 32 cumulative scans were acquired with a resolution of 2 cm^{-1} in absorbance mode. The cured resins typically had a thickness of 3-4 mm and their respective near-IR spectra were acquired in the same method as the uncured resins. By measuring the peak absorbance intensities of the styrenic vinyl (~ 6135 cm^{-1}) and methacrylate vinyl (~ 6165 cm^{-1}) bonds (i.e. polymerizable groups) before and after curing, Equation 14 was used to determine the overall extent of cure based on the conversion of polymerizable groups [43, 78]. The peak at ~ 5900 cm^{-1} was chosen as the internal standard because this peak was not affected by the polymerization.

$$X(Polymerizable\ Groups) = \frac{\left(\frac{ABS_{6135-6165cm^{-1}}}{ABS_{5900cm^{-1}}}\right)_{unreacted} - \left(\frac{ABS_{6135-6165cm^{-1}}}{ABS_{5900cm^{-1}}}\right)_{reacted}}{\left(\frac{ABS_{6135-6165cm^{-1}}}{ABS_{5900cm^{-1}}}\right)_{unreacted}} \qquad Eq.\ 14$$

3.2.7 Polymer properties. The thermogravimetric properties of the cured resins were measured using a TA Instruments Discovery Thermogravimetric Analyzer 550 (TGA). Approximately 10 mg of cured resin was placed on a platinum pan and heated to 700 °C at a rate of 10 °C min^{-1} in a N_2 atmosphere (40 mL min^{-1} balance gas flow rate

and 25 mL min^{-1} sample gas flow rate). This process was repeated in an oxidative (air) environment. Thermogravimetric properties including initial decomposition temperature (IDT), temperature at 50% weight loss ($T_{50\%}$), temperature at maximum decomposition rate (T_{max}), and char content were reported. TGA was repeated in N_2 and oxidative atmospheres for replicates to evaluate consistency in data.

The viscoelastic properties of the cured VERs were measured using a TA Instruments Q800 DMA. Each sample was prepared with appropriate dimensions (35 x 12 x 2.5 mm^3) and tested using a single cantilever geometry in accordance with McAninch et al [32]. The tests were performed at a frequency of 1.0 Hz, oscillatory deflection amplitude of 7.5 μm, and a Poisson's ratio of 0.35. The heating ramp rate was 2 °C min^{-1} from -50.0 °C to 250 °C. The T_g of each sample was measured as the peak of the tan δ curve. Polymer densities were measured at room temperature according to Archimedes' principle [29].

Fracture toughness was tested to compare the synthesized, bio-based polymers and the commercially available cured VERs. Three-point single edge notched bend (SENB) samples of all cured resins were prepared in accordance with ASTM D5045 at room temperature. Samples were prepared to be 44 x 10 x 4 mm^3 to ensure plane-strain. Using a diamond saw, samples were notched and then tapped using a single edged razor blade in order to "instantly propagate" a crack. Upon cracking the samples, the tip of the crack was marked with ink. Capillary action drew the ink down and the initial location of the crack could be determined after fracture [35]. Samples were then tested on an Instron 4442 with a 500 N load cell and a 3-point bend flexure fixture at a cross head speed of 10 mm min^{-1}. The plane-strain fracture toughness, K_{1C}, and the critical strain energy release

rate, G_{1C}, were determined upon fracture [34]. Five replicates of each cured VER system were prepared and tested using this procedure.

3.3 Results and Discussion

3.3.1 Resin characterization. The synthesized and commercially available cured and uncured resins were analyzed and compared. VE828 was used as a comparable industry standard along with BPADM. Due to structural similarities, BPADM is a close comparison to the synthesized monomers. When combined with a reactive diluent (styrene) at room temperature, the VE828 uncured resin was a clear, green liquid due to the catalysts used in the synthesis of VE828, while all the bio-based uncured resins were clear, yellow liquids. BPADM did not dissolve in the reactive diluent at room temperature. After heating to dissolve solids, the BPADM uncured resin was a clear liquid similar to the bio-based resins; however ,BPADM does not remain soluble in styrene when cooled to room temperature. BGDM was found to be insoluble in styrene at room and elevated temperatures; therefore, the evaluation of thermal and mechanical properties of cured BGDM with 35 wt% styrene was not carried out further in this study. The bio-based (VACDM & VAHCDM) and BPADM cured resins were transparent with a slight yellow color, while the VE828 cured resin had a green hue.

The viscosities of the synthesized monomers and the uncured resins were measured using a rheometer at a constant temperature of 25 °C. All synthesized monomers and blends were run with the exception of those containing BPADM and BGDM. BPADM is insoluble in styrene at 25 °C; however, BPADM is soluble in styrene at elevated temperatures, yet crashes out of solution when cooled back to 25 °C. BGDM was insoluble in styrene at 25 °C and at elevated temperatures. Newtonian nature was

observed for all synthesized monomers and uncured resins. The viscosities of each monomer and resin were obtained by averaging three steady-state viscosity data points at multiple shear rates for each sample. Three replicates were performed for each sample, and the resulting viscosity data are found in Table 1. The viscosities of the styrene monomer and VE828 are shown for comparison [5].

Table 1

Viscosity of monomers and resins at 25 °C

Sample	Viscosity at 25 °C (cP)
Styrene [5]	0.7
VE828 [78]	6×10^7
BPADM	-
VACDM	567 ± 51
VAHCDM	1290 ± 84
VE828 35 wt% Styrene	134 ± 24
BPADM 35 wt% Styrene	-
VACDM 35 wt% Styrene	22 ± 6
VAHCDM 35 wt% Styrene	22 ± 6

To be processed using liquid molding techniques, a viscosity of 50 cP to 1000 cP at or slightly above 25 °C is recommended; however, resins that fall outside of the desired range are used occasionally [81, 82]. When comparing the monomer viscosities, pure VE828 has the highest viscosity of 6×10^7 cP at 25 °C. Therefore, VE828 has limited use as a resin without the use of a low viscosity reactive diluent [5]. VACDM had a viscosity of 567 cP, significantly less than the viscosity of VAHCDM at 1290 cP. Both VACDM and VAHCDM are liquids whereas BPADM and BGDM are solids at room temperature. Therefore, the aliphatic substituents of both VACDM and VAHCDM as

well as a likely contribution from molecular asymmetry provided benefits in terms of monomer and resin processing, especially when compared to the symmetric BGDM which was unable to be processed in the same manner as all other dimethacrylates used in this work. The unsaturated, alkyl chain of VACDM forms kinks due to the cis conformation of the carbon-carbon double bonds, decreasing the intermolecular interactions in the uncured resin. In contrast, as the unsaturation level decreases, the intermolecular interactions increase. The hydrogenated bonds present in the C15 chain increase the intermolecular interactions present in VAHCDM as compared to VACDM, resulting in the higher viscosity (Table 1) [81].

The uncured resins followed a similar trend as the synthesized monomers with VE828 35 wt% Styrene had a higher viscosity (134 cP) than VACDM 35 wt% Styrene and VAHCDM 35 wt% Styrene (each 22 cP). The hydrogenation of the C15 chain did not impart significant viscosity changes between the VACDM 35 wt% Styrene and VAHCDM 35 wt% Styrene uncured resins at 25 °C. The addition of styrene increases the amount of space between the chains (i.e., acts as a solvent), allowing for lower intermolecular interactions among the crosslinkers and subsequently lower viscosities than those of the synthesized monomers (crosslinkers) by themselves [81].

Compared to the high viscosity of VE828, the synthesized monomers and uncured resins fall within or close to the desired processing range for resin transfer molding of 50 cP to 1000 cP at or slightly above 25 °C [81, 82]. Both VACDM and VAHCDM fall directly within the range, and VACDM 35 wt% Styrene and VAHCDM 35 wt% Styrene systems fall 28 cP below the range. The viscosity range is used as a guideline; however, resins that fall slightly outside of the range can be used in industry as it is easy to increase

the viscosity of resins through use of less reactive diluent (i.e., styrene) or addition of thickening agents like fumed silica. Thus, all of the bio-based synthesized monomers and uncured resins are potentially processable by industry standards [83].

3.3.2 Extent of cure. Figure 12 shows the mid-IR spectra within the relevant wavenumber region as a function of time for VAHCDM 35 wt% Styrene. The full width spectra are available in Appendix B. The methacrylate and styrene peaks are shown to decrease in peak intensity as a function of time relative to that of the ester and styrene internal standards. This method allows for calculation of the individual conversions of the methacrylates and styrene groups according to Equation 13, which is much more difficult using near-IR as the peaks are too close to effectively resolve. Additionally, DSC does not allow for the measurement of the individual component extents of cure and requires the use of a ramp to high temperatures where it is assumed 100% extent of cure occurs, but this is not necessarily what occurs in every resin. A similar analysis of the mid-IR results was possible for the samples containing BPADM and VE828 but was not possible with VACDM due to concurrent unsaturation peaks in the region of 900-950 cm^{-1}.

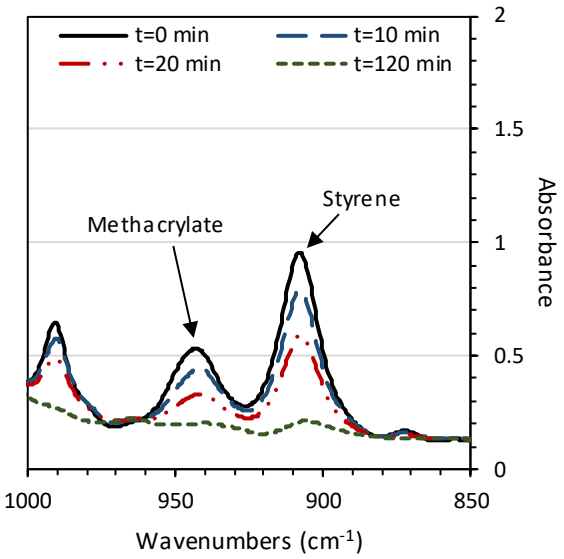

Figure 12. The styrene vinyl and methacrylate region of interest of the mid-IR spectra of VAHCDM 35 wt% Styrene as a function of cure time at 90 °C.

Near-IR spectral analysis and Equation 14 were used to obtain the extent of cure of the VACDM 35 wt% Styrene and VAHCDM 35 wt% Styrene resins. Representative spectra for this study are shown in Figure 13, which shows VACDM 35 wt% Styrene resin both cured and uncured. The overall extents of cure determined using Equation 14 for VACDM and VAHCM blended with 35 wt% Styrene are shown in Table 2. The methacrylate and styrene vinyl groups, at 6165 cm^{-1} and 6135 cm^{-1}, respectively, participate in the free radical polymerization to form the linkages between the reactive diluent and VE monomers in the cured resin.

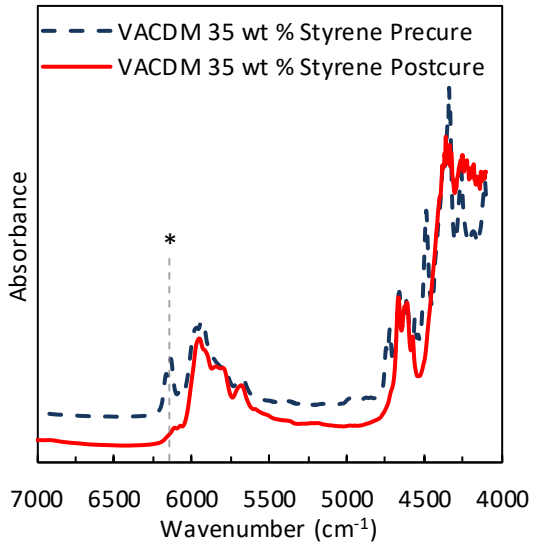

Figure 13. Near-IR spectra of VACDM 35 wt% Styrene resin and cured resin. Methacrylate (*) absorption is indicated. Spectra are offset vertically for clarity.

Table 2 lists the methacrylate, styrene, and overall conversions of the four resins studied. Importantly, the mid-IR and near-IR results for VAHCDM 35 wt% Styrene are within experimental error of each other (± 2%), confirming the validity of these results. The near-IR analysis indicates the final extent of cure was very similar for both VACDM and VAHCDM systems, with VACDM potentially having a slightly lower extent of cure due to chain transfer to the unsaturation sites. Given the similarity of VACDM and VAHCDM molecular structures, we can assume that VACDM has similar methacrylate and styrene conversions relative to VAHCDM, although we cannot say this for sure. For VAHCDM 35 wt% Styrene, the methacrylate and styrene extents of cure were approximately 90% after cure at 90 °C (provided in Appendix B), and 91% after postcure at 160 °C, whereas VE828 and BPADM samples had significantly more conversion during the postcure steps. The methacrylate conversions were fairly low for the VE828 and BPADM after cure (48% and 56%, respectively) while the styrene conversion for

both was very similar to that what was measured for the VAHCDM resin. After postcure, the methacrylate conversions for VE828 and BPADM rise to 62% and 60%, respectively, while the styrene conversion rises to 96% and 99%, respectively. Interestingly, despite the higher extents of cure of VAHCDM relative to VE828 and BPADM, VAHCDM has a lower conversion of styrene, likely due to the much higher conversion of the methacrylates on VAHCDM which crosslinks the resin, thus limits diffusion rates and prevent near complete cure of the styrene. In all, the overall extent of cure increased as the flexibility of the crosslinker molecules increased (VAHCDM & VACDM are the most flexible, while BPADM is the least flexible).

Table 2

Extent of cure of resins via mid-IR and near-IR spectroscopy after postcure based on styrenic vinyl and methacrylate vinyl bonds, taken at room temperature. (Denotes near-IR results)*

System	Methacrylate Conversion (%)	Styrene Conversion (%)	Overall Extent of Cure (%)
VE828 35 wt% Styrene	62	96	82
BPADM 35 wt% Styrene	60	99	79
VACDM 35 wt% Styrene	-	-	90*
VAHCDM 35 wt% Styrene	91	91	91 (92*)

3.3.3 Polymer properties. Thermogravimetric properties of the cured VERs were analyzed. Figure 14 shows the weight percentages and the derivative of the weight percentages for all cured resins. The IDT, $T_{50\%}$, T_{max}, and char content values are shown in Table 3. BPADM 35 wt% Styrene exhibited the lowest IDT (336 °C), $T_{50\%}$ (403 °C), and T_{max} (409 °C) which correlates to the low extent of cure of the system. VE828 35

wt% Styrene showed slightly improved thermogravimetric properties, due to the higher extent of cure of the system, with IDT = 344 °C, $T_{50\%}$ = 403 °C, and T_{max} = 401 °C. The cured resins containing VACDM and VAHCDM exhibited directly comparable thermal resistances to the VE828 cured resin and higher thermal resistances compared the BPADM cured resin. Thermal stability of the VACDM and VAHCDM cured resins relative to structurally similar BPADM were mostly affected by the differences in extent of cure; however, the presence of the alkyl substituent, which adds increased carbon content relative to the methoxy substituent, could play a role in the increased thermal stability of these systems. Methoxy substituents are known to decrease the thermal stability of systems due to electron donating to the aromatic ring, however the presence of the alkyl chain likely overshadowed this effect, as the presence of cardanol units in thermosetting systems have been shown to impart enhanced thermal stability [84, 85]. Additionally, the unsaturation points on the C15 chain of VAC require more energy to degrade, since alkenes are shown to have higher thermal stabilities than alkanes, which could cause the slight differences in IDT between VACDM and VAHCDM cured resins [86, 87].

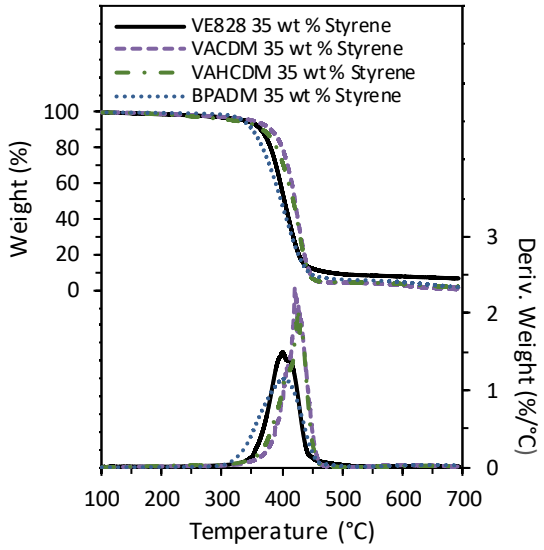

Figure 14. TGA thermograms and their respective 1st derivatives of VERs cured with 35 wt% Styrene in N_2.

Table 3

Thermogravimetric properties of the cured VERs in N_2

System	IDT (°C)	$T_{50\%}$ (°C)	T_{max} (°C)	Char Content (%)
VE828 35 wt% Styrene	344 ± 6	403 ± 3	401 ± 3	1.0 ± 0.4
BPADM 35 wt% Styrene	336 ± 4	403 ± 5	409 ± 6	2.3 ± 0.6
VACDM 35 wt% Styrene	354 ± 1	420 ± 1	424 ± 3	1.5 ± 1.1
VAHCDM 35 wt% Styrene	347 ± 3	419 ± 1	429 ± 3	1.3 ± 0.5

Similar trends were observed when the resins were tested in an oxidative environment (provided in Appendix B). The only notable difference was a second degradation in all the cured resins, which was attributed to combustion of the char from the first step due to the oxidative environment and high temperature [88].

The thermomechanical properties of the cured VERs were measured to quantify and compare the viscoelastic behavior. Figure 15 shows the thermograms of storage moduli (E') and loss moduli (E''). The storage modulus represents the elastic response of

the polymer by measuring the amount of energy stored during the deformation process, while the loss modulus measures the energy dissipated as heat [89]. The BPADM 35 wt% Styrene showed the highest E' value (3.0 GPa), while the VAHCDM 35 wt% Styrene and VACDM 35 wt% Styrene showed nearly identical E' values (1.7 GPa), lower than both BPADM 35 wt% Styrene and VE828 35 wt% Styrene (2.8 GPa), all at 25 °C. The density values reported in Table 4 follow the same trend as the storage moduli.

Density and storage modulus properties are related to the stacking of the polymer chains [90]. The C15 alkyl chains present in VACDM 35 wt% Styrene and VAHCDM 35 wt% Styrene inhibit close packing of the polymer chains resulting in lower densities and lower storage moduli. Comparing VACDM 35 wt% Styrene and VAHCDM 35 wt% Styrene, the density values and E' values were similar, indicating the difference in quantity of unsaturation points in the alkyl chain had minimal effect on the polymer network packing. VE828 35 wt% Styrene and BPADM 35 wt% Styrene blends had tighter packing due to the lack of aliphatic substituents [90].

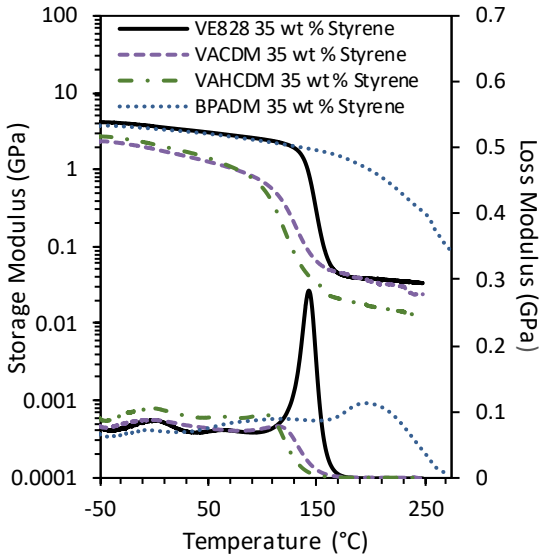

Figure 15. DMA thermograms of *E′* and *E″* of the VERs cured with 35 wt% Styrene.

Table 4

Thermomechanical properties of VERs cured with 35 wt% Styrene

System	E′ @ 25 °C GPa	Peak of tan δ (°C)	ρ @ 25 °C (g cm^{-3})
VE828 35 wt% Styrene	2.8 ± 0.3	152.9 ± 2.0	1.157 ± 0.005
BPADM 35 wt% Styrene	3.0 ± 0.1	234.4 ± 1.6	1.135 ± 0.001
VACDM 35 wt% Styrene	1.7 ± 0.2	136.9 ± 1.9	1.083 ± 0.003
VAHCDM 35 wt% Styrene	1.7 ± 0.1	127.7 ± 2.0	1.070 ± 0.001

Tan δ, shown in Figure 16, is a measure of the ratio of the loss modulus to storage modulus (*E″*/*E′*). The width of the tan δ peak represents homogeneity in the polymer network [91, 92]. The wider peak of BPADM 35 wt% Styrene indicated a more heterogeneous network than the VE828 35 wt% Styrene and bio-based cured VERs. Following the Twinkling Fractal Theory, heterogeneity increases within the network when there is a wide distribution of solid fractal clusters that shift to the liquid phase

upon heating [91, 93]. Additionally, the extent of polymer chain segmental mobility is indicated by the maximum value of the tan δ curve [92]. VACDM 35 wt% Styrene and VAHCDM 35 wt% Styrene cured resins had lower polymer chain segmental mobilities relative to the VE828 35 wt% Styrene cured resin, yet higher than BPADM 35 wt% Styrene, which may be a result of crosslink densities of the cured bio-based resins being between that of the two petroleum-derived systems.

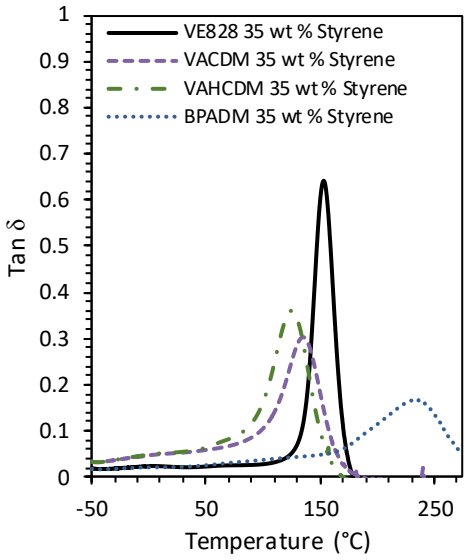

Figure 16. Tan δ thermograms of the VERs cured with 35 wt% Styrene.

The peak of the tan δ, shown in Table 4, indicates the value of T_g. Typically, the peak of the loss modulus is a more conservative value for T_g, however, most of the tested polymers do not exhibit a clear peak of the loss modulus (Figure 15). A clear peak of the loss modulus does not form due to the continual β-relaxation on the long, alkyl chain [2]. The T_g is reported using the peak of the tan δ when a clear peak is not formed for E'' [44]. The trend of the T_gs follows that of the storage moduli, BPADM 35 wt% Styrene

possesses the highest T_g (234.4 °C), then VE828 35 wt% Styrene (152.9 °C). VACDM 35 wt% Styrene and VAHCDM 35 wt% Styrene exhibit lower T_gs, at 136.9 °C and 127.7 °C, respectively.

T_g is closely related to the chemical structure of the units and packing of the polymer chains. A longer, flexible backbone in the repeating unit will decrease the T_g as shown by the comparison between VE828 35 wt% Styrene and BPADM 35 wt% Styrene [94] . With no difference in substituent groups, the drop of T_g between VE828 35 wt% Styrene and BPADM 35 wt% Styrene was attributed to the increased rotational freedom in the backbone of the VE828 35 wt% Styrene polymer network. BPADM, VACDM, and VAHCDM are similar in structure, in that the backbone is the same length, while the substituent groups on the aromatic rings vary. Therefore, the drop in T_g was attributed to the added substituent groups. Additional free volume resulting from the alkyl chain substituent group, as well as the methoxy moiety, likely increased the ability for rotational motion, accounting for the drop in T_g between VE828 and BPADM and the bio based monomers [94].

The difference in T_g between VACDM 35 wt% Styrene and VAHCDM 35 wt% Styrene was due to the difference in unsaturation points along the alkyl chain, given that the VAHCDM sample cured to the same, if not greater extent. The fully saturated alkyl chains in VAHCDM had a lower T_g than the chains with unsaturation points in VACDM. Previous studies of fatty acids demonstrate that unsaturation sites interact with free radical polymerizations due to transfer of radicals and can potentially polymerize to a small degree; therefore, the increase in T_g for VACDM 35 wt% Styrene was accredited to chain entanglement and interaction of the unsaturation sites [5, 95]. However, both

VACDM 35 wt% Styrene and VAHCDM 35 wt% Styrene had T_gs above the industrial standard for high performance thermosetting resins of 120 °C [78].

To determine the effects of the structural differences between the monomers on the mechanical properties of the polymer, fracture toughness testing was conducted. The plane-strain fracture toughness, $K_{1C,}$ and the critical strain energy release rate, G_{1C}, were obtained and are shown in Table 5. All samples showed brittle behavior; the load and deformation increase linearly until the point of fracture as shown in Figure 17 [96]. VE828 35 wt% Styrene displayed the highest K_{1C} and G_{1C} values of 0.14 MPa $m^{1/2}$ and 221 J m^{-2}, respectively, indicating that VE828 35 wt% Styrene was the toughest of the polymers tested. The most brittle sample was BPADM 35 wt% Styrene with a K_{1C} of 0.03 MPa $m^{1/2}$ and G_{1C} of 24 J m^{-2}. The VE828 sample was more tough than the BPADM sample because it has a lower crosslink density and increased aliphatic content that generally provides toughening [97]. The K_{1C} and the G_{1C} values of VAHCDM 35 wt% Styrene were 0.09 MPa $m^{1/2}$ and 67 J m^{-2}, respectively, whereas the K_{1C} and the G_{1C} values of VACDM 35 wt% Styrene were 0.08 MPa $m^{1/2}$ and 66 J m^{-2}, respectively. VAHCDM 35 wt% Styrene did not show significant improvements to the toughness of the polymer compared to that of VACDM 35 wt% Styrene. Therefore, for the desired application of high-performance thermosetting resins, there were no significant improvements between the saturation and unsaturation points in the long, alkyl chain. VACDM 35 wt% Styrene and VAHCDM 35 wt% Styrene were more tough than BPADM 35 wt% Styrene due to the increased aliphatic nature, where the cardanol alkyl chain provides increased flexibility as demonstrated through its reduced T_g, modulus, and increased toughness. Despite the VACDM and VAHCDM having more aliphatic

character than VE828, the cardanol alkyl chains are not along the backbone of the polymer and thus provide a reduced matrix toughening effect.

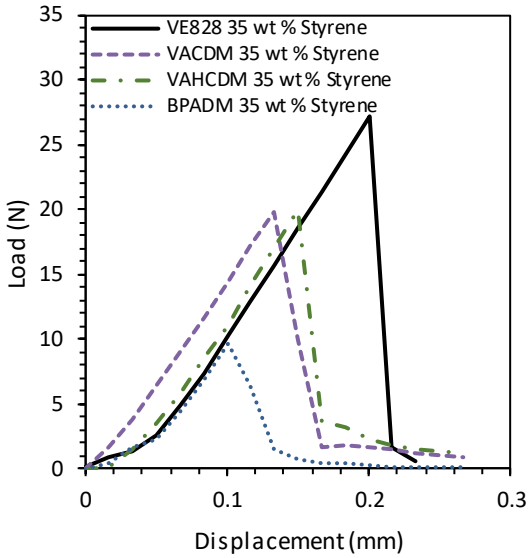

Figure 17. Load displacement curves for VERs cured with 35 wt% Styrene.

Table 5

Fracture toughness K_{1c} and G_{1c} values of VERs cured with 35 wt% Styrene

System	K_{1c} MPa $m^{1/2}$	G_{1c} J m^{-2}
VE828 35 wt% Styrene	0.14 ± 0.04	221 ± 22
BPADM 35 wt% Styrene	0.03 ± 0.01	24 ± 6
VACDM 35 wt% Styrene	0.08 ± 0.01	66 ± 1
VAHCDM 35 wt% Styrene	0.09 ± 0.04	67 ± 13

3.4 Conclusions

Vanillyl alcohol and cardanol were successfully coupled to create an asymmetric bisphenol, VAC. The C15 side chain of VAC was hydrogenated to create VAHC, and both VAC and VAHC were methacrylated to prepare VACDM and VAHCDM for

incorporation into thermosetting VERs and compared to resins containing a commercial VER (VE828), structurally similar BPA dimethacrylate (BPADM), and structurally similar bisguaiacol dimethacrylate (BGDM), which was prepared from a bio-based bisphenol, bisguaiacol (BG). The collected results suggest that both VACDM and VAHCDM are suitable for use in VERs. VACDM and VAHDCM exhibited lower viscosities relative to VE828 and are processable liquids at room temperature due to the structural asymmetry and aromatic substituents. Relative to BPADM and BGDM, which are both solids at room temperature, VACDM and VAHCDM offer significant improvements in processability, especially when compared to BGDM which was unable to be solubilized in styrene as the reactive diluent and therefore unable to be cured and compared in this study. Cured resins with VACDM and VAHCDM exhibit comparable thermal resistances, lower densities, and lower T_gs relative to both VE828- and BPADM-based resins cured with 35 wt% styrene; however, VACDM and VAHCDM show improved toughness over BPADM due to the C15 side chain contributing to matrix toughening. Although the T_gs were lower for the bio-based bisphenols compared to the BPA based bisphenols, the T_gs were within range for high performance VER applications, exceeding 120 °C. The collected results associated with VAHC did not show a significant improvement in polymer properties compared to those of VAC. Therefore, the saturation and unsaturation levels did not improve the polymer properties for this application, however both VAC and VAHC are shown to be promising building blocks for thermoset applications.

Chapter 4

Molecularly Hybrid, Ester-Spaced, Aromatic Diglycidyl Ethers From Bio-Based Feedstocks

4.1 Introduction

While Chapter 3 focused on the development of molecularly hybrid, asymmetric bisphenolic analogues, Chapter 4 continues the molecularly hybrid concept from a slightly different approach. Rather than having the alkyl functionality as a pendant group as shown in Chapter 3, this chapter aims to impart alkyl functionality into the core of the bisphenolic structure. As mentioned and as demonstrated in Chapter 3, vanillyl alcohol (VA), the reduced form of vanillin and lignin-derivative, can be a platform chemical for the production of bisphenolic analogues as the hydroxymethyl group provides the necessary functionality for phenolic coupling [36, 61, 71]. Interestingly, VA bears both aromatic and aliphatic hydroxyls, in which the aromatic hydroxyl is more acidic, thus more reactive towards epichlorohydrin [61, 98]. Studies preparing the diglycidyl ether of VA have reported moderate to low yields of the monoglycidyl ether of VA (MGEVA) as a byproduct due to this difference in reactivity, and the utilization of MGEVA as a building block for other chemical modifications has not been explored [61, 98]. The synthesis of MGEVA was adapted from literature [98], whereby MGEVA was produced as the major product in which the aliphatic hydroxyl was unreacted. The monoglycidyl ether of VA (see ^{1}H-NMR spectrum in Appendix D) confirms that the aliphatic methylene is adjacent to an unreacted hydroxyl [61].

To incorporate aliphatic character into the core of the monomer structure, MGEVA was reacted via transesterification with three renewably sourced dimethyl

esters: dimethyl adipate, dimethyl dodecanedioate, and dimethyl octadecanedioate to prepare DGEVBA-Ad, DGEBVA-C12, and DGEBVA-C18, respectively (Figure 18). Furthermore, to achieve a sustainable process and preserve the glycidyl functionality during transesterification, an enzymatic catalyst, *Candida antarctica* Lipase B (CALB), was utilized [99-101]. The use of CALB for polycondensations and transesterifications is well documented and avoids the use of metal-based catalysts, which typically require high temperatures, and, in this case, releases a byproduct of methanol, a green solvent [102-104]. DGEVBA-Ad, DGEBVA-C12, and DGEBVA-C18 were cured with stoichiometric equivalents of diethyl toluene diamine (Epikure W) and the effect of the aliphatic chain length on the thermomechanical properties of the cured polymers was evaluated.

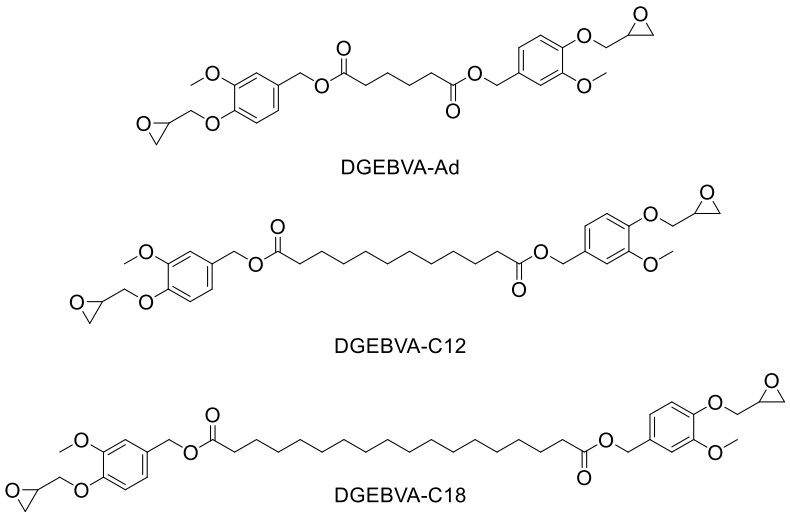

Figure 18. Ester-spaced, aromatic diglycidyl ethers prepared.

4.2 Experimental Methods & Procedures

4.2.1 Materials. Epichlorohydrin (99%), vanillyl alcohol (4-hydroxy-3-methoxybenzyl alcohol, 99%), dimethyl adipate (99%), dimethyl dodecanedioate (C12ME, 98%), dichloromethane (DCM, 99.6%), and chloroform-d_3 ($CDCl_3$, 99.8 atom % d) were purchased from Acros Organics. Ethyl acetate (99.9%) and hexanes (99.9%) were purchased from Fisher Scientific. Benzyltriethylammonium chloride (TEBAC, 99%) and *Candida antarctica* lipase B (CALB, Novozyme 435) were purchased from Sigma Aldrich. Compressed nitrogen (N_2, 99.998%), and compressed argon (Ar, 99.999%) were purchased from Airgas. Dimethyl octadecanedioate (C18ME, 99%) was provided by Elevance Renewable Sciences. Epikure Curing Agent W (Diethyl toluene diamine) was obtained from Hexion. Sodium hydroxide was purchased from VWR. All chemicals mentioned above were used without further purification.

4.2.2 Synthesis of ester-spaced, aromatic diglycidyl ethers. Vanillyl alcohol (5 g), epichlorohydrin (25.43 mL), and TEBAC (0.74 g) were added to a three-neck round bottom flask equipped with a mechanical mixer. The reaction mixture was heated to 80 °C for 1 h. After 1 h, the reaction was cooled to room temperature, and a mixture of 5 M $NaOH_{(aq)}$ (25.9 mL) and TEBAC (0.74 g) was added dropwise. The reaction was worked up and washed with a solution of equal parts de-ionized (DI) water and ethyl acetate. Flash chromatography (hexanes/ethyl acetate) was used to purify the intermediate product, mono-glycidyl ether of vanillyl alcohol (MGEVA, 55% yield, white powder).MGEVA (4 g) and dimethyl octadecanedioate (C18ME, 3.1 g) were charged to a round bottom flask equipped with a magnetic stir bar and an inlet for dry argon gas. The flask was continuously purged with argon and the reactants were melted together at 75

°C. After 2 h, 0.7 g of *Candida antarctica* lipase B (CALB, Novozyme 435) was added to the flask under a continuous argon purge and allowed to react at room temperature for 2 h. Over the course of the next 6 hours, the flask was slowly put under complete vacuum and heated to 95 °C to facilitate the removal of methanol (the byproduct of the reaction) thus driving the reaction towards completion. The flask was left under complete vacuum at 95 °C for 3 d, after which the reaction mixture was cooled to room temperature and dissolved in dichloromethane. The solution was filtered to remove the CALB, washed with 2.5 M $NaOH_{(aq)}$, and concentrated under reduced pressure to yield diglycidyl ether of bis-vanillyl alcohol C18 (DGEBVA-C18; white solid; 71% yield; T_m = 93 °C). A similar procedure was used to prepare diglycidyl ether of bis-vanillyl alcohol adipate (DGEBVA-Ad; white solid; 79% yield; T_m = 98 °C) and diglycidyl ether of bis-vanillyl alcohol C12 (DGEBVA-C12; white solid; 74% yield; T_m = 112 °C). The general reaction scheme is provided in Figure 19, whereby R equals 4, 10, and 16 -CH_2- repeating units for the adipate, C12, and C18, respectively.

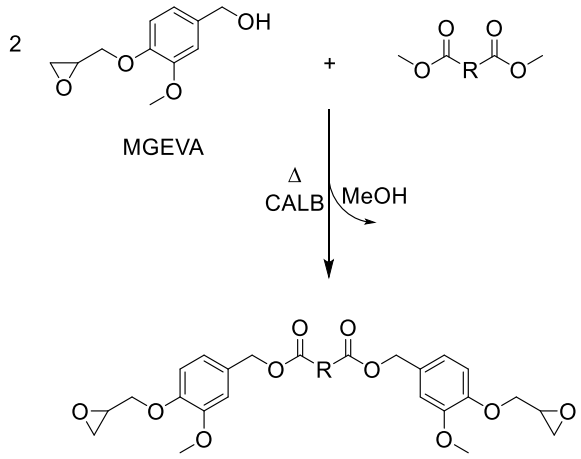

Figure 19. Synthetic route to prepare ester-spaced, aromatic diglycidyl ethers.

4.2.3 Monomer characterization. All molecules synthesized in this work were characterized by ^{1}H-NMR (400.15 MHz, 32 scans at 298 K) using a Varian 400 MHz FT-NMR spectrometer. Relevant ^{1}H-NMR spectra are provided in Appendix C.

The melting points of the monomers were measured in triplicate using a TA Instruments Discovery DSC 2500. Approximately 10 mg of sample was placed into a Tzero pan with a Tzero Hermetic lid and heated from 0 °C to 100 °C at a rate of 10 °C min^{-1} in a N_2 atmosphere.

4.2.4 Resin cure. All ester-spaced diglycidyl ethers were pre-melted, mixed with Epikure W in stoichiometric quantities of epoxy and amine reactivity, and cured at 100 °C for 4 h and post-cured at 180 °C for 2 h in air.

4.2.5 Polymer properties. The thermogravimetric properties of the cured resins were measured using a TA Instruments Discovery Thermogravimetric Analyzer 550 (TGA). 10 mg of cured resin was placed on a platinum pan and heated to 700 °C at a rate of 10 °C min^{-1} in a N_2 atmosphere (40 mL min^{-1} balance gas flow rate and 25 mL min^{-1} sample gas flow rate). This process was repeated in an oxidative environment. Thermogravimetric properties including initial decomposition temperature (IDT), temperature at 50% weight loss ($T_{50\%}$), temperature at maximum decomposition rate (T_{max}), and char content were reported.

Thermophysical properties of all polymers were determined using a TA Instruments Discovery DSC 2500. A Tzero aluminium pan was loaded with 3-6 mg of sample and sealed with a Tzero Hermetic lid. Three heating and cooling cycles were performed at a rate of 10 °C min^{-1} under continuous N_2 flow (50 mL min^{-1}) over a

temperature ramp range of -50-150 °C. The T_g was determined as the midpoint of the inflection in the second heating cycle.

The viscoelastic properties of the cured resins were measured using a TA Instruments Q800 DMA. Each sample was prepared with appropriate dimensions (35 x 12 x 2.5 mm^3) and tested using a single cantilever geometry [32]. The tests were performed at a frequency of 1.0 Hz, oscillatory deflection amplitude of 7.5 μm, and a Poisson's ratio of 0.35. The heating ramp rate was 2 °C min^{-1} from -50.0 to 150 °C. Polymer densities were measured according to Archimedes' principle [29]. The molecular weight between crosslinks, M_c, was estimated using the Theory of Rubber Elasticity [31].

4.3 Results and Discussion

4.3.1 Synthesis of ester-spaced, aromatic diglycidyl ethers. The transesterification of MGEVA with the selected dimethyl esters in the presence of CALB was successful. The ^{1}H-NMR spectrum of DGEBVA-C18 is provided in Figure 20. ^{1}H-NMR spectra of DGEBVA-Ad and DGEBVA-C12 are provided in Appendix C. The synthetic route to prepare the coupled, ester-spaced, aromatic diglycidyl ethers as described does not go to full completion. In the ^{1}H-NMR spectrum, it can be observed that there is a distribution of products that are formed during the reaction. Of note, due to incomplete conversion, some MGEVA is still present as shown by the residual peak at 4.6 ppm which represents the protons adjacent to the unreacted, aliphatic hydroxyl of MGEVA. The successful transesterification to couple the hydroxyl moiety to the dimethyl ester causes these protons to shift to 5 ppm. Furthermore, the peak at 3.7 ppm is indicative of unreacted methyl ester functionality; therefore, the composition of the final

reaction product is, in general, a combination of the desired DGEBVA-C18, mono-coupled MGEVA-C18 whereby the MGEVA is only attached to one side of the C18ME, and unreacted MGEVA. Residual unreacted dimethyl ester is assumed to be mostly removed during the purification process. Similar results are observed for DGEBVA-Ad and DGEBVA-C12.

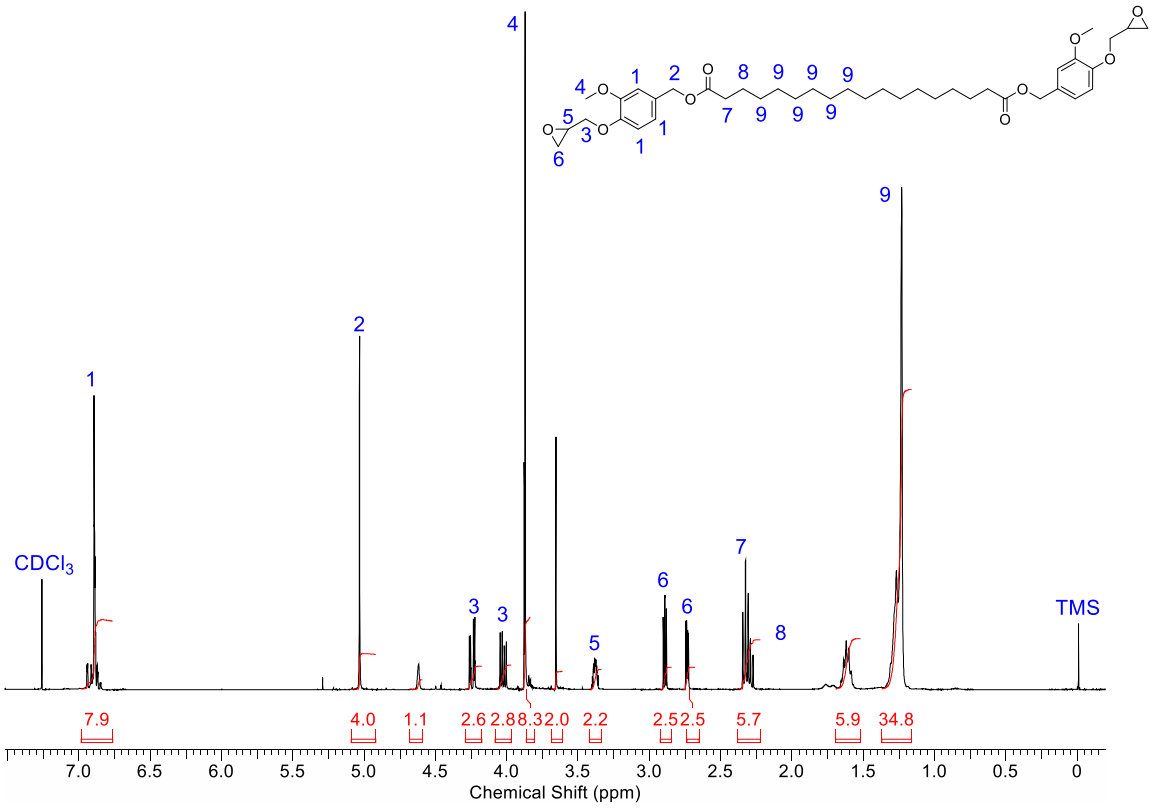

Figure 20. ^{1}H-NMR spectrum of DGEBVA-C18 with peak assignments and integrations.

4.3.2 Polymer properties. The ester-spaced, aromatic diglycidyl ether monomers were cured with stoichiometric amounts of Epikure W at 100 °C for 4 h and post-cured at 180 °C for 2 h in air and the resulting polymers were glassy and yellow in color.

Thermogravimetric analysis was performed on all post-cured samples to determine the thermal stability of all prepared, bio-based thermosets. The thermograms in N_2 of the post-cured materials is shown in Figure 21. The IDT, $T_{50\%}$, T_{max}, and char content values are presented in Table 6.

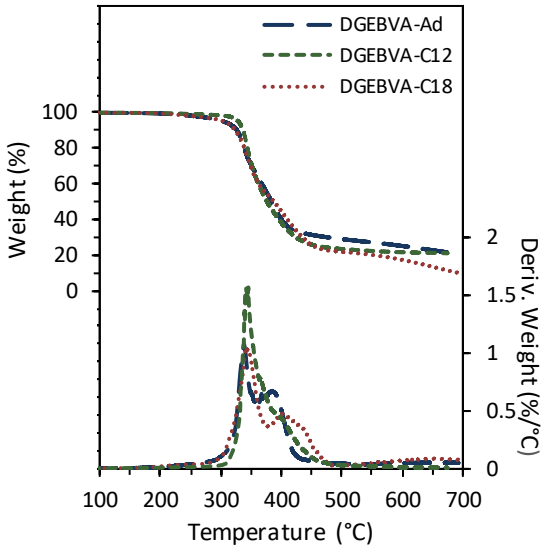

Figure 21. TGA thermograms and the respective first derivatives of the cured epoxy-amine thermosets in N_2.

Table 6

Thermogravimetric properties for all ester-spaced, aromatic diglycidyl ether samples cured with Epikure W in N_2

Sample	IDT (°C)	$T_{50\%}$ (°C)	T_{max} (°C)	Char Content (%)
DGEBVA-Ad	306 ± 4	382 ± 3	335 ± 2	20.5 ± 2.4
DGEBVA-C12	318 ± 7	386 ± 6	342 ± 2	17.0 ± 3.1
DGEBVA-C18	305 ± 3	382 ± 3	343 ± 4	9.2 ± 1.4

All cured, bio-based thermosets exhibit lower thermal stabilities compared to cured epoxy-amine thermosets containing BPA-derived epoxy resins [61]. In general, all prepared materials exhibited comparable thermal stabilities relative to one another, indicating that the length of ester spacer in the core of the monomer has minimal impact on thermal stability of the resulting polymer. However, as the chain length of the ester increases, the overall char content remaining after the experiment decreases.

DSC was performed on all post-cured samples to determine the thermophysical properties of all epoxy-amine thermosets, including the determination of T_g and any other thermal phenomena associated with the samples. The DSC thermograms are provided in Figure 22 and the tabulated DSC results are shown in Table 7.

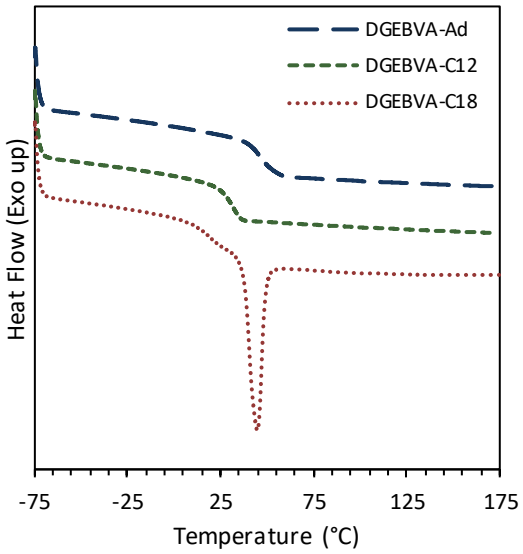

Figure 22. DSC traces of the cured epoxy-amine thermosets.

Table 7

DSC results for all ester-spaced, aromatic diglycidyl ether samples cured with Epikure W

Sample	T_g (°C)	T_m (°C)	Enthalpy (J g^{-1})
DGEBVA-Ad	48 ± 1	-	-
DGEBVA-C12	30 ± 1	-	-
DGEBVA-C18	16 ± 1	44 ± 1	16 ± 5

As expected, T_g is a function of ester length whereby T_g decreases as the aliphatic chain length between the aromatic units increases [105]. DGEBVA-Ad has the shortest chain length, and exhibits highest T_g of 48 °C. Further increasing aliphatic chain length between the aromatic units for DGEBVA-C12 and DGEBVA-C18 results in cured polymers with T_gs of 30 °C and 16 °C, respectively. Interestingly, the cured sample containing DGEBVA-C18 exhibits a melting transition at 44 °C, which is consistently repeatable when cycling the sample on DSC, whereas the other samples do not exhibit such behavior. TGA experiments confirm that this transition is not associated with bulk material weight loss at the temperature which this occurs, therefore the presence of the long, C18 chain is hypothesized to be forming regions of crystallinity that are chemically bound to the thermoset matrix. Thermosetting matrices with regions of crystallinity are of general interest due to their potential for use in highly advanced materials and the possibility to yield unexpected mechanical properties, such as significant improvements in fracture behavior [106, 107].

Viscoelastic properties of all cured epoxy-amine systems were evaluated using DMA. Representative thermograms for the storage modulus (E') and the loss modulus (E'') for each sample are provided in Figure 23. The tan δ thermograms are shown in

Figure 24. The thermomechanical property values for each sample are included in Table 8.

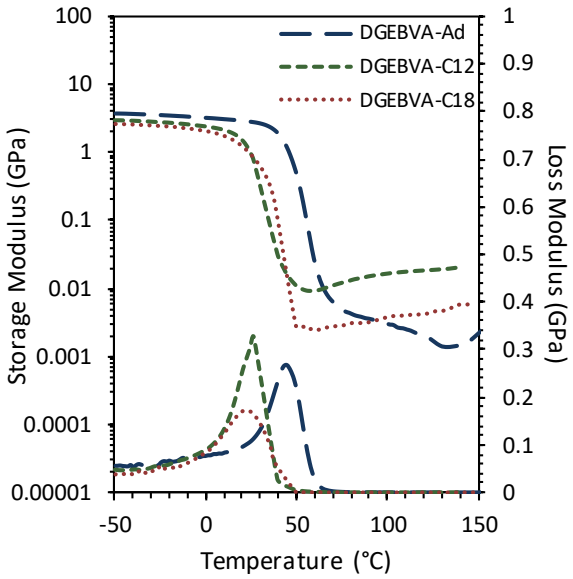

Figure 23. DMA thermograms of *E′* and *E″* for the epoxy-amine thermosets.

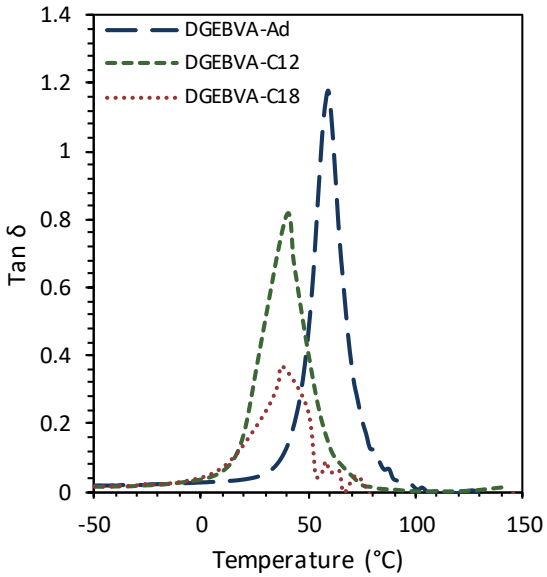

Figure 24. Tan δ thermograms of the cured epoxy-amine thermosets.

Table 8

Thermomechanical results for all ester-spaced, aromatic diglycidyl ether samples cured with Epikure W

Sample	E′ @ -40 °C (GPa)	E′ @ 25 °C (Gpa)	Peak of E″ (°C)	Peak of Tan δ (°C)	eff. M_c (g mol $^{-1}$)	ρ @ 25 °C (g cm^{-3})
DGEBVA-Ad	3.6 ± 0.1	2.8 ± 0.1	46 ± 1	60 ± 1	7334 ± 2597	1.236 ± 0.007
DGEBVA-C12	3.0 ± 0.1	0.8 ± 0.1	24 ± 4	37 ± 3	1008 ± 64	1.177 ± 0.005
DGEBVA-C18	2.5 ± 0.1	0.8 ± 0.1	22 ± 1	37 ± 2*	3562 ± 543	1.150 ± 0.003

The cured sample containing DGEBVA-Ad had the highest E' of 3.6 GPa at – 40 °C and 2.8 GPa at 25 °C due to the low flexibility of the short aliphatic chain. As the chain length of the methyl ester utilized in the synthesis increased, the E' of the cured epoxy-amine thermoset decreased due to the increase in aliphatic character resulting in an increase in flexibility of the resulting polymer network [11, 17]. The peak of E'' was used to estimate T_g. The peak of E'' gives a more conservative value for the T_g while the peak of the tan δ provides an upper limit [44]. The T_g based on the peak of E'' follows the same trend as observed in the DSC experiments and similar values were obtained, whereby the thermoset containing DGEBVA-Ad displayed the highest T_g of 46 °C. Increasing aliphatic chain length between the aromatic units for DGEBVA-C12 and DGEBVA-C18 resulted in the reduction of T_g to 24 °C and 22 °C, respectively. The cured sample containing DGEBVA-C18 once again displayed interesting behavior, whereby at approximately 40 °C, the sample seems to lose all rigidity, and the E' begins to drop in a linear fashion. Additionally, the tan δ thermogram for the DGEBVA-C18 containing thermoset, shown in Figure 24, displays odd, asymmetric behavior. This behavior is

likely due to the semi-crystalline transition which was observed in DSC at approximately the same temperature.

The polymer chain segmental mobility can be interpreted by the maximum value of the tan δ, where a higher peak indicates a higher chain mobility [92]. In general, as the aliphatic content was increased from -Ad to -C12 to -C18, the chain mobility appears to decrease. The molecular weight between crosslinks (M_c) was calculated using the Theory of Rubber Elasticity. M_c is expected to be a linear function of epoxy molecular weight, whereby a lower molecular weight epoxy would yield a material with a lower value of M_c; however, the DGEBVA-Ad containing thermoset does not fit this trend. This result is likely due to a low degree of cure of the DGEBVA-Ad sample as a result of the curing procedure used. The melting point of DGEBVA-Ad is approximately the same value of the cure temperature of 100 °C, therefore mixing of DGEBVA-Ad in Epikure W at 100 °C likely resulted in imperfect cure and rapid vitrification of the bulk material, thus leading to the significant increase in M_c for that sample.

4.4 Conclusions

Bio-based, ester-spaced, aromatic diglycidyl ethers were prepared via the intermediate preparation of monoglycidyl ether of vanillyl alcohol (MGEVA), which was subsequently coupled via an enzyme-catalyzed transesterification with three different, renewably sourced dimethyl esters including dimethyl adipate, dimethyl dodecanedioate, and dimethyl octadecanedioate to prepare DGEVBA-Ad, DGEBVA-C12, and DGEBVA-C18. DGEVBA-Ad, DGEBVA-C12, and DGEBVA-C18 were cured with stoichiometric amounts of amine curing agent, Epikure W, and evaluated for their thermophysical and thermomechanical properties to determine the effect of ester length on resulting polymer

properties. In general, as ester chain length was increased, the glass transition temperatures of the resulting epoxy-amine thermoset decreased. Interestingly DGEBVA-C18 exhibited a melting transition at 44 °C, which is confirmed to not be associated with bulk material weight loss. Thus, the presence of the long, C18 chain at the core of the molecule is hypothesized to be forming regions of crystallinity that are chemically bound to the epoxy-amine polymer. The potential crystallinity could lead to unexpected mechanical properties and significant improvements in fracture behavior; however, this was not tested in this work.

Chapter 5

Functionally Hybrid Monomers From Aromatic, Bio-Based, Asymmetric Diols and Their Respective Epoxy-Functional Homopolymers

Text and figures are reproduced and adapted with permission from A.W. Bassett, K.R. Sweet, R.M. O'Dea, A.E. Honnig, C.M. Breyta, J.H. Reilly, J.J. La Scala, T.H. Epps III, and J.F. Stanzione III, "Dual-functional, Aromatic, Epoxy-Methacrylate Monomers from Bio-based Feedstocks and Their Respective Epoxy-functional Thermoplastics," *Journal of Polymer Science*, 2020, 58 (5), 673-682, reference [108].

5.1 Introduction

Currently, glycidyl methacrylate (GMA) is the only commercially available, functionally hybrid, dual-functional monomer with both terminal epoxy and methacrylate functionalities. Multi-functional vinyl ester monomers can be prepared via the reaction of a polyepoxide with less than stoichiometric amount of methacrylic acid; however, this approach does not follow the same structural motif as GMA and yields relatively large molecules with high viscosities that make processing difficult [4]. Therefore, the development of unique, aromatic GMA complements provides chemical variety and characteristics for a wide range of applications.

Kim et al. have presented a dual-functional monomer with both epoxy and methacrylate functionalities for holographic recording from 2-(oxiranylmethoxy)ethyl 2-methyl-2-propenoate (OEMP) [109]. This dual-functional monomer was efficient for holographic recording with high photosensitivity and low shrinkage for unique optical properties [109]. However, to the authors' knowledge, no other synthesized monomers

that include both terminal epoxy and methacrylate functional groups, specifically those with aromatic character, are readily available.

Additionally, epoxy-functional thermoplastic polymers are highly desired for their tunable properties for consumer plastic goods, coatings, and adhesives [14, 15]. GMA has been homopolymerized and copolymerized with many other (meth)acrylate monomers to produce polymers with pendant oxirane rings [110]. These pendant groups allow for further modifications through various chemistries, including ring-opening reactions with nucleophiles, and facilitating the robust attachment of films to surfaces [16]. Polymerized GMA, poly(GMA), is known for biocompatibility and versatility as previous research has found utility for poly(GMA) and its copolymers in gene delivery, polymer scaffolds, and self-healing materials [111, 112]. Poly(GMA) has additional uses in industrial and consumer settings including automotive coatings, protective finishes, adhesives, and electrical laminates. While GMA and poly(GMA) have been well researched, GMA has no commercial complements with similar functionality which could broaden and diversify the applications of epoxy-functional materials [15].

Vanillyl alcohol (VA) and syringyl alcohol (SA), lignin-based aromatic diols and products of lignin depolymerization [19, 57, 61, 113, 114], gastrodigenin (GD), a bio-based aromatic diol found in the Chinese *Gastrodia elata* Blume herb and *Coelogossum* orchid [115, 116], and tyrosol, a naturally derived aromatic diol found in olive oil which can be recovered from olive oil wastewater streams [117], are suitable platform chemicals for the preparation of unique, aromatic GMA complements due to their natural asymmetry. While these compounds have been previously investigated for thermosetting

resins [8, 61, 98], their potential to be transformed into dual-functional monomers has not been explored.

In the present work, we detail the synthesis of novel, aromatic, epoxy-methacrylate monomers: vanillyl alcohol epoxy-methacrylate (VAEM), syringyl alcohol epoxy-methacrylate (SAEM), gastrodigenin epoxy-methacrylate (GDEM), and tyrosol epoxy-methacrylate (TEM), derived from vanillyl alcohol, syringyl alcohol, gastrodigenin, and tyrosol, respectively (Figure 25). The natural asymmetry and differences in reactivity of the aromatic and aliphatic hydroxyls enable the facile, selective synthesis of dual-functional, epoxy-methacrylate monomers.

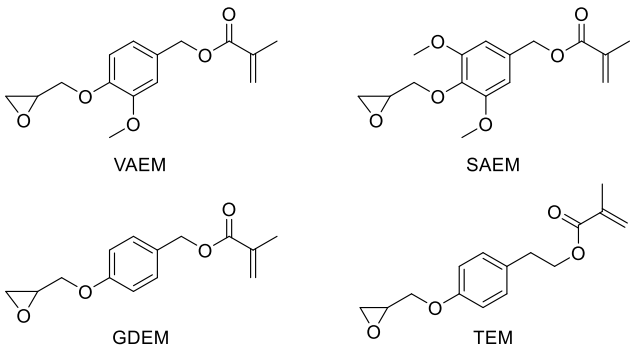

Figure 25. Structures of dual-functional monomers prepared.

Additionally, this work highlights the preparation of epoxy-functional thermoplastic homopolymers comprised of VAEM, SAEM, GDEM, and TEM. The resultant homopolymers were compared to poly(GMA) to assess the effect of molecular structure on thermal and surface properties. All polymers were characterized for their molecular weight, thermal stability and glass transition temperature (T_g), with surface energies evaluated for thin films prepared by flow coating [118-120]. These bio-based

materials exhibited substantially higher thermal stabilities and comparable surface energies relative to poly(GMA), leading to potential for use in high-temperature applications including coatings and adhesives.

5.2 Experimental Methods & Procedures

5.2.1 Materials. Epichlorohydrin (99%), gastrodigenin (4-hydroxybenzyl alcohol, 97%), dichloromethane (DCM, 99.6%), vanillyl alcohol (4-hydroxy-3-methoxybenzyl alcohol, 99%), diiodomethane (99%, stabilized), and chloroform-d_3 ($CDCl_3$, 99.8 atom% d) were purchased from Acros Organics. Ethyl acetate (99.9%), hexanes (99.9%), methanol (99.8%), toluene (99.9%), tetrahydrofuran (Optima THF, 99.9%), and triethylamine (TEA, 99%) were purchased from Fisher Scientific. Syringyl alcohol [(4-(3-hydroxyprop-1-enyl)-2,6-dimethoxyphenol, 99%] and methacryloyl chloride (97%) were purchased from Alfa Aesar. Tyrosol [2-(4-Hydroxyphenol) ethanol, 98%], *N*,*N*-Dimethylformamide (DMF, 99.8%), benzyltriethylammonium chloride (TEBAC, 99%), and poly(GMA) (M_n=10,000-20,000 Da) were purchased from Sigma Aldrich. 2,2′-Azobis(2-methylpropinitrile) (AIBN, 95%) was purchased from AstaTech. Compressed nitrogen (N_2, 99.998%) and compressed argon (Ar, 99.999%) were purchased from Airgas. Sodium hydroxide was purchased from VWR. All chemicals mentioned above were used without further purification. Unidentified peaks in the ^{1}H-NMR spectra for all synthesized dual-functional monomers are associated with methacryloyl chloride dimers and impurities that were not able to be removed during chromatographic purification [121].

5.2.2 Synthesis of 3-methoxy-4-(oxiran-2-ylmethoxy)benzyl methacrylate (VAEM). Vanillyl alcohol (5 g), epichlorohydrin (25.43 mL), and TEBAC (0.74 g) were

added to a three-neck round bottom flask equipped with a mechanical mixer. The reaction mixture was heated to 80 °C for 1 h. After 1 h, the reaction was cooled to room temperature and a mixture of 5 M $NaOH_{(aq)}$ (25.9 mL) and TEBAC (0.74 g) was added dropwise. Then, the reaction was worked up and washed with a solution of equal parts de-ionized (DI) water and ethyl acetate. Flash chromatography (hexanes/ethyl acetate) was used to purify the intermediate product, mono-glycidyl ether of vanillyl alcohol (MGEVA; 55% yield; white powder).

(3-methoxy-4-(oxiran-2-ylmethoxy)phenyl)methanol (MGEVA, $C_{11}H_{14}O_4$). White solid, mp. 71-73 °C. ^{1}H-NMR ($CDCl_3$): 2.7 (1 H, dd), 2.9 (1 H, t), 3.4 (1 H, m), 3.9 (3 H, s), 4.0 (1 H, dd), 4.2 (1 H, dd), 4.6 (2 H, s), 6.9 (3 H, m).

MGEVA (3.726 g) was added to a three-neck round bottom flask containing DCM (5.26 mL) and triethylamine (4.944 mL). The flask was placed in an ice bath, equipped with a magnetic stir bar, pressure-equalizing dropping funnel, and an inlet for dry argon gas. Once the contents were cooled to 0 °C, a DCM (10.91 mL) and methacryloyl chloride (1.821 mL) solution was added dropwise with constant stirring. After 24 h, DCM was added to the mixture and then washed once with a 2.5 M $NaOH_{(aq)}$ solution. The organic phase was isolated, and the solvent removed using reduced pressure. The product, vanillyl alcohol epoxy methacrylate (VAEM; 62% yield; white solid) was further purified using flash chromatography (hexanes/ethyl acetate).

3-methoxy-4-(oxiran-2-ylmethoxy)benzyl methacrylate (VAEM, $C_{15}H_{18}O_5$). White solid, mp. 79-81 °C. ^{1}H-NMR ($CDCl_3$): δ 2.0 (3 H, t), 2.7 (1 H, dd), 2.9 (1 H, t), 3.4 (1 H, m), 3.9 (3 H, s), 4.0 (1 H, dd), 4.2 (1 H, dd), 5.1 (2 H, s), 5.6 (1 H, d), 6.1 (1 H, d), 6.9 (3 H, m). ^{13}C-NMR ($CDCl_3$): δ 18.2, 44.7, 50.0, 55.8, 66.2, 70.1, 112.0, 113.7, 120.8, 125.6,

129.6, 136.1, 147.8, 149.4, 167.1. High-resolution mass spectrometry (HRMS) Calculated: 278.1154. Found: 278.1172.

5.2.3 Synthesis of 3,5-dimethoxy-4-(oxiran-2-ylmethoxy)benzyl methacrylate (SAEM). Syringyl alcohol (4 g), epichlorohydrin (17.03 mL), and TEBAC (0.49 g) were added to a three-neck round bottom flask equipped with a mechanical mixer. The reaction mixture was heated to 80 °C for 1 h. After 1 h, the reaction was cooled to room temperature and a mixture of 5 M $NaOH_{(aq)}$ (17.4 mL) and TEBAC (0.49 g) was added dropwise. Then, the reaction was worked up and washed with a solution of equal parts DI water and ethyl acetate. Flash chromatography (hexanes/ethyl acetate) was used to purify the intermediate product, mono-glycidyl ether of syringyl alcohol (MGESA; 28% yield; pale yellow liquid).

(3,5-dimethoxy-4-(oxiran-2-ylmethoxy)phenyl)methanol (MGESA, $C_{12}H_{16}O_5$). Pale yellow liquid. ^{1}H-NMR ($CDCl_3$): δ 2.6 (1 H, dd), 2.8 (1 H, t), 3.4 (1 H, m), 3.9 (6 H, s), 4.0 (1 H, dd), 4.2 (1 H, dd), 4.6 (2 H, s), 6.6 (2 H, s).

MGESA (1 g) was added to a three-neck round bottom flask containing DCM (1.24 mL) and triethylamine (1.16 mL). The flask was placed in an ice bath, equipped with a magnetic stir bar, pressure-equalizing dropping funnel, and an inlet for dry argon gas. Once the contents were cooled to 0 °C, a DCM (2.56 mL) and methacryloyl chloride (0.43 mL) solution was added dropwise with constant stirring. After 24 h, DCM was added to the mixture and then washed once with a 2.5 M $NaOH_{(aq)}$ solution. The organic phase was isolated, and the solvent removed using reduced pressure. The product, syringyl alcohol epoxy methacrylate (SAEM; 48% yield; white solid), was further purified using flash chromatography (hexanes/ethyl acetate).

3,5-dimethoxy-4-(oxiran-2-ylmethoxy)benzyl methacrylate (SAEM, $C_{16}H_{20}O_6$). White solid, mp. 73-75 °C. ^{1}H-NMR ($CDCl_3$): δ 2.0 (3 H, t), 2.6 (1 H, dd), 2.8 (1 H, t), 3.4 (1 H, m), 3.9 (6 H, s), 4.0 (1 H, dd), 4.2 (1 H, dd), 5.1 (2 H, s), 5.6 (1 H, d), 6.2 (1 H, d), 6.6 (2 H, s). ^{13}C-NMR ($CDCl_3$): δ 18.3, 44.7, 50.5, 56.1, 66.5, 74.1, 105.1, 125.9, 132.0, 136.1, 136.5, 153.2, 167.2. HRMS Calculated: 308.1260. Found: 308.1284.

5.2.4 Synthesis of 4-(oxiran-2-ylmethoxy)benzyl methacrylate (GDEM). Gastrodigenin (30 g), epichlorohydrin (189.48 mL), and TEBAC (5.50 g) were added to a three-neck round bottom flask equipped with a mechanical mixer. The reaction mixture was heated to 80 °C for 1 h. After 1 h, the reaction was cooled to room temperature and a mixture of 5 M $NaOH_{(aq)}$ (193.3 mL) and TEBAC (5.50 g) was added dropwise. Then, the reaction was worked up and washed with a solution of equal parts DI water and ethyl acetate. Flash chromatography (hexanes/ethyl acetate) was used to purify the intermediate product, mono-glycidyl ether of gastrodigenin (MGEGD; 60% yield; white powder).

(4-(oxiran-2-ylmethoxy)phenyl)methanol (MGEGD, $C_{10}H_{12}O_3$). White solid, mp. 63-64 °C. ^{1}H-NMR ($CDCl_3$): δ 2.7 (1 H, dd), 2.9 (1 H, t), 3.4 (1 H, m), 4.0 (1 H, dd), 4.2 (1 H, dd), 4.6 (2 H, s), 6.9 (2 H, m), 7.3 (2 H, m).

MGEGD (25.49 g) was added to a three-neck round bottom flask containing DCM (42.00 mL) and triethylamine (39.46 mL). The flask was placed in an ice bath, equipped with a magnetic stir bar, pressure-equalizing dropping funnel, and an inlet for dry argon gas. Once the contents were cooled to 0 °C, a DCM (87.10 mL) and methacryloyl chloride (14.53 mL) solution was added dropwise with constant stirring. After 24 h, DCM was added to the mixture and then washed once with a 2.5 M $NaOH_{(aq)}$

solution. The organic phase was isolated, and the solvent removed using reduced pressure. The product, gastrodigenin epoxy methacrylate (GDEM; 66% yield; white solid) was further purified using flash chromatography (hexanes/ethyl acetate).

4-(oxiran-2-ylmethoxy)benzyl methacrylate (GDEM, $C_{14}H_{16}O_4$). White solid, mp. 63-65 °C. ^{1}H-NMR ($CDCl_3$): δ 2.0 (3 H, t), 2.7 (1 H, dd), 2.9 (1 H, t), 3.4 (1 H, m), 4.0 (1 H, dd), 4.2 (1 H, dd), 5.1 (2 H, s), 5.6 (1 H, d), 6.1 (1 H, d), 6.9 (2 H, m), 7.3 (2 H, m). ^{13}C-NMR ($CDCl_3$): δ 18.3, 44.6, 50.0, 66.1, 68.7, 114.5, 125.6, 128.8, 129.8, 136.2, 158.4, 167.2. HRMS Calculated: 248.1049. Found: 248.1081.

5.2.5 Synthesis of 4-(oxiran-2-ylmethoxy)phenethyl methacrylate (TEM). Tyrosol (4 g), epichlorohydrin (22.70 mL), and TEBAC (0.66 g) were added to a three-neck round bottom flask equipped with a mechanical mixer. The reaction mixture was heated to 80 °C for 1 h. After 1 h, the reaction was cooled to room temperature and a mixture of 5 M $NaOH_{(aq)}$ (23.2 mL) and TEBAC (0.66 g) was added dropwise. Then, the reaction was worked up and washed with a solution of equal parts DI water and ethyl acetate. Flash chromatography (hexanes/ethyl acetate) was used to purify the intermediate product, mono-glycidyl ether of tyrosol (MGET; 74% yield; white powder).

2-(4-(oxiran-2-ylmethoxy)phenyl)ethan-1-ol (MGET, $C_{11}H_{14}O_3$). White solid, mp. 60-62 °C. ^{1}H-NMR ($CDCl_3$): δ 2.7 (1 H, dd), 2.8 (2 H, t), 2.9 (1 H, t), 3.3 (1 H, m), 3.8 (2 H, q), 3.9 (1 H, dd), 4.2 (1 H, dd), 6.9 (2 H, m), 7.1 (2 H, m).

MGET (3.50 g) was added to a three-neck round bottom flask containing DCM (5.35 mL) and triethylamine (5.03 mL). The flask was placed in an ice bath, equipped with a magnetic stir bar, pressure-equalizing dropping funnel, and an inlet for dry argon gas. Once the contents were cooled to 0 °C, a DCM (11.09 mL) and methacryloyl

chloride (1.85 mL) solution was added dropwise with constant stirring. After 24 h, DCM was added to the mixture and then washed once with a 2.5 M $NaOH_{(aq)}$ solution. The organic phase was isolated, and the solvent removed using reduced pressure. The product tyrosol epoxy methacrylate (TEM; 35% yield; white solid) was further purified using flash chromatography (hexanes/ethyl acetate).

4-(oxiran-2-ylmethoxy)phenethyl methacrylate (TEM, $C_{15}H_{18}O_4$). White solid, sample auto-polymerized before reaching mp. ^{1}H-NMR ($CDCl_3$): δ 2.0 (3 H, t), 2.7 (1 H, dd), 2.9 (3 H, m), 3.4 (1 H, m), 4.0 (1 H, dd), 4.2 (1 H, dd), 4.3 (2 H, t), 5.5 (1 H, d), 6.1 (1 H, d), 6.9 (2 H, m), 7.2 (2 H, m). ^{13}C-NMR ($CDCl_3$): δ 18.2, 34.1, 44.6, 50.0, 65.2, 68.7, 114.5, 125.3, 129.8, 130.5, 136.2, 157.1, 167.2. HRMS Calculated: 262.1205. Found: 262.1208.

5.2.6 Preparation of homopolymers. VAEM was mixed with 1 wt.% of AIBN and 3.32 mL DMF per gram of monomer. The solution was sparged with argon for 10 min, after which the reaction vessel was sealed, and the solution was heated to 60 ºC while stirring. After 24 h, the solution was precipitated in excess methanol. The resulting product, poly(VAEM) was dissolved in DCM and re-precipitated in hexanes to remove any residual monomer and/or initiator. The procedure was repeated for GDEM, SAEM, and TEM to form poly(GDEM), poly(SAEM), and poly(TEM), respectively. A representative reaction scheme for the homopolymer synthesis is provided in Figure 26.

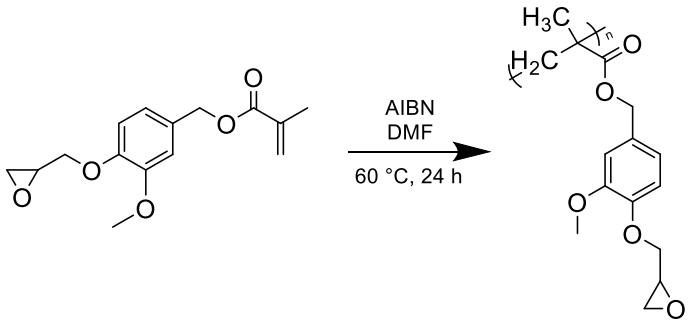

Figure 26. Representative reaction scheme for homopolymers; solution polymerization of VAEM to prepare poly(VAEM).

5.2.7 Characterization of monomers & homopolymers. All molecules and homopolymers synthesized in this work were characterized by ^{1}H-NMR spectroscopy (400.15 MHz, 32 scans at 298 K). Additionally, all new molecules were characterized by ^{13}C-NMR spectroscopy (111 MHz, 512 scans at 298 K) using a Varian 400 MHz FT-NMR Spectrometer. High resolution mass spectrometry (TOF HRMS) was used to determine the exact mass of the monomers synthesized in this study. Spectra were recorded on a Waters Xevo G2 XS QToF Mass Spectrometer.

The melting points of the monomers were measured using a TA Instruments Discovery Differential Scanning Calorimeter (DSC) 2500. Approximately 10 mg of sample was placed within a Tzero pan with a Tzero Hermetic lid and heated from 30 °C at a rate of 10 °C min^{-1} in a N_2 atmosphere. Based on characterization methods, all final dual functional monomers were determined to be > 98% pure.

The number-average molecular weight (M_n), weight-average molecular weight (M_w), and dispersity ($Đ$) were obtained on a Waters Acquity Advanced Polymer Chromatography (APC) instrument with THF as the eluent (0.6 mL min^{-1}), using

polystyrene standards with M_n of 537,000 Da ($Đ$=1.03), 59,300 Da ($Đ$=1.05), and 8,650 Da ($Đ$=1.03) as a reference.

Glass transition temperatures (T_gs) of all polymers were determined using a TA Instruments Discovery DSC 2500. A Tzero aluminium pan was loaded with 3-6 mg of sample and sealed with a Tzero Hermetic lid. Three heating and cooling cycles were performed at a rate of 10 °C min^{-1} under continuous N_2 flow (50 mL min^{-1}) over a temperature range of 0-150 °C. The second and third cycles had no significant changes for all samples. The T_g was determined as the midpoint of the inflection in the second heating cycle.

The thermal degradation properties of the polymers including initial decomposition temperature (IDT), temperature at 50% weight loss ($T_{50\%}$), temperature at maximum degradation rate (T_{max}), and char content were characterized using a TA Instruments Discovery Thermogravimetric Analyzer 550 (TGA). A powdered sample of 4-6 mg of each polymer was loaded into a platinum pan and heated a rate of 10 °C min^{-1} to 700 °C in either a N_2 or air atmosphere (40 mL min^{-1} balance gas flow rate and 25 mL min^{-1} sample gas flow rate). Each polymer was run in triplicate for oxidative (air) and inert (N_2) environments.

Surface properties were measured for thin films (< 50 nm) prepared by flow coating onto silicon wafers (N<100>, Wafer World, Inc.) [118, 119]. For each polymer [except poly(TEM) due to reduced thermal stability], a 2 wt.% solution in THF was prepared, and 50 µL of filtered (0.45 µm) solution was flow coated onto a clean (triple rinsed with toluene), ultraviolet-ozone-treated (Jelight, Model 342, 30 min. treatment) silicon wafer at 10 mm/s with an acceleration and deceleration of 100 mm/s^2 and a gap

height of 20 µm. The samples were annealed overnight at 120 °C under dynamic vacuum. The epoxy functional group was expected to bond to the UVO-treated silicon surface at elevated temperatures, yielding a covalently-bound polymer layer [122]. The reflectance curve for each film was obtained using a spectral reflectometer (Filmetrics, Inc. F20-UV) and fit using a constant refractive index to estimate the thicknesses of the annealed samples. Then, the films were washed with THF and toluene to remove any non-bound polymer, followed by annealing under the same conditions as described above. The film thicknesses were re-measured to quantify any changes after the washing process. Static contact angles were measured in triplicate for DI water and diiodomethane (CH_2I_2) using a contact angle goniometer (Krüss Drop Shape Analyzer, DSA25S) with a sessile drop technique (2 µL drop size) [118, 120]. Images were analyzed using Krüss Advance software with a Young-Laplace model for water and an ellipse-tangent model for CH_2I_2, and surface energies were calculated using the two-fluid Owens-Wendt model [118, 120].

5.3 Results and Discussion

5.3.1 Monomer synthesis and characterization. VA, SA, GD, and tyrosol bear aromatic and aliphatic hydroxyls, with the aromatic hydroxyl being more acidic and more reactive towards epichlorohydrin [61, 98]. Previous studies preparing diglycidyl ethers of VA and GD have reported moderate to low yields of monoglycidyl ethers as byproducts due to this slight difference in acidity [61, 98]. Intentional synthesis of monoglycidyl ethers of these compounds as intermediate building blocks for other modifications have not been performed. The syntheses for all monoglycidyl ethers were adapted from literature [98], whereby the monoepoxidized intermediate is produced as the major product, in which the aliphatic hydroxyl is unreacted. The monoglycidyl ethers of VA,

SA, and GD exhibit a characteristic singlet at 4.6 ppm in $CDCl_3$ (see ^{1}H-NMR spectra in Appendix D), confirming that the aliphatic methylene is adjacent to an unreacted hydroxyl [61]. The monoglycidyl ether of tyrosol exhibits a similar characteristic peak, a triplet at 3.8 ppm in $CDCl_3$ (see ^{1}H-NMR spectra in Appendix D), indicating that the aliphatic hydroxyl is unreacted. The unreacted aliphatic hydroxyl was then esterified with methacryloyl chloride to prepare the dual-functional monomers VAEM, SAEM, GDEM, and TEM. Excess triethylamine was utilized in the synthesis to ensure the rapid trapping of hydrochloric acid that is formed during the reaction, thus preventing epoxy ring opening. Esterification of the aliphatic hydroxyl was confirmed via ^{1}H-NMR, as the aliphatic methylene protons shift to 5.1 ppm in $CDCl_3$ for the synthesis of VAEM, SAEM, and GDEM. Similarly, esterification of the aliphatic hydroxyl was confirmed in the synthesis of TEM, as the protons adjacent to the aliphatic hydroxyl shift to 4.3 ppm in $CDCl_3$. The general synthesis scheme for the production of the dual-functional monomers is shown in Figure 27.

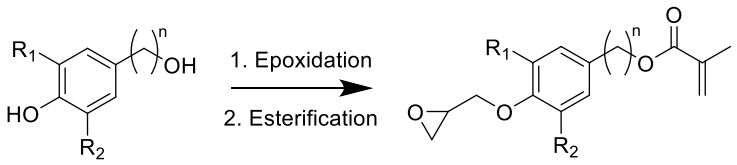

Monomer	R_1	R_2	n
GDEM	H	H	1
VAEM	H	OCH_3	1
SAEM	OCH_3	OCH_3	1
TEM	H	H	2

Figure 27. General synthesis route for the preparation of dual functional monomers.

The ^{1}H-NMR spectrum of VAEM with peak assignments is shown in Figure 28. The ^{1}H-NMR spectra of all other dual functional monomers are provided in Appendix D. VAEM, SAEM, and GDEM are similar in structure: VAEM bears a methoxy moiety *ortho* to the glycidyl ether, SAEM bears two methoxy moieties that are both *ortho* to the glycidyl ether, and GDEM does not bear any substituents on the aromatic ring. TEM and GDEM also are similar in structure, with the only difference being that TEM bears an ethylene spacer between the aromatic ring and methacrylate, whereas GDEM bears a methylene spacer.

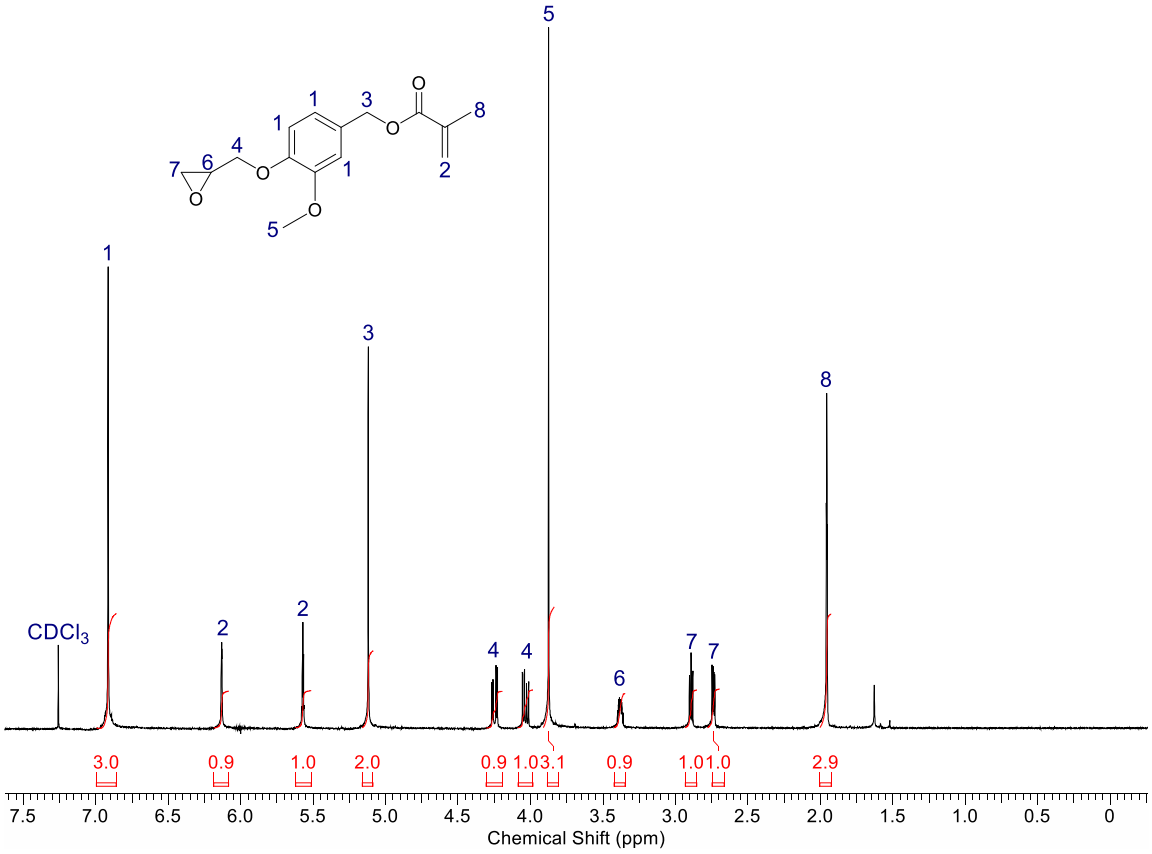

Figure 28. [1]H-NMR spectrum for synthesized VAEM molecule with peak assignments and integrations.

These monomers have both methacrylate and epoxy functionalities similar to GMA, yet contain aromaticity at the core of the molecule, which has the potential to enhance material properties, such as thermal stability and hydrophobicity. Additionally, the synthesized monomers are all solids at room temperature (DSC traces provided in Appendix D), potentially increasing storage stability and significantly reducing volatility relative to GMA.

5.3.2 Polymer characterization. Each of the synthesized monomers was individually polymerized via methods adapted from Fei et al [123]. The resulting homopolymers were white solids at 25 °C. Poly(GMA), a white solid at 25 °C, was

purchased from Sigma-Aldrich and used as a reference. The structures of the homopolymers are shown in Figure 29.

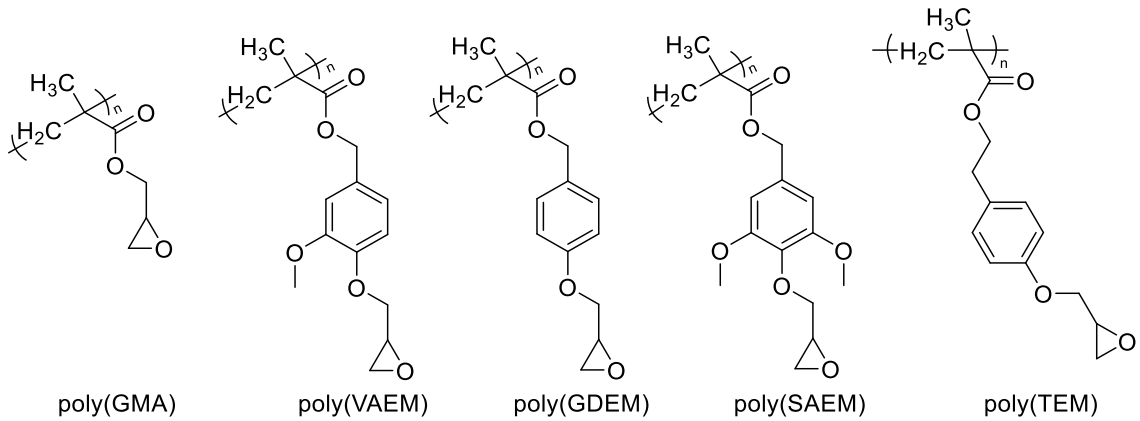

Figure 29. Epoxy-functional thermoplastics prepared.

The presence of the epoxy group on the pendant chain was confirmed via ^{1}H-NMR spectroscopy for each homopolymer. The ^{1}H-NMR spectrum of poly(VAEM) is shown in Figure 30. The ^{1}H-NMR spectra for poly(GMA), poly(GDEM), poly(VAEM), and poly(TEM) are provided in Appendix D. The reference peak of the two hydrogens on the methylene bridge, located at 4.8 ppm, was set to an integration of 2. The protons present on the epoxy are labeled as 5 and 6 shown at 3.3 ppm and 2.6 – 2.8 ppm, respectively. Each epoxy proton peak integrated to 1, indicating the preservation of three protons on the epoxy ring.

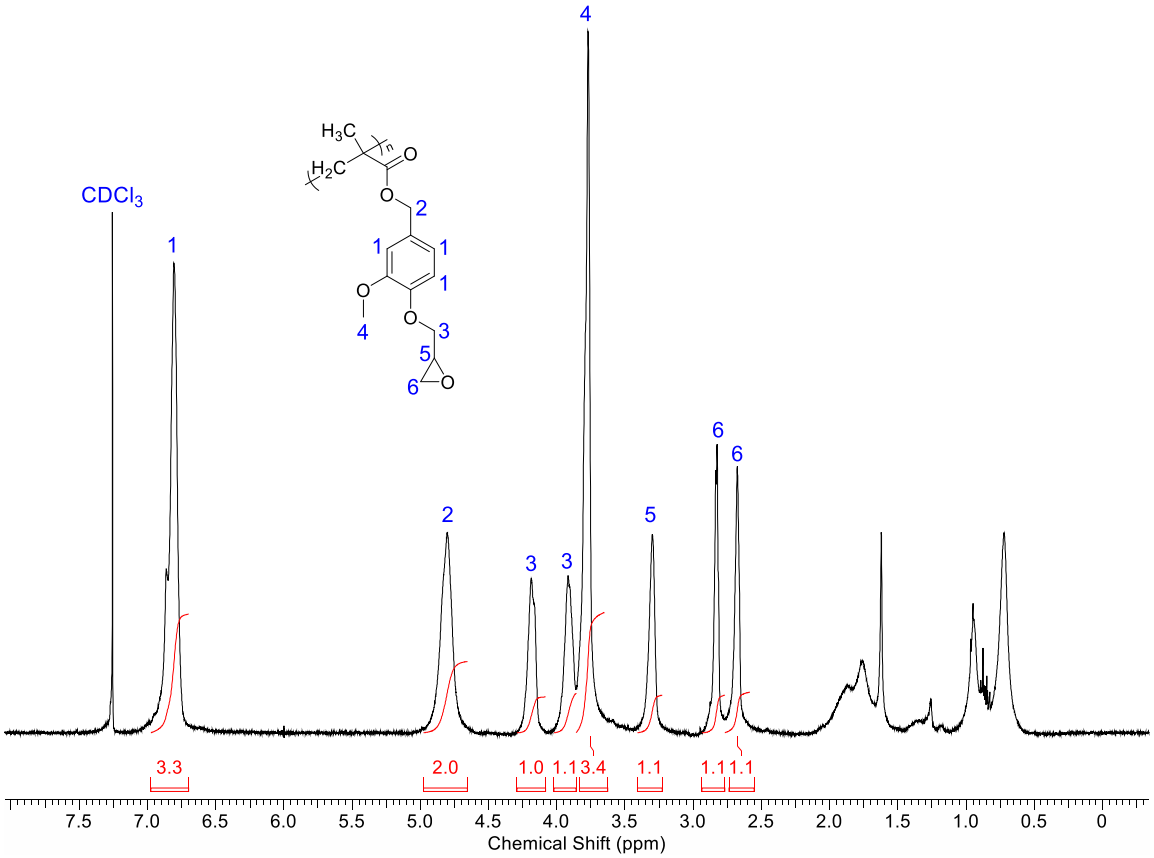

Figure 30. Representative ^{1}H-NMR spectrum with partial peak integrations of poly(VAEM).

The molecular weights and T_gs of each polymer were determined using size exclusion chromatography (SEC) and DSC, respectively. The resulting data are shown in Table 9, with DSC and SEC traces provided in Appendix D. The M_n values of all prepared homopolymers are similar; however, the dispersities of the prepared homopolymers relative to poly(GMA) are higher, likely because these homopolymers were prepared via uncontrolled radical polymerizations [124, 125]. All synthesized polymers exhibited T_gs within the range of 60-68 ºC, similar to that of poly(GMA), with the exception of poly(TEM) at 46 ºC. The similarities in the T_gs indicate the methacrylate backbone has a more substantial effect on the T_g than the aromatic ring in the pendant

group of the prepared homopolymers as the presence of the aromatic ring is likely muted by the methylene spacer. Additionally, the methoxy substituents of the poly(VAEM) and poly(SAEM) have minimal impact on T_g. However, when considering the additional carbon between the polymer backbone and the aromatic ring present in poly(TEM), the T_g of the homopolymer decreases by approximately 20 °C, which is a likely result of the enhanced free rotation in the pendant group [94].

Table 9

Molecular weight and T_gs of prepared homopolymers

Sample	**M_n (Da)**	**M_w (Da)**	***Đ***	***T_g* (°C)**
poly(GMA)	14,300	20,400	1.43	66 ± 1
poly(GDEM)	46,700	152,300	3.26	62 ± 1
poly(VAEM)	52,700	88,500	1.68	60 ± 5
poly(SAEM)	53,000	121,800	2.30	68 ± 1
poly(TEM)	46,900	151,900	3.24	46 ± 1

The thermogravimetric properties of each homopolymer were analyzed using TGA in both inert (N_2) and oxidative (air) atmospheres. The thermograms and first derivates of each polymer tested in N_2 are shown in Figure 31. The thermograms and first derivatives of each polymer tested in air are available in the Appendix D. The IDT, $T_{50\%}$, T_{max}, and char content average values are listed in Table 10 for N_2 (air atmosphere provided in Appendix D).

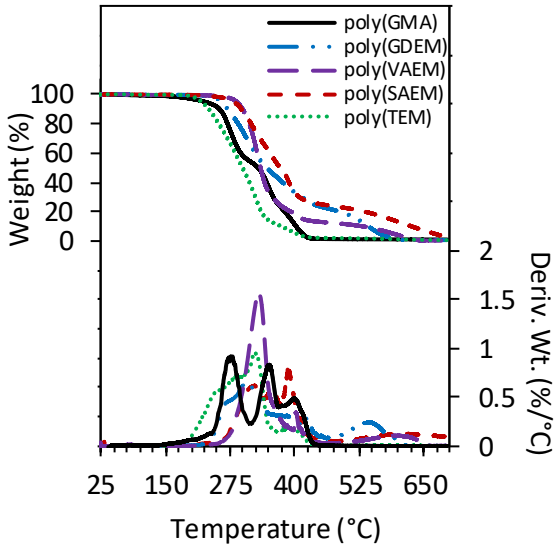

Figure 31. TGA thermograms and the respective first derivatives of the polymers in N_2.

Table 10

Thermogravimetric properties of the epoxy-functional homopolymers in N_2

Sample	IDT (°C)	$T_{50\%}$ (°C)	T_{max} (°C)	Char Content (%)
poly(GMA)	236 ± 11	327 ± 2	278 ± 2	0.7 ± 0.4
poly(GDEM)	261 ± 1	365 ± 6	307 ± 1	0.1 ± 0.1
poly(VAEM)	288 ± 1	335 ± 1	330 ± 1	0.2 ± 0.1
poly(SAEM)	281 ± 2	368 ± 6	388 ± 8	0.3 ± 0.2
poly(TEM)	217 ± 5	294 ± 7	325 ± 1	0.5 ± 0.1

Most of the prepared homopolymers had considerably higher thermal stabilities than poly(GMA). Poly(GDEM), poly(VAEM), and poly(SAEM) had significantly higher IDT values than poly(GMA), likely due to the added aromaticity in the pendant chain enhancing thermal stability [126]. Between poly(GDEM), poly(VAEM), and poly(SAEM), the placement and number of methoxy moieties had minimal effects on

thermal stability; however, the added carbon on the pendant chain of poly(TEM) allows for a higher degree of rotation of the side group, subsequently decreasing the thermal stability to below that of poly(GMA) [94]. The noted decrease in thermal stability of poly(TEM) in direct comparison to poly(GDEM) is consistent with the known trend of increased pendant chain length decreasing thermal stability of linear thermoplastics [127]. Based on the observed trends, the additional free rotation of the alkyl, epoxy terminated pendant group para to the ester moiety on the aromatic ring had a more consequential effect on the thermal properties, in both N_2 and air, than the presence, position, and number of methoxy moieties on the aromatic ring. Similar thermal degradation trends are noted for the $T_{50\%}$ and the T_{max} data, and the char content was similar for all of the homopolymers in both atmospheres. Overall, the thermal behavior of the new thermoplastics indicate similar glass transitions, but improved thermal stability in comparison to poly(GMA), with poly(TEM) being the exception having a lower T_g value and a decreased thermal stability.

Surface energy determines the behavior of coatings on substrates and their interactions with fluids, and comparing surface energies to poly(GMA) is useful for determining the possible applications of the homopolymerized epoxy-methacrylates [118, 128-133]. Static contact angles for DI water and CH_2I_2 were measured for thin films (< 50 nm) prepared by flow coating onto silicon wafers as described above [118, 119]. The relationship between the three-phase contact angle and interfacial interactions is given by Young's equation [134]. Surface energies were calculated using the two-liquid Owens-Wendt model [120]. The surface energies of DI water and CH_2I_2 can be found in the Appendix D. Thickness measurements and contact angle data for each sample after

washing and re-annealing are shown in Table 11. In all cases, the films were not removed by the washing step, indicating the polymers were covalently-bound to the silicon surface. Interestingly, the thicknesses did not decrease significantly after washing for the bio-based polymers, whereas the thickness of the poly(GMA) film decreased substantially (see Appendix D).

Table 11

Film thicknesses and static contact angles of the flow coated polymer samples

Sample[a]	**Film Thickness (nm)**	**Contact Angle Water (°)**	**Contact Angle CH_2I_2 (°)**
poly(GMA)	22.4 ± 1.4	59.8 ± 1.6	32.7 ± 0.2
poly(SAEM)	28.8 ± 0.1	64.3 ± 0.8	31.4 ± 0.2
poly(VAEM)	32.6 ± 1.9	66.1 ± 0.2	24.8 ± 0.6
poly(GDEM)	41.5 ± 0.4	68.3 ± 1.3	25.6 ± 0.8

[a]The surface properties of poly(TEM) were not investigated in detail due to the reduced thermal stability of that material, as determined through the above-mentioned TGA experiments.

Despite the differences in washing behavior, all films exhibited comparable contact angles and surface energies. The DI water contact angles ranged from 59° to 68°, with the prepared homopolymers being slightly more hydrophobic than poly(GMA). Additionally, the CH_2I_2 contact angles were between 25° and 33°, with all prepared homopolymers exhibiting slightly lower contact angles than poly(GMA). The total surface energies, shown in Table 12, are comparable for all films and range from 52.4 mJ/m^2 to 54.4 mJ/m^2; however, the polar and dispersive components of the surface energies differ, with the prepared homopolymers having higher dispersive surface energies and lower polar surface energies in comparison to poly(GMA). Among the

prepared homopolymer films, the polar components appear to be driven by *o*-methoxy content, a trend that is consistent with previous literature, whereas there is no clear trend for the dispersive surface energies [118].

Table 12

Surface energies for each film

Sample	γ_s^D (mJ/m^2)	γ_s^P (mJ/m^2)	γ_s (mJ/m^2)
poly(GMA)	43.1	11.3	54.4
poly(SAEM)	43.7	8.9	52.6
poly(VAEM)	46.2	7.4	53.6
poly(GDEM)	45.9	6.5	52.4

5.4 Conclusions

A synthetic route to prepare aromatic GMA complements from bio-based feedstocks was designed successfully. The functionalization pathway carried out for the production of VAEM, SAEM, GDEM, and TEM can be applied to a multitude of asymmetric phenolic diol and multi-ol compounds, thus enabling the design of a library of GMA complements for a wide variety of applications. Additionally, epoxy-functional homopolymers poly(VAEM), poly(SAEM), poly(GDEM), and poly(TEM) were successfully prepared and were shown to have increased thermal stabilities while retaining similar glass transition and surface properties in comparison to poly(GMA), demonstrating their potential utility in higher-temperature surface coatings applications.

Chapter 6

Vanillin-Based Resin for Additive Manufacturing

Text and figures are reproduced and adapted with permission from A.W. Bassett, A.E. Honnig, C.M. Breyta, I.C. Dunn, J.J. La Scala, and J.F. Stanzione III, "Vanillin-based Resin for Additive Manufacturing," *In preparation,* reference [26].

6.1 Introduction

Additive manufacturing (AM) encompasses a class of manufacturing methods that produce parts layer-by-layer. The concept of AM is the opposite of conventional subtractive manufacturing wherein parts are produced by selectively removing material from a monolithic bulk substance. Building parts layer-by-layer can produce complex geometries that would be, otherwise, difficult to manufacture at industrial scales with conventional manufacturing methods. The removal of typical geometric manufacturing constraints opens the door to a host of new technological developments; e.g., polymeric parts with cellular infills that can be optimized for high strength-to-weight ratios [135]. Other attractive prospects of AM, such as efficient use of material and disruption of conventional supply-chain operations, have been drawing substantial interest from industry, military, and academic communities as of late. Global consumption of AM systems, supplies, and related services amounted to $6 billion (USD) in 2016 and several institutions have predicted annual growth rates in excess of 20% [136-138]. The growth of the AM industry comes with an expected increase in demand for new materials to be developed for AM applications. It is known that the mechanical properties of AM printed parts can be affected by both the unprinted material and the manufacturing method(s) employed [139, 140]. Thus, there is a need to characterize these affects and ascertain that

the performance of AM parts can achieve at least parity with conventionally manufactured parts [141, 142].

Stereolithography (SLA) is an AM method in which layers are formed on a build platform in a vat of liquid photoreactive polymer/resin by directing a UV/visible light laser beam onto the surface of the pool of resin. The laser beam causes localized curing of the resin, forming a part layer. The build platform is moved vertically by a distance equal to the layer thickness, allowing the resin to backfill and a new layer to be cured and bonded to the previous layer [143, 144]. When initially formed, the printed part is not fully cured. Due to this, the printed part is typically subjected to a post-cure process to reach a greater degree of cure [141]. Currently, SLA is capable of producing high resolution parts with layer thicknesses ranging from 25 to 200 microns [138, 143-145]. Mechanical anisotropy as a result of layer-wise fabrication is an issue that plagues AM technologies; however, SLA printed parts have been shown to be effectively isotropic [135, 138, 140].

In order to be used for SLA, a polymer resin must be able to cure sufficiently fast in typical printing conditions. The rate-limiting step in SLA is the time required to scan an entire layer. This typically spans 10-300 seconds; therefore, a resin must cure at relevant layer thicknesses and irradiance on a timescale significantly less than the scanning timescale. More reactive resins that reach their gel-point with less exposure can be printed with a higher laser scanning speed and, thus, reduce overall print time [143]. Resins must also have sufficiently low viscosities in order to be used in SLA. Typical commercial resins for SLA have viscosities ranging from 500-1500 cPs at room temperature [13]. When the build platform is moved between scanning layers, the resin

must backfill and evenly recoat the cured part and the surface being irradiated. Many existing radiation curable resins are viscous enough that the time required for recoating is prohibitively long and must be assisted by a physical recoating mechanism such as a "recoating blade" [143, 144].

Commercial SLA resins are typically (meth)acrylate-based and/or epoxy-based. Acrylate-based resins are favorable due to their high reactivity and rapid cure times; however, the primary disadvantage of acrylates is the tendency to produce parts with poorer accuracy and mechanical properties caused by shrinkage and curling. Epoxy resins exhibit significantly less shrinkage and produce more accurate, harder, and stronger parts. The main disadvantage of epoxy resin systems is slow cure times. As a result, commercial resins for SLA often contain both acrylates and epoxies [141, 146].

The majority of photocurable resin systems are derived from petroleum feedstocks. Petroleum is a finite resource with price volatility and negative environmental impacts. These concerns provide impetus for the development of bio-based photocurable resin systems for use in new and existing applications [146, 147]. The earliest research in bio-based resins for SLA was a result of the desire to develop biocompatible resins for medical applications, such as 3D cellular scaffolds. Such research utilized acrylated oligomers derived from bio-based aliphatic diols and yielded printable structures with low glass transition temperatures (T_gs) and mechanical properties [148-152]. A small amount of academic research has been conducted in adapting plant oil based resins for SLA with the use of acrylated epoxidized soybean oil, glycerol diglycidyl ether, and epoxidized linseed oil [153-156]. These resins have been reported as having prohibitively slow cure times under typical irradiance, high viscosities, and low T_gs when cured.

Despite these drawbacks, modified vegetable oil resins still present attractive prospects for SLA resin systems because of the ability to impart toughness within the cured polymer network. Additional bio-based resin systems have been developed for SLA including bio-based acrylates [157]. For example, Ding et al in 2019 synthesized a natural phenolic based meth(acrylate) and investigated the polymer properties of systems including the synthesized monomer, bio-based crosslinkers and a reactive diluent. The resins were cured in photorheological studies to prove the potential to transition to SLA printing the resins [158]. To our knowledge, there are currently no publications examining SLA printed samples of bio-based resin systems outside those mentioned herein.

Vinyl ester resins (VERs) are a widely-used class of high-performance resins with superior mechanical properties, thermal stability, and chemical resistances [36]. Produced from the esterification of epoxide resins, VERs are unsaturated, thermosetting resins used in the formulation of composites for a wide variety of commercial applications, such as the transportation and construction industries [13]. VERs are composed of vinyl ester monomers and contain reactive diluents, typically styrene, to lower the viscosity for processability. VERs are conventionally thermally cured to produce parts using resin transfer molding [143] and the majority of commercially available VERs are petroleum-based [12].

Significant work has been done towards the development of bio-based VERs. Stanzione et al in 2012 presented a method for the synthesis of a vanillin-based VER [159]. Vanillin, which can be derived from lignin as well as other biomass feedstocks, was identified as a suitable bio-based molecule for use in VERs. The aromatic character

of vanillin imparts structural rigidity and thermal stability on the final polymer network by inhibiting rotational freedom. The synthesis presented in Stanzione et al was a 1 Pot, 2 Step (1P2S) reaction sequence that generated the mono-functional monomer, methacrylated vanillin (MV), and a cross-linking agent, glycerol dimethacrylate (GDM) in a 1:1 mole ratio. The synthesis possessed several desirable sustainable characteristics: (1) the use of renewable reactants, (2) no by-product formation, (3) no solvent, and (4) the use of relatively small quantities of catalyst at moderate reaction temperatures [160]. The addition of a reactive diluent is not necessary as the neat resin has a sufficiently low viscosity at room temperature [159].

Our work described herein demonstrates the transition of the aforementioned vanillin-based resin from conventional manufacturing to AM via SLA. Due to the methacrylate components, low viscosity, and aromatic character, the described resin system has the potential to enable the sustainable production of high-performance printable materials. The suitability for use in SLA was characterized by determining the working curve parameters for the resin as well as the rheological and photorheological properties of the resin. The resin was printed into samples for viscoelastic, thermogravimetric, and mechanical analyses and the effect of post-processing on polymer properties was evaluated.

6.2 Experimental Methods & Procedures

6.2.1 Materials. Vanillin (4-hydroxy-3-methoxybenzyl alcohol, 99%), 4-dimethylaminopyridine (DMAP, 99%), glycidyl methacrylate (GMA, 97%), and chloroform-d_3 for NMR were purchased from Acros Organics. Methacrylic anhydride (94%) was purchased from Alfa Aesar. AMC-2 catalyst was purchased from AMPAC

Fine Chemicals. Diphenyl (2,4,5-trimethylbenzoyl) phosphine oxide (TPO) was purchased from TCI. Isopropyl alcohol (IPA) was purchased from VWR. Compressed nitrogen (N_2, 99.998%) and compressed argon (Ar, 99.999%) were purchased from Airgas. All chemicals purchased were used as received.

6.2.2 Resin synthesis. The resin was synthesized following the one-pot reaction methodology described in Stanzione et. al [159]. In a 3-neck round bottom flask equipped with a magnetic stirring bar, vanillin (75.00 g) and DMAP (1.22 g) were added. The mixture was purged with argon for 10 minutes and then methacrylic anhydride (42.95 g) was added. The reaction mixture was heated to 50-55 °C with continuous stirring. After 24 hours, the reaction mixture was cooled to room temperature and a stoichiometric amount of GMA (70.93 g) was added along with AMC-2 catalyst (0.11 g). The mixture was then heated to 70 °C and monitored via acid number titration until completion (when the free acid number was < 10, corresponding to ~3% acid) [159]. The synthesized VER (1P2S MV-GMA) was comprised of mono-functional monomer, methacrylated vanillin (MV), and crosslinker, glycerol dimethacrylate (GDM) in a 1:1 mole ratio. The complete reaction is shown in Figure 32 and the ^{1}H-NMR spectrum of the resin with peak assignments is provided in the Appendix E.

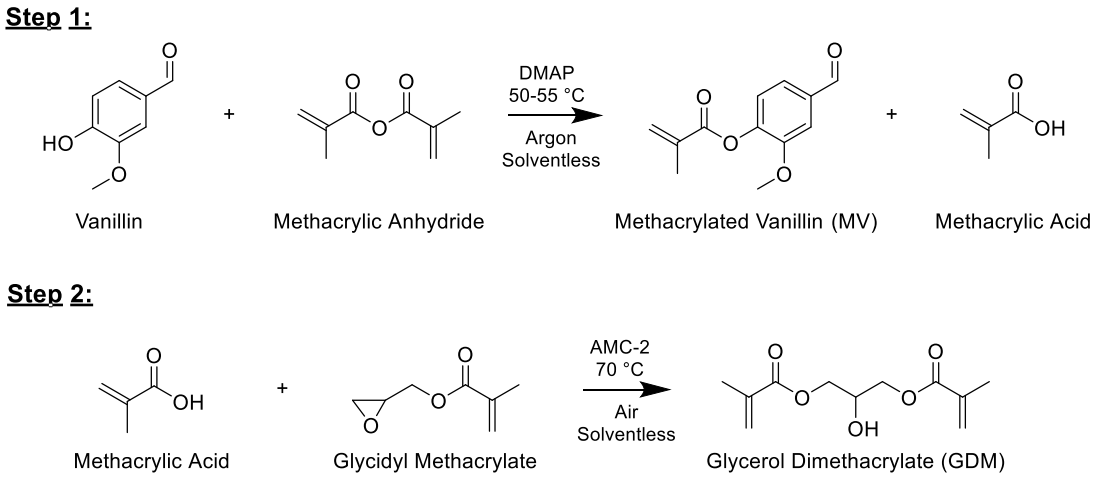

Figure 32. 1P2S MV-GMA reaction scheme.

6.2.3 Resin characterization & photorheology. The synthesized resin was characterized by ^{1}H-NMR (400.15 MHz, 32 scans at 298 K) using a Varian 400 MHz FT-NMR spectrometer. The spectrum is provided in the Appendix E. The viscosity of the resin was obtained using a TA Instruments Discovery Hybrid Rheometer (Discovery HR-2) using a 1° 40 mm cone geometry with the Peltier plate held at a constant 25 °C. The shear rate was ramped logarithmically ascending from 1 to 100 s^{-1} and descending back to 1 s^{-1}. Three measurements were collected per decade to determine the Newtonian behavior or thixotropic properties of the resin [44, 78].

The same Discovery HR-2 was used in conjunction with a UV/Visible light curing accessory (OmiCure Series 2000) to photopolymerize the resin (blended with TPO as the photoinitiator at a loading of 2 wt% of the total resin mass) at room temperature. The light source was filtered to 320-480 nm at an irradiation intensity of 250 mW cm^{-2}. Oscillation and strain of the rheometer was set to 10%. The gel point, or modulus crossover, was recorded in triplicate.

6.2.4 Determination of working curve parameters. The fundamental working curve model for SLA is described in Chapter 2.5 [27]. D_p and E_c are considered the characteristic parameters of an SLA resin. D_p and E_c were estimated for the 1P2S MV-GMA resin by varying resin exposure and measuring the resulting cure depth. Three parts were printed with scanning speeds of 80 mm/s and of 200 mm/s. Confidence intervals on E_c were approximated by assuming the logarithmic distribution is essentially normal.

6.2.5 Resin additive manufacturing. 1P2S MV-GMA was prepared for free radical photopolymerization via SLA by adding TPO as the photoinitiator at 2 wt% of the total resin mass. The resin with the TPO was mixed with a Thinky ARE-310 planetary mixer for 10 minutes and defoamed for 2 minutes. Digital models were prepared for viscoelastic and tensile testing samples (sample geometries and dimensions are provided in the subsequent sections). The models were processed with Formlabs PreForm software to build a scaffold system to support the samples. The final model was uploaded to a Formlabs Form 2 SLA 3D printer. The printing method was set to the preprogrammed "Grey Resin" setting in "Open Mode" with no heating of the resin tank. A layer thickness of 100 μm was selected. After printing, the printed samples were washed with IPA in a Formlabs Form Wash for 20 minutes to remove any unreacted resin. These samples were denoted as 1P2S MV-GMA AM. Additionally, some samples were further post processed in a Formlabs Form Cure (FC) with UV/visible light (λ= 405 nm) and slight heat (80 °C) for 2 hrs. FC samples were denoted as 1P2S MV-GMA AM-FC.

6.2.6 Extent of cure. The extent of cure of the 1P2S MV-GMA AM and 1P2S MV-GMA AM-FC cured resins were determined via near-infrared (near-IR) spectroscopy using a Thermo Scientific Nicolet iS50 FTIR. The uncured resin was

contained in a glass reservoir with a thickness of 3 mm. 32 cumulative scans with a resolution of 2 cm^{-1} were collected. The cured resins had a thickness of 2.5 mm and their near-IR spectra were acquired in the same method as the uncured resins. The methacrylate peak was measured at ~ 6165 cm^{-1} before and after curing and compared to a reference peak at 5900 cm^{-1} which is not affected by the polymerization [78].

6.2.7 Polymer properties. Thermogravimetric analysis was conducted on the 1P2S MV-GMA AM and 1P2S MV-GMA AM-FC cured resins using a TA Instruments Discovery Thermogravimetric Analyzer 550 (TGA). Approximately 10 mg of sample was placed on a platinum pan and heated to 700 °C at a rate of 10 °C min^{-1} in a N_2 atmosphere (40 mL min^{-1} balance gas flow rate and 25 mL min^{-1} sample gas flow rate). This process was repeated in an oxidative (air) environment. Initial decomposition temperature (IDT), temperature at 50 wt% degradation ($T_{50\%}$), temperature at maximum degradation (T_{max}), and char content are reported.

A TA Instruments Q800 dynamic mechanical analyzer (DMA) was used to evaluate the viscoelastic properties of the 1P2S MV-GMA AM and 1P2S MV-GMA AM-FC cured resins. A single cantilever geometry with a frequency of 1.0 Hz, a Poisson's ratio of 0.35 and a deflection amplitude of oscillation equal to 7.5 μm were used. Samples were printed with appropriate dimensions (35 x 12 x 2.5 mm^3 and 35 x 12 x 1.5 mm^3) and tested in accordance with McAninch et al [32]. The heating ramp was 2 °C per minute from 0 °C to 250 °C. The molecular weight between crosslinks, M_c, was estimated using the Theory of Rubber Elasticity [31]. The density of each sample was calculated using Archimedes' principle [5, 161, 162].

Mechanical properties of 1P2S MV-GMA AM and 1P2S MV-GMA AM-FC cured resins were evaluated via tensile testing. Tensile testing was conducted using an Instron 5966 with a 1 kN load cell and a crosshead speed of 1 mm min^{-1}. Type IV samples were printed such that the printed layers are parallel to the direction of the crosshead movement and analyzed according to ASTM D638 [157]. Support structures on the tensile samples were carefully removed via cutting tools followed by wet sanding to limit the possibility of the supports to impart failure sites in the bulk specimen.

6.3 Results and Discussion

6.3.1 Rheology. The viscosity of the synthesized, uncured resin, 1P2S MV-GMA, was measured to be 99 ± 1 cP at a constant 25 °C and Newtonian behavior was observed, similar to what was reported previously [159]. The viscosity was determined using the average of three steady state points at different shear rates. The relatively low viscosity resulted from low interactions between resin monomers and low molecular weights of the monomers. Low viscosities are desirable for SLA printing to allow for the surface of the resin tank to be recoated between layer additions and movement of the build platform. Viscosities under 3000 cP at room temperature have shown success with producing high resolution objects in rapid prototyping techniques [163-165]. Thus, this resin meets viscosity requirements for rapid prototyping, in general, and SLA.

The photopolymerization characteristics of the resin were evaluated with a rheometer and light attachment. The viscoelastic properties of the resin were tracked as it cured via free radical light-initiated polymerization. By tracking the shear storage modulus (G'), shear loss modulus (G''), and the complex viscosity (η), the point at which polymerization occurred can be discerned using the gel point time. The gel point, also

known as the modulus crossover, occurred when G'' crossed G' indicating the formation of a polymer network [166]. Figure 33 shows the gel point (modulus crossover), shear storage and loss moduli and complex viscosity of the 1P2S MV-GMA resin as the sample cures via light polymerization.

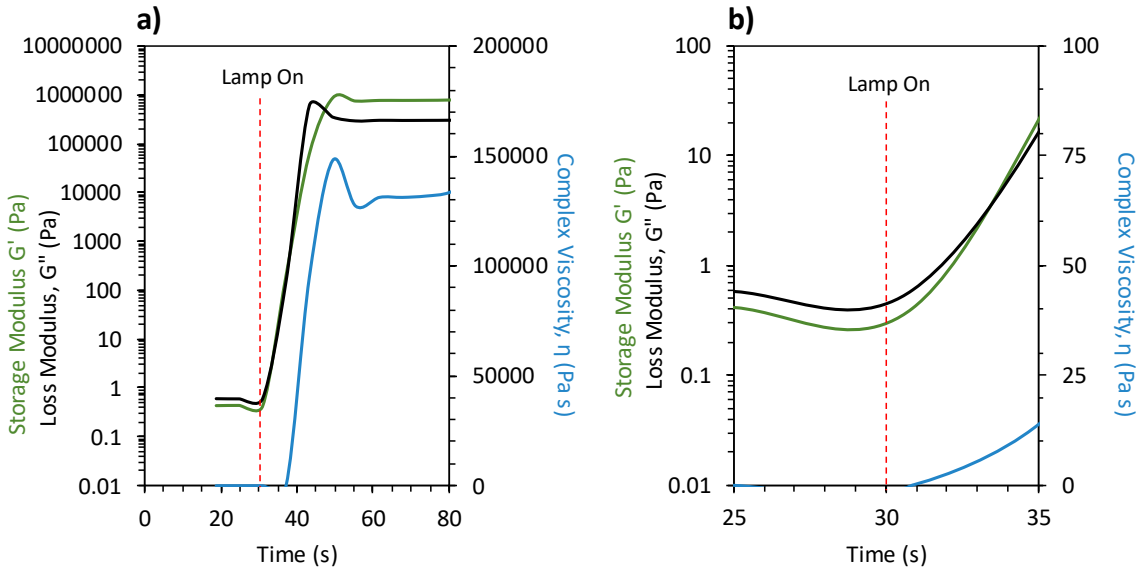

Figure 33. a) Shear storage and loss moduli and the complex viscosity for the 1P2S MV-GMA resin during photorheology and b) Zoomed shear storage and loss moduli and the complex viscosity for the 1P2S MV-GMA resin at modulus crossover. Light turns on at 30 s.

The gel point of 1P2S MV-GMA occurred 2.18 ± 0.69 s after the lamp turned on using an irradiation of 250 mW cm^{-2} and a sample thickness of 1000 μm. A gel time of approximately 2 s could be used in a conventional 3D printer. However, a typical SLA printer uses a higher irradiance and a smaller layer thickness than what was used for photorheology. The actual cure time on an SLA printer would be less than the representative cure time found. The quick polymerization after contact with light is a

strong indication the resin would cure quickly in an SLA printer and could be suitable for rapid prototyping [167]. After the gel point, the moduli and viscosity increase to a peak before reaching a steady state, likely due to hysteresis as a result of rapid vitrification of the polymer network [168].

6.3.2 Working curve parameters. The working curve parameters E_c and D_p were estimated by OLS regression of cure depth (C_d) against the natural logarithm of E_{max}. The fit of the working curve model with the estimated parameters is shown in Figure 34. Parameter estimations and variances are presented in Table 13.

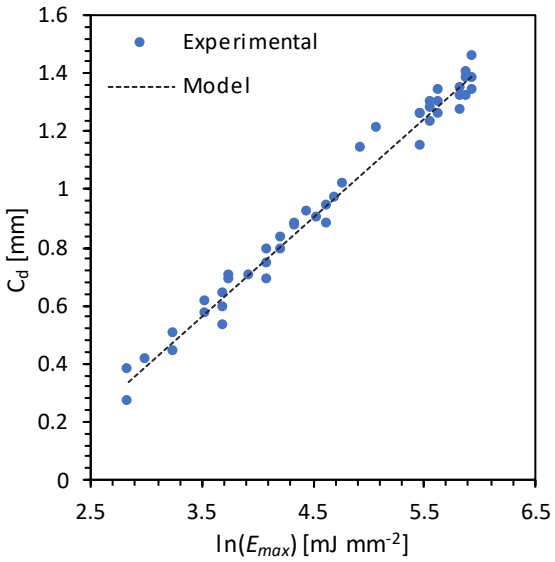

Figure 34. Comparison of OLS model and observed data points.

Table 13

Working Curve Parameter Estimates

Parameter	Mean	Standard Deviation	95% CI
$E_c \left(\frac{mJ}{mm^2}\right)$	1.87	0.07	1.74 - 1.99
$D_p\ (mm)$	0.34	0.007	0.32 - 0.35
R^2	0.981		

The working curve model is in good agreement with the data collected as indicated by an R^2 value of 0.981. The E_c value determined is comparable to that found in other resin formulations [169]. However, it is important to note that the 1P2S MV-GMA resin does not contain any photo-blockers, which could be used to reduce the sensitivity of the resin to light. Additionally, the 1P2S MV-GMA resin is comprised of two low molecular weight methacrylates; thus, causing the overall reactive (methacrylate) concentration to be high. This is also observed on the D_p, where the 1P2S MV-GMA resin has a higher D_p than that of other commercial based resin formulations, such as PR48 which has a D_p of 0.105 mm, due to the absence of photo-blockers [169]. Nevertheless, and if desired, the 1P2S MV-GMA resin has the potential to be combined with photo-blocking agents and other higher molecular weight additives, due to its very low viscosity, to tune the curing parameters.

6.3.3 Extent of cure. Near-IR was used to obtain the extent of cure for the synthesized 1P2S MV-GMA resin before and after FC for a layer thickness of 100 µm.

Figure 35 shows representative near-IR spectra of the cured resins as well as the uncured resin.

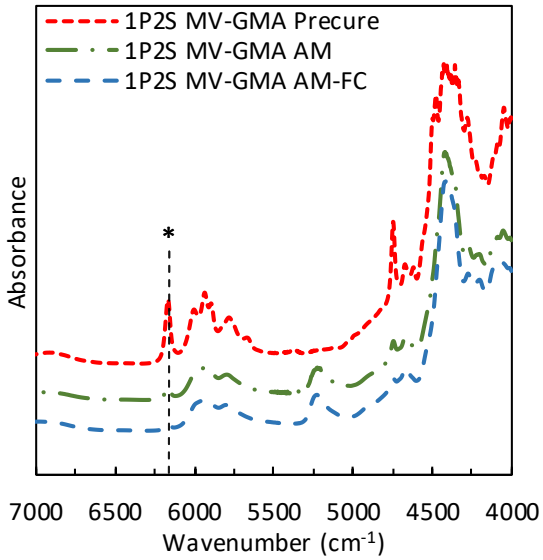

Figure 35. Near-IR spectra of 1P2S MV-GMA Resin, AM and AM-FC. Methacrylate (*) absorption is indicated. Spectra are offset vertically for clarity.

The polymerizable groups are the methacrylate groups of GDM and MV. These groups have an absorbance at 6165 cm^{-1}. The ratio between the methacrylate peak before and after cure steps were compared to a stagnant (unreactive) control peak (5900 cm^{-1}) to calculate the extent of cure percentage. At a 100 µm layer thickness, 1P2S MV-GMA AM had an extent of cure of 66 ± 0.2 %. With the FC, the extent of cure increased to 89 ± 1.5 % (for 1P2S MV-GMA AM-FC). The FC acted as a traditional post cure to increase the extent of cure of the polymer network. FC requires less heat than traditional thermal cures and incorporates UV light around the printed parts [36, 170]. Interestingly, the extent of cure values obtained via AM with the addition of the FC post processing step are significantly higher than that of traditional thermal curing of the same resin. Previous

work shows that thermal cure in an inert atmosphere (90 °C for 4 hours) and post cure (130 °C for 2 hours) using a thermal initiator with the same resin only achieves extents of cure after postcure of approximately 78%, which is approximately 10% lower than that of what was found via AM-FC. Thus, demonstrating that the AM process can yield materials with high extents of cure without needing high temperature postcures [159].

6.3.4 Polymer properties. The resulting AM polymers were hard, glassy, dull yellow samples. FC samples experienced slight oxidation and were brown-tinted and yellow in color. Thermal degradation of the 1P2S MV-GMA AM and 1P2S MV-GMA AM-FC was analyzed. A representative thermogram is shown in Figure 36, with the derivative of the weight percent. The IDT, $T_{50\%}$, T_{max}, and char content values are shown in Table 14.

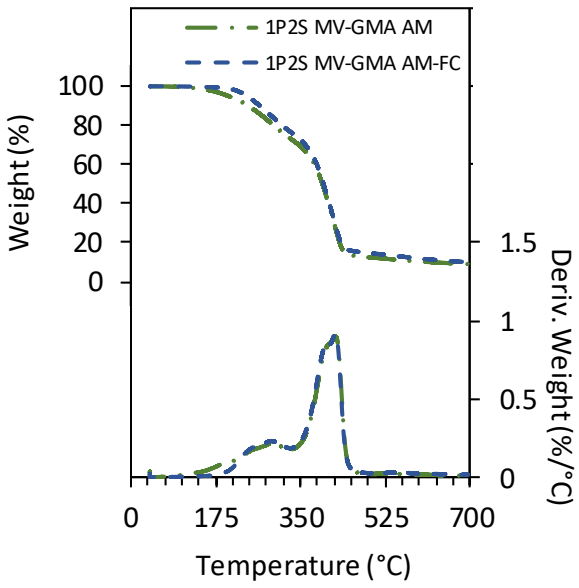

Figure 36. TGA thermograms and their respective 1st derivatives of the 1P2S MV-GMA AM and 1P2S MV-GMA AM-FC cured samples in N_2.

Table 14

Thermogravimetric results for the 1P2S MV-GMA AM and 1P2S MV-GMA AM-FC in N_2

System	IDT (°C)	$T_{50\%}$ (°C)	T_{max} (°C)	Char Content (%)
1P2S MV-GMA AM	204 ± 4	396 ± 1	423 ± 1	9.0 ± 0.1
1P2S MV-GMA AM-FC	240 ± 1	397 ± 1	421 ± 1	9.7 ± 0.1

1P2S MV-GMA AM showed a lower IDT of 204 °C compared to the IDT of 1P2S MV-GMA AM-FC, 240 °C. The increase in IDT upon FC is a result of increasing the extent of cure. For the light cured only samples, unpolymerized molecules degrade before the linked polymer chains causing the lower degradation temperature [171]. The data from the oxidative environment exhibited similar trends, where a lower extent of cure correlated to the lower IDT. Oxidative environment data can be found in the Appendix E. 1P2S MV-GMA AM and 1P2S MV-GMA AM-FC have $T_{50\%}$ and T_{max} values that were within error of each other as seen in Table 14. These samples exhibited similar $T_{50\%}$ and T_{max} values compared to Vinyl Ester 828 with 35 wt% styrene, an industry standard that is traditionally used to produce high performance polymer composites and that is typically processed via resin molding techniques, often times with heat ($T_{50\%}$ = 403 °C and T_{max} = 401 °C) [36]. Additionally, 1P2S MV-GMA AM-FC has comparable thermogravimetric properties to the same resin which was thermally cured, despite the difference in extent of cure between the two curing techniques [159]. In an oxidative environment, any char produced combusts and subsequently generates a second degradation trace [172]. The resulting char content is less than the char content in an N_2 environment.

Viscoelastic properties were obtained using DMA. Figure 37 shows representative thermograms for the storage modulus (*E′*) and the loss modulus (*E″*). The measurement of the energy stored during deformation is the storage modulus and represents the elastic behavior of the polymer, while the loss modulus is the measurement of the heat dissipated as energy during deformation and represents the viscous behavior [78]. Figure 38 shows the tan δ thermograms. Table 15 includes the thermomechanical data for 1P2S MV-GMA AM and 1P2S MV-GMA AM-FC.

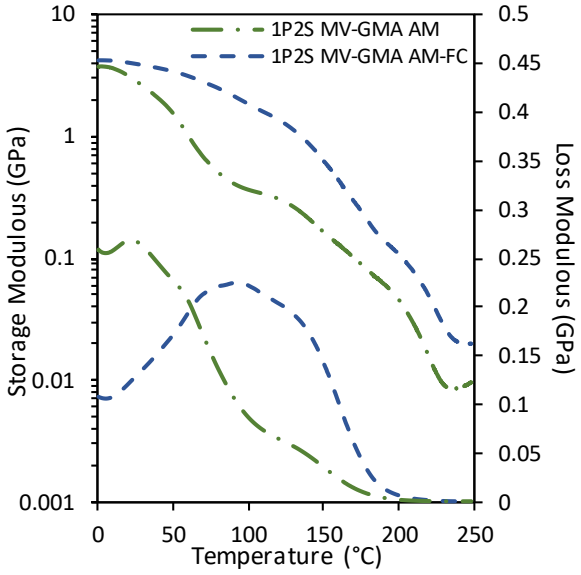

Figure 37. DMA thermograms of *E′* and *E″* of 1P2S MV-GMA AM and 1P2S MV-GMA AM-FC.

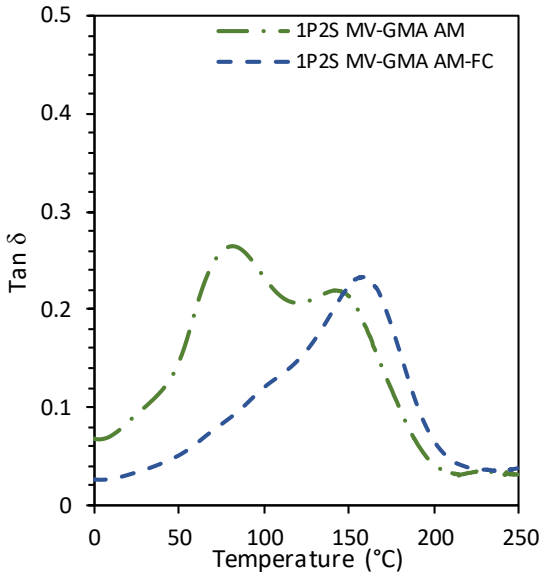

Figure 38. Tan δ thermograms of 1P2S MV-GMA AM and 1P2S MV-GMA AM-FC.

Table 15

Viscoelastic properties of 1P2S MV-GMA AM and 1P2S MV-GMA AM-FC

Sample	**E′ @ 25 °C (GPa)**	**Peak of E″ (°C)**	**Peak of Tan δ (°C)**	**M_c (g mol $^{-1}$)**	**ρ @ 25 °C (g cm^{-3})**
1P2S MV-GMA AM	2.5 ± 0.3	16 ± 4	80 ± 2	4159 ± 1784	1.273 ± 0.006
1P2S MV-GMA AM-FC	3.8 ± 0.3	72 ± 12	153 ± 4	1536 ± 498	1.283 ± 0.001

1P2S MV-GMA AM-FC had the highest *E′* of 3.8 GPa at 25 °C which is comparably higher to commercially available Vinyl Ester 828 with 35 wt% styrene (2.8 GPa at 25 °C) [36]. 1P2S MV-GMA AM had a lower *E′* (2.5 GPa at 25 °C) resulting from the lower extent of cure of 66%. *E′* is dependent on the packing of the polymer chains. At lower extents of cure, the unreacted molecules act as plasticizers. Additionally,

lower extents of cure result in lower crosslink densities; thus, facilitating easier polymer deformation [94, 173, 174].

The peak of E'' and the peak of tan δ were both used to estimate the T_g or the temperature at which the polymer goes from a rigid state to a more flexible and rubbery state. Traditionally, the peak of E'' gives a more conservative value for the T_g while the peak of the tan δ provides an upper limit value [44]. 1P2S MV-GMA AM-FC had the highest T_g values of 72 °C and 153 °C based on the peak of E'' and the peak of tan δ, respectively. The low extent of cure for 1P2S MV-GMA AM was attributed to the lower T_g values. The unreacted monomers act as matrix plasticizers in the network decreasing the T_g of the formed network [175, 176]. The T_g value of 1P2S MV-GMA AM-FC based on the peak of tan δ was similar to that of commercially available high performance VERs [36]. Furthermore, the T_g values of 1P2S MV-GMA AM-FC based on the peak of E'' is approximately 10 °C higher, while the peak of the tan δ is approximately identical, to that achieved from the same resin which was cured thermally, indicating that the processing techniques had minimal effect on the final T_g [159, 177].

The width of the tan δ peak is associated with the heterogeneity of the polymer network. A broader peak indicates a more heterogeneous network and a wider distribution of relaxation modes. The Twinkling Fractal Theory can be used to further describe the distribution of relaxation modes as an increase in relaxation modes will cause an increase in the solid fractals that will twinkle into the liquid upon heating [93, 178-180]. The peaks of tan δ for 1P2S MV-GMA AM and 1P2S MV-GMA AM-FC are broad and represent the creation of highly crosslinked, heterogenous networks with broad relaxation modes and twinkling solid fractals [93]. Two T_g regions typically appear when

a thermoset is under cured, and this is shown in the tan δ thermogram for 1P2S MV-GMA AM. A second peak becomes more prominent and/or the sole peak once enough chain mobility has been reached and the polymer starts to polymerize again [181-186].

M_c was calculated using the Theory of Rubber Elasticity and is shown in Table 15. The Theory of Rubber Elasticity was derived for branched and lightly crosslinked polymer networks; however, literature has shown that it can be applied to highly crosslinked polymer networks as well [31]. The addition of FC decreased the M_c due to the formation of a more complete polymer network, as indicated by the higher extent of cure. In addition, the decrease in M_c for 1P2S MV-GMA AM-FC was attributed to the increase in T_g [187]. Interestingly, the M_c of the same resin with traditional thermal curing has been shown to be 825 g mol^{-1}, which is approximately half of that of what was achieved via AM-FC [159]. Typically, lower M_c values closer to the theoretical M_c (224.22 g mol^{-1} in this case) indicate the material is cured to a higher degree, yet based on our observations the opposite occurs; however, more likely is that different polymerization methods could be forming thermosets with vastly different interconnectivity, although the overall thermomechanical polymer properties seem to be largely unaffected. We hypothesize that the AM-FC material may, in fact, be more heterogenous than the thermally cured material even though the breadth of the tan δ peaks are observed to be similar. Because the 1P2S MV-GMA resin has one aromatic monomer and one aliphatic monomer, we speculate that the aromatic monomer (MV) may be absorbing enough of the light such that it inhibits the polymerization of the MV monomer to a slight degree; thus, potentially yielding a less random formation of the polymer network as indicated by the higher value of M_c.

Tensile testing was conducted to determine the effects of FC on the mechanical properties of the polymers. Figure 39 shows a representative stress-strain curve for 1P2S MV-GMA AM and 1P2S MV-GMA AM-FC samples. All samples showed linear behavior until the point of break and were deemed brittle. Table 16 shows the data for the mechanical properties for 1P2S MV-GMA AM and 1P2S MV-GMA AM-FC.

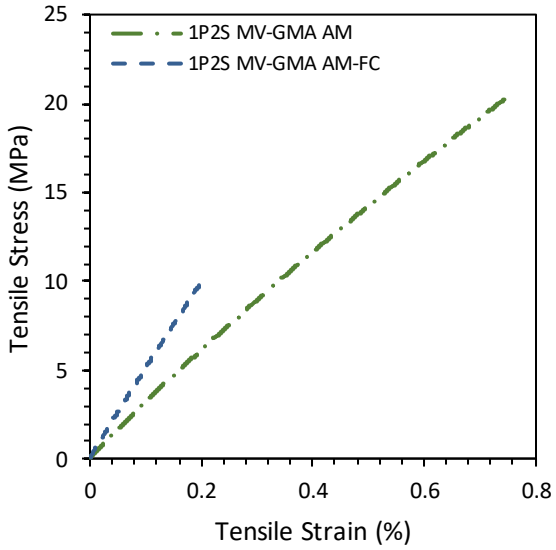

Figure 39. Stress-strain curves of 1P2S MV-GMA AM and 1P2S MV-GMA AM-FC.

Table 16

Tensile testing values of 1P2S MV-GMA AM and 1P2S MV-GMA AM-FC

Sample	Energy at Max Force (J)	Young's Modulus (MPa)	Force at Break (kN)	Tensile Strain at Break (%)	Tensile Stress at Break (MPa)
1P2S MV-GMA AM	0.084 ± 0.023	2920 ± 149	0.74 ± 0.11	0.83 ± 0.10	20.27 ± 2.24
1P2S MV-GMA AM-FC	0.013 ± 0.003	4903 ± 120	0.35 ± 0.04	0.27 ± 0.05	12.49 ± 1.63

1P2S MV-GMA AM-FC had a higher slope than 1P2S MV-GMA AM as shown in Figure 39. The slope of the stress-strain curve relates to the Young's modulus, which is a measure of the stiffness of the polymer. 1P2S MV-GMA AM-FC had a Young's modulus of 4,900 MPa compared to 2,920 MPa for 1P2S MV-GMA AM. Young's modulus is known to have a direct correlation with the overall monomer structure, degree of crosslinking, as well as M_c [188-190]. Generally, as M_c is decreased and the degree of crosslinking is increased, an overall increased Young's modulus is expected [191-193]. With the 1P2S MV-GMA resin, 50 mol% of the resin system is comprised of a short, aliphatic crosslinker that provides minimal flexibility due to its chemical structure. Since there are stoichiometric quantities of low molecular weight crosslinker to monofunctional monomer (MV), the crosslink density is effectively increased substantially over conventional epoxy resins. Additionally, the hydroxyl substituent on the crosslinker is known to hydrogen bond with the methoxy moiety at room temperature which, in this case, are of equal molar concentration, thus leading to the extraordinarily high Young's modulus [77]. Yet, the high degree of crosslinking led to the embrittlement of the material as shown by the reduction in the energy at maximum force, force at break, and tensile stress as there are little to no excess unreacted monomers acting as matrix plasticizers [194-198].

6.4 Conclusions

A low viscosity, vanillin-based resin was prepared via a 100% atom efficient and solventless technique. The vanillin-based resin was evaluated for its photocure parameters and additively manufactured using stereolithography (SLA). The effect of post-processing after print was evaluated, whereby post processing is shown to increase

the overall extent of cure by 23%, subsequently increasing the final cured polymer properties. Additive manufacturing with post-processing was shown to have a 10% increase in extent of cure compared to the same material that was thermally cured and subsequently post cured, yet the thermogravimetric and thermomechanical properties are minimally affected. The vanillin-based resin prepared via SLA with post-processing is shown to have a T_g of 153 °C (based on the peak of tan δ) and Young's modulus of 4,900 MPa, demonstrating the potential for the resin to be used as a standalone high T_g and high strength material for SLA. Due to the low viscosity and low critical energy of cure, the vanillin-based resin also has potential to be used as a component in the development of bio-based, high T_g, high strength materials for SLA.

Chapter 7

CNSL-Isosorbide-Lignin Derived (Formulated Hybrid) Resins for Additive Manufacturing

7.1 Introduction

While Chapters 3 and 4 focused on a molecularly hybrid approach towards developing performance advantaged materials and Chapter 6 focused on the development of a vanillin-based resin for AM, Chapter 7 adopts the formulation hybrid approach as discussed in Chapter 1 to explore the effect of combining the unique molecular structures of bio-based materials from different feedstocks for stereolithography (SLA). Individual feedstocks offer unique attributes that can address specific performance needs, depending on the intended application; yet, the majority of applications typically require that several performance characteristics be fulfilled simultaneously.

Lignin is an abundant, natural resource with a complex, three dimensional, substituted polyphenol structure [57-59]. Lignin, a waste product of the paper and pulp industry, accounts for up to 18-35% by weight of wood with an annual production of up to 50 million tons [60, 62, 77]. Due to the high aromatic content of lignin, lignin depolymerization has gained significant interest. Ongoing research has shown that the strategic depolymerization of lignin can result in a variety of aromatics and phenolics that can be more easily processed [63, 64]. Previous studies have demonstrated that lignin-based methacrylates are suitable replacements for styrene, a volatile organic compound (VOC) and hazardous air pollutant (HAP), in commercial, petroleum-derived vinyl ester resins (VERs) [78].

Cardanol, derived from cashew nutshell liquid (CNSL), is a non-edible byproduct of the cashew production industry with a unique phenolic structure bearing a saturated and/or unsaturated carbon chain [55, 72, 73]. CNSL makes up approximately one third of the total cashew nut weight; therefore, CNSL is largely available as a byproduct of the mechanical process of removing the cashew kernel from the shell [11]. CNSL can be extracted from the largely available, and otherwise unused, shell of the cashew nut at a relatively low cost [54]. Production of crude CNSL approaches 1 million tons annually as a mixture of different unsaturated long-chain phenols with up to three unsaturation points. The aliphatic chain of cardanol can have double bonds in positions (8), (8, 11), or (8, 11, 14) with an average number of two alkyl double bonds per molecule [54, 55, 74]. The phenolic lipid structure of cardanol provides the flexibility to create monomers with unique properties to impart both water and thermal resistance into polymeric materials [18, 75, 76]. The phenolic lipid structure of cardanol has shown promise in the development of VERs [11, 54, 55]. Cardanol-based vinyl esters have exhibited reduced viscosities relative to BPA-based VE828, improving processability; however, depending on the ultimate formulation, comparable T_gs to commercial VERs have been difficult to obtain from modified cardanols [11, 17, 18].

Previous studies have identified isosorbide as a potential building block for VERs. Derived from the hydrolysis of glucose, the fused bicyclic structure of isosorbide, which bears chiral diols, has been shown to provide structural integrity and thermal stability when used in thermosetting resins [44-47]. Isosorbide dimethacrylate (IM) is a low viscosity resin that could be cured with or without a reactive diluent. The cured resin

containing neat IM resulted in a thermoset with a T_g of approximately 245 °C, the highest known T_g for a VER system [44].

This chapter details the combination of building blocks from lignin, CNSL, and carbohydrates for thermosetting, SLA materials. The one-pot reaction synthesis route detailed in Chapter 6 was employed using starting, bio-based materials phenol (potentially lignin-derived) and NC-514s, a commercially available CNSL-based epoxy resin. The one-pot reaction synthesis scheme was performed to prepare a resin containing phenyl methacrylate (PM), and NC-514sVE in a 1 to 0.5 mole ratio. Due to the aliphatic nature of CNSL derived materials, it is to be expected that the T_g of the PM-NC514sVE system would be low. Therefore, IM was formulated in amounts of 10 wt% and 20 wt% in an effort to take advantage of the chemical structure of IM to significantly enhance T_g while attempting to maintain the flexibility and toughness provided by the CNSL-derived NC514sVE. The rheological and photocure properties of the resin formulations as well as the thermogravimetric, thermomechanical, tensile, and fracture toughness properties of the SLA printed, post-processed polymers were evaluated to determine the effect of combining unique structures, with their own different performance attributes, on the properties of cured thermosetting VERs.

7.2 Experimental Methods & Procedures

7.2.1 Materials. Phenol (99%), 4-dimethylaminopyridine (DMAP, 99%), and chloroform-d_3 for NMR were purchased from Acros Organics. Methacrylic anhydride (94%) was purchased from Alfa Aesar. AMC-2 catalyst was purchased from AMPAC Fine Chemicals. Diphenyl (2,4,5-trimethylbenzoyl) phosphine oxide (TPO) was purchased from TCI. Isopropyl alcohol (IPA) was purchased from VWR. Compressed

nitrogen (N2, 99.998%) and compressed argon (Ar, 99.999%) were purchased from Airgas. NC-514s was provided by Cardolite Corporation. IM was prepared as described in literature [44]. All chemicals purchased were used as received.

7.2.2 Resin synthesis. The resin was synthesized following the one-pot reaction methodology described Chapter 6. In a three-neck round bottom flask equipped with a mechanical mixer, phenol (50.00 g) and DMAP (3.28 g) were added. The mixture was purged with argon for 10 minutes and then methacrylic anhydride (82.73 g) was added. The reaction mixture was heated to 50-55 °C with continuous stirring. After 24 hours, the reaction mixture was cooled to room temperature and NC-514s (224.47 g) was added along with AMC-2 catalyst (0.27 g). The mixture was then heated to 70 °C and monitored via acid number titration until completion (when the free acid number was < 10, corresponding to ~3% acid) [159]. The synthesized resin (1P2S PM-NC514sVE) was comprised of mono-functional monomer, phenyl methacrylate (PM), and crosslinker, NC514sVE in a 1:0.5 mole ratio. The complete reaction is shown in Figure 40 and the ^{1}H-NMR spectrum of the resin with peak assignments is provided in Appendix F.

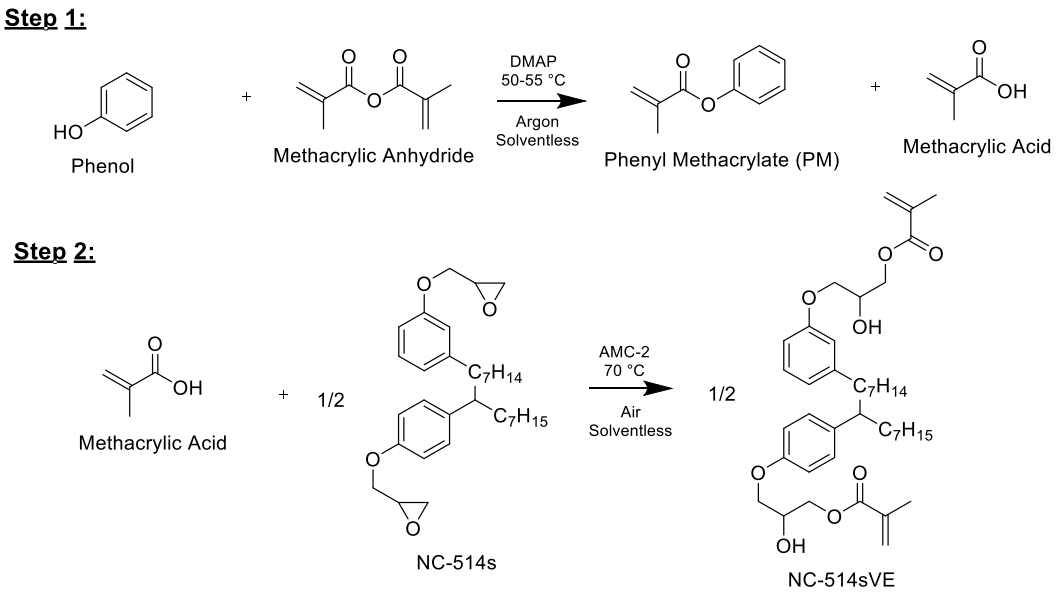

Figure 40. 1P2S PM-NC514sVE reaction scheme.

The PM-NC514sVE resin was utilized as a standalone resin and also blended with both 10 wt% and 20 wt% IM (Figure 41) to determine the effect of increasing IM content on resin properties.

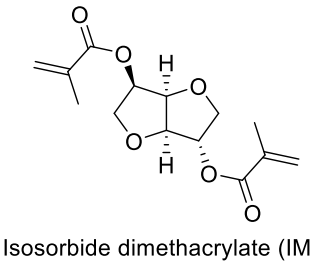

Figure 41. Structure of isosorbide dimethacrylate.

7.2.3 Resin characterization & photorheology. The synthesized resin was characterized by ^{1}H-NMR (400.15 MHz, 32 scans at 298 K) using a Varian 400 MHz FT-NMR spectrometer. The viscosity of the resin was obtained using a TA Instruments Discovery Hybrid Rheometer (Discovery HR-2) using a 1° 40 mm cone geometry with

the Peltier plate held at a constant 25 °C. The shear rate was ramped logarithmically ascending from 1 to 100 s^{-1} and descending back to 1 s^{-1}. Three measurements were collected per decade to determine the Newtonian behavior or thixotropic properties [44, 78].

The same TA Instruments Discovery HR-2 instrument was used with a UV/Visible light curing accessory (OmiCure Series 2000) to photopolymerize the resin (blended with TPO as the photoinitiator at a loading of 2 wt% of the total resin mass) at room temperature. The light source was filtered to 320-480 nm at an irradiation intensity of 250 mW cm^{-2}. Oscillation and strain of the rheometer were set to 10%. The gel point, or modulus crossover, was recorded in triplicate.

7.2.4 Determination of working curve parameters. The determination of fundamental working curve model for SLA is described in Chapter 2.5. In brief, the working curve parameters were estimated for the resins by varying resin exposure and measuring the resulting cure depth and were estimated by ordinary least squares (OLS) regression of cure depth (C_d) against the maximum exposure on the surface of the resin [$\ln(E_{max})$] as described in Chapter 2.5.

7.2.5 Resin additive manufacturing. All resins were prepared for free radical photopolymerization via SLA by adding TPO as the photoinitiator at 2 wt% of the total resin mass. The resin with the TPO was mixed with a Thinky ARE-310 planetary mixer for 10 minutes and defoamed for 2 minutes. Digital models were prepared for viscoelastic, tensile, and fracture testing. The resin was printed on a Formlabs Form 2 SLA 3D printer. The printing method was set to the preprogrammed “Tough Resin” setting in “Open Mode” with no heating of the resin tank. A layer thickness of 100 μm

was selected. After printing, the printed samples were washed with IPA in a Formlabs Form Wash for 20 minutes to remove any unreacted resin and further post processed in a Formlabs Form Cure (FC) with UV/visible light (λ= 405 nm) and slight heat (80 °C) for 2 hrs.

7.2.6 Extent of cure. The extents of cure were determined via near-infrared (near-IR) spectroscopy using a Thermo Scientific Nicolet iS50 FTIR. The uncured resin was contained in a glass reservoir with a thickness of 3 mm. 32 cumulative scans with a resolution of 2 cm^{-1} were collected. The cured resins had a thickness of 2.5 mm and their near-IR spectra were acquired in the same method as the uncured resins. The methacrylate peak was measured at ~ 6165 cm^{-1} before and after curing and compared to a reference peak at 5900 cm^{-1}, which is not affected by the polymerization [78].

7.2.7 Polymer properties. Thermogravimetric analysis was conducted on the cured resins using a TA Instruments Discovery Thermogravimetric Analyzer 550 (TGA). 10 mg of sample was placed on a platinum pan and heated to 700 °C at a rate of 10 °C min^{-1} in either a N_2 or oxidative (air) atmosphere (40 mL min^{-1} balance gas flow rate and 25 mL min^{-1} sample gas flow rate). Initial decomposition temperature (IDT), temperature at 50 wt% degradation ($T_{50\%}$), temperature at maximum degradation (T_{max}), and char content are reported.

A TA Instruments Q800 dynamic mechanical analyzer (DMA) was used to evaluate the viscoelastic properties of the cured resins. A single cantilever geometry with a frequency of 1.0 Hz, a Poisson's ratio of 0.35 and a deflection amplitude of oscillation equal to 7.5 μm were used. Samples were printed with appropriate dimensions (35 x 12 x 2.5 mm^3 and 35 x 12 x 1.5 mm^3) and tested in accordance with McAninch et al [32]. The

heating ramp was 2 °C per minute from -50 °C to 250 °C. The molecular weight between crosslinks, M_c, was estimated using the Theory of Rubber Elasticity. The density of each sample was calculated using Archimedes' principle [5, 161, 162].

Mechanical properties of the cured resins were evaluated via tensile testing and fracture toughness. Tensile testing was conducted using an Instron 5966 with a 10 kN load cell and a crosshead speed of 1 mm min^{-1}. Type IV samples were printed such that the printed layers were parallel to the direction of the crosshead movement and analyzed according to ASTM D638 [157]. Fracture toughness was performed in accordance with ASTM D5045 at room temperature. Three-point single edge notched bend (SENB) samples were printed such that the printed layers were perpendicular to the direction of the crosshead. Samples were prepared to be 44 x 10 x 4 mm^3 to ensure plane-strain. Using a diamond saw, samples were notched and then tapped using a single edged razor blade in order to "instantly propagate" a crack. Samples were tested on an Instron 5966 equipped with a 1 kN load cell and a 3-point bend flexure fixture at a crosshead speed of 10 mm min^{-1}. The plane-strain fracture toughness, K_{1C}, and the critical strain energy release rate, G_{1C}, were determined upon fracture [34]. Five replicates of each cured system were prepared and tested.

7.3 Results and Discussion

7.3.1 Rheology. To determine the feasibility of the bio-based resins for SLA, viscosities of the resin formulations were obtained, and the results are shown in Figure 42 and Table 17. The viscosity was determined using the average of three steady state points at varying shear rates. All resin blends exhibited Newtonian behavior. In order for a resin to be processed via SLA, viscosities under 3000 cP at room temperature are generally

recommended [163-165]. Therefore, the resin blends meet viscosity requirements for SLA. In general, the viscosity of the resin system decreased as the concentration of IM increased. This is due to the IM, which has a viscosity on its own of approximately 157 cP at room temperature, acting as a diluent [44]. The viscosities experimentally determined are expected based on a logarithmic simple rule of mixtures of the individual viscosities of the 1P2S PM-NC514sVE (PM: 3.1 cP and NC514s: 2.9 x 10^7 cP) and IM [78].

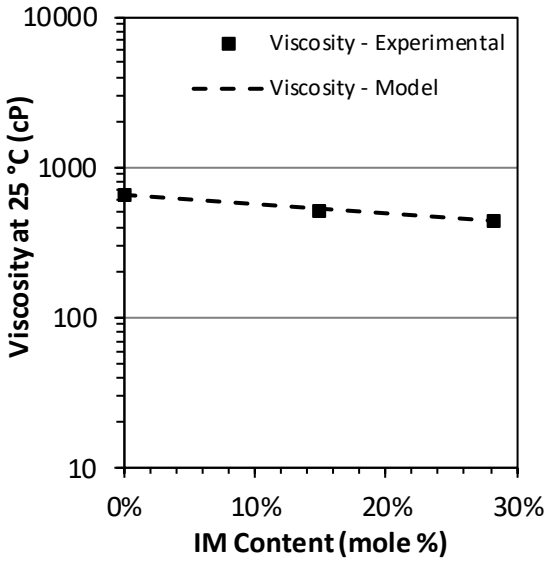

Figure 42. Viscosity of 1P2S PM-NC514sVE with varying IM content.

Table 17

Viscosity at room temperature for 1P2S PM-NC514sVE with varying IM weight percent

Sample	Viscosity at 25°C (cP)
1P2S PM NC514sVE 0% IM	651 ± 25
1P2S PM NC514sVE 10% IM	501 ± 15
1P2S PM NC514sVE 20% IM	436 ± 5

7.3.2 Working curve parameters. The working curve parameters, E_c (the exposure per unit area required for the resin to reach its gel point) and D_p (the depth at which the irradiance is 13.5% of the irradiance at the interface where the laser contacts the resin), were estimated by OLS regression of cure depth against the natural logarithm of E_{max}. The fit of the working curve model for 1P2S PM-NC514sVE 20% IM with the estimated parameters is shown in Figure 43. The models for the other two resin systems are provided in Appendix F. Parameter estimations for all resin systems are provided in Table 18.

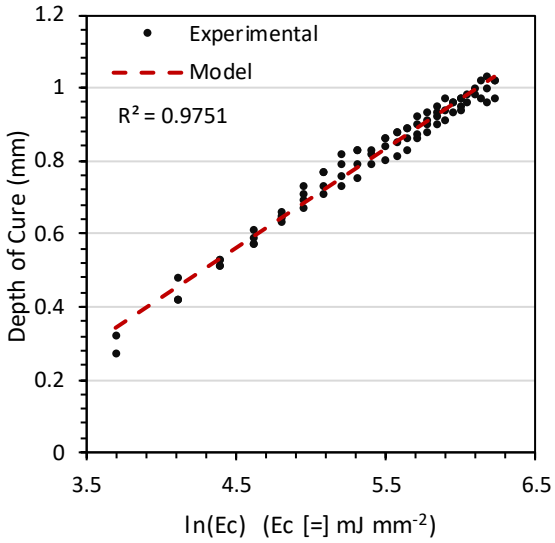

Figure 43. Working curve for 1P2S PM-NC514sVE 20% IM.

Table 18

Working curve parameters for 1P2S-PM NC514sVE with varying IM weight percent

Sample	D_p (mm)	E_{Crit} (mJ cm^{-2})
1P2S PM NC514sVE 0% IM	0.30 ± 0.03	2.90 ± 0.45
1P2S PM NC514sVE 10% IM	0.28 ± 0.02	2.05 ± 0.20
1P2S PM NC514sVE 20% IM	0.27 ± 0.01	1.94 ± 0.10

The working curve model is in good agreement with the data. The E_c value determined is comparable to that found in other resin formulations as well as with the resin system described in Chapter 6 [169]. The resin blends show a general trend, whereby the increase in IM content yields a decrease in both E_c and D_p. The addition of IM increases the overall methacrylate concentration in the resin, ultimately reducing the overall sensitivity to light as observed by the lower E_c. Similarly, the increasing IM contend yields a decrease in the D_p as the higher methacrylate concentration yields a

higher crosslink density polymer network, thus decreasing the penetration depth of light through the cured resin surface.

7.3.3 Extent of cure. Near-IR was used to determine the extent of cure for the formulated resins after print (denoted as AM) and after post-processing in a Formlabs Form Cure (denoted as FC). Representative near-IR spectra are provided in Figure 44 and the obtained extent of cure values are presented in Table 19

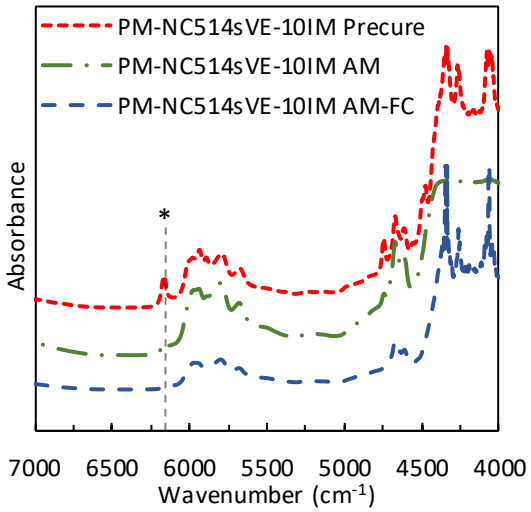

Figure 44. Near-IR spectra for 1P2S PM-NC514sVE Resin, AM and AM-FC for 10% IM. Methacrylate (*) absorption is indicated. Spectra are offset vertically for clarity.

Table 19

Extent of cure for before and after FC of printed samples for 1P2S PM-NC514sVE with varying IM weight percent

Sample	Extent of Cure AM (%)	Extent of Cure AMFC (%)
1P2S PM NC514sVE 0% IM	81.1 ± 0.5	96.5 ± 0.4
1P2S PM NC514sVE 10% IM	80.2 ± 3.6	96.6 ± 0.9
1P2S PM NC514sVE 20% IM	81.9 ± 3.6	95.8 ± 0.3

The polymerizable methacrylate groups have an absorbance at 6165 cm^{-1}. The ratio between the methacrylate peak before and after cure stages were compared to a reference peak (5900 cm^{-1}) to calculate the extents of cure. In general, all resin blends exhibited similar extents of cure both after printing and after post-processing. The addition of the FC increased the overall extent of cure by approximately 16%, acting as a traditional post-cure to increase the extents of cure of the formed polymer networks [36, 170].

7.3.4 Polymer properties. The resulting polymers were glassy and brown in color, due to the color of the NC-514s utilized in the resin synthesis. TGA was performed on all post-processed samples to determine the thermal stability of all prepared, bio-based thermosets. The thermograms in N_2 of the post-cured resins are shown in Figure 45. The IDT, $T_{50\%}$, T_{max}, and char content values are presented in Table 20. The thermogravimetric data for the same samples evaluated in air (an oxidative environment) are provided in Appendix F.

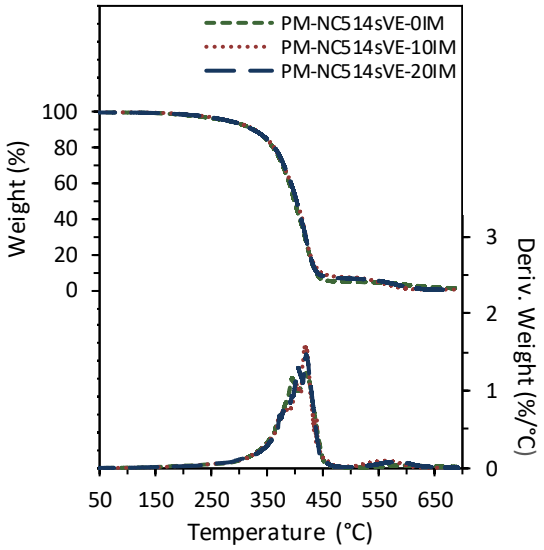

Figure 45. TGA thermograms and respective 1st derivatives of 1P2S PM-NC514sVE with varying IM weight percent in N_2.

Table 20

Thermogravimetric properties for 1P2S PM-NC514sVE samples with varying IM weight percent in N_2

Sample	IDT (°C)	$T_{50\%}$ (°C)	T_{max} (°C)	Char Content (%)
1P2S PM NC514sVE 0% IM	287 ± 5	399 ± 1	420 ± 1	1.9 ± 1.2
1P2S PM NC514sVE 10% IM	288 ± 1	403 ± 1	417 ± 1	0.3 ± 0.1
1P2S PM NC514sVE 20% IM	281 ± 6	402 ± 2	419 ± 3	0.3 ± 0.1

In general, all samples possess values for IDT, $T_{50\%}$, T_{max}, and char content which are within error of one another; therefore, the addition of IM into the base 1P2S PM-NC514sVE resin does not have any significant impact on thermal stability. This is expected, as cured IM by itself possesses similar thermal stability to that of the neat, cured 1P2S PM-NC514sVE resin [44]. Analogous thermogravimetric results to those reported in N_2 were achieved in an air atmosphere.

Viscoelastic properties were evaluated using DMA. Representative thermograms for the storage modulus (E') and the loss modulus (E'') for each sample are shown in Figure 46. The tan δ thermograms are provided in Figure 47. Table 21 includes the thermomechanical property values for each cured resin.

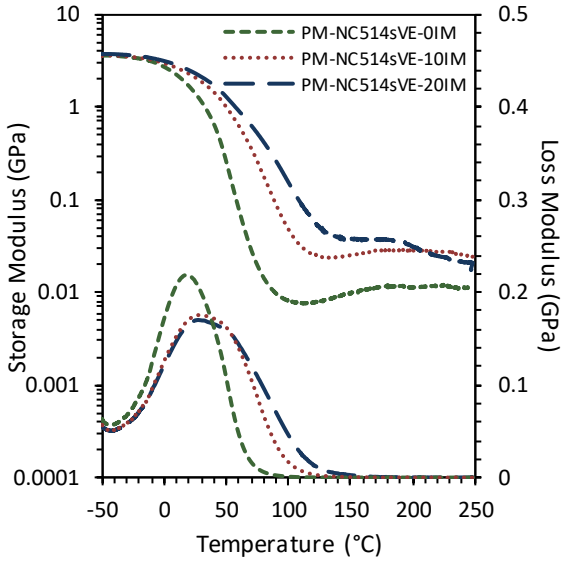

Figure 46. DMA thermograms of E' and E'' of 1P2S PM-NC514sVE samples with varying IM weight percent.

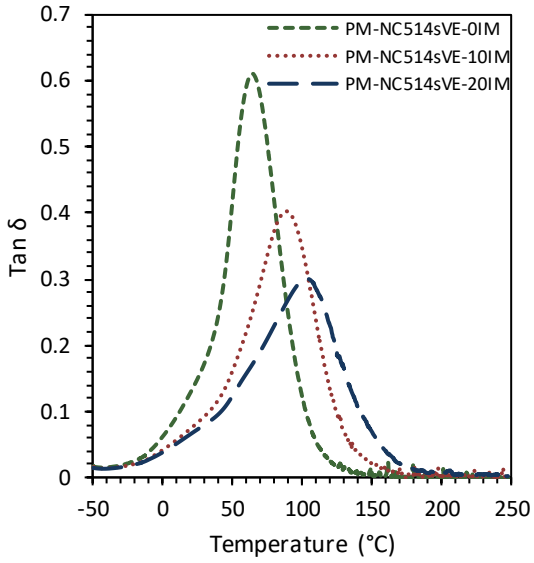

Figure 47. Tan δ thermograms for 1P2S PM-NC514sVE samples with varying IM weight percent.

Table 21

Thermomechanical results for 1P2S PM-NC514sVE samples with varying IM weight percent

Sample	**E′ @ -40 °C (GPa)**	**E′ @ 25 °C (GPa)**	**Peak of E″ (°C)**	**Peak of Tan δ (°C)**	**eff. M_c (g mol $^{-1}$)**	**ρ @ 25 °C (g cm^{-3})**
1P2S PM NC514sVE 0% IM	3.5 ± 0.3	1.0 ± 0.3	11.5 ± 4.8	62.7 ± 1.3	3015 ± 357	1.123 ± 0.002
1P2S PM NC514sVE 10% IM	3.7 ± 0.2	2.0 ± 0.2	25.3 ± 2.2	90.8 ± 2.9	547 ± 77	1.146 ± 0.001
1P2S PM NC514sVE 20% IM	4.0 ± 0.2	2.2 ± 0.1	27.0 ± 3.5	108.6 ± 1.5	388 ± 47	1.158 ± 0.006

The cured 1P2S PM-NC514sVE resin had the lowest *E′* of 3.5 GPa at – 40 °C and 1.0 GPa at 25 °C due to the flexible character of CNSL-derived NC514sVE [11, 17]. The addition of IM at 10 wt% and 20 wt% increases the *E′* at – 40 °C and at 25 °C as expected, since IM alone has a *E′* of 4 GPa at 25 °C [44]. The peak of *E″* and the peak of

tan δ were both used to estimate the T_g, or the temperature at which the polymer goes from a rigid state to a more flexible and rubbery state upon heating. Generally, the peak of E'' gives a more conservative value for the T_g while the peak of the tan δ provides an upper limit value [44]. Due to concerns of peak overlap from the continual β-relaxation on the long, alkyl chain of NC514sVE, the peak of the tan δ was utilized as the value of T_g for comparative purposes [2]. Overall, the T_g follows the same trends as the E', whereby the base 1P2S PM-NC514sVE resin, when cured, displayed a T_g, based on the peak of the tan δ, of 63 °C and the addition of 10 wt% and 20 wt% IM yielded cured resins with T_gs, based on the peak of the tan δ, of 91 °C and 109 °C, respectively.

The width of the tan δ peak is associated with the heterogeneity of the polymer network and a broader peak indicates a more heterogeneous network and a wider distribution of relaxation modes [93, 178-180]. As IM is formulated into the 1P2S PM-NC514sVE resin system, the width of the tan δ peak increases due to increasing the heterogeneity of the formulation, since there are now three different components with vastly different molecular structures within the polymer matrix. The polymer chain segmental mobility is specified by the maximum value of the tan δ, whereby a higher peak indicates a higher chain mobility [92]. As the IM content is increased, the stiff nature of the IM structure restricts the chain mobility within the entirety of the polymer matrix, thus reducing the peak height of the tan δ as shown in Figure 47.

M_c, calculated using the Theory of Rubber Elasticity, is shown in Table 21. In general, as the content of IM is increased the value of M_c decreases. This is due to the low molecular weight of IM, which yields a polymer matrix with a higher degree of

crosslink density. Similarly, the increase in crosslink density and decrease in M_c directly correlate to the increase in bulk polymer density as the IM content is increased.

Tensile testing was conducted to determine the effects of increasing IM content on the mechanical properties of the prepared polymers. Figure 48 shows the representative stress-strain curves for the prepared samples. The properties for the tensile tests including energy at max force, Young's modulus, force at break, tensile strain, and tensile stress are reported in Table 22.

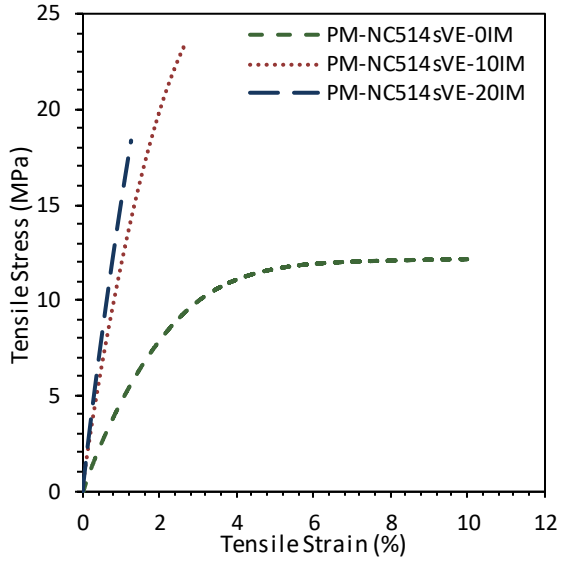

Figure 48. Stress-strain curves of 1P2S PM-NC514sVE with varying IM weight percent.

Table 22

Tensile testing results for 1P2S PM-NC514sVE with varying IM weight percent

Sample	Energy at Max Force (J)	Young's Modulus (MPa)	Force at Break (N)	Tensile Strain at Break (%)	Tensile Stress at Break (MPa)
1P2S PM NC514sVE 0% IM	0.62 ± 0.09	543 ± 16	314 ± 9	9.44 ± 1.13	12.29 ± 0.50
1P2S PM NC514sVE 10% IM	0.32 ± 0.08	1285 ± 56	463 ± 43	3.11 ± 0.58	17.57 ± 1.74
1P2S PM NC514sVE 20% IM	0.09 ± 0.01	1787 ± 48	509 ± 31	1.27 ± 0.11	19.15 ± 1.23

The cured 1P2S PM-NC514sVE resin exhibited the lowest Young's modulus and highest tensile strain at break of 543 MPa and 9.44%, respectively. The low Young's modulus and high strain at break is due to the chemical structure of the NC514sVE component, which is known to exhibit elastic behavior and yield low modulus materials. However, upon the addition of IM, the Young's modulus increases significantly, while the strain at break is significantly decreased. Generally, as M_c is decreased, an increased Young's modulus is expected [191-193]. As shown in the DMA results, the blends follow this trend, whereby the addition of IM causes a decrease in M_c, thus directly correlating to the increase in Young's modulus and decrease in strain at break. However, while the addition of IM substantially increased the overall material strength, the addition of IM led to the embrittlement of the material as shown by the significant decrease in the energy at max force.

The results displayed in the tensile evaluation are also affirmed in the fracture toughness experiments. All samples displayed linear deformation to failure as shown in

Figure 49. The plane-strain fracture toughness, $K_{1C,}$ and the critical strain energy release rate, G_{1C}, were obtained and are shown in Table 23 [96]. In general, as the IM content in the cured 1P2S PM-NC514sVE resin is increased, both the K_{1C} and G_{1C} decreased. The cured 1P2S PM-NC514sVE resin with no IM had the highest K_{1C} and G_{1C} values of 0.39 MPa $m^{1/2}$ and 761 J m^{-2}, respectively, indicating that the 1P2S PM-NC514sVE cured system was the toughest of the polymers printed and tested. The most brittle sample was the cured 1P2S PM-NC514sVE blended with 20 wt% IM resin with a K_{1C} of 0.34 MPa $m^{1/2}$ and G_{1C} of 167 J m^{-2}. The decrease in toughness is due to the IM containing resins yielding polymer matrices with higher crosslink densities, as indicated by the DMA results, and decreased aliphatic content, which usually provides toughening [97]. The presence of IM decreased flexibility as demonstrated through its increased T_g, modulus, and decreased toughness.

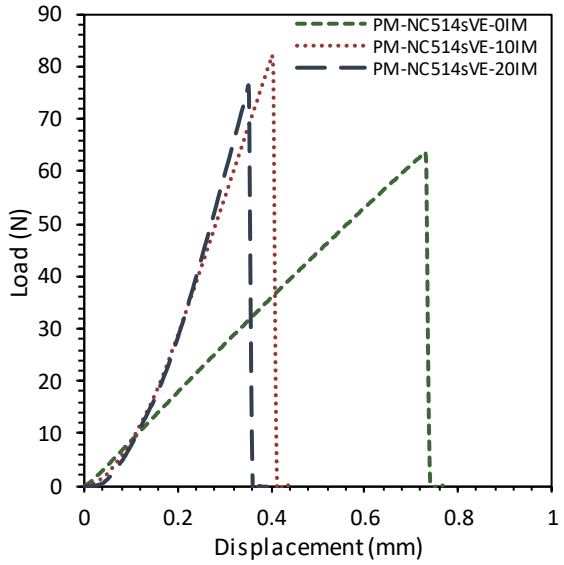

Figure 49. Load displacement curves for 1P2S PM-NC514sVE with varying IM weight percent.

Table 23

Fracture toughness K_{1C} and G_{1C} for 1P2S PM-NC514sVE with varying IM weight percent

Sample	K_{1c} MPa $m^{1/2}$	G_{1c} J m^{-2}
1P2S PM NC514sVE 0% IM	0.39 ± 0.01	761 ± 26
1P2S PM NC514sVE 10% IM	0.38 ± 0.01	340 ± 57
1P2S PM NC514sVE 20% IM	0.34 ± 0.03	167 ± 67

7.4 Conclusions

A bio-based resin comprised of phenyl methacrylate (PM, a potentially lignin-derived methacrylate), NC514sVE (derived from cashew nutshell liquid, CNSL), and isosorbide methacrylate (IM, derived from carbohydrates) was prepared by formulating varying weight percentages of 10 wt% and 20 wt% IM into a base resin of PM and NC514sVE. The bio-based resin formulations were evaluated for their respective photocure parameters and additively manufactured using stereolithography (SLA). The effect of the addition of IM into the formulation was evaluated, whereby the addition of IM is shown to linearly decrease resin viscosity as predicted by a logarithmic rule of mixing. The base resin, comprised of PM and NC514sVE is shown to have a T_g of 63 °C, Young's modulus of 543 MPa, and critical strain energy release rate, G_{1C}, of 761 J m^{-2}, yielding a material with a relatively low T_g but high toughness when cured. IM was added in amounts of 10 wt% and 20 wt% in an effort to increase the T_g of the cured resin up to that of conventionally cured vinyl ester resins while maintaining high toughness; however, while the addition of IM did increase the T_g, the increase the T_g was achieved at a significant detriment to the fracture toughness, where the cured 1P2S PM-NC514sVE

with 20 wt% IM resin exhibited a T_g of 109 °C and a G_{1C} of 167 J m^{-2}, demonstrating a significant tradeoff between T_g and toughness for these materials.

Chapter 8

Network Toughening of Additively Manufactured, High Glass Transition Temperature Materials via Sequentially Cured, Interpenetrating Polymers

Text and figures are reproduced and adapted with permission from A.W. Bassett, A.E. Honnig, J.J La Scala, and J.F. Stanzione III, "Network Toughening of Additively Manufactured, High Glass Transition Temperature Materials via Sequentially Cured, Interpenetrating Polymers," *In preparation*, reference [199].

8.1 Introduction

Interpenetrating polymer networks (IPNs) are defined as a combination of two or more individual polymer networks whereby at least one of the polymer networks is formed in the presence of the other [22, 200]. There exist numerous types of IPNs, including sequential, simultaneous, latex, gradient, and thermoplastic IPNs, which are formed via different methods of polymerization and/or utilizing different initial blended components in the IPN formulation [201]. IPNs are utilized in a broad range of applications such as biomedical materials, sound and vibration damping materials, and ion exchange resins [202]. Moreover, IPNs have found utility in a variety of additive manufacturing (AM) applications [203-206].

The utilization of AM, a layer-wise process more commonly known as 3D printing, has gained significant traction in industry, military, and academia due to efficient material use, rapid production times, and the ability to create complex parts on-demand while removing manufacturing constraints that typically exist with conventional methods [136-138, 203]. Stereolithography (SLA) is an AM method in which layers are formed via the photopolymerization of a liquid resin via UV/visible light. Localized curing of the resin occurs due to the laser beam scanning specific locations on the surface

of the resin, after which the material is raised vertically by the desired layer thickness, which typically ranges from 25 to 200 microns, allowing the resin to backfill and a new layer to be cured and polymerized to the previously formed layer [138, 143-145, 203]. Parts printed via SLA are usually exposed to post-processing to reach higher degrees of cure [141]. Layered fabrication as a result of SLA typically leads to mechanical anisotropy; yet, SLA printed parts are effectively isotropic due to inter-layer crosslinks formed during photopolymerization [135, 138, 140]. SLA resins that are readily available usually contain both (meth)acrylate and/or epoxy functionality, both of which are polymerized via light. (Meth)acrylate-based resins typically lead to less accurate parts and overall distortion, resulting in lower mechanical properties; however, (meth)acrylate-based resins can be polymerized quickly due to high cure rates. Furthermore, epoxy resins, while having prohibitively slow cure rates, have less shrinkage and produce more accurate geometries leading to increased mechanical performance [141]. As a result, most SLA resins are comprised of both (meth)acrylate and epoxy functionality to combine their independent advantages [141, 146, 203].

Thermosetting polymers including epoxy and vinyl ester resins (VERs) are widely used in commercial and military applications due to their outstanding properties including high glass transition temperatures (T_gs), moduli, strengths, chemical resistances, and toughness [1, 2, 20, 36, 207, 208]. Epoxy resins are characterized by an oxirane moiety, which can be polymerized via multiple mechanisms including ionic polymerizations and, more commonly for higher performance materials, epoxy-amine step-growth polymerizations [3]. VERs are generally produced via the esterification of epoxy resins to incorporate vinyl moieties that are capable of being polymerized via

radical-based polymerization mechanisms [2]. Both epoxy and vinyl ester resins are commonly cured and molded via conventional, thermally driven procedures; however, the properties displayed by epoxy-amine and vinyl ester resins and their versatility of polymerization makes them intriguing candidates for AM, in general.

In this work, IPNs comprised of vinyl ester and epoxy-amine components, shown in Figure 50, were prepared via sequential cure using SLA. SLA was utilized to photopolymerize the vinyl ester components and encapsulate the epoxy and amine monomers within the methacrylate-based polymer matrix. The samples were subsequently post-processed to facilitate the sequential thermal cure of the epoxy-amine network to form the IPN. The effect of macromolecular inter-network connections and IPN formation was subsequently evaluated via thermomechanical, thermogravimetric, tensile, and fracture testing to determine the influence of network connectivity on SLA printed, IPN polymer properties.

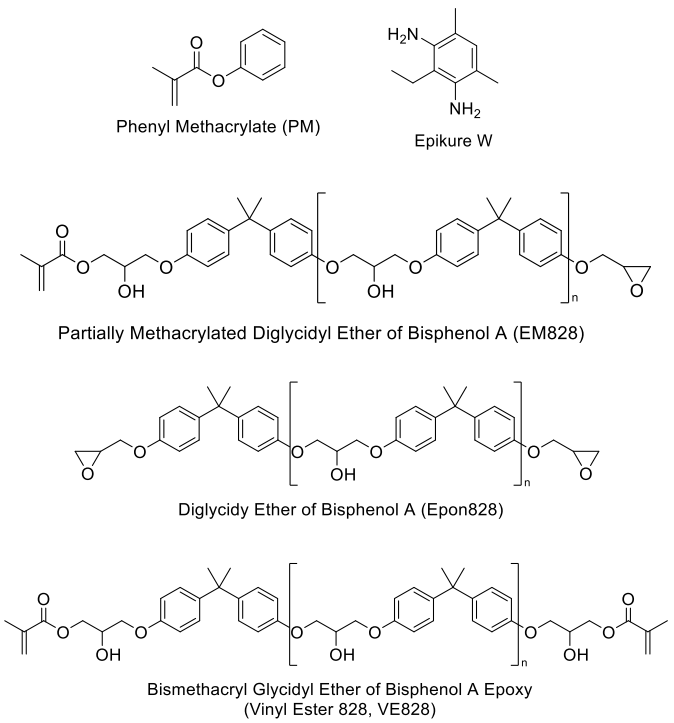

Figure 50. Chemical structures used in this study.

8.2 Experimental Methods & Procedures

8.2.1 Materials Phenol (99.5%), 4-dimethylaminopyridine (DMAP, 99%), and chloroform-d_3 for NMR were purchased from Acros Organics. Methacrylic anhydride (94%) was purchased from Alfa Aesar. AMC-2 catalyst was purchased from AMPAC Fine Chemicals. Diphenyl (2,4,5-trimethylbenzoyl) phosphine oxide (TPO) was purchased from TCI. Isopropyl alcohol (IPA) was purchased from VWR. Compressed nitrogen (N_2, 99.998%) and compressed argon (Ar, 99.999%) were purchased from Airgas. Epon Resin 828 (diglycidyl ether of bisphenol A, DGEBA, Epon828) and Epikure Curing Agent W (diethyl toluene diamine, Epikure W) were obtained from Hexion. Epon828 was transformed into bismethacryl glycidyl ether of bisphenol A and is denoted as vinyl ester 828 (VE828). Synthesis and characterization of VE828 described

in literature were performed with similar results [4, 5]. All chemicals were used as received.

8.2.2 Dual-cure resin synthesis. The resin was synthesized via a one-pot reaction methodology [159]. In a three-neck round bottom flask equipped with a mechanical mixer, phenol (200.00 g) and DMAP (13.11 g) were added. The mixture was purged with argon for 10 minutes and then methacrylic anhydride (330.91 g) was added. The reaction mixture was heated to 50-55 °C with continuous stirring. After 24 hours, the reaction mixture was cooled to room temperature and a stoichiometric amount of Epon828 (804.75 g) was added along with AMC-2 catalyst (1.00 g). The mixture was then heated to 70 °C and monitored via acid number titration until completion (when the free acid number was < 10, corresponding to ~3% acid) [159]. The final, synthesized VER (PM-EM828) was comprised of mono-functional monomer, phenyl methacrylate (PM), and partially methacrylated bisphenol A epoxy (EM828), as a dual-functional crosslinker, in a 1:1 mole ratio. The complete reaction is shown in Figure 51 and the ^{1}H-NMR spectrum of the resin with peak assignments is provided in Appendix G. A fully methacrylated VER analogous to the PM-EM828 system was also prepared for comparative purposes, whereby Epon828 was added in a 0.5 mole ratio relative to methacrylic acid to facilitate the complete conversion of Epon828 to the corresponding difunctional vinyl ester, VE828.

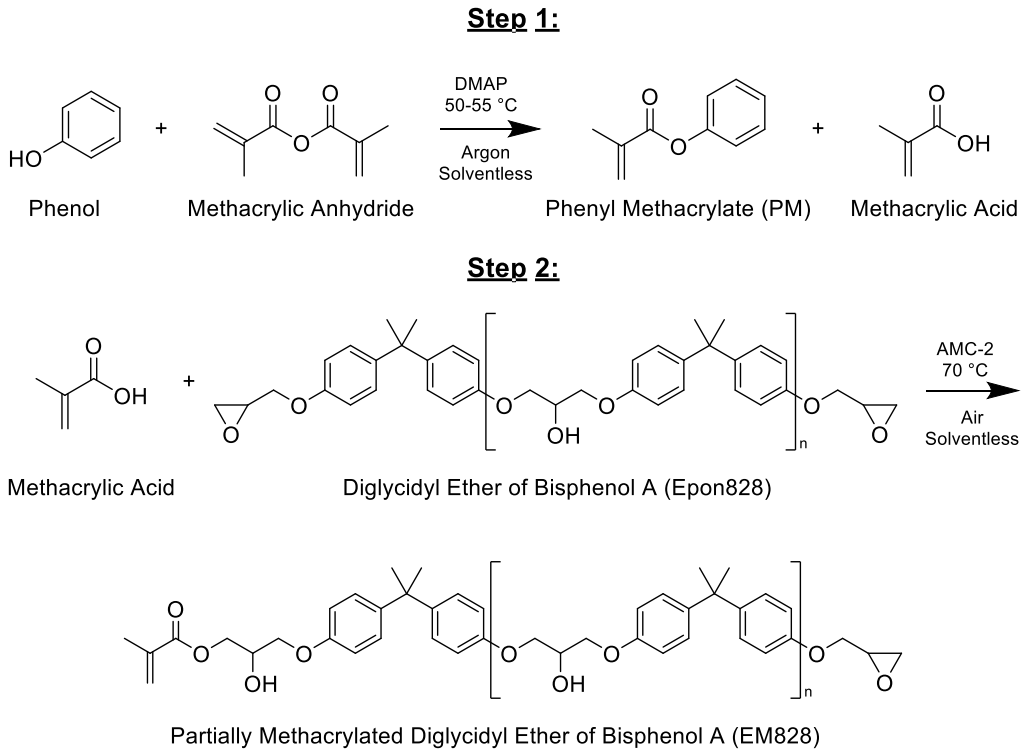

Figure 51. PM-EM828 reaction scheme.

8.2.3 Resin formulation. Resins containing epoxy moieties were blended with stochiometric amounts of Epikure W to facilitate the cure of the epoxy-amine network. Furthermore, resin formulations were prepared in specific molar compositions as shown in Table 24. The PM-VE828 resin alone was utilized as a basis of comparison for this work.

Table 24

Resin formulation composition

Sample	Formulation Composition			
	PM (mol)	**VE828 (mol)**	**EM828 (mol)**	**Epon828 (mol)**
PM-VE828	1	0.5	0	0
PM-EM828	1	0	1	0
PM-VE828 - Epon828 Blend	1	0.5	0	0.5
PM-EM828_025VE828	1	0.25	1	0
PM-EM828_05Epon828_025VE828	1	0.25	1	0.5

The effect of network connectivity was evaluated by comparing the PM-EM828 to the PM-VE828 – Epon828 Blend, due to the fact that these two resins have the exact same molar concentration of reactive epoxy and methacrylate groups; however, the PM-EM828 resin allows the vinyl ester and the epoxy-amine networks to be chemically connected to one another due to the EM828 monomer bearing both functionalities, whereas the PM-VE828 – Epon828 Blend does not enable such molecular level connections.

Furthermore, the PM-EM828 was blended with either VE828 or VE828 and Epon828 to evaluate the effect of molecular distance between the connections of the vinyl ester and epoxy-amine networks on overall polymer properties. A visual representation of the networks formed is provided in Figure 52.

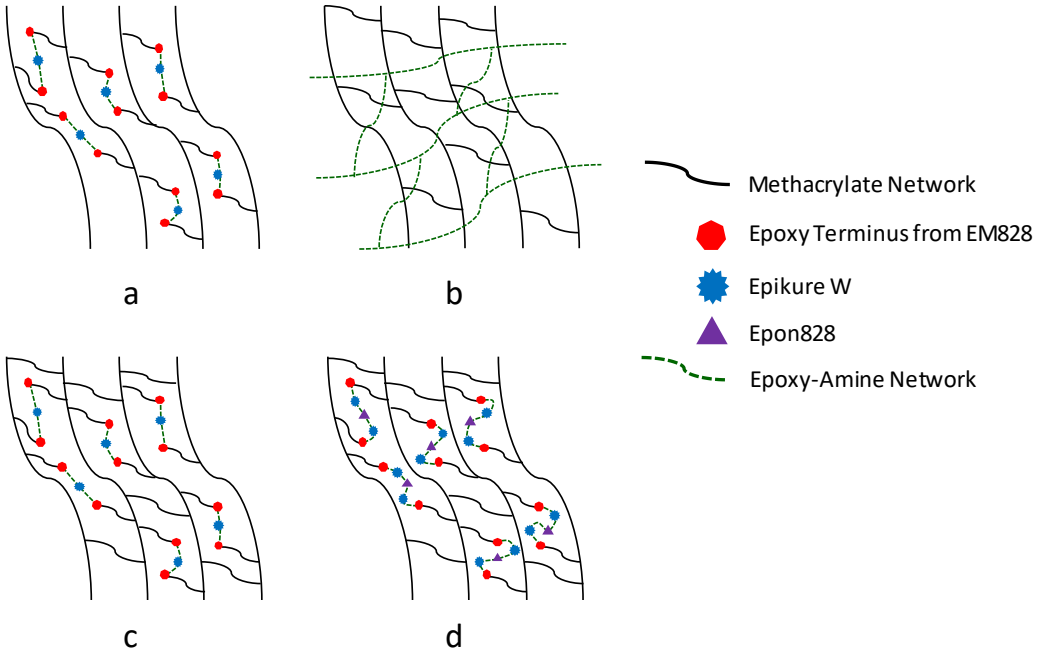

Figure 52. Visual representations of a) the PM-EM828 network, b) the PM-VE828 – Epon828 Blend network, c) the PM-EM828_025VE828 network, and d) the PM-EM828_05Epon828_025VE828 network.

8.2.4 Resin rheology. The synthesized resins were characterized by ^{1}H-NMR spectroscopy (400.15 MHz, 32 scans at 298 K) using a Varian 400 MHz FT-NMR spectrometer. The spectra are provided in the Appendix G. The viscosity of the resins and formulations were obtained using a TA Instruments Discovery Hybrid Rheometer (DHR-2) using a 1° 40 mm cone geometry at a temperature of 25 °C. The shear rate was ramped logarithmically ascending from 1 to 100 s^{-1} and descending from 100 to 1 s^{-1} [44, 78].

8.2.5 Resin additive manufacturing & cure. All resins were prepared for free radical photopolymerization via SLA by adding TPO as the photoinitiator at an amount of 2 wt% of the total, formulated resin mass. The resins, along with TPO, were mixed in a Thinky ARE-310 planetary mixer for 15 minutes and defoamed for 2 minutes. Digital models were prepared for viscoelastic, tensile, and fracture testing. The final models were

uploaded to a Formlabs Form 2 SLA 3D printer, with the printer set to the preprogrammed “Tough Resin” setting in “Open Mode” with no heating of the resin tank. A layer thickness of 100 μm was selected. After printing, the printed samples were washed with IPA in a Formlabs Form Wash for 20 minutes to remove any unreacted resin from the surface of the printed samples. These samples were denoted as AM samples. Additionally, the samples were further post-processed in a Formlabs Form Cure (denoted as FC) with UV/visible light (λ= 405 nm) and heat (80 °C) for 2 hrs and then further post-cured at 180 °C for 2 hours in a thermal oven (denoted as PC).

8.2.6 Extent of cure. The extent of cure of the resins after print (AM), Form Cure (FC) and post-cure (PC) were determined via near-infrared (near-IR) spectroscopy using a Thermo Scientific Nicolet iS50 FTIR. The uncured resin was contained in a glass reservoir with a thickness of 3 mm. 64 cumulative scans with a resolution of 2 cm^{-1} were collected. The cured resins had a thickness of 2.5 mm and their near-IR spectra were acquired in the same method as the uncured resins. The methacrylate peak was measured at ~ 6165 cm^{-1} before and after curing and compared to a reference peak at 5900 cm^{-1}, which is not affected by the polymerization. Similarly, the oxirane ring of the epoxy was measured at ~ 4530 cm^{-1} [61, 78].

8.2.7 Polymer properties. Thermogravimetric analysis was performed using a TA Instruments Discovery Thermogravimetric Analyzer 550 (TGA). 10 mg of sample was placed on a platinum pan and heated to 700 °C at a rate of 10 °C min^{-1} in both N_2 (inert) and air (oxidative) atmospheres (40 mL min^{-1} balance gas flow rate and 25 mL min^{-1} sample gas flow rate). Initial decomposition temperature (IDT), temperature at 50

wt% degradation ($T_{50\%}$), temperature at maximum degradation (T_{max}), and char content are reported.

A TA Instruments Q800 dynamic mechanical analyzer (DMA) was used to evaluate the viscoelastic properties of all cured resins. A single cantilever geometry with a frequency of 1.0 Hz, Poisson's ratio of 0.35, and a deflection amplitude of oscillation of 7.5 μm were used. The heating ramp was 2 °C per minute from 0 °C to 250 °C. Samples were printed with appropriate dimensions (35 x 12 x 2.5 mm^3 and 35 x 12 x 1.5 mm^3) with the length-by-thickness plane parallel to the build platform and tested in accordance with McAninch et al [32]. The molecular weight between crosslinks, M_c, was determined using the Theory of Rubber Elasticity [31]. The density of each sample at 25 °C was calculated using Archimedes' principle [5, 161, 162].

Tensile testing of all cured resins was conducted using an Instron 5966 equipped with a 10 kN load cell and at a crosshead speed of 1 mm min^{-1}. Type IV samples were printed such that the printed layers were parallel to the direction of the crosshead movement and analyzed according to ASTM D638 [157]. Fracture toughness was evaluated according to ASTM D5045 [34]. Three-point, single edge notched bend (SENB) samples of all cured resins were printed such that the printed layers were perpendicular to the direction of the crosshead movement. Samples were prepared to be 44 x 10 x 4 mm^3 to ensure plane-strain. Using a diamond saw, samples were notched and then a single edged razor blade was used to instantly propagate a crack. Upon cracking the samples, the tip of the crack was marked with ink [35]. Samples were tested on an Instron 5966 with a 1 kN load cell and a 3-point bend flexure fixture at a cross head speed of 10 mm min^{-1}. The plane-strain fracture toughness, K_{1C}, and the critical strain

energy release rate, G_{1C}, were determined upon fracture. All mechanical testing was performed with a minimum of five replicates.

8.3 Results and Discussion

8.3.1 Resin rheology. All resin compositions exhibited Newtonian behavior. The viscosity of each resin was determined via the average of three steady state points at different shear rates and is shown in Table 25. In general, low viscosities are preferred for printing via SLA in order to facilitate recoating of the resin tank surface between layers [145]. Resins with viscosities under 3000 cP at room temperature have shown success with producing high resolution objects in rapid prototyping techniques; however, this does not preclude the use of resins with viscosities above 3000 cP [163-165].

Table 25

Viscosity of resins at 25 °C

Sample	Viscosity at 25°C (cP)	Viscosity at 25°C with Epikure W (cP)
PM-VE828	578 ± 11	-
PM-EM828	1172 ± 34	1226 ± 15
PM-VE828 - Epon828 Blend	1734 ± 63	1783 ± 20
PM-EM828_025VE828	2774 ± 18	2996 ± 15
PM-EM828_05Epon828_025VE828	5003 ± 36	5014 ± 54

The viscosities of each resin system increased as the overall molar concentration of crosslinker, either EM828, Epon828, or VE828, was increased. Interestingly, although the PM-EM828 and PM-VE828 – Epon828 Blend resins contain the exact same molar quantities of PM, crosslinkers, and bisphenolic content with identical molar quantities of

methacrylate and epoxy moieties, the PM-EM828 resin exhibits a significantly reduced viscosity relative to the blended counterpart. This is due to the EM828 monomer alone having a viscosity of 1.1 x 10^5 cP, whereas the equimolar blend of VE828 (6 x 10^7 cP at 25 °C) and Epon828 (1.3 x 10^4 cP at °C) has a viscosity of approximately 3 x 10^7 cP based on a logarithmic simple rule of mixtures [78]. Therefore, the preparation of the multi-functional EM828 provides reduced resin viscosity for the same molar content of reactive functionalities, thus potentially increasing processability.

8.3.2 Extent of cure. Near-IR spectroscopy was used to obtain the extent of cure for all resins at the various stages of cure. Figure 53 shows representative near-IR spectra of cured resins as well as an uncured resin. The extent of cure values are provided in Table 26.

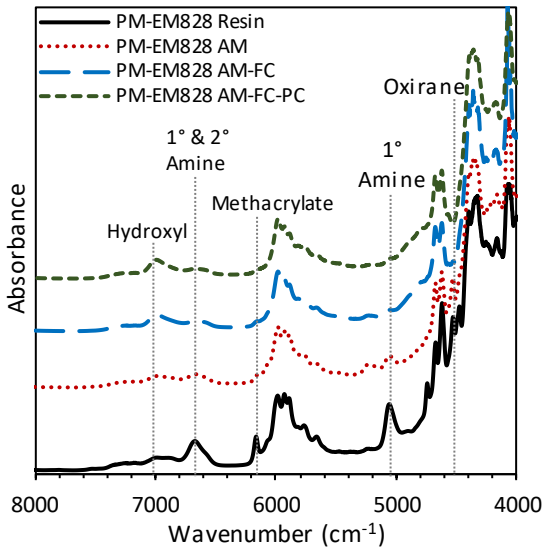

Figure 53. Near-IR spectra of the PM-EM828 resin, and the resin at the AM, FC, and PC stages of cure. Spectra are vertically offset for clarity.

Table 26

Extent of cure of resins via near-IR spectroscopy at various stages of cure, taken at room temperature

Sample	Methacrylate Extent of Cure (%)		
	AM	**AM-FC**	**AM-FC-PC**
PM-VE828	74.8 ± 0.6	89.7 ± 0.6	-
PM-EM828	84.5 ± 1.5	90.9 ± 0.7	92.7 ± 0.7
PM-VE828 - Epon828 Blend	84.1 ± 0.9	90.1 ± 2.3	90.0 ± 2.3
PM-EM828_025VE828	82.0 ± 0.6	91.7 ± 1.3	91.9 ± 0.5
PM-EM828_05Epon828_025VE828	87.3 ± 0.1	95.4 ± 0.8	94.8 ± 0.9
Sample	**Epoxy Extent of Cure (%)**		
	AM	**AM-FC**	**AM-FC-PC**
PM-VE828	-	-	-
PM-EM828	0	92.1 ± 1.6	99.9 ± 0.9
PM-VE828 - Epon828 Blend	0	96.4 ± 2.0	98.0 ± 2.3
PM-EM828_025VE828	0	86.6 ± 0.5	99.9 ± 0.1
PM-EM828_05Epon828_025VE828	0	82.9 ± 0.5	99.9 ± 0.1

The only photopolymerizable groups within the resins are the methacrylate functionalities which have an absorbance in near-IR at 6165 cm^{-1}. The ratio between the methacrylate peak before and after cure steps were compared to an unreactive control peak at 5900 cm^{-1} to calculate the extent of cure of the methacrylate network. Similarly, the oxirane ring on the epoxy has an absorbance in near-IR at 4530 cm^{-1}, which was utilized to determine the extent of cure of the epoxy-amine network [61]. After printing, the extent of cure of the methacrylate functionality for all resins were between 75 – 90% and all epoxy conversions were 0%, as the epoxy-amine reaction is not initiated during SLA printing; thus, the epoxy and amine monomers are plasticized within the shell of the methacrylate-based network. The addition of the FC post-processing at 80 °C with irradiation of UV/visible light around the printed part further increases the extent of cure of the methacrylates to approximately 90% [170]. Additionally, the FC stage at 80 °C

initiates the epoxy-amine cure as this temperature is within the range of typical epoxy-amine cures [61, 161, 186, 209]. The overall epoxy extent of cure is shown to increase to between 83 – 93% for all samples, demonstrating that the approach of using staged cure via SLA with a thermal post process enables *in-situ* IPN formation whereby the epoxy-amine monomers are initially plasticized within the SLA-printed, methacrylate-based polymer matrix and sequentially initiated during FC. A traditional post-cure was further employed at 180 °C to ensure the near-complete conversion of the epoxy-amine network. This post-cure was not employed for the fully methacrylate-based PM-VE828 due to the absence of epoxy-amine reactivity. After all stages of cure, every sample exhibited similar degrees of cure for both the methacrylate and epoxy-amine networks. Therefore, the polymer properties resulting from these samples will be attributed to the overall network connectivity of the bulk IPN, and not a function of extent of cure.

8.3.3 Polymer properties. The resulting polymers were hard, glassy, dull green/brown samples due to the color of the AMC-2 catalyst used in the resin synthesis and the post-processing processing steps causing slight oxidation. Thermal degradation of all cured resins was analyzed. The TGA thermograms are provided in Figure 54. The IDT, $T_{50\%}$, T_{max}, and char content values are reported in Table 27.

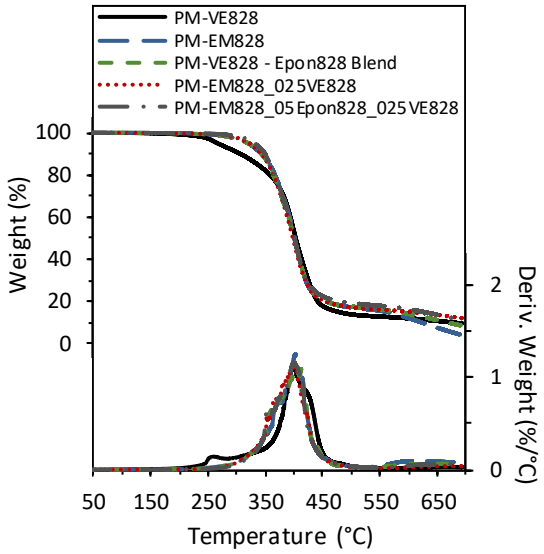

Figure 54. TGA thermograms and the respective 1st derivatives of all IPNs in N_2.

Table 27

Thermogravimetric properties of all IPNs in N_2

Sample	IDT (°C)	$T_{50\%}$ (°C)	T_{max} (°C)	Char Content (%)
PM-VE828	267 ± 1	402 ± 1	395 ± 1	9.6 ± 0.3
PM-EM828	318 ± 3	400 ± 1	402 ± 1	5.7 ± 2.0
PM-VE828 - Epon828 Blend	320 ± 1	400 ± 1	408 ± 6	9.3 ± 1.3
PM-EM828_025VE	324 ± 3	396 ± 2	399 ± 3	12.1 ± 0.2
PM-EM828_05Epon828_025VE828	330 ± 1	401 ± 2	400 ± 1	8.1 ± 4.2

In general, all IPNs exhibit comparable thermogravimetric properties with IDT values of approximately 320 °C, $T_{50\%}$ and T_{max} values of approximately 400 °C, and char contents ranging from 5 – 12%. The fully methacrylate-based PM-VE828 was the only sample that showed a reduction in IDT. The lower IDT of the methacrylate-based PM-VE828 could be a result of the absence of the secondary network, which is likely contributing to higher IDT values of the IPNs and preventing premature degradation of

the bulk material [171]. Similar thermogravimetric trends were observed in an oxidative environment (provided in Appendix G) with the only difference being that char content is lower due to combustion of the char at high temperature [172].

Viscoelastic properties of all IPNs were evaluated using DMA. Figure 55 shows representative storage modulus (E') and loss modulus (E'') thermograms for all IPN samples. Figure 56 shows the tan δ thermograms for each IPN. Table 28 shows the specific thermomechanical properties for all cured IPNs.

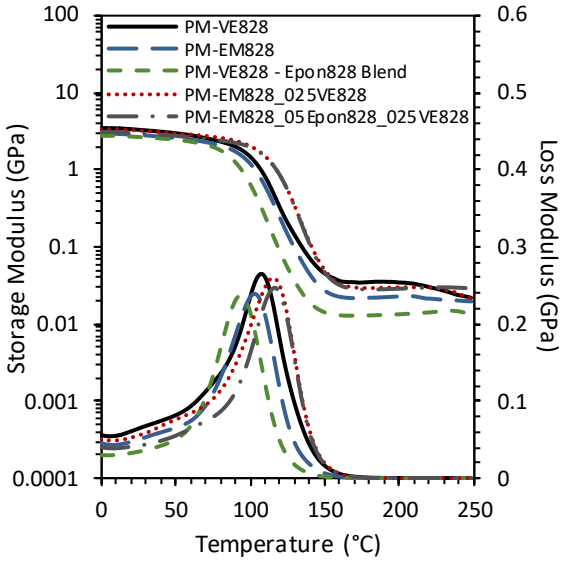

Figure 55. DMA thermograms of E' and E'' of all IPNs.

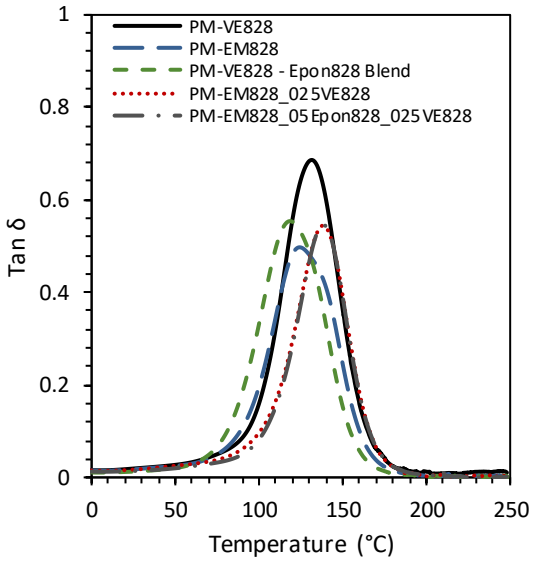

Figure 56. Tan δ thermograms of all IPNs.

Table 28

Viscoelastic properties of all IPNs

Sample	E′ @ 25 °C (GPa)	Peak of E″ (°C)	Peak of Tan δ (°C)	eff. M_c (g mol $^{-1}$)	ρ @ 25 °C (g cm^{-3})
PM-VE828	3.1 ± 0.2	109 ± 1	134 ± 2	378 ± 20	1.2157 ± 0.002
PM-EM828	3.1 ± 0.2	103 ± 2	138 ± 2	511 ± 104	1.1989 ± 0.003
PM-VE828 - Epon828 Blend	2.7 ± 0.2	92 ± 2	121 ± 6	906 ± 102	1.1957 ± 0.002
PM-EM828_025VE828	3.2 ± 0.1	114 ± 2	139 ± 2	469 ± 18	1.1955 ± 0.003
PM-EM828_05Epon828_025VE828	3.1 ± 0.1	117 ± 1	140 ± 2	468 ± 20	1.1880 ± 0.002

The differences in *E′* at 25 °C were statistically insignificant for all samples, which exhibited comparable *E′* values to conventional styrene diluted vinyl esters at 25 °C [4, 36]. The peak of *E″* and the peak of tan δ were both used to determine the T_g, the

temperature at which the polymer goes from a glassy state to rubbery state. Traditionally, the peak of E'' gives a more conservative value for the T_g while the peak of the tan δ provides an upper limit value [44]. Comparing the PM-EM828 and PM-VE828 – Epon828 Blend cured systems, which contain the exact same molar quantities of PM, crosslinkers, and bisphenolic content with identical molar quantities of methacrylate and epoxy moieties, demonstrates that the interconnection of the two networks at the molecular level yield a material with a T_g approximately 10 °C higher than that of the non-interconnected IPN. Furthermore, additional formulation of VE828 into the PM-EM828 resin further increases T_g based on the peak of E'' by approximately 11 °C due to the increase in crosslinker content in the overall system, yet the formulation of both VE828 and Epon828 does not offer any additional increase in T_g. Therefore, the increase in molecular distance between the connection of the methacrylate and epoxy-amine network does not have a significant impact on T_g. Nevertheless, all of the prepared IPNs exhibit similar T_g values to traditionally cured styrene diluted VERs [36].

The width of the tan δ peak is associated with the heterogeneity of the polymer network. A broader peak indicates a more heterogeneous network and a wider distribution of relaxation modes [93, 178-180]. The tan δ thermograms of all IPNs show similar widths, indicating all IPNs exhibited similar levels of heterogeneity [93]. The maximum value of the tan δ can be used to provide insight in to the overall polymer chain segmental mobility, whereby a higher peak indicates a higher chain mobility [92]. In general, the prepared IPNs exhibit similar chain mobility, therefore the differences in interconnection of the two networks and the differences in molecular spacing show

minimal to no effect on heterogeneity or segmental mobility, likely because all of the components within the resin have similar, bisphenol-A like structures.

M_c was calculated using the Theory of Rubber Elasticity and is shown in Table 28. The Theory of Rubber Elasticity was originally derived for branched and lightly crosslinked polymer networks; however, literature has demonstrated this theory applied to highly crosslinked polymer can provide some insight into overall polymer network trends [31]. In comparing the fully methacrylate-based PM-VE828 to all other polymers prepared, it is observed that the PM-VE828 had the lowest M_c of all prepared polymers, likely due to the fact that no secondary network is present in the system and an IPN is not formed. The PM-VE828 – Epon828 Blend exhibited the highest M_c of all samples, which is likely a result of the formation of the non-interconnected, meshed IPN. Since the two networks are not connected, the fully methacrylated portion likely results in the AM polymer having a higher T_g than all other IPNs prepared, thus causing vitrification of the network to happen quicker, resulting in non-uniform formation of the secondary network, leading to the higher value of M_c [187]. All interconnected IPNs of PM-EM828, PM-EM828_025VE828, and PM-EM828_05Epon828_025VE828 display similar values of M_c. This result is due to all the crosslinkers (EM828, VE828, and Epon828) having similar molecular weights. The increase in molecular distance between the connection of the methacrylate and epoxy-amine network does not affect M_c because, although the molecular weight between the two connected polymer networks is changing, the numerical M_c exists independently from the overall IPN connection and accounts for the M_c within each individual network, which in this case are all of similar magnitude.

Tensile testing was conducted to determine the effects of IPN connection on the resulting mechanical properties of the polymers. Figure 57 shows representative stress-strain curves for all samples. All samples showed linear behavior until break. Table 29 shows the tensile data for all cured polymers.

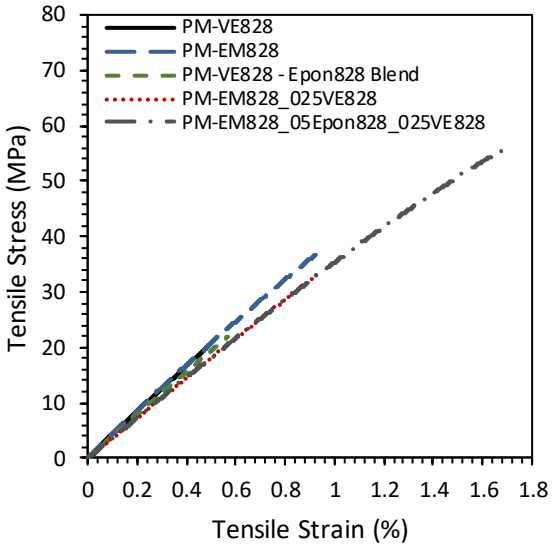

Figure 57. Stress-strain curves of all IPNs.

Table 29

Tensile testing values of all IPNs

Sample	Energy at Max Force (J)	Young's Modulus (MPa)	Force at Break (N)	Tensile Strain at Break (%)	Tensile Stress at Break (MPa)
PM-VE828	0.04 ± 0.02	3947 ± 280	542 ± 2	0.45 ± 0.20	20.35 ± 1.83
PM-EM828	0.11 ± 0.04	3807 ± 75	993 ± 133	0.91 ± 0.20	34.56 ± 4.64
PM-VE828 – Epon828 Blend	0.04 ± 0.01	3940 ± 58	566 ± 84	0.55 ± 0.06	20.86 ± 2.58
PM-EM828_025VE828	0.08 ± 0.01	3957 ± 106	813 ± 57	0.81 ± 0.07	30.16 ± 2.29
PM-EM828_05Epon828_025VE828	0.30 ± 0.05	3543 ± 86	1360 ± 132	1.54 ± 0.21	51.30 ± 5.20

Young's modulus, which is a measure of the stiffness of the polymer, has a direct correlation with the overall monomer structure, degree of crosslinking, as well as macromolecular architecture of the polymer network [188-190, 193]. The differences in Young's modulus were statistically insignificant for most samples, with the exception of PM-EM828_05Epon828_025VE828, likely due to the increasing molecular distance between the two formed networks as a result of the additional formulation of VE828 and Epon828. The fully methacrylate-based PM-VE828 cured resin exhibited the lowest tensile strain and tensile stress at break, on average. The PM-VE828 – Epon828 Blend IPN yielded near-identical results to that of the fully methacrylate-based PM-VE828. Interestingly, the PM-EM828, interconnected IPN yielded a material with significantly improved tensile properties over the PM-VE828 – Epon828 Blend, which contains the exact same molar quantities of resin constituents and reactive species, thus demonstrating that the interconnection of the vinyl ester and epoxy-amine network yielded significant

tensile strength enhancements. Yet, the addition of VE828 into the PM-EM828 resin resulted in an overall decrease in the resulting IPN tensile properties, which is a result of increasing the number of crosslinks within the methacrylate network, subsequently decreasing in molecular distance between network-level connections. However, the addition of Epon828 offsets this, causing an increase in the molecular distance between the two interconnected networks formed. While this increase in molecular distance causes as slight reduction in Young's modulus as stated earlier, the change in network connectivity affords significant improvements in all other tensile properties measured including energy at maximum force, force at break, tensile strain at break, and tensile stress at break.

The results obtained via tensile testing are further affirmed by the fracture toughness experiments. All samples displayed linear deformation to failure as shown in Figure 58. The plane-strain fracture toughness, $K_{1C,}$ and the critical strain energy release rate, G_{1C}, were obtained and are shown in Table 30 [96].

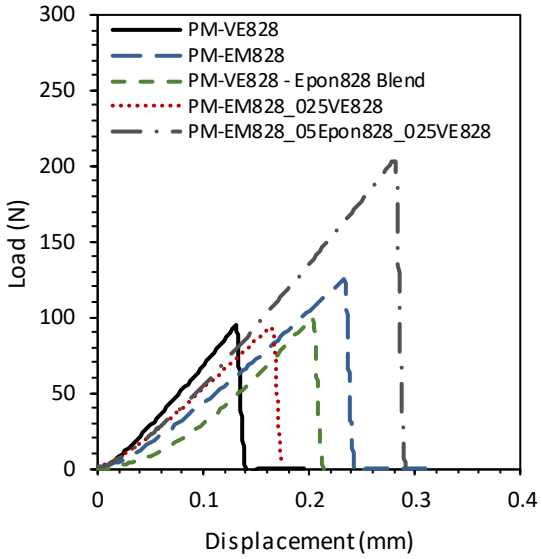

Figure 58. Load-displacement curves of all IPNs.

Table 30

Fracture toughness K_{1C} and G_{1C} values of all IPNs

Sample	G_{1C} (J m^{-2})	K_{1C} (MPa m$^{1/2}$)
PM-VE828	255 ± 36	0.48 ± 0.07
PM-EM828	753 ± 76	0.56 ± 0.03
PM-VE828 - Epon828 Blend	234 ± 32	0.47 ± 0.06
PM-EM828_025VE828	314 ± 21	0.44 ± 0.04
PM-EM828_05Epon828_025VE828	974 ± 41	0.70 ± 0.03

The fully methacrylate-based PM-VE828 system exhibited similar fracture toughness to that of styrene-diluted VERs [36]. The PM-VE828 – Epon828 Blend displayed the lowest fracture toughness of all IPNs prepared. Interestingly, the PM-VE828 – Epon828 Blend yields intermediate fracture properties based on the individual components of the network, whereby the PM-VE828 component is shown in Table 30

(G_{1C} of 255 J m^{-2}) and the G_{1C} of Epon828-Eplikure W is shown in literature to be 135 J m^{-2} [210]. This intermediate fracture toughness is a result of the formation of the non-interconnected, meshed IPN. However, the PM-EM828, interconnected IPN which contains the exact same molar quantities of PM, crosslinkers, and bisphenolic content and the same molar quantities of methacrylate and epoxy moieties to the PM-VE828 – Epon828 Blend, yields significant gains in fracture toughness as a result of interconnecting the vinyl ester and epoxy-amine network via the dual-functionality of the EM828 monomer. The G_{1C} of 753 J m^{-2} for the additively manufactured PM-EM828 IPN rivals that of thermally cured, rubber and/or particle toughened vinyl ester and epoxy resins [4, 96, 198, 211-214]. The addition of VE828 into the PM-EM828 resin resulted in a decrease in the G_{1C} to 314 J m^{-2} due to the increasing number of crosslinks within the methacrylate network and resulting decrease in molecular distance between network-level connections. However, the formulation of Epon828 offsets the decrease in mechanical properties from the addition of VE828, whereby the PM-EM828_05Epon828_025VE828 IPN is shown to have a remarkably high fracture toughness of 974 J m^{-2}, which is a result of the increase in the total molecular distance between the connection of the two interconnected networks formed.

The G_{1C} of 974 J m^{-2} for the additively manufactured PM-EM828_05Epon828_025VE828 IPN not only surpasses that of many particle toughened vinyl ester and epoxy resins, but now rivals that of some engineered thermoplastics [211-213, 215]. It is also important to note that this high fracture toughness is achieved without reduction in T_g, which is typical of rubber toughened systems due to the plasticizing effect of the particles.

8.4 Conclusions

A dual-cure mechanism for the *in-situ* creation of interpenetrating polymer networks (IPNs) for additive manufacturing (AM) was investigated and the effect of network connectivity on overall polymer properties was evaluated. Resins and formulations of individual monomers bearing both vinyl ester and epoxy functionality were prepared. Vinyl ester components capable of polymerizing by photo-induced, free radical polymerization were mixed with thermally driven epoxy-amine systems to facilitate sequential cure of the two systems, whereby the vinyl ester component was photopolymerized using stereolithography (SLA), an AM technique, and the epoxy-amine network was formed during thermal post-curing. The formation of a multi-mechanistic, interconnected, sequentially cured IPN via SLA is shown to produce polymeric materials with T_gs that exceed 120 °C. Overall, polymer network connectivity is shown to have a relatively minimal impact on thermomechanical and thermogravimetric properties; however, manipulation of network level connections is shown to afford materials with high toughness (G_{1C} values as high as 974 J m^{-2}), tensile strength (as high as 51 MPa), and Young's moduli (exceeding 3.5 GPa). Thus, IPNs prepared via multi-cure, AM-based techniques have the potential to be utilized for high performance applications.

Chapter 9

Conclusions and Recommendations for Future Work

9.1 Conclusions

This dissertation focused on molecular-level approaches towards developing performance-enhanced materials, specifically those with improved thermal properties and mechanical integrities (such as toughness) over current, market-dominant resins that can be applied to both classical and upcoming manufacturing methodologies. The first approach via a molecularly hybrid combination of building blocks from bio-based resources, namely lignin and cashew nutshell liquid or long-chain dimethyl esters detailed in Chapters 3 and 4, show that the molecular level combination yields materials that exhibit either comparable thermal properties to that of common, industrial standards and significantly reduced toughness or, in the case of Chapter 4 low thermal properties. Chapters 6 and 7 detail the applicability of bio-based resins toward additive manufacturing techniques, namely stereolithography (SLA). Chapter 6 details a lignin-based resin which does achieve thermal properties comparable to that of industry standards; however, this comes at a significant detriment to the toughness of the material. The formulation approach, detailed in Chapter 7, demonstrates the formulation of tough and high glass transition temperature materials yields intermediate properties that do not exhibit both improved thermal integrities and toughness. In sum, the molecularly hybrid and formulation hybrid approaches did lead to the discovery of novel materials that could have potential uses in commercial and military applications; however, these materials specifically did not achieve the goal of this dissertation: glass transition temperatures

(T_gs) exceeding 120 °C and fracture toughness exceeding industrial standards (G_{1C} > 250 J m^{-2}).

The functionally hybrid approach detailed in Chapter 5 demonstrated the ability to make aromatic monomers with unique functionality, namely both methacrylate and epoxy functionalities. These materials were homopolymerized to prepare thermoplastic aromatic compliments to industrially viable poly(glycidyl methacrylate) for applications such as coatings and adhesives. While these thermoplastic materials yielded interesting results and higher thermal stabilities relative to poly(glycidyl methacrylate), the applicability of the functionally hybrid monomers detailed in Chapter 5 were not applied to thermosetting systems. However, the dual functionality of the monomers prepared in Chapter 5, inspired the preparation of the functionally hybrid, petrochemical-derived resins detailed in Chapter 8. The inclusion of two different polymerizable moieties within the same thermosetting resin was shown to facilitate the preparation of interpenetrating polymers. Furthermore, SLA techniques enabled the sequential conversion of the different polymerizable moieties which, in turn, facilitated unique, interconnected, interpenetrating polymer networks. The utilization of the functionally hybrid resins in Chapter 8, which enabled the manipulation of network-level connections, led to the development of materials with T_gs that exceeded 120 °C and fracture toughness values that approached 1000 J m^{-2}, approximately 4 times higher than conventional cured resins with the same T_g. Thus, the functionally hybrid, sequentially cured, interpenetrating polymers developed in Chapter 8 achieved every goal of this dissertation, including the ability to be applicable to additive manufacturing techniques such as SLA. A summary of all the thermosetting materials prepared in this dissertation is shown in Figure 59, which

detail the toughness, G_{1C}, and T_g, based on the peak of the tan δ observed via dynamic mechanical analysis with arrows indicating general trends.

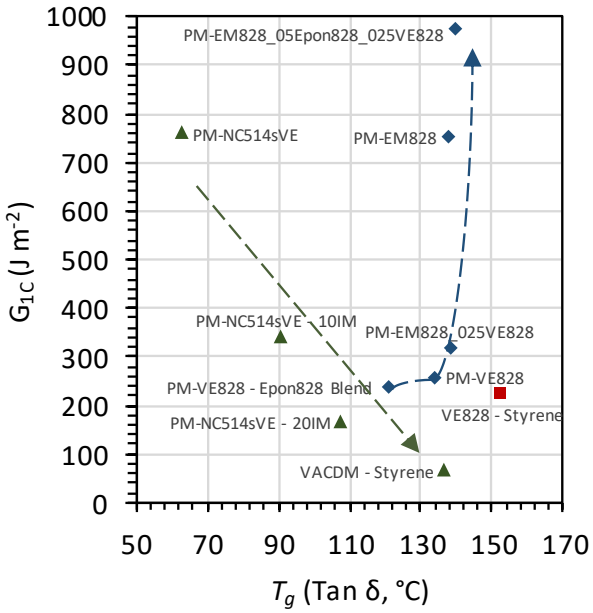

Figure 59. Summary of the fracture toughness values and glass transition temperatures of all thermosets prepared in this dissertation.

While Chapter 8 demonstrates the ability to develop materials with significant improvements in toughness while maintaining high T_gs, it is anticipated that the ultimate utility and applicability of these materials will be hindered due to the slow build rates of SLA. Alternative manufacturing methods to increase production rates of geometric parts and broaden the applicability of the materials presented in Chapter 8 are discussed in the remaining sections.

Furthermore, the spirit of the utilization of bio-based resources as alternatives to petroleum-derived building blocks is heavily explored throughout this dissertation and,

although bio-based materials specifically did not yield the results that were ultimately desired, the remaining sections discuss how bio-based resins could be applied in a similar fashion as discussed in Chapter 8 to further advance material properties in general, most notably high toughness materials where the T_gs are lower than that of conventional, high-performance epoxy and vinyl ester resins.

9.2 Recommendations for Increased Manufacturing Rate of Sequential Interpenetrating Polymers

9.2.1 Photoreactive extrusion. Stereolithography (SLA) additive manufacturing (AM) techniques, which were employed in this dissertation, generally have low build rates on the order of tenths of mL min^{-1}. While the materials prepared in this dissertation, namely those in Chapter 8, exhibit superior performance to that of industrial standards, it is anticipated that the prohibitively slow build rates and geometric size limitations of SLA will limit the use of such materials in higher end applications. Therefore, to increase the applicability of these materials, alternative, larger format manufacturing methods should be explored to circumvent the shortcomings of SLA. One such example is reactive extrusion, which has larger build volumes and build rates on the order of L min^{-1}. However, reactive extrusion is typically designed for click chemistries which enable polymerization and crosslinking upon deposition [216]. It is recommended to employ a modified reactive extrusion methodology as shown in Figure 60, hereafter referred to as photoreactive extrusion, or PRE.

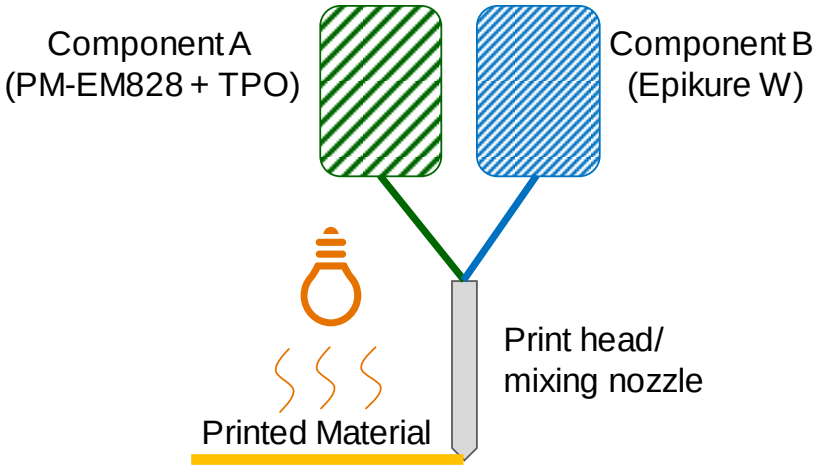

Figure 60. Visual representation of the photoreactive extrusion (PRE) process.

PRE has the potential to increase the scalability of manufacturing of the materials described in Chapter 8, whereby each reservoir contains individual components of the interpenetrating polymer (IPN) formulation, such as the one shown in Figure 60, and the components are subsequently mixed within the print head before deposition. The print head then deposits the resin in a layer-wise fashion and each layer is photocured with UV/visible light. The maximum layer thickness that could be employed in this process would be dependent on the depth of penetration of light into the resin, which could be determined from the SLA working curve characterization technique described in Chapter 2. Determination of the depth of penetration parameter for the IPNs in Chapter 8 is highly recommended. Furthermore, reactive extrusion techniques that exist in the literature have general rheological guidelines in order to determine printability for thermoset systems [216]. The guidelines described, including initial modulus and gel time, could easily be adapted to PRE via the use of photoirradiation rheology accessories, such as that described in Chapter 6, to determine the moduli and gel time when the fully formulated resin is exposed to varying light intensities and wavelengths. However, when applying

the IPN formulations described in Chapter 8 to PRE, it is important to note that only the photosensitive methacrylates of the resin will polymerize during deposition, and the deposited material will be partially cured as the epoxy-amine reaction would not be initiated. Thus, the epoxy and amine monomers would be plasticized within the methacrylate-based polymer matrix. Therefore, a second stage thermal cure analogous to that described in Chapter 8 would need to be employed in order to create the epoxy-amine network and facilitate the interconnection between the IPN components, which ultimately was shown to provide significant performance benefits.

Furthermore, reactive extrusion technologies can handle materials with significantly higher viscosities than SLA [216]. Therefore, in a process such as PRE, fillers, viscosity modifiers, and particulates could easily be incorporated. Additionally, PRE processes could enable the utility of epoxy-amine accelerators to initiate the formation of the second network at ambient conditions, thus curing the individual networks simultaneously and subsequently limiting the need for a high-temperature, second stage cure.

9.2.2 Cold spray. Direct write approaches, such as cold spray (CS), can also be employed to increase manufacturing throughput and diversify the use of the IPNs prepared in Chapter 8. CS is a technique that can be utilized to deposit materials such as metals, polymers, and ceramics onto substrates via the supersonic acceleration of small particles [217]. Upon impact, the particles exhibit plastic deformation and adhere to the substrate. CS is of primary interest for the development of coatings as well as coating repair and refinish processes [217]. While polymeric materials have been investigated in CS manufacturing techniques, the study of reactive polymeric particles in CS is limited

[218]. Since the materials derived in Chapter 8 are prepared via sequential cure, and the final IPNs prepared exhibit outstanding properties, these materials have the potential to be interesting candidates in reactive CS techniques such as that pictured in Figure 61.

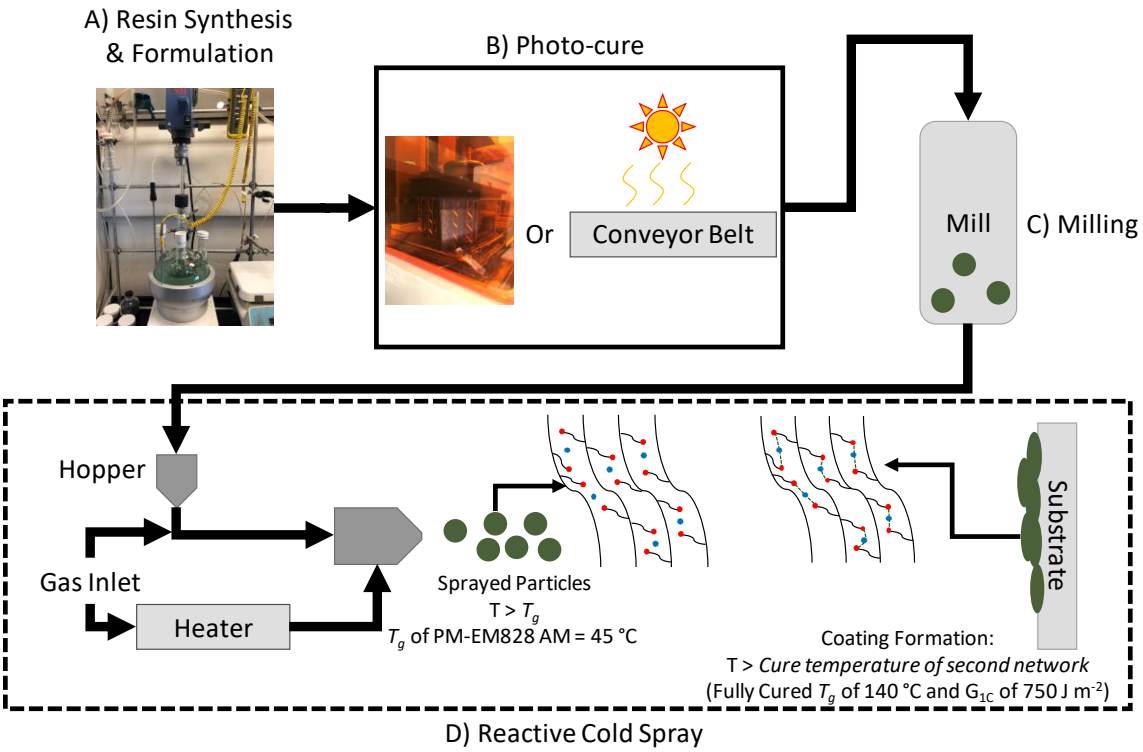

Figure 61. Proposed reactive cold spray (CS) process diagram.

The proposed process in Figure 61 demonstrates the potential use of the IPNs in Chapter 8, such as the PM-EM828 resin for example, in CS; whereby the formulated resin is irradiated with light (either via SLA printing or simple thin-film, high-throughput techniques such as passing the resin under a light via a conveyor belt) to form the methacrylate network which is plasticized with epoxy and amine monomers. The partially cured material would then be subjected to milling processes to create particles of

the correct size for applicability in CS. It is then hypothesized that these partially cured particles could then be sprayed at a temperature above the T_g, which in the case of PM-EM828 is 45 °C, such that the material exhibits a rubbery behavior, thus facilitating easier deformation upon impact with the substrate to create the coating. Furthermore, the substrate can be heated to a temperature that initiates the polymerization of the epoxy-amine network which, in turn, could lead to chemical connections between each of the individual polymer particles that are deposited, thus creating a robust, uniform coating.

In order to evaluate this hypothesis, it is recommended that the applicability of the partially cured particles in CS be evaluated. Furthermore, the cure kinetics of the secondary network (epoxy-amine) should be investigated to determine the time scales on which the formation of the secondary network takes place. Finally, the robustness of the fully cured, IPN-based coating should be evaluated.

9.3 Recommendations for Bio-Based, Sequential Interpenetrating Polymers

The formation of sequentially cured, interpenetrating polymers (IPNs) detailed in Chapter 8 exhibit not only comparable thermal properties to that of high-performance epoxies and vinyl ester resins, but also remarkably improved toughness as a result of the unique network-level connections. Interestingly, the network connectivity in Chapter 8 is shown to have a relatively minimal impact on thermal properties, but a substantial impact on mechanical properties. The T_g of the resulting IPN appears to be a function of the monomeric structures utilized in the IPN formulation and the toughness appears to be a result of the network connectivity. Therefore, the starting molecules which, on a structure-property relationship basis have inherently lower T_gs and higher G_{1C} values than that of the bisphenol A derived materials discussed in Chapter 8, should yield

thermosetting IPNs which exhibit overall lower T_gs and higher G_{1C} values exceeding 1000 J m^{-2}.

For example, the bio-based PM-NC514sVE cured resin discussed in Chapter 7 has a T_g of 63 °C and a G_{1C} of 761 J m^{-2} and the petroleum-derived PM-VE828 has a T_g of 134 °C and a G_{1C} of 255 J m^{-2}. Therefore, the structure-property differences between using bio-based NC514sVE instead of petroleum- and bisphenol A-based VE828 results in a decrease in T_g of approximately 70 °C and increase of G_{1C} by approximately 510 J m^{-2}. The manipulation of network connectivity using bisphenol A-based building blocks to create the PM-EM828 IPN results in a T_g of approximately 138 °C and a G_{1C} of 753 J m^{-2}. Compared to the PM-VE828 cured resin, this results in a minor change in T_g and a major, threefold increase in G_{1C}. Therefore, it is hypothesized that the structure-property relationships observed in bio-based monomers can be used to manipulate the properties that are enhanced through network connectivity changes. Thus, it is recommended to develop bio-based, functionally hybrid materials analogous to those described in Chapter 8 to take advantage of the performance enhancement benefits of the IPN formation. An example is given in Figure 62, the preparation of functionally hybrid resin PM-EMNC514s. Because of the structure property-relationships detailed earlier, it is anticipated for this material, when cured, to exhibit a T_g comparable to that of PM-NC514sVE (63 °C); however, the network connectivity is hypothesized to enhance the fracture toughness of the final material similar to that which occurred with the petroleum-derived IPNs, thus increasing the G_{1C} from 753 J m^{-2} to a value exceeding 2,250 J m^{-2}.

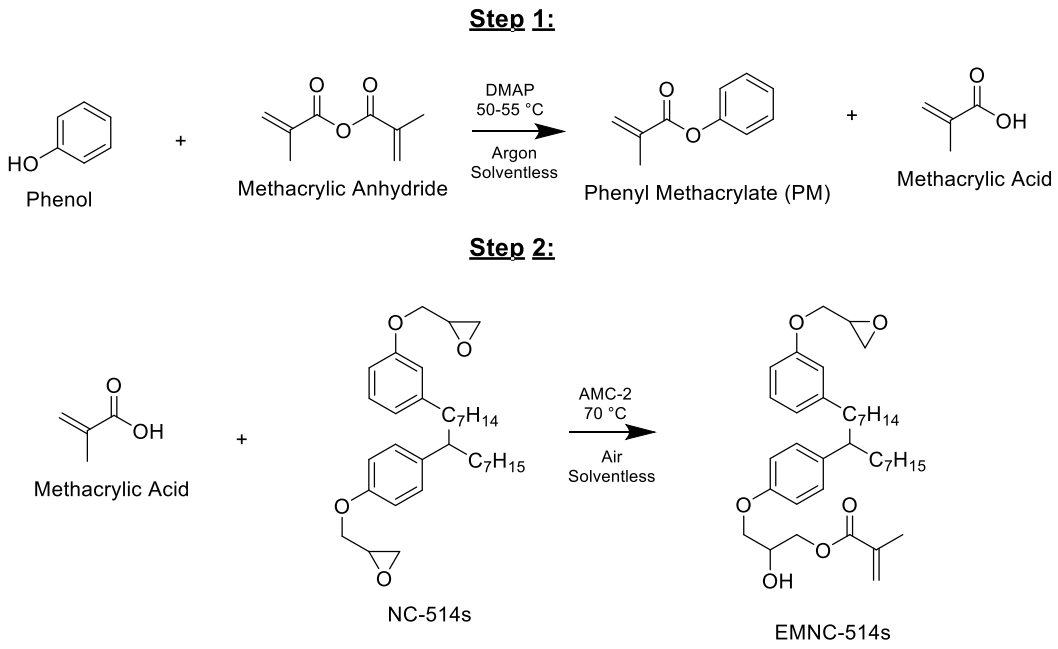

Figure 62. Reaction scheme for the preparation of PM-EMNC514s.

Efforts to incorporate some bio-based content into the IPN formulation was studied preliminarily. The best performing IPN described in Chapter 8 (PM-EM828_05Epon828_025VE828) was utilized as a basis for this study, whereby the Epon828 component was replaced with either cashew nutshell liquid (CNSL) derived NC514s or epoxidized VAC (EVAC), which was prepared via the epoxidation of the VAC bisphenol presented in Chapter 3, to prepare PM-EM828_05NC514s_025VE828 and PM-EM828_05EVAC_025VE828, respectively. These materials were made via sequential cure using SLA as described in Chapter 8 and the final materials were evaluated for their fracture toughness. The load-displacement curves are shown in Figure 63 and the K_{1C} and G_{1C} values are presented in Table 31.

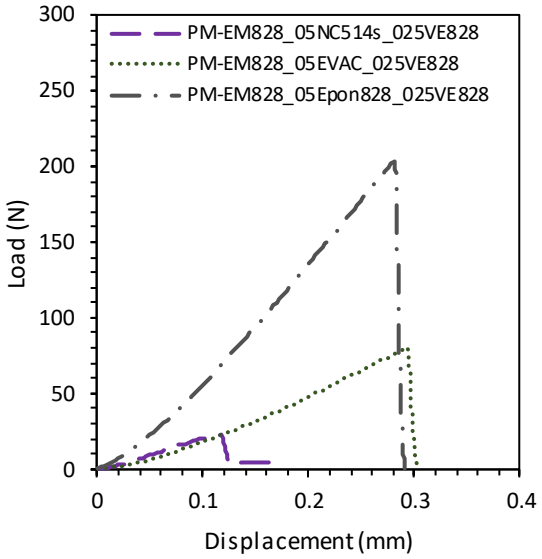

Figure 63. Load-displacement curves of IPNs containing bio-based epoxies.

Table 31

Fracture toughness K_{1C} and G_{1C} values of IPNs containing bio-based epoxies

Sample	G_{1C} (J m^{-2})	K_{1C} (MPa m$^{1/2}$)
PM-EM828_05NC514s_025VE828	64 ± 4	0.08 ± 0.01
PM-EM828_05EVAC_025VE828	805 ± 51	0.30 ± 0.02
PM-EM828_05Epon828_025VE828	974 ± 41	0.70 ± 0.03

In sum, the incorporation of the bio-based epoxies decreased the fracture toughness relative to the PM-EM828_05Epon828_025VE828 IPN. The decrease in fracture toughness for the PM-EM828_05NC514s_025VE828 IPN is likely a result of the material exhibiting macroscopic level phase separation throughout all stages of cure, thus likely resulting in poor interconnectivity between the independent components of the IPN. Furthermore, the utilization of EVAC also resulted in a decrease in fracture toughness, although not to the magnitude as shown with NC514s. This result is

hypothesized to be a result of non-uniformity of the monomers utilized in the total IPN formulation. Therefore, it is recommended to repeat this procedure whereby each component of the IPN is comprised of monomers with the same exact molecular backbones with the only variation being the reactive handles on the terminus of the monomer structure. An example of this would be a resin such as PM_EMNC514s_05NC514s_025NC514sVE, of which the molecular structures are shown in Figure 64. Homogenizing the backbone of the monomeric structures is hypothesized to reduce phase separation and create three-dimensional networks that are relatively uniform, thus improving the overall toughness of these materials as expected.

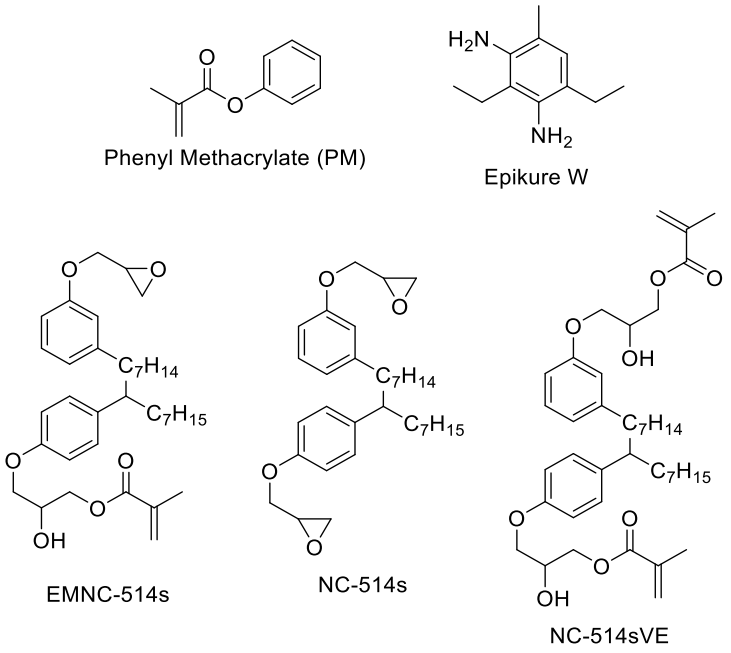

Figure 64. Proposed, bio-based IPN components.

References

[1] D. Feldman and A. Barbalata, *Synthetic Polymers: Technology, Properties, Applications*, 1st ed. London: Chapman Hill, 1996.

[2] J. R. Fried, *Polymer Science and Technology*, 2nd ed. Upper Saddle River, NJ: Prentice Hall Professional Technical Reference, 2003.

[3] G. G. Odian, *Principles of Polymerization*, 3rd ed. New York: Wiley, 1991.

[4] J. J. La Scala, J. A. Orlicki, C. Winston, E. J. Robinette, J. M. Sands, and G. R. Palmese, "The use of bimodal blends of vinyl ester monomers to improve resin processing and toughen polymer properties," (in English), *Polymer,* vol. 46, no. 9, pp. 2908-2921, Apr 15 2005.

[5] J. J. La Scala, J. M. Sands, J. A. Orlicki, E. J. Robinette, and G. R. Palmese, "Fatty acid-based monomers as styrene replacements for liquid molding resins," (in English), *Polymer,* vol. 45, no. 22, pp. 7729-7737, Oct 13 2004.

[6] S. Ziaee and G. R. Palmese, "Effects of temperature on cure kinetics and mechanical properties of vinyl-ester resins," (in English), *Journal of Polymer Science Part B-Polymer Physics,* vol. 37, no. 7, pp. 725-744, Apr 1 1999.

[7] C. A. May, *Epoxy resins : chemistry and technology*. New York: Marcel Dekker, 1988.

[8] E. A. Baroncini, S. K. Yadav, G. R. Palmese, and J. F. Stanzione III, "Recent advances in bio-based epoxy resins and bio-based epoxy curing agents," (in English), *Journal of Applied Polymer Science,* vol. 133, no. 45, Dec 5 2016.

[9] M. Sultania, J. S. P. Rai, and D. Srivastava, "Studies on the synthesis and curing of epoxidized novolac vinyl ester resin from renewable resource material," (in English), *European Polymer Journal,* vol. 46, no. 10, pp. 2019-2032, Oct 2010.

[10] J. J. La Scala, M. S. Logan, J. M. Sands, and G. R. Palmese, "Composites based on bimodal vinyl ester resins with low hazardous air pollutant contents," (in English), *Composites Science and Technology,* vol. 68, no. 7-8, pp. 1869-1876, Jun 2008.

[11] E. Can, E. Kinaci, and G. R. Palmese, "Preparation and characterization of novel vinyl ester formulations derived from cardanol," (in English), *European Polymer Journal,* vol. 72, pp. 129-147, Nov 2015.

[12] S. Jaswal and B. Gaur, "New trends in vinyl ester resins," (in English), *Reviews in Chemical Engineering,* vol. 30, no. 6, pp. 567-581, Dec 2014.

[13] P. N. Shah *et al.*, "Environmentally benign synthesis of vinyl ester resin from biowaste glycerin," *RSC Advances,* vol. 5, no. 48, pp. 38673-38679, 2015.

[14] M. Kumar, S. Mohanty, S. K. Nayak, and M. Rahail Parvaiz, "Effect of glycidyl methacrylate (GMA) on the thermal, mechanical and morphological property of biodegradable PLA/PBAT blend and its nanocomposites," *Bioresource Technology,* vol. 101, no. 21, pp. 8406-15, Nov 2010.

[15] (2018). *How is Glycidyl Methacrylate (GMA) used and what are the key benefits?* Available: https://dowac.custhelp.com/app/answers/detail/a_id/4249/~/gma---applications-and-benefits.

[16] P. K. Kuroishi, M. J. Bennison, and A. P. Dove, "Synthesis and post-polymerisation modification of an epoxy-functional polycarbonate," *Polymer Chemistry*, vol. 7, no. 46, pp. 7108-7115, 2016.

[17] F. Jaillet, H. Nouailhas, R. Auvergne, A. Ratsimihety, B. Boutevin, and S. Caillol, "Synthesis and characterization of novel vinylester prepolymers from cardanol," (in English), *European Journal of Lipid Science and Technology,* vol. 116, no. 7, pp. 928-939, Jul 2014.

[18] C. Voirin, S. Caillol, N. V. Sadavarte, B. V. Tawade, B. Boutevin, and P. P. Wadgaonkar, "Functionalization of cardanol: towards biobased polymers and additives," (in English), *Polymer Chemistry,* vol. 5, no. 9, pp. 3142-3162, 2014.

[19] M. Fache, B. Boutevin, and S. Caillol, "Epoxy thermosets from model mixtures of the lignin-to-vanillin process," *Green Chemistry,* vol. 18, no. 3, pp. 712-725, 2016.

[20] S. K. Yadav, K. M. Schmalbach, E. Kinaci, J. F. Stanzione, and G. R. Palmese, "Recent advances in plant-based vinyl ester resins and reactive diluents," (in English), *European Polymer Journal,* vol. 98, pp. 199-215, Jan 2018.

[21] J. A. Carioscia, J. W. Stansbury, and C. N. Bowman, "Evaluation and Control of Thiol-ene/Thiol-epoxy Hybrid Networks," *Polymer,* vol. 48, no. 6, pp. 1526-1532, Mar 8 2007.

[22] L. H. Sperling, "Interpenetrating Polymer Networks: An Overview," in *Interpenetrating Polymer Networks*, vol. 239 (Advances in Chemistry, no. 239): American Chemical Society, 1994, pp. 3-38.

[23] L. G. Wade, *Organic Chemistry*, 6th ed. Upper Saddle River, N.J.: Pearson Prentice Hall, 2006.

[24] M. Balci, *Basic 1H-13C-NMR Spectroscopy*. Amsterdam: Elsevier, 2005.

[25] V. Shah, *Handbook of plastics testing technology*. *Second edition*. New York, NY (United States); John Wiley and Sons, 1998, p. 527.

[26] A. W. Bassett, A. E. Honnig, C. M. Breyta, I. C. Dunn, J. J. La Scala, and J. F. Stanzione III, "Vanillin-based Resin for Additive Manufacturing," *In Preparation*.

[27] P. F. Jacobs, *Rapid Prototyping and Manufacturing: Fundamentals of StereoLithography*. McGraw-Hill, Inc., 1993.

[28] M. A. Durivage, "6.4.2.4 Log-Normal Distribution," in *Certified Reliability Engineer Handbook (3rd Edition)*: American Society for Quality (ASQ).

[29] D. Halliday, R. Resnick, and J. Walker, *Fundamentals of Physics*. Hoboken, NJ: Wiley, 2014.

[30] J. Duncan, "Principles and Applications of Mechanical Thermal Analysis," in *Principles and Applications of Thermal Analysis* Oxford, UK: Blackwell Publishing LTD, 2008, pp. 119-163.

[31] P. J. Flory, *Principles of Polymer Chemistry*. Ithaca: Cornell University Press, 1953.

[32] I. M. McAninch, G. R. Palmese, J. L. Lenhart, and J. J. La Scala, "DMA Testing of Epoxy Resins: The Importance of Dimensions," *Polymer Engineering and Science,* vol. 55, no. 12, pp. 2761-2774, 2015.

[33] *ASTM D638 Standard Test Method for Tensile Properties of Plastics,* 2018.

[34] *ASTM D5045-14 Standard Test Methods for Plane-Strain Fracture Toughness and Strain Energy Release Rate of Plastic Materials,* 2014.

[35] I. M. McAninch, J. J. La Scala, G. R. Palmese, and E. J. Robinette, "Thin film initiation of cracks for fracture toughness measurements in epoxy resins," *Journal of Applied Polymer Science,* vol. 134, no. 1, 2017.

[36] A. W. Bassett *et al.*, "Synthesis and characterization of molecularly hybrid bisphenols derived from lignin and CNSL: Application in thermosetting resins," *European Polymer Journal,* vol. 111, pp. 95-103, 2019.

[37] "European Union Summary Risk Assessment Report - 4,4'-isopropylidenediphenol (Bisphenol A)," European Chemicals Bureau, United Kingdom, 2003.

[38] "Report on Carcinogens, Thirteenth Edition.," National Toxicology Program. Department of Health and Human Services, Public Health Service NC, USA 2014, Available: http://ntp.niehs.nih.gov/pubhealth/roc/roc13/.

[39] "NTP-CERHR Expert Panel Report on the Reproductive and Developmental Toxcity of Bisphenol A," National Toxicology Program, Research Triangle Park, NC, 2007.

[40] L. N. Vandenberg, R. Hauser, M. Marcus, N. Olea, and W. V. Welshons, "Human exposure to bisphenol A (BPA)," *Reproductive Toxicololgy,* vol. 24, no. 2, pp. 139-177, 2007.

[41] J. A. Rogers, L. Metz, and V. W. Yong, "Review: Endocrine disrupting chemicals and immune responses: A focus on bisphenol-A and its potential mechanisms," *Molecular Immunology,* vol. 53, pp. 421-430, 2013.

[42] S. Eladak *et al.*, "A new chapter in the bisphenol A story: bisphenol S and bisphenol F are not safe alternatives to this compound," *Fertility and Sterility*, vol. 103, no. 1, pp. 11-21, 2015.

[43] J. F. Stanzione, P. A. Giangiulio, J. M. Sadler, J. J. La Scala, and R. P. Wool, "Lignin-Based Bio-Oil Mimic as Biobased Resin for Composite Applications," (in English), *ACS Sustainable Chemistry & Engineering*, vol. 1, no. 4, pp. 419-426, Apr 2013.

[44] J. M. Sadler *et al.*, "Isosorbide-methacrylate as a bio-based low viscosity resin for high performance thermosetting applications," (in English), *Journal of Materials Chemistry A*, vol. 1, no. 40, pp. 12579-12586, 2013.

[45] M. L. B. Duarte, L. A. R. Medina, P. T. Reyes, S. E. G. Perez, and A. M. H. Gonzalez, "Biobased isosorbide methacrylate monomer as an alternative to bisphenol A glycerolate dimethacrylate for dental restorative applications," (in English), *Journal of Applied Polymer Science*, vol. 134, no. 11, Mar 2017.

[46] Y. Mansoori, S. Hemmati, P. Eghbali, M. R. Zamanloo, and G. Imanzadeh, "Nanocomposite materials based on isosorbide methacrylate/Cloisite 20A," (in English), *Polymer International*, vol. 62, no. 2, pp. 280-288, Feb 2013.

[47] Z. Vazifehasl, S. Hemmati, M. Zamanloo, and M. Jaymand, "Synthesis and Characterization of Novel Diglycidyl Methacrylate-Based Macromonomers on Isosorbide for Dental Composites," (in English), *Macromolecular Research*, vol. 21, no. 4, pp. 427-434, Apr 2013.

[48] K. Liu, *Soybeans: Chemistry, Technology and Utilization*. New York: Chapman & Hall, 1997.

[49] D. P. S. Verma and R. C. Shoemaker, *Soybean: Genetics, Molecular Biology and Biotechnology*. Wallingford, UK: Cab International, 1996.

[50] A. Campanella, M. J. Zhan, P. Watt, A. T. Grous, C. C. Shen, and R. P. Wool, "Triglyceride-based thermosetting resins with different reactive diluents and fiber reinforced composite applications," (in English), *Composites Part A-Applied Science and Manufacturing*, vol. 72, pp. 192-199, May 2015.

[51] E. S. Beach, Z. Cui, P. T. Anastas, M. J. Zhan, and R. P. Wool, "Properties of Thermosets Derived from Chemically Modified Triglycerides and Bio-Based Comonomers," (in English), *Applied Sciences,* vol. 3, no. 4, pp. 684-693, Dec 2013.

[52] E. Can, R. P. Wool, and S. Kusefoglu, "Soybean and castor oil based monomers: Synthesis and copolymerization with styrene," (in English), *Journal of Applied Polymer Science,* vol. 102, no. 3, pp. 2433-2447, Nov 5 2006.

[53] E. Can, R. P. Wool, and S. Kusefoglu, "Soybean- and castor-oil-based thermosetting polymers: mechanical properties," (in English), *Journal of Applied Polymer Science,* vol. 102, no. 2, pp. 1497-1504, Oct 15 2006.

[54] D. Balgude and A. S. Sabnis, "CNSL: an environment friendly alternative for the modern coating industry," (in English), *Journal of Coatings Technology and Research,* vol. 11, no. 2, pp. 169-183, Mar 2014.

[55] M. Banchhor and R. Baid, "CNSL (cashew nut shell liquid) - A versatile renewable natural resource," (in English), *Plant Archives,* vol. 7, no. 2, pp. 497-501, Oct 2007.

[56] H. X. Hong *et al.,* "Experimental Data Extraction and in Silico Prediction of the Estrogenic Activity of Renewable Replacements for Bisphenol A," (in English), *International Journal of Environmental Research and Public Health,* vol. 13, no. 7, Jul 2016.

[57] F. G. Calvo-Flores and J. A. Dobado, "Lignin as Renewable Raw Material," *ChemSusChem,* vol. 3, no. 11, pp. 1227-1235, 2010.

[58] F. S. Chakar and A. J. Ragauskas, "Review of current and future softwood kraft lignin process chemistry," (in English), *Industrial Crops and Products,* vol. 20, no. 2, pp. 131-141, Sep 2004.

[59] J. Holladay, J. White, J. Bozell, and D. Johnson, "Top Value-Added Chemicals from Biomass - Volume II—Results of Screening for Potential Candidates from Biorefinery Lignin," Pacific Northwest National Laboratory, Richland, WA2007.

[60] T. Saito *et al.*, "Turning renewable resources into value-added polymer: development of lignin-based thermoplastic," *Green Chemistry,* vol. 14, no. 12, pp. 3295-3303, 2012.

[61] E. D. Hernandez, A. W. Bassett, J. M. Sadler, J. J. La Scala, and J. F. Stanzione III, "Synthesis and Characterization of Bio-based Epoxy Resins Derived from Vanillyl Alcohol," *ACS Sustainable Chemistry & Engineering,* vol. 4, no. 8, pp. 4328-4339, 2016.

[62] P. J. De Wild, W. J. J. Huijgen, and R. J. A. Gosselink, "Lignin pyrolysis for profitable lignocellulosic biorefineries," (in English), *Biofuels Bioproducts & Biorefining,* vol. 8, no. 5, pp. 645-657, Sep-Oct 2014.

[63] D. K. Shen, S. Gu, K. H. Luo, S. R. Wang, and M. X. Fang, "The pyrolytic degradation of wood-derived lignin from pulping process," *Bioresource Technology,* 10.1016/j.biortech.2010.02.078 vol. 101, no. 15, pp. 6136-6146, 2010.

[64] T. D. H. Bugg, M. Ahmad, E. M. Hardiman, and R. Rahmanpour, "Pathways for degradation of lignin in bacteria and fungi," (in English), *Natural Product Reports,* vol. 28, no. 12, pp. 1883-1896, 2011.

[65] J. D. Araujo, "Production of vanillin from lignin present in the Kraft black liquor of the pulp and paper industry," Doctor of Philosophy, Chemical Engineering, University of Porto, 2008.

[66] H.-R. Bjorsvik and F. Minisci, "Fine Chemicals from Lignosulfonates. 1. Synthesis of Vanillin by Oxidation of Lignosulfonates," *Organic Process Research & Development,* vol. 3, no. 5, pp. 330-340, 1999.

[67] E. A. Borges da Silva *et al.*, "An integrated process to produce vanillin and lignin-based polyurethanes from Kraft lignin," *Chemical Engineering Research & Design, v*ol. 87, no. 9, pp. 1276-1292, 2009.

[68] J. D. P. Araujo, C. A. Grande, and A. E. Rodrigues, "Vanillin production from lignin oxidation in a batch reactor," *Chemical Engineering Research & Design,* vol. 88, no. 8, pp. 1024-1032, 2010.

[69] M. B. Hocking, "Vanillin: Synthetic flavoring from spent sulfite liquor," *Journal of Chemical Education,* vol. 74, no. 9, pp. 1055-1059, 1997.

[70] "Part 3 - Aroma chemicals from petrochemical feedstocks, in: Study into the establishment of an aroma and fragrance fine chemicals value chain in South Africa," Triumph Venture Capital, Ltd, South Africa, 2004.

[71] C. S. Lecher. (2007). *Sodium Borohydride Reduction of Vanillin: A Low Solvent Synthesis of Vanillyl Alcohol*. Available: http://greenchem.uoregon.edu/PDFs/GEMsID90.pdf.

[72] T. S. Gandhi, B. Z. Dholakiya, and M. R. Patel, "Extraction protocol for isolation of CNSL by using protic and aprotic solvents from cashew nut and study of their physico-chemical parameter," (in English), *Polish Journal of Chemical Technology,* vol. 15, no. 4, pp. 24-27, 2013.

[73] F. Jaillet, E. Darroman, A. Ratsimihety, R. Auvergne, B. Boutevin, and S. Caillol, "New biobased epoxy materials from cardanol," (in English), *European Journal of Lipid Science and Technology,* vol. 116, no. 1, pp. 63-73, Jan 2014.

[74] S. K. Sanjeeva *et al.*, "Distilled technical cashew nut shell liquid (DT-CNSL) as an effective biofuel and additive to stabilize triglyceride biofuels in diesel," (in English), *Renewable Energy,* vol. 71, pp. 81-88, Nov 2014.

[75] F. Jaillet, E. Darroman, A. Ratsimihety, B. Boutevin, and S. Caillol, "Synthesis of cardanol oil building blocks for polymer synthesis," (in English), *Green Materials,* vol. 3, no. 3, pp. 59-70, Sep 2015.

[76] F. Jaillet, E. Darroman, B. Boutevin, and S. Caillol, "A chemical platform approach on cardanol oil: from the synthesis of building blocks to polymer synthesis," (in English), *Ocl-Oilseeds and Fats Crops and Lipids,* vol. 23, no. 5, Sep-Oct 2016.

[77] E. D. Hernandez, A. W. Bassett, J. M. Sadler, J. J. La Scala, and J. F. Stanzione, "Synthesis and Characterization of Bio-based Epoxy Resins Derived from Vanillyl Alcohol," *ACS Sustainable Chemistry & Engineering,* vol. 4, no. 8, pp. 4328-4339, 2016.

[78] A. W. Bassett, D. P. Rogers, J. M. Sadler, J. J. La Scala, R. P. Wool, and J. F. Stanzione, "The effect of impurities in reactive diluents prepared from lignin model compounds on the properties of vinyl ester resins," (in English), *Journal of Applied Polymer Science,* vol. 133, no. 45, Dec 5 2016.

[79] R. P. Brill and G. R. Palmese, "An investigation of vinyl-ester - Styrene bulk copolymerization cure kinetics using Fourier transform infrared spectroscopy," (in English), *Journal of Applied Polymer Science,* vol. 76, no. 10, pp. 1572-1582, Jun 6 2000.

[80] C. J. Pouchert and Aldrich Chemical Company., *The Aldrich library of infrared spectra*, Ed. 3. ed. Milwaukee, Wis. (940 W. St. Paul Ave., Milwaukee 53233): Aldrich Chemical Co., 1981, pp. xxiii, 1873 p.

[81] J. La Scala and R. P. Wool, "Rheology of chemically modified triglycerides," *Journal of Applied Polymer Science,* vol. 95, no. 3, pp. 774-783, 2005.

[82] R. Wool and X. S. Sun, *Bio-Based Polymers and Composites*, 1 ed. Burlington, MA: Elsevier Academic Press, 2005, p. 640.

[83] R. C. Petersen, "Reactive Secondary Sequence Oxidative Pathology Polymer Model and Antioxidant Tests," *International Research Journal of Pure amd Applied Chemistry,* vol. 2, no. 4, pp. 247-285, 2012.

[84] B. Lochab, I. K. Varma, and J. Bijwe, "Thermal behaviour of cardanol-based benzoxazines," (in English), *Journal of Thermal Analysis and Calorimetry,* vol. 102, no. 2, pp. 769-774, Nov 2010.

[85] B. G. Harvey *et al.*, "Effects of o-Methoxy Groups on the Properties and Thermal Stability of Renewable High-Temperature Cyanate Ester Resins," (in English), *Macromolecules,* vol. 48, no. 10, pp. 3173-3179, May 26 2015.

[86] C. S. Song, W. C. Lai, and H. H. Schobert, "Hydrogen-Transferring Pyrolysis of Long-Chain Alkanes and Thermal-Stability Improvement of Jet Fuels by Hydrogen Donors," (in English), *Industrial & Engineering Chemistry Research,* vol. 33, no. 3, pp. 548-557, Mar 1994.

[87] J. Yu and S. Eser, "Thermal decomposition of C-10-C-14 normal alkanes in near-critical and supercritical regions: Product distributions and reaction mechanisms,"

(in English), *Industrial & Engineering Chemistry Research*, vol. 36, no. 3, pp. 574-584, Mar 1997.

[88] H. W. Moeller, *Progress in Polymer Degradation and Stability Research*. Nova Publishers, 2007.

[89] L. E. N. a. R. F. Landel, *Mechanical Properties of Polymers and Composites*. New York, NY: Marcel Dekker Inc., 1994.

[90] S. Miura, Y. Shidara, T. Yunoki, M. A. A. Mamun, Y. Shibasaki, and A. Fujimori, "High-Density Packing of Amorphous Polymer with Bulky Aromatic Rings in Interfacial Molecular Films," *Macromolecular Chemistry and Physics*, vol. 218, no. 7, 2017.

[91] R. P. Wool, "Twinkling fractal theory of the glass transition," *Journal of Polymer Science Part B: Polymer Physics*, vol. 46, no. 24, pp. 2765-2778, 2008.

[92] J. Park, J. Eslick, Q. Ye, A. Misra, and P. Spencer, "The influence of chemical structure on the properties in methacrylate-based dentin adhesives," *Dental Materials*, vol. 27, no. 11, pp. 1086-93, Nov 2011.

[93] J. F. Stanzione, K. E. Strawhecker, and R. P. Wool, "Observing the twinkling fractal nature of the glass transition," (in English), *Journal of Non-Crystalline Solids*, vol. 357, no. 2, pp. 311-319, Jan 15 2011.

[94] B. Yancey and J. E. Ritchie, "Adding free volume to PEG based anhydrous proton conducting electrolytes with bulky copolymers," (in English), *Journal of Electroanalytical Chemistry*, vol. 706, pp. 117-126, Oct 1 2013.

[95] X. Lu, G. Xue, and Y. Mi, "Understanding the effect of chain entanglement on the glass transition of a hydrophilic polymer," *Journal of Applied Polymer Science*, vol. 119, no. 4, pp. 2310-2317, 2011.

[96] I.M. McAninch, G. R. Palmese, J. L. Lenhart, and J. J. L. Scala, "Characterization of Epoxies Cured with Bimodal Blends of Polyetheramines," *Journal of Applied Polymer Science*, 2013.

[97] T. Liu, Y. Nie, L. Zhang, R. Chen, Y. Meng, and X. Li, "Dependence of epoxy toughness on the backbone structure of hyperbranched polyether modifiers," *RSC Advances*, vol. 5, no. 5, pp. 3408-3416, 2015.

[98] M. Fache, E. Darroman, V. Besse, R. Auvergne, S. Caillol, and B. Boutevin, "Vanillin, a promising biobased building-block for monomer synthesis," *Green Chemistry*, vol. 16, no. 4, pp. 1987-1998, 2014.

[99] S. Curia, A. F. Barclay, S. Torron, M. Johansson, and S. M. Howdle, "Green process for green materials: viable low-temperature lipase-catalysed synthesis of renewable telechelics in supercritical CO_2," (in English), *Philosophical Transactions of the Royal Society a-Mathematical Physical and Engineering Sciences*, vol. 373, no. 2057, Dec 28 2015.

[100] J. X. Zhang *et al.*, "Recent developments in lipase-catalyzed synthesis of polymeric materials," (in English), *Process Biochemistry*, vol. 49, no. 5, pp. 797-806, May 2014.

[101] A. Olsson, M. Lindstrom, and T. Iversen, "Lipase-catalyzed synthesis of an epoxy-functionalized polyester from the suberin monomer cis-9,10-epoxy-18-hydroxyoctadecanoic acid," (in English), *Biomacromolecules*, vol. 8, no. 2, pp. 757-760, Feb 2007.

[102] G. Montaudo and P. Rizzarelli, "Synthesis and enzymatic degradation of aliphatic copolyesters," (in English), *Polymer Degradation and Stability*, vol. 70, no. 2, pp. 305-314, 2000.

[103] C. Capello, U. Fischer, and K. Hungerbuhler, "What is a green solvent? A comprehensive framework for the environmental assessment of solvents," (in English), *Green Chemistry*, vol. 9, no. 9, pp. 927-934, 2007.

[104] P. G. Jessop, "Searching for green solvents," (in English), *Green Chemistry*, vol. 13, no. 6, pp. 1391-1398, 2011.

[105] S. Curia *et al.*, "Betulin-Based Thermoplastics and Thermosets through Sustainable and Industrially Viable Approaches: New Insights for the Valorization of an Underutilized Resource," (in English), *ACS Sustainable Chemistry & Engineering*, vol. 7, no. 19, pp. 16371-16381, Oct 7 2019.

[106] G. G. Barclay, C. K. Ober, K. I. Papathomas, and D. W. Wang, "Liquid-Crystalline Epoxy Thermosets Based on Dihydroxymethylstilbene - Synthesis and Characterization," (in English), *Journal of Polymer Science Part A-Polymer Chemistry*, vol. 30, no. 9, pp. 1831-1843, Aug 1992.

[107] C. Carfagna, E. Amendola, and M. Giamberini, "Liquid crystalline epoxy based thermosetting polymers," (in English), *Progress in Polymer Science*, vol. 22, no. 8, pp. 1607-1647, 1997.

[108] A. W. Bassett *et al.*, "Dual-functional, aromatic, epoxy-methacrylate monomers from bio-based feedstocks and their respective epoxy-functional thermoplastics," *Journal of Polymer Science*, vol. 58, no. 5, pp. 673-682, 2020.

[109] J. Kim, H. Oh, and E. Kim, "A dual-functional monomer having an epoxy and methacrylate group for holographic recording," *Journal of Materials Chemistry*, vol. 18, no. 40, 2008.

[110] P. Jiang, Y. Shi, P. Liu, and Y. Cai, "Synthesis of well-defined glycidyl methacrylate based block copolymers with self-activation and self-initiation behaviors via ambient temperature atom transfer radical polymerization," *Journal of Polymer Science Part A: Polymer Chemistry*, vol. 45, no. 14, pp. 2947-2958, 2007.

[111] Ezzah M. Muzammil, A. Khan, and M. C. Stuparu, "Post-polymerization modification reactions of poly(glycidyl methacrylate)s," *RSC Advances*, vol. 7, no. 88, pp. 55874-55884, 2017.

[112] X. Luo, R. Ou, D. E. Eberly, A. Singhal, W. Viratyaporn, and P. T. Mather, "A thermoplastic/thermoset blend exhibiting thermal mending and reversible adhesion," *ACS Applied Materials & Interfaces*, vol. 1, no. 3, pp. 612-20, Mar 2009.

[113] B. G. Harvey *et al.*, "Renewable thermosetting resins and thermoplastics from vanillin," *Green Chemistry*, vol. 17, no. 2, pp. 1249-1258, 2015.

[114] A. L. Holmberg, K. H. Reno, N. A. Nguyen, R. P. Wool, and T. H. Epps III, "Syringyl Methacrylate, a Hardwood Lignin-Based Monomer for High-Tg Polymeric Materials," *ACS Macro Letters*, vol. 5, no. 5, pp. 574-578, May 17 2016.

[115] T. S. Junko Hayashia, Shigeyoshi Deguchia, Qing Linb, Syunji Horiea, Shizuko Tsuchiyaa, Shingo Yanoa, Kazuo Watanabea, Fumio Ikegamia, "Phenolic compounds from Gastrodia rhizome and relaxant effects of related compounds on isolated smooth muscle preparation," *Phytochemistry,* vol. 59, pp. 513-519, 2001.

[116] S. Y. Huang, G. Q. Li, J. G. Shi, and S. Y. Mo, "Chemical constituents of the rhizomes of Coeloglossum viride var. bracteatum," *Journal of Asian Natural Products Research,* vol. 6, no. 1, pp. 49-61, Mar 2004.

[117] M. Larriba, S. Omar, P. Navarro, J. García, F. Rodríguez, and M. Gonzalez-Miquel, "Recovery of tyrosol from aqueous streams using hydrophobic ionic liquids: a first step towards developing sustainable processes for olive mill wastewater (OMW) management," *RSC Advances,* vol. 6, no. 23, pp. 18751-18762, 2016.

[118] J. A. Emerson, N. T. Garabedian, D. L. Burris, E. M. Furst, and T. H. Epps III, "Exploiting Feedstock Diversity To Tune the Chemical and Tribological Properties of Lignin-Inspired Polymer Coatings," (in English), *ACS Sustainable Chemistry & Engineering,* vol. 6, no. 5, pp. 6856-6866, May 2018.

[119] C. M. Stafford, K. E. Roskov, T. H. Epps III, and M. J. Fasolka, "Generating thickness gradients of thin polymer films via flow coating," *Review of Scientific Instruments,* vol. 77, no. 2, p. 023908, 2006.

[120] D. K. Owens and R. C. Wendt, "Estimation of the surface free energy of polymers," *Journal of Applied Polymer Science,* vol. 13, no. 8, pp. 1741-1747, 1969.

[121] J. Warneke, Z. Y. Wang, M. Zeller, D. Leibfritz, M. Plaumann, and V. A. Azov, "Methacryloyl chloride dimers: from structure elucidation to a manifold of chemical transformations," (in English), *Tetrahedron,* vol. 70, no. 37, pp. 6515-6521, Sep 16 2014.

[122] Q. Lou and D. A. Shipp, "Poly(glycidyl methacrylate-*block*-styrene) for Photolithographically Patternable Resist Materials," in *Progress in Controlled Radical Polymerization: Materials and Applications,* vol. 1101(ACS Symposium Series, no. 1101): American Chemical Society, 2012, pp. 115-125.

[123] X. Fei, Y. Shi, and Y. Cao, "Synthesis of photosensitive poly(methyl methacrylate-co-glycidyl methacrylate) for optical waveguide devices," *Applied Physics A,* vol. 100, no. 2, pp. 409-414, 2010.

[124] J. Chiefari *et al.*, "Living free-radical polymerization by reversible addition-fragmentation chain transfer: The RAFT process," (in English), *Macromolecules,* vol. 31, no. 16, pp. 5559-5562, Aug 11 1998.

[125] S. Perrier, "50th Anniversary Perspective: RAFT Polymerization-A User Guide," (in English), *Macromolecules,* vol. 50, no. 19, pp. 7433-7447, Oct 10 2017.

[126] B. G. Harvey *et al.*, "Synthesis and characterization of a renewable cyanate ester/polycarbonate network derived from eugenol," *Polymer,* vol. 55, no. 20, pp. 5073-5079, 2014.

[127] S. Radhakrishnan, N. Somanathan, and M. Thelakkat, "Thermal Degradation Studies of Polythiophenes Containing Hetero Aromatic Side Chains," (in English), *International Journal of Thermophysics,* vol. 30, no. 3, pp. 1074-1087, Jun 2009.

[128] M. Geoghegan and G. Krausch, "Wetting at polymer surfaces and interfaces," *Progress in Polymer Science,* vol. 28, no. 2, pp. 261-302, 2003.

[129] C. K. Shelton and T. H. Epps III, "Decoupling Substrate Surface Interactions in Block Polymer Thin Film Self-Assembly," *Macromolecules,* vol. 48, no. 13, pp. 4572-4580, 2015/07/14 2015.

[130] C. K. Shelton and T. H. Epps III, "Mapping Substrate Surface Field Propagation in Block Polymer Thin Films," *Macromolecules,* vol. 49, no. 2, pp. 574-580, 2016/01/26 2016.

[131] K. M. Ashley, D. Raghavan, J. F. Douglas, and A. Karim, "Wetting−Dewetting Transition Line in Thin Polymer Films," *Langmuir,* vol. 21, no. 21, pp. 9518-9523, 2005.

[132] F. M. Fowkes, "Attractive Forces at Interfaces," *Industrial & Engineering Chemistry,* vol. 56, no. 12, pp. 40-52, 1964.

[133] J. N. Israelachvili, "17 - Adhesion and Wetting Phenomena," in *Intermolecular and Surface Forces (Third Edition)*, J. N. Israelachvili, Ed. San Diego: Academic Press, 2011, pp. 415-467.

[134] G. Whyman, E. Bormashenko, and T. Stein, "The rigorous derivation of Young, Cassie-Baxter and Wenzel equations and the analysis of the contact angle hysteresis phenomenon," (in English), *Chemical Physics Letters,* vol. 450, no. 4-6, pp. 355-359, Jan 4 2008.

[135] D. J. McGregor, S. Tawfick, and W. P. King, "Mechanical properties of hexagonal lattice structures fabricated using continuous liquid interface production additive manufacturing," (in English), *Additive Manufacturing,* vol. 25, pp. 10-18, Jan 2019.

[136] "The Great Re-make: Manufacturing for Modern Times," McKinsey & Company, 2017.

[137] *Wohlers Report 2017: 3D Printing and Additive Manufacturing State of the Industry, Annual Worldwide Progress Report*. Wohlers Associates Inc., 2017.

[138] J. R. C. Dizon, A. H. Espera, Q. Y. Chen, and R. C. Advincula, "Mechanical characterization of 3D-printed polymers," (in English), *Additive Manufacturing,* vol. 20, pp. 44-67, Mar 2018.

[139] N. Chantarapanich, P. Puttawibul, K. Sitthiseripratip, S. Sucharitpwatskul, and S. Chantaweroad, "Study of the mechanical properties of photo-cured epoxy resin fabricated by stereolithography process," *Songklanakarin Journal of Science and Technology,* vol. 35, no. 1, pp. 91-98, 2013.

[140] R. Quintana, J. W. Choi, K. Puebla, and R. Wicker, "Effects of build orientation on tensile strength for stereolithography-manufactured ASTM D-638 type I specimens," (in English), *International Journal of Advanced Manufacturing Technology,* vol. 46, no. 1-4, pp. 201-215, Jan 2010.

[141] I. Gibson, D. W. Rosen, and B. Stucker, *Additive Manufacturing Technologies: Rapid Prototyping to Direct Digital Manufacturing*. Springer Publishing Company, 2009, p. 462.

[142] J. Stampfl, M. Cziferszky, S. Baudis, H. Lichtenegger, and R. Liska, "Biodegradable stereolithography resins with defined mechanical properties," in *Virtual and Rapid Manufacturing*, P. J. Bartolo, Ed.: VRAP, 2007, pp. 283-288.

[143] P. J. Halley and G. A. George, "6.9.1.1 Stereolithography," in *Chemorheology of Polymers - From Fundamental Principles to Reactive Processing*: Cambridge University Press, 2009, pp. 420-422.

[144] M. Kutz, "28.2.2 Selective Laser Sintering," in *Applied Plastics Engineering Handbook - Processing, Materials, and Applications (2nd Edition)*: Elsevier, 2017, pp. 618-619.

[145] S. Killi, "A.4.1 Stereolithography," in *Additive Manufacturing - Design, Methods, and Processes*: CRC Press, pp. 60-61.

[146] S. A. Madbouly, C. Zhang, and M. R. Kessler, "7.4.2 Resins of Acrylated-Epoxidized Plant Oils," in *Bio-Based Plant Oil Polymers and Composites*: Elsevier.

[147] L. Shen, J. I. Haufe, and M. Patel, *Product Overview and Market Projection of Emerging Bio-Based Plastics-PRO-BIP 2009–Final Report*. 2009.

[148] T. Matsuda, M. Mizutani, and S. C. Arnold, "Molecular design of photocurable liquid biodegradable copolymers. 1. Synthesis and photocuring characteristics," (in English), *Macromolecules,* vol. 33, no. 3, pp. 795-800, Feb 8 2000.

[149] T. Matsuda and M. Mizutani, "Liquid acrylate-endcapped biodegradable poly(epsilon-caprolactone-co-trimethylene carbonate). II. Computer-aided stereolithographic microarchitectural surface photoconstructs," *Journal of Biomedical Materials Research,* vol. 62, no. 3, pp. 395-403, Dec 5 2002.

[150] K. W. Lee, S. Wang, B. C. Fox, E. L. Ritman, M. J. Yaszemski, and L. Lu, "Poly(propylene fumarate) bone tissue engineering scaffold fabrication using stereolithography: effects of resin formulations and laser parameters," *Biomacromolecules,* vol. 8, no. 4, pp. 1077-84, Apr 2007.

[151] F. P. Melchels, J. Feijen, and D. W. Grijpma, "A poly(D,L-lactide) resin for the preparation of tissue engineering scaffolds by stereolithography," *Biomaterials,* vol. 30, no. 23-24, pp. 3801-9, Aug 2009.

[152] F. A. Gonçalves *et al.*, "3D printing of new biobased unsaturated polyesters by microstereo-thermal-lithography," *Biofabrication,* vol. 6, no. 3, p. 035024, 2014.

[153] G. Miezinyte, J. Ostrauskaite, E. Rainosalo, E. Skliutas, and M. Malinauskas, "Photoresins based on acrylated epoxidized soybean oil and benzenedithiols for optical 3D printing," *Rapid Prototyping Journal,* vol. 25, no. 2, pp. 378-387, 2019.

[154] E. Skliutas *et al.*, *Bioresists from renewable resources as sustainable photoresins for 3D laser microlithography: material synthesis, cross-linking rate and characterization of the structures* (Proceesings of SPIE). SPIE, 2017.

[155] E. Skliutas, S. Kašėtaitė, L. Jonušauskas, J. Ostrauskaite, and M. Malinauskas, "Photosensitive naturally derived resins toward optical 3-D printing," *Optical Engineering,* vol. 57, no. 4, pp. 1-9, 2018.

[156] D. S. Branciforti *et al.*, "Visible light 3D printing with epoxidized vegetable oils," (in English), *Additive Manufacturing,* vol. 25, pp. 317-324, Jan 2019.

[157] V. S. D. Voet *et al.*, "Biobased Acrylate Photocurable Resin Formulation for Stereolithography 3D Printing," (in English), *Acs Omega,* vol. 3, no. 2, pp. 1403-1408, Feb 2018.

[158] R. Ding, Y. Du, R. B. Goncalves, L. F. Francis, and T. M. Reineke, "Sustainable near UV-curable acrylates based on natural phenolics for stereolithography 3D printing," *Polymer Chemistry,* vol. 10, no. 9, pp. 1067-1077, 2019.

[159] J. F. Stanzione III, J. M. Sadler, J. J. La Scala, K. H. Reno, and R. P. Wool, "Vanillin-based resin for use in composite applications," *Green Chemistry,* vol. 14, no. 8, pp. 2346-2352, 2012.

[160] P. T. Anastas and J. C. Warner, "Green Chemistry: Theory and Practice," New York: Oxford University Press, 1998, p. 130.

[161] G. R. Palmese and R. L. Mccullough, "Effect of Epoxy Amine Stoichiometry on Cured Resin Material Properties," (in English), *Journal of Applied Polymer Science,* vol. 46, no. 10, pp. 1863-1873, Dec 5 1992.

[162] L. H. Sperling, Introduction to Physical Polymer Science, 4 ed. New York: John Wiley & Sons, 2006. [Online]. Available.

[163] M. Wozniak, Y. de Hazan, T. Graule, and D. Kata, "Rheology of UV curable colloidal silica dispersions for rapid prototyping applications," (in English), *Journal of the European Ceramic Society,* vol. 31, no. 13, pp. 2221-2229, Nov 2011.

[164] C. Hinczewski, S. Corbel, and T. Chartier, "Ceramic suspensions suitable for stereolithography," (in English), *Journal of the European Ceramic Society,* vol. 18, no. 6, pp. 583-590, 1998.

[165] Z. X. Weng, Y. Zhou, W. X. Lin, T. Senthil, and L. X. Wu, "Structure-property relationship of nano enhanced stereolithography resin for desktop SLA 3D printer," (in English), *Composites Part A-Applied Science and Manufacturing,* vol. 88, pp. 234-242, Sep 2016.

[166] C. Y. M. Tung and P. J. Dynes, "Relationship between Viscoelastic Properties and Gelation in Thermosetting Systems," (in English), *Journal of Applied Polymer Science,* vol. 27, no. 2, pp. 569-574, 1982.

[167] J. Herzberger, V. Meenakshisundaram, C. B. Williams, and T. E. Long, "3D Printing All-Aromatic Polyimides Using Stereolithographic 3D Printing of Polyamic Acid Salts," (in English), *ACS Macro Letters,* vol. 7, no. 4, pp. 493-497, Apr 2018.

[168] A. Puisto, M. Mohtaschemi, M. J. Alava, and X. Illa, "Dynamic hysteresis in the rheology of complex fluids," (in English), *Physical Review E - Statistical, Nonlinear and Soft Matter Physics,* vol. 91, no. 4, p. 042314, Apr 2015.

[169] J. T. Sutton, K. Rajan, D. P. Harper, and S. C. Chmely, "Lignin-Containing Photoactive Resins for 3D Printing by Stereolithography," (in English), *ACS Applied Materials & Interfaces,* vol. 10, no. 42, pp. 36456-36463, Oct 24 2018.

[170] R. Hague, S. Mansour, and N. Saleh, "Material and design considerations for Rapid Manufacturing," (in English), *International Journal of Production Research,* vol. 42, no. 22, pp. 4691-4708, Nov 15 2004.

[171] A. Witkowski, A. A. Stec, and T. R. Hull, "Thermal Decomposition of Polymeric Materials," in *SFPE Handbook of Fire Protection Engineering*, M. J. Hurley *et al.*, Eds. New York, NY: Springer New York, 2016, pp. 167-254.

[172] *Progess in Polymer Degradation and Stability Research*. New York, NY: Nova Science Publishers, Inc., 2007.

[173] J. K. Herman Teo, K. C. Teo, B. Pan, Y. Xiao, and X. Lu, "Epoxy/polyhedral oligomeric silsesquioxane (POSS) hybrid networks cured with an anhydride: Cure kinetics and thermal properties," *Polymer,* vol. 48, no. 19, pp. 5671-5680, 2007.

[174] S. Miura, Y. Shidara, T. Yunoki, M. A. Al Mamun, Y. Shibasaki, and A. Fujimori, "High-Density Packing of Amorphous Polymer with Bulky Aromatic Rings in Interfacial Molecular Films," (in English), *Macromolecular Chemistry and Physics,* vol. 218, no. 7, Apr 2017.

[175] M. Daronch, F. A. Rueggeberg, and M. F. De Goes, "Monomer conversion of pre-heated composite," (in English), *Journal of Dental Research,* vol. 84, no. 7, pp. 663-7, Jul 2005.

[176] D. W. van Krevelen and K. te Nijenhuis, *Properties of Polymers - Their Correlation with Chemical Structure; Their Numerical Estimation and Prediction from Additive Group Contributions*, 4 ed. Elsevier, 2009.

[177] J. F. Stanzione III, "Lignin-Based Monomers: Utilization In High-Performance Polymers And The Effects Of Their Structures On Polymer Properties," Ph.D., Chemical and Biomolecular Engineering, University of Delaware, Newark, DE, 2013.

[178] R. P. Wool, "Twinkling Fractal Theory of the Glass Transition," (in English), *Journal of Polymer Science Part B-Polymer Physics,* vol. 46, no. 24, pp. 2765-2778, Dec 15 2008.

[179] A. R. Kannurpatti, J. W. Anseth, and C. N. Bowman, "A study of the evolution of mechanical properties and structural heterogeneity of polymer networks formed by photopolymerizations of multifunctional (meth)acrylates," (in English), *Polymer,* vol. 39, no. 12, pp. 2507-2513, Jun 1998.

[180] L. Song *et al.*, "Synthesis and evaluation of novel dental monomer with branched carboxyl acid group," (in English), *Journal of Biomedical Materials Research Part B: Applied Biomaterials,* vol. 102, no. 7, pp. 1473-84, Oct 2014.

[181] W. D. Cook, G. P. Simon, P. J. Burchill, M. Lau, and T. J. Fitch, "Curing kinetics and thermal properties of vinyl ester resins," (in English), *Journal of Applied Polymer Science,* vol. 64, no. 4, pp. 769-781, Apr 25 1997.

[182] W. D. Cook, T. F. Scott, S. Quay-Thevenon, and J. S. Forsythe, "Dynamic mechanical thermal analysis of thermally stable and thermally reactive network polymers," (in English), *Journal of Applied Polymer Science,* vol. 93, no. 3, pp. 1348-1359, Aug 5 2004.

[183] A. R. Kannurpatti, K. J. Anderson, J. W. Anseth, and C. N. Bowman, "Use of "living" radical polymerizations to study the structural evolution and properties of highly crosslinked polymer networks," (in English), *Journal of Polymer Science Part B-Polymer Physics,* vol. 35, no. 14, pp. 2297-2307, Oct 1997.

[184] J. K. Gillham, J. A. Benci, and A. Noshay, "Isothermal Transitions of a Thermosetting System," (in English), *Abstracts of Papers of the American Chemical Society,* 1974.

[185] J. B. Enns and J. K. Gillham, "The Time-Temperature-Transformation (Ttt) Cure Diagram - Modeling the Cure Behavior of Thermosets," (in English), *Abstracts of Papers of the American Chemical Society,* vol. 184, no. Sep, 1982.

[186] G. Wisanrakkit and J. K. Gillham, "Continuous Heating Transformation (Cht) Cure Diagram of an Aromatic Amine Epoxy System at Constant Heating Rates," (in English), *Journal of Applied Polymer Science,* vol. 42, no. 9, pp. 2453-2463, May 5 1991.

[187] K. Bandzierz, L. Reuvekamp, J. Dryzek, W. Dierkes, A. Blume, and D. Bielinski, "Influence of Network Structure on Glass Transition Temperature of Elastomers," (in English), *Materials,* vol. 9, no. 7, Jul 22 2016.

[188] H. A. Khonakdar, J. Morshedian, U. Wagenknecht, and S. H. Jafari, "An investigation of chemical crosslinking effect on properties of high-density polyethylene," (in English), *Polymer,* vol. 44, no. 15, pp. 4301-4309, Jul 2003.

[189] S. R. Yang and J. M. Qu, "Computing thermomechanical properties of crosslinked epoxy by molecular dynamic simulations," (in English), *Polymer,* vol. 53, no. 21, pp. 4806-4817, Sep 28 2012.

[190] E. Urbaczewskiespuche, J. Galy, J. F. Gerard, J. P. Pascault, and H. Sautereau, "Influence of Chain Flexibility and Cross-Link Density on Mechanical-Properties of Epoxy Amine Networks," (in English), *Polymer Engineering and Science,* vol. 31, no. 22, pp. 1572-1580, Nov 1991.

[191] I. Krupa and A. S. Luyt, "Mechanical properties of uncrosslinked and crosslinked linear low-density polyethylene/wax blends," (in English), *Journal of Applied Polymer Science,* vol. 81, no. 4, pp. 973-980, Jul 25 2001.

[192] B. Kim, J. Choi, S. Yang, S. Yu, and M. Cho, "Influence of crosslink density on the interfacial characteristics of epoxy nanocomposites," (in English), *Polymer,* vol. 60, pp. 186-197, Mar 9 2015.

[193] A. Bandyopadhyay, P. K. Valavala, T. C. Clancy, K. E. Wise, and G. M. Odegard, "Molecular modeling of crosslinked epoxy polymers: The effect of crosslink density on thermomechanical properties," (in English), *Polymer,* vol. 52, no. 11, pp. 2445-2452, May 13 2011.

[194] J. Lu and R. P. Wool, "Additive toughening effects on new bio-based thermosetting resins from plant oils," (in English), *Composites Science and Technology,* vol. 68, no. 3-4, pp. 1025-1033, Mar 2008.

[195] K. Cho, D. Lee, and C. E. Park, "Effect of molecular weight between crosslinks on fracture behaviour of diallylterephthalate resins," (in English), *Polymer,* vol. 37, no. 5, pp. 813-817, Mar 1996.

[196] I. Giannakopoulos and A. C. Taylor, "An essential work of fracture study of the toughness of thermoset polyester coatings," (in English), *Progress in Organic Coatings,* vol. 78, pp. 265-274, Jan 2015.

[197] H. L. Bos and J. J. H. Nusselder, "Toughness of Model Polymeric Networks in the Glassy State - Effect of Cross-Link Density," (in English), *Polymer,* vol. 35, no. 13, pp. 2793-2799, 1994.

[198] G. Levita, S. Depetris, A. Marchetti, and A. Lazzeri, "Cross-Link Density and Fracture-Toughness of Epoxy-Resins," (in English), *Journal of Materials Science,* vol. 26, no. 9, pp. 2348-2352, May 1 1991.

[199] A. W. Bassett, A. E. Honnig, J. J. La Scala, and J. F. Stanzione III, "Network Toughening of Additively Manufactured, High Glass Transition Temperature Materials via Sequentially Cured, Interpenetrating Polymers," *In Preparation*.

[200] L. H. Sperling, "An Introduction to Polymer Networks and IPNs," in *Interpenetrating Polymer Networks and Related Materials*Boston, MA: Springer US, 1981, pp. 1-10.

[201] L. H. Sperling, "Interpenetrating polymer networks and related materials," vol. 12, no. 1, pp. 141-180, 1977.

[202] L. H. Sperling and R. Hu, "Interpenetrating Polymer Networks," in *Polymer Blends Handbook*, L. A. Utracki, Ed. Dordrecht: Springer Netherlands, 2003, pp. 417-447.

[203] S. C. Ligon, R. Liska, J. Stampfl, M. Gurr, and R. Mulhaupt, "Polymers for 3D Printing and Customized Additive Manufacturing," (in English), *Chemical Reviews,* vol. 117, no. 15, pp. 10212-10290, Aug 9 2017.

[204] N. Naseri, B. Deepa, A. P. Mathew, K. Oksman, and L. Girandon, "Nanocellulose-Based Interpenetrating Polymer Network (IPN) Hydrogels for Cartilage Applications," (in English), *Biomacromolecules,* vol. 17, no. 11, pp. 3714-3723, Nov 2016.

[205] K. Bootsma *et al.*, "3D printing of an interpenetrating network hydrogel material with tunable viscoelastic properties," (in English), *Journal of the Mechanical Behavior of Biomedical Materials,* vol. 70, pp. 84-94, Jun 2017.

[206] X. Kuang, K. J. Chen, C. K. Dunn, J. T. Wu, V. C. F. Li, and H. J. Qi, "3D Printing of Highly Stretchable, Shape-Memory, and Self-Healing Elastomer toward Novel 4D Printing," (in English), *ACS Applied Materials & Interfaces,* vol. 10, no. 8, pp. 7381-7388, Feb 28 2018.

[207] R. Auvergne, S. Caillol, G. David, B. Boutevin, and J. P. Pascault, "Biobased Thermosetting Epoxy: Present and Future," (in English), *Chemical Reviews,* vol. 114, no. 2, pp. 1082-1115, Jan 22 2014.

[208] F. L. Jin, X. Li, and S. J. Park, "Synthesis and application of epoxy resins: A review," (in English), *Journal of Industrial and Engineering Chemistry,* vol. 29, pp. 1-11, Sep 25 2015.

[209] F. S. Hu, J. J. La Scala, J. M. Sadler, and G. R. Palmese, "Synthesis and Characterization of Thermosetting Furan-Based Epoxy Systems," (in English), *Macromolecules,* vol. 47, no. 10, pp. 3332-3342, May 27 2014.

[210] F. Hu, "Structure - Property Relationships of Furanyl Thermosetting Polymer Materials Derived from Biobased Feedstocks," Doctor of Philosophy, Drexel University, Philadelphia, PA, 2016.

[211] S. K. Yadav, F. S. Hu, J. J. La Scala, and G. R. Palmese, "Toughening Anhydride-Cured Epoxy Resins Using Fatty Alkyl-Anhydride-Grafted Epoxidized Soybean Oil," (in English), *ACS Omega,* vol. 3, no. 3, pp. 2641-2651, Mar 2018.

[212] W. P. Liu, S. V. Hoa, and M. Pugh, "Fracture toughness and water uptake of high-performance epoxy/nanoclay nanocomposites," (in English), *Composites Science and Technology,* vol. 65, no. 15-16, pp. 2364-2373, Dec 2005.

[213] A. T. Seyhan, M. Tanoglu, and K. Schulte, "Mode I and mode II fracture toughness of E-glass non-crimp fabric/carbon nanotube (CNT) modified polymer based composites," (in English), *Engineering Fracture Mechanics,* vol. 75, no. 18, pp. 5151-5162, Dec 2008.

[214] A. T. Grous, "Toughening Bimodal Vinyl Ester Blends Using Bio-rubber Monomers," Master of Science, Drexel University, Philadelphia, PA, 2011.

[215] G. T. Hahn, M. F. Kanninen, and A. R. Rosenfield, "Fracture Toughness of Materials," vol. 2, no. 1, pp. 381-404, 1972.

[216] O. Rios *et al.*, "3D printing via ambient reactive extrusion," (in English), *Materials Today Communications,* vol. 15, pp. 333-336, Jun 2018.

[217] A. Moridi, S. M. Hassani-Gangaraj, M. Guagliano, and M. Dao, "Cold spray coating: review of material systems and future perspectives," (in English), *Surface Engineering*, vol. 30, no. 6, pp. 369-U29, Jun 2014.

[218] G. Z. Yang *et al.*, "Polymer Particles with a Low Glass Transition Temperature Containing Thermoset Resin Enable Powder Coatings at Room Temperature," (in English), *Industrial & Engineering Chemistry Research*, vol. 58, no. 2, pp. 908-916, Jan 16 2019.

[219] A. W. Bassett *et al.*, "Alternative monomers for 4,4 '-methylenedianiline in thermosetting epoxy resins," (in English), *Journal of Applied Polymer Science*, vol. 137, p. 48707, Nov 14 2020.

[220] B. Dao, A. M. Groth, and J. H. Hodgkin, "PMR type polyimides by aqueous cyclization methods - Chemistry," (in English), *High Performance Polymers*, vol. 20, no. 1, pp. 38-52, Feb 2008.

[221] D. Wilson, "PMR-15 Processing, Properties and Problems - a Review," (in English), *British Polymer Journal*, vol. 20, no. 5, pp. 405-416, 1988.

[222] J. H. Luft, "Improvements in Epoxy-Resin Embedding Methods," (in English), *The Journal of Cell Biology*, vol. 2, no. 9, pp. 409-414, 1961.

[223] C. A. Mcqueen and G. M. Williams, "Review of the Genotoxicity and Carcinogenicity of 4,4'-Methylene-Dianiline and 4,4'-Methylene-Bis-2-Chloroaniline," (in English), *Mutation Research*, vol. 239, no. 2, pp. 133-142, Sep 1990.

[224] A. G. Siraki, T. S. Chan, G. Galati, S. Teng, and P. J. O'Brien, "N-oxidation of aromatic amines by intracellular oxidases," (in English), *Drug Metabolism Reviews*, vol. 34, no. 3, pp. 549-564, 2002.

[225] S. Rendic and F. P. Guengerich, "Contributions of Human Enzymes in Carcinogen Metabolism," (in English), *Chemical Research in Toxicology*, vol. 25, no. 7, pp. 1316-1383, Jul 2012.

[226] M. F. Kanz, L. Kaphalia, B. S. Kaphalia, E. Romagnoli, and G. A. S. Ansari, "Methylene Dianiline - Acute Toxicity and Effects on Biliary Function," (in

English), *Toxicology and Applied Pharmacology,* vol. 117, no. 1, pp. 88-97, Nov 1992.

[227] H. Bartsch and R. Montesano, "Relevance of Nitrosamines to Human Cancer," (in English), *Carcinogenesis,* vol. 5, no. 11, pp. 1381-1393, 1984.

[228] G. Y. Wu, Y. Z. Fang, S. Yang, J. R. Lupton, and N. D. Turner, "Glutathione metabolism and its implications for health," (in English), *Journal of Nutrition,* vol. 134, no. 3, pp. 489-492, Mar 2004.

[229] V. Aruoja, M. Sihtmae, H. C. Dubourguier, and A. Kahru, "Toxicity of 58 substituted anilines and phenols to algae Pseudokirchneriella subcapitata and bacteria Vibrio fischeri: Comparison with published data and QSARs," (in English), *Chemosphere,* vol. 84, no. 10, pp. 1310-1320, Sep 2011.

[230] K. T. Chung, S. C. Chen, T. Y. Wong, Y. S. Li, C. I. Wei, and M. W. Chou, "Mutagenicity studies of benzidine and its analogs: Structure-activity relationships," (in English), *Toxicological Sciences,* vol. 56, no. 2, pp. 351-356, Aug 2000.

[231] D. Hinks, H. S. Freeman, M. Nakpathom, and J. Sokolowska, "Synthesis and evaluation of organic pigments and intermediates. 1. Nonmutagenic benzidine analogs," (in English), *Dyes and Pigments,* vol. 44, no. 3, pp. 199-207, Feb 2000.

[232] G. R. Yandek *et al.*, "Balancing Performance and Sustainability in Next-Generation PMR Technologies for OMC (Organic Matrix Composites) Structures," presented at the SAMPE, Long Beach CA, 2016.

[233] A. H. Soeriyadi *et al.*, "Synthesis and modification of thermoresponsive poly(oligo(ethylene glycol) methacrylate) via catalytic chain transfer polymerization and thiol-ene Michael addition," (in English), *Polymer Chemistry,* vol. 2, no. 4, pp. 815-822, 2011.

[234] *Polyimides and Other High Temperature Polymers: Synthesis, Characterization and Applications*. The Netherlands: VSP, 2001, p. 320.

[235] *ASTM E2552-08, Standard Guide for Assessing the Environmental and Human Health Impacts of New Energetic Compounds*, 2008.

[236] B. G. Harvey, G. R. Yandek, J. T. Lamb, W. S. Eck, M. D. Garrison, and M. C. Davis, "Synthesis and characterization of a high temperature thermosetting polyimide oligomer derived from a non-toxic, sustainable bisaniline," *RSC Advances,* vol. 7, no. 37, pp. 23149-23156, 2017.

[237] G. Reifferscheid and J. Heil, "Validation of the SOS/umu test using test results of 486 chemicals and comparison with the Ames test and carcinogenicity data," *Mutation Research/Genetic Toxicology,* vol. 369, no. 3, pp. 129-145, 1996.

[238] D. P. Middaugh, S. M. Resnick, S. E. Lantz, C. S. Heard, and J. G. Mueller, "Toxicological assessment of biodegraded pentachlorophenol: Microtox® and fish embryos," *Archives of Environmental Contamination and Toxicology,* vol. 24, no. 2, pp. 165-172, 1993.

[239] *ASTM E729-96, Standard Guide for Conducting Acute Toxicity Tests on Test Materials with Fishes, Macroinvertebrates, and Amphibians,* 2014.

[240] D. M. L. Morgan, "Tetrazolium (MTT) Assay for Cellular Viability and Activity," in *Polyamine Protocols,* D. M. L. Morgan, Ed. Totowa, NJ: Humana Press, 1998, pp. 179-184.

[241] K. H. Jones and J. A. Senft, "An improved method to determine cell viability by simultaneous staining with fluorescein diacetate-propidium iodide," *Journal of Histochemistry & Cytochemistry,* vol. 33, no. 1, pp. 77-79, 1985.

[242] I. M. McAninch, G. R. Palmese, J. L. Lenhart, and J. J. La Scala, "Characterization of epoxies cured with bimodal blends of polyetheramines," (in English), *Journal of Applied Polymer Science,* vol. 130, no. 3, pp. 1621-1631, Nov 5 2013.

[243] J. J. La Scala and R. P. Wool, "Fundamental thermo-mechanical property modeling of triglyceride-based thermosetting resins," (in English), *Journal of Applied Polymer Science,* vol. 127, no. 3, pp. 1812-1826, Feb 5 2013.

[244] Hazardous Substances Data Bank [Online]. Available: http://toxnet.nlm.nih.gov.

[245] W. D. Ross, J. D. Noble, J. A. Gridley, J. M. Fullenkamp, M. T. Wininger, and J. A. Graham, "Mutagenic Screening of Diamine Monomers," Washington, D. C.,

1983, Available: https://ntrs.nasa.gov/archive/nasa/casi.ntrs.nasa.gov/19830013482.pdf.

[246] M. G. Gonzalez, J. C. Cabanelas, and J. Baselga, "Applications of FTIR on epoxy resins - identification, monitoring the curing process, phase separation and water uptake," presented at the Infrared Spectroscopy: Materials Science, Engineering and Technology, 2012.

[247] I. Javni, W. Zhang, and Z. S. Petrovic, "Effect of different isocyanates on the properties of soy-based polyurethanes," (in English), *Journal of Applied Polymer Science,* vol. 88, no. 13, pp. 2912-2916, Jun 24 2003.

[248] G. H. Kwak, K. Inoue, Y. Tominaga, S. Asai, and M. Sumita, "Characterization of the vibrational damping loss factor and viscoelastic properties of ethylene-propylene rubbers reinforced with micro-scale fillers," (in English), *Journal of Applied Polymer Science,* vol. 82, no. 12, pp. 3058-3066, Dec 13 2001.

[249] M. Palusiak and S. J. Grabowski, "Methoxy group as an acceptor of proton in hydrogen bonds," *Journal of Molecular Structure,* vol. 642, no. 1–3, pp. 97-104, 2002.

[250] *STP1249-EB, The Glass Transition Temperature of Glassy Polymers using Dynamic Mechanical Analysis*, 1994.

[251] P. J. Flory, *Principles of Polymer Chemistry* (The George Fisher Baker non-resident lectureship in chemistry at Cornell University). Ithaca,: Cornell University Press, 1953, p. 672.

[252] R. F. Landel and L. E. Nielsen, *Mechanical Properties of Polymers and Composites, Second Edition*. Taylor & Francis, 1993.

[253] J. Park, J. Eslick, Q. Ye, A. Misra, and P. Spencer, "The influence of chemical structure on the properties in methacrylate-based dentin adhesives," (in English), *Dental Materials,* vol. 27, no. 11, pp. 1086-1093, Nov 2011.

Appendix A

Alternative Monomers to 4,4′-methylenedianiline in Thermosetting Epoxy Resins

Text and figures are reproduced and adapted with permission from A.W. Bassett, J.D. Cosgrove, K.M. Schmalbach, O.M. Stecca, C.M. Paquette, V.H. Adams, W.S. Eck, J.M. Sadler, J.J. La Scala, and J.F. Stanzione III, "Alternative Monomers to 4,4′-methylenedianiline in Thermosetting Epoxy Resins," *Journal of Applied Polymer Science*, 2020, 137 (20), 48707, reference [219].

A.1 Introduction

4,4'-Methylenedianiline (MDA) is an industrial chemical used in epoxy resins, composites, and various polymer applications. In particular, MDA has been used in the production of high temperature epoxies for aerospace and is used in PMR-15, a polyimide developed by the NASA Lewis Research Center in the 1970s [220-222]. Unfortunately, MDA is toxic to the liver and is a known carcinogen [223]. MDA toxicity results from the oxidation of MDA by cytochrome P450 (CYP) into a reactive intermediate that is subsequently transformed into a nitrosamine or rearranged into a different, stabilized carbocation [224-226]. Nitrosamines are highly carcinogenic to many animal species, suggesting that they can also cause cancer in humans [227]. The rearranged carbocation is capable of irreversibly binding to glutathione, a key antioxidant protein involved in the detoxification of reactive intermediates generated by CYP enzymes [228]. Depletion of functional glutathione results in the increase of free radicals that cause DNA damage and impacts nutrient metabolism and DNA and protein synthesis [226].

Since handling MDA is an occupational risk, there has been an increase in costs for the resin systems containing MDA, as workers are required to use adequate personal protective equipment (PPE). Considering all the current risks of using MDA in polymer production, there is a need for the development of newer, less toxic dianilines. In order to successfully replace MDA, the dianiline must reduce toxicity, maintain thermal and mechanical properties of the polymer, simplify composite processing, and reduce lifecycle costs. Slight modifications to the structure of MDA may result in reduced toxicity and data from aniline substituents suggest a substantial reduction in toxicity is possible [229]. Interestingly, dianilines with a single methyl substituent are still highly toxic [230, 231]. Thus, the addition of one or more substituents around the aromatic ring, the type of substituents added, the placement of the amine, and the type of spacer-bridge between the aromatic rings could all affect the toxicity of the dianiline. Similar research on the molecular toxicity of MDA alternatives showed that these potential changes to the structures all have observable effects on the oxidation rate of the amine [232]. However, modifications to the structure of MDA can also affect the mechanical and thermal properties of the developed materials, leading to the possibility of reducing overall material performance.

While known for its use in PMR-15, MDA and its potential alternatives can be utilized as curing agents in epoxy resins or as co-monomers in Michael addition polymerizations [222, 233]. Utilizing MDA and its potential alternatives in epoxy resins provides a more facile way to determine structure-property relationships relative to preparing polyimides. Several dianilines have been investigated in the past for the replacement of MDA and for use in epoxy resin systems. Previous replacements of MDA

include 3,4'-oxydianiline (3,4'-ODA) and 2,2-bis[4-(4-aminophenoxy)phenyl]propane (BAPP). However, both of these dianilines possess ether linkages, producing polyimides with lower glass transition temperatures (T_g) and thermal-oxidative stabilities [234]. Additionally, both 3,4' ODA and BAPP demonstrate toxicity equivalent to MDA and are therefore not sustainable alternatives. Another potential dianiline is 2,2'-dimethylbenzidine (DMBZ), which is used to produce the DMBZ-15 polyimide. DMBZ-15 has a T_g of 414-418 °C, which is a significant improvement on the 345 °C T_g of PMR-15. The higher T_g is attributed to both the biphenyl linkage that stiffens the molecule, and the addition of methyl groups to the aromatic rings that which limits rotation in the polyimide during the glass transition phase [234]. Yet, the processing characteristics of the resin and toughness of the resulting polymer are worsened [234].

In this work, variety of dianilines were prepared and blended with a commercial curing agent, Epikure W, and cured with EPON 828 (low molecular weight oligomer of diglycidyl ether of bisphenol A). It is hypothesized that structure-property trends for dianilines in epoxy resins will be qualitatively similar in PMR polyimides. The structure-toxicity relationships of these monomers were examined using quantitative structure activity relationships (QSAR) coupled with *in vitro* tests that evaluate DNA damage (bacterial mutagenicity), aquatic toxicity/water quality, and acute oral toxicity (cell-based cytotoxicity assay). The synthesized dianilines were mixed individually in an equal weight ratio with Epikure W and cured with stoichiometric equivalents of EPON 828 to determine the effect of dianiline architecture on polymer properties. The properties of the cured polymers were tested via differential scanning calorimetry (DSC), dynamic

mechanical analysis (DMA), and thermal gravimetric analysis (TGA) to determine whether these substituted dianilines are suitable alternatives to MDA.

A.2 Experimental Methods & Procedures

A.2.1 Materials. Paraformaldehyde (96%, extra pure), 2,5-dimethylaniline (2,5-dMA, 98%), 2,6-dimethylaniline (2,6-dMA, 99%), 3,5-dimethylaniline (3,5-dMA, 98%), hydrochloric acid (HCl, 37%), bisphenol A (4,4'-isopropylenediphenol, 97%), chloroform-d_3 ($CDCl_3$, 99+%), potassium carbonate (anhydrous 99+%), and dichloromethane (DCM, 99.6%, ACS reagent) were purchased from Acros Organics. Hexanes, ethyl acetate, sodium bicarbonate, methanol, 1,4-dioxane, and sodium hydroxide (NaOH) pellets were purchased from Fisher Scientific. Nitric acid (70%), *N*,*N*-dimethylformamide (DMF, 99.8+%), methyl iodide, magnesium sulfate, 10% Pd/C, 4,4'-methylenedianiline (MDA, ≥ 97%), 2-methylaniline (2-MA, 99+%), 3-methoxyaniline (3-MeOA, ≥ 99%), 3-methylaniline (3-MA, 99%), and 4,4'-diaminobenzophenone (DABP, 97%) were purchased from Sigma-Aldrich. 4,4'-diaminodiphenylsulfone (Dapsone, 98%) was purchased from Alfa Aesar. EPON 828 (diglycidyl ether of bisphenol A – DGEBA) was obtained from Momentive Specialty Chemicals (EEW = 190 g mol^{-1}). Epikure Curing Agent W was received from Hexion. Compressed nitrogen (N_2, 99.999%) and compressed hydrogen (H_2, 99.995%) were purchased from Airgas. All chemicals were used as received.

A.2.2 General synthesis of dianilines. For most of the prepared dianilines, anilines were coupled using paraformaldehyde under acidic conditions (Figure A1). The aniline of choice (3 g), paraformaldehyde (0.25 molar equivalents), and 14 mL DI water were added to a round-bottom flask equipped with a magnetic stir bar. The reactants were

mixed vigorously as 9 mL $HCl_{(aq)}$ (37 wt%) was slowly added. The reaction was then heated to 90 °C for 4 hours. The reaction mixture was cooled to 0 °C and was slowly neutralized to pH 10 with NaOH pellets. The mixture was extracted with DCM and the organic extract was dried using magnesium sulfate before it was concentrated under reduced pressure. The resulting solid was filtered and chromatographed to afford the dianiline of interest (approx. 42.5% yield) as an off-white solid. This procedure was used to synthesize 4,4'-methylenebis(2,5-dimethylaniline) (2,5-dMAC), 4,4'-methylenebis(2,6-dimethylaniline) (2,6-dMAC), 4,4'-methylenebis(2-methylaniline) (2-MAC), 4,4'-methylenebis(2-methoxyaniline) (2-MeOAC), and 6,6'-methylenebis(3-methylaniline) (3-MAC).

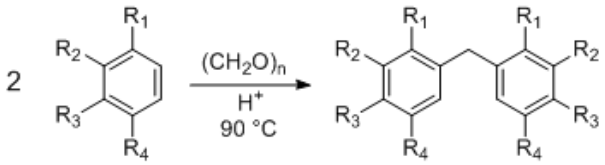

MDA: R1 = H, R2 = H, R3 = NH_2, R4 = H
2,5-dMAC: R1 = CH_3, R2 = H, R3 = NH_2, R4 = CH_3
2,6-dMAC: R1 = H, R2 = CH_3, R3 = NH_2, R4 = CH_3
2-MAC: R1 = H, R2 = H, R3 = NH_2, R4 = CH_3
2-MeOAC: R1 = H, R2 = H, R3 = NH_2, R4 = OCH_3
3-MAC: R1 = NH_2, R2 = H, R3 = CH_3, R4 = H

Figure A1. General synthesis of dianilines.

5,5'-isopropylenebis(2-methoxyaniline) (BPA-N) was prepared using bisphenol A as the starting chemical, which was subsequently nitrated, esterified at the hydroxyl moieties, and the nitrates reduced to amines.

4,4'-methylenebis(2,5-dimethylaniline) (2,5-dMAC) ($C_{17}H_{22}N_2$): ^{1}H NMR ($CDCl_3$) δ 2.08 (6 H, s), 2.17 (6 H, s), 3.48 (4 H, bs), 3.68 (2 H, s), 6.54 (2 H, s), 6.59 (2 H, s).

4,4'-methylenebis(2,6-dimethylaniline) (2,6-dMAC) ($C_{17}H_{22}N_2$): ^{1}H NMR ($CDCl_3$) δ 2.18 (12 H, s), 3.48 (4 H, bs), 3.71 (2 H, s), 6.79 (4 H, s).

4,4'-methylenebis(2-methylaniline) (2-MAC) ($C_{15}H_{18}N_2$): ^{1}H NMR ($CDCl_3$) δ 2.14 (6 H, s), 3.48 (4 H, bs), 3.75 (2 H, s), 6.61 (2 H, d), 6.86 (4 H, m).

4,4'-methylenebis(2-methoxyaniline) (2-MeOAC) ($C_{15}H_{18}N_2O_2$): ^{1}H NMR ($CDCl_3$) δ 3.61 (4 H, bs), 3.80 (6 H, s), 3.81 (2 H, s), 6.62 (6 H, m).

6,6'-methylenebis(3-methylaniline) (3-MAC) ($C_{15}H_{18}N_2$): ^{1}H NMR ($CDCl_3$) δ 2.18 (6 H, s), 3.51 (4 H, bs), 3.71 (2 H, s), 6.45 (2 H, dd), 6.56 (2 H, d), 6.69 (2 H, d).

5,5'-isopropylenebis(2-methoxyaniline) (BPA-N) ($C_{17}H_{18}N_2O_2$): ^{1}H NMR ($CDCl_3$) δ 1.58 (6 H, s), 3.61 (4 H, bs), 3.82 (6 H, s), 6.57 (2 H, d), 6.66 (4 H, m).

A.2.3 Characterization of monomers. Dianilines synthesized in this work were characterized by ^{1}H-NMR (400.15 MHz, 32 scans at 298 K) using a Varian 400 MHz FT-NMR Spectrometer. DSC experiments were carried out on a TA Instruments Discovery Series DSC2500. Approximately 3 mg of dianiline was placed in a Tzero aluminum pan and sealed with a hermetic lid to obtain the melting temperatures (T_m) and molar enthalpies of melting of the pure dianilines. The sample was heated to 170 °C at a rate of 5 °C min^{-1} in a N_2 atmosphere. For Dapsone, the sample was heated to 210 °C at a rate of 5 °C min^{-1} in a N_2 atmosphere. For DABP, the sample was heated to 270 °C at a rate of 5 °C min^{-1} in a N_2 atmosphere.

A.2.4 Toxicity analysis. Human health and environmental hazard assessments were conducted in accordance with ASTM Guideline E-2552, Standard Guide for

Assessing the Environmental and Human Health Impacts of New Energetic Compounds [235]. The guideline organizes the hazard assessment using a tiered approach that matches the complexity and cost of testing with the availability and candidacy of the compound. A first step is to use *in silico* methods for predicting toxicity and physical/chemical properties. The Quantitative Structure-Activity Relationship (QSAR) programs TOPKAT (Toxicity Prediction by Komputer Assisted Technology, Ver. 6.2, BIOVIA Dassault Systems, Inc., EPI Suite Program (Estimation Programs Interface, Ver. 4.11) and ECOSAR (ECOtoxicity Structure Activity Relationship, Ver. 1.11) were utilized to make predictions based on interactions that have been reported for compounds with similar chemical groups. For each compound of interest, the chemical structure was entered as a SMILES (simplified molecular-input line entry system) string; described previously [236]. Data generated by TOPKAT, EpiSuite and ECOSAR included physiochemical properties, bacterial mutagenicity, mammalian toxicity, and aquatic toxicity, along with confidence information were collected for each of the candidate MDA replacements. TOPKAT and ECOSAR predict toxicity based on structural alerts and similarities with experimental data available in the modeling databases. Experimental data for MDA is contained within these databases.

Specifically, the toxicity of the various dianilines developed were assessed using three basic *in vitro* tests that evaluate DNA damage (bacterial mutagenicity), aquatic toxicity/water quality, and oral toxicity (cytotoxicity assay). All *in vitro* tests were conducted using good laboratory practice (GLP) and repeated at least twice. Briefly, the Ames test measures whether a chemical causes mutagenicity in Salmonella tester strain bacteria (ANIARA, Mason, OH). The Salmonella tester strains are dependent on histidine

for growth due to errors in a critical gene. If, after exposure to the chemical, the strains are capable of growth in medium without histidine, the chemical has caused changes to the critical gene and is considered mutagenic [237]. The five tester strains were exposed to a concentration range of each compound and mutagenicity was assessed after a two-day incubation. The assay was also conducted in the presence of liver enzymes to test if the chemical was biotransformed (detoxified) or bioactivated (increased toxicity). The most sensitive strain (TA100) was screened first. If the chemical evoked mutagenicity, it was not tested further.

The Microtox ™ assay (Modern Water, New Castle DE) was used to test water quality and estimate aquatic toxicity. The marine bacteria (Aliivibrio fischeri) are naturally bioluminescent at an intensity directly related to cell health [238]. The bacteria were exposed to a concentration range of the compound and bioluminescence was measured sequentially at 5, 15 and 30 minutes using a spectrophotometer (Modern Water Analyzer, Modern Water Inc, New Castle Delaware). Raw luminescence data were collected and analyzed with the MicrotoxOmni Software ver. 4.3 (Modern Water Inc, New Castle Delaware) Reduction in bioluminescence in the presence of the test compound indicated toxicity [239]. An algorithm was then used to correlate acute aquatic toxicity.

The mammalian cell line cytotoxicity assay is an *in vitro* surrogate for *in vivo* acute oral toxicity testing [240, 241]. A toxic chemical interferes with the cell division and growth processes, resulting in a reduction of growth rate, reduced viability and ultimately cell death. Cytotoxicity (or loss of viability) was expressed as a concentration-dependent reduction of the indicator dye after chemical exposure. Two similar methods,

either neutral red uptake (NRU) or propidium iodide (PI) exclusion, were used to evaluate the cytotoxicity of the chemicals [240, 241]. Data were analyzed and an estimated mammalian LD_{50}, or the amount of an ingested substance that kills 50% of a test sample, was calculated and used to determine the acute hazard classification.

A.2.5 Resin cure. Dianilines could not be used alone as the curing agent with the EPON 828 as many of the dianilines were solids at temperatures exceeding 140 °C. As a result, it was not possible to blend the epoxy and dianilines without curing during the blending phase, thereby making the preparation of the desired polymers quite difficult. Therefore, blends of synthesized dianilines and Epikure W, a liquid at room temperature, were prepared by mixing the two amines together at equal weight ratios. The stoichiometric quantities of the epoxy (EPON 828) were calculated according to Equation 15:

$$phr = \frac{AHEW_{Blend} \times 100}{\text{EEW}} \qquad \textit{Eq. 15}$$

where *phr* is the parts by weight amine per hundred parts by weight epoxy resin and AHEW is the amine hydrogen equivalent weight. Tabel B1 shows the AHEW and structure of each dianiline.

Table A1

Structures and AHEW of all dianilines

Dianiline	Dianiline AHEW ($g\ mol^{-1}$)	Dianiline Structure
4,4'-methylenedianiline (MDA)	49.57	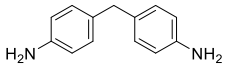
4,4'-methylenebis(2,5-dimethylaniline) (2,5-dMAC)	63.60	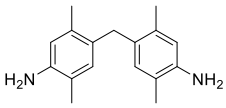
4,4'-methylenebis(2,6-dimethylaniline) (2,6-dMAC)	63.60	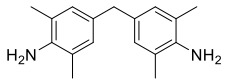
4,4'-methylenebis(2-methylaniline) (2-MAC)	56.58	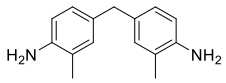
4,4'-methylenebis(2-methoxyaniline) (2-MeOAC)	64.58	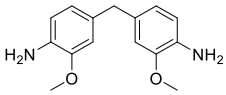
6,6'-methylenebis(3-methylaniline) (3-MAC)	56.58	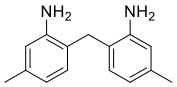
5,5'-isopropylenebis(2-methoxyaniline) (BPA-N)	71.60	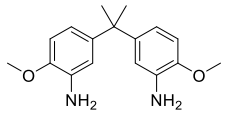
4,4'-diaminodiphenylsulfone (Dapsone)	62.08	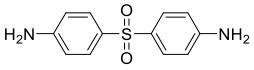
4,4'-diaminobenzophenone (DABP)	53.06	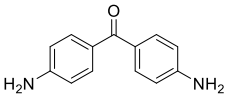

All epoxy-amine resins were well mixed by hand, heated to melt any crystallized material, and degassed under vacuum for approximately 10 minutes to remove any trapped air. The resins were then poured into an aluminum mold with uniform dimension

(75 × 13 × 3.5 mm^3) and cured for 5 h at 140 °C and post-cured at 230 °C for 3 hours. The cured samples were removed from the oven and allowed to cool to room temperature. All samples were transparent indicating the lack of macroscopic phase separation. Following the curing process, the samples were cut and shaped to uniform dimensions for DMA. DABP was not soluble in the resin mixture, even at temperatures as high as 120 °C. Blends up to 25/75 by weight DABP to Epikure W were also not able to form a soluble mixture even at 120 °C. Therefore, no additional experiments were performed on DABP formulations.

A.2.6 Extent of cure. The extent of cure was measured using near-infrared (N-IR) spectroscopy. N-IR spectra (64 scans, 8 cm^{-1} resolution) of the epoxy-amine systems both before cure and after post-cure were obtained in the range of 4000-8000 cm^{-1} in transmission mode at room temperature on a Thermo Scientific Nicolet iS50 FTIR spectrometer [242].

A.2.7 Polymer properties. The thermogravimetric properties of the cured epoxy-amine thermosets were measured in duplicate using a TA Instruments Q500 Thermogravimetric Analyzer (TGA). Approximately 5 mg of sample was placed in a platinum pan and heated to 650 °C at a rate of 20 °C min^{-1} in a N_2 atmosphere (10 mL min^{-1} balance gas flow rate and 25 mL min^{-1} sample gas flow rate). Thermogravimetric properties including initial decomposition temperature (*IDT*), temperature at 50% weight loss ($T_{50\%}$), temperature at maximum decomposition rate (T_{max}), and char content are reported.

The thermophysical properties of all cured epoxy-amine thermosets were measured in duplicate using a TA Instruments Discovery Series DSC2500.

Approximately 5 mg of sample was placed in a Tzero aluminum pan, sealed with a hermetic lid, and the temperature was increased to 220 °C at a rate of 10 °C min^{-1} in a N_2 atmosphere. The sample was then cooled to -25 °C then heated at 10 °C min^{-1} to 220 °C to measure the glass transition temperature (T_g).

The viscoelastic properties of the cured epoxy-amine thermosets were measured using a TA Instruments Q800 Dynamic Mechanical Analyzer (DMA). T_g, storage modulus (E') at 25 °C, rubbery temperature, rubbery E', and molecular weight between crosslinks (M_c) are reported. M_c was calculated using the Theory of Rubber Elasticity [31]. The Theory of Rubber Elasticity was derived for branched and lightly crosslinked polymer networks; however, literature has shown that the application of this theory to highly crosslinked polymer networks can still provide insight into polymer behavior and trends [5, 61, 243]. Polymer densities at room temperature were measured using Archimedes' principle [29]. Samples were prepared with uniform dimensions of 35 × 11 × 2.5 mm^3 and 35 × 11 × 1.5 mm^3 and tested using single cantilever geometry in accordance with McAninch et al [32]. The tests were performed at a frequency of 1.0 Hz, a deflection amplitude of oscillation of 7.5 μm, and a Poisson's ratio of 0.35. The temperature was increased from 0 °C to 220 °C at a rate of 2 °C min^{-1}.

A.3 Results and Discussion

A.3.1 Synthesis and characterization of dianilines. After flash chromatography and subsequent solvent removal, all dianilines were white solids. The structures of all dianilines were confirmed via ^{1}H-NMR. Integration of the ^{1}H-NMR spectra confirmed that the number of protons associated with each peak agreed with the proposed structure. The melting points and enthalpies of melting for all dianilines are provided in Table A2.

Table A2

Melting points and enthalpies of melting of all dianilines

Dianiline	**Melting Point (°C)**	**Enthalpy of Melting (kJ mol^{-1})**
MDA	94.9 ± 0.1	21.61 ± 0.68
2,5-dMAC	143.1 ± 0.1	38.12 ± 1.05
2,6-dMAC	122.2 ± 0.3	23.97 ± 0.31
2-MAC	159.2 ± 0.7	32.52 ± 3.53
2-MeOAC	101.9 ± 0.2	28.11 ± 0.50
3-MAC	124.4 ± 0.5	19.60 ± 0.44
BPA-N	103.6 ± 0.4	34.12 ± 1.73
Dapsone	180.1 ± 0.1	20.80 ± 0.43
DABP	245.5 ± 2.3	32.48 ± 1.61

All of the selected dianilines have higher melting points than MDA, due to the effects of the additional substituents on the aromatic rings and different structural motifs. Dapsone has a very high T_m, likely due to the rigidity of the sulfone bridge. Similarly, DABP has a significantly elevated T_m likely due to the rigidity of the carbonyl bridge. For 2-MeOAC, the methoxy moieties ortho to the amines increased the melting point by 7 °C. Similarly, BPA-N, which also bears methoxy moieties, has a melting point 9 °C higher than that of MDA. Methyl moieties are shown to have a significantly greater impact on melting point, where 2-MAC has a melting point that is 65 °C higher than that of MDA. A dianiline of the same molecular weight, 3-MAC, only has a 29 °C higher melting point than MDA, showing the effect of the placement of the methyl moieties and

the position of the amines relative to the methylene bridge connecting the two aromatic rings. 2,5-dMAC has a melting point that is 48 °C higher than MDA, whereas 2,6-dMAC has a melting point that is only 27 °C higher, showing the effect of multiple methyl moieties and their respective locations on the aromatic ring. Unfortunately, too few unique monomers were prepared to quantify the exact effect of amine location and methyl placement on T_m, yet it was seen that the proposed MDA alternatives all have a higher T_ms and enthalpy of melting than MDA. The increase in both T_m and enthalpy is generally not beneficial for composites manufacturing as it requires blending with a co-monomer (e.g., Epikure W) to be liquid processable at desired temperatures. Alternatively, high temperature processing can be used for resin systems based on these dianilines, although this would not be possible for epoxies as the resins would cure during processing. In all, these higher T_ms would likely increase overall processing costs of these materials without factoring in toxicity benefits.

A.3.2 Toxicity of dianilines. MDA toxicity has been tested in several animal species. The dose that causes 50% death in rats (LD50) is 517 mg/kg, which is considered moderately toxic. MDA is mutagenic in the Ames assay and carcinogenic in animals [244]. Dapsone is not a mutagen or carcinogen [31]. Despite DABP's use in commercial polymers, it was surprising to find that much information on its toxicity was lacking. Our experimental results (Table A3) indicate than DABP is not mutagenic – a predictor of carcinogenic potential.

The alternative diamines were evaluated for oral and aquatic toxicity by reviewing the literature for reported toxicity and conducting QSAR and in vitro testing where data were lacking (Table A3). The highly used amine hardener Dapsone has

slightly lower toxicity (i.e., lower LD50 and LC50) compared to MDA showing that MDA's primary hazard is carcinogenicity compared to Dapsone acute toxicity. Compared to the NRU and/or rat acute toxicity values, QSAR under-estimated the oral toxicities. Compared to the microtox data, QSAR overestimated the aquatic toxicity for these compounds by approximately one order of magnitude. For the endpoints compared in this report, there does not seem to be a common trend among structural effects on oral and aquatic toxicities, reflecting the need to experimentally measure these results.

Of the synthesized alternative anilines, QSAR predicted that only 2,6-dMAC and BPA-N were not mutagens at high probability (Table A3). The 2,6-dMAC is likely not mutagenic resulting from steric effects on the amine that likely limit the nitrosamine formation. The use of an isopropyl linkage may also contribute to the reduced mutagenicity of 5,5'-(propane-2,2-diyl)bis(2-methoxyaniline), although the different position of the amine may also contribute to the reduced mutagenicity. All of the other synthesized anilines were mutagens at high probability. Except for BPA-N and 2,5-dMAC, the experimental Ames test results were in agreement with the QSAR predictions with one false positive and one false negative (Table A3). From an oral and aquatic toxicity perspective, no synthesized chemicals were significantly better than MDA or each other.

The nitrosamine forms on the amine, and thus sterics and electronics of the amine and the sterics of interactions of the molecule with the CYP enzyme are likely to play a role. Yet, the sterics on the amine for 3-MAC and BPA-N are comparable, so amine sterics is not likely the main reason. Yet, the shape of the BPA-N molecule is significantly different than that of 3-MAC and 2-MeOC because of both its methoxy and

isopropyl linkage between phenyl rings, which can affect the ability of the CYP enzyme to come in close contact with BPA-N on a relative basis. Alternatively, BPA-N has its amine meta to the aliphatic linkage between phenyl rings, while all the other molecules are ortho or para. This meta substitution may have a disruptive electronics effect that reduces the formation of the nitrosamine. Yet, this work and past work [38] show that 2,6-dMAC is not mutagenic and this molecule has para bonding of the amine and has a methylene linkage between the phenyl rings indicating that an available position on the ring ortho to the amine may contribute to nitrosamine formation. For 4,4'-methylenebis(2,6-dimethylaniline), the positions ortho to the amine is not available. For BPA-N, one of the ortho sites on each phenyl ring is not available, but the other is significantly more sterically hindered than any of the other molecule tested. Additionally, 2,5-dMAC is mutagenic and has an available, non-sterically hindered site ortho to the amine. Thus, it seems that both sterics and electronics of the whole aniline structure is important in the actual mutagenicity.

Table A3

QSAR and in vitro toxicity predictions.

Dianiline	TOPKAT Prediction Oral LD50 in mg/kg [data confidence]	In vitro NRU Estimated LD50 in mg/kg (toxicity category)	Ames Mutagenicity, TOPKAT Prediction*	Ames Mutagenicity, Experimental	Daphnia LC50, (mg L^{-1}) ECOSAR Prediction	Aquatic Toxicity mg L^{-1} +/-C.I. (toxicity category)
MDA	1900 [high] 517 (rat) DB [32]	944 (Moderate toxicity)	Positive; DB [53]	Positive (at/above 10.0 ug/mL)	1.41 (Moderate toxicity)	14.3 ± 1.1 (Low toxicity)
2,5-dMAC	2500 [high]	650 (Moderate toxicity)	Unlikely [low]	Positive (at/above 1.1 ug/mL)	0.67 (Highly toxic)	35.4 ± 10.0 (slightly toxic)
2,6-dMAC	2400 [high]	NT, Insoluble	Negative DB [245]	Negative	0.67 (Highly toxic)	39.4 ± 5.0 (Slightly toxic)
2-MAC	2200 [high]	532 (Moderate toxicity)	Positive; DB [245]	Positive (at/above 3.2 ug/mL)	3.45 (Moderate toxicity)	14.3 ± 1.7 (Low toxicity)
2-MeOAC	6900 [high]	781 (Moderate toxicity)	Positive [high]	Positive (at/above 3.2 ug/mL)	1.83 (Moderate toxicity)	6.3 ± 1.3 (Moderate toxicity)
3-MAC	2000 [high]	684 (Moderate toxicity)	Probable [high]	Positive (at/above 3.2 ug/mL)	3.45 (Moderate toxicity)	42.3 ± 1.2 (Low toxicity)
BPA-N	6300 [high]	512 (Moderate Toxicity)	Positive [high]	Negative	1.82 (Moderate toxicity)	51.3 ± 1.0 (Slightly toxic)
Dapsone	1000 (rat) DB [31]	NT	NA	Negative; DB [31]	1.82 (Moderate toxicity)	NT
DABP	2400 [high]	NT	Positive [high]	Negative	1.54 (Moderate toxicity)	NT

NT=not tested
DB=database value
NA=TOPKAT uses experimental value for compound

A.3.3 Extent of cure. The extent of reaction is typically measured by DSC; however, infrared spectroscopy, particularly N-IR, is a more powerful tool allowing for accurate determination of both epoxy and amine conversions [246]. Since the absorbance peak at 4530 cm^{-1} does not overlap other peaks, it can be used to quantitatively determine the extent of cure according to Equation 16 in which absorbance peaks at 6000 cm^{-1} were used as internal references.

$$Extent\ of\ cure = \frac{\left(ABS_{4530cm^{-1}}/ABS_{ref}\right)_{precure} - \left(ABS_{4530cm^{-1}}/ABS_{ref}\right)_{postcure}}{\left(ABS_{4530cm^{-1}}/ABS_{ref}\right)_{precure}} \qquad Eq.\ 16$$

Within the limits of N-IR spectroscopy, all resins were determined to exhibit extents of cure ≥ 99% following post-cure. Figure A2 only shows the spectra of the resin system containing Dapsone pre- and post-cure; however, all other resins showed similar results.

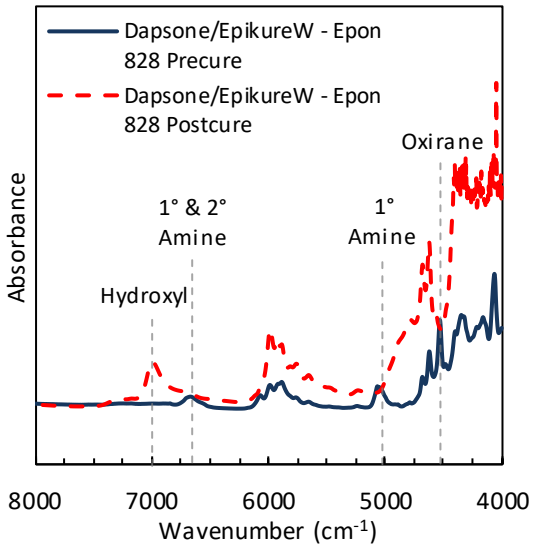

Figure A2. Overlay of near-IR spectra of pre-cured and post-cured an epoxy resin system; spectra offset for clarity.

A.3.4 Polymer properties. All synthesized cured epoxy resin systems were transparent, indicating the lack of macroscopic phase separation. Figure A3 shows both the weight percentage and derivative of the weight percent for the selected dianilines: MDA, Dapsone, 2,6-dMAC, and BPA-N, as a function of temperature. The thermogravimetric properties of the epoxy-amine thermosets are summarized in Table A4. Each cured epoxy-amine resin containing a dianiline was tested using TGA to determine the effect of dianiline structure on thermogravimetric properties. As seen in Table A4 and Figure A3, most of the thermosets exhibit *IDT*s between 356 °C and 368 °C, $T_{50\%}$ values between 392 °C and 399 °C and T_{max} values between 384 °C and 392 °C, indicating that all the cured epoxy systems containing alternative MDA dianilines had comparable thermal stabilities to those containing MDA. The exception to this trend is the Dapsone-containing cured resin, which has a slightly higher *IDT* (378 °C), $T_{50\%}$ (409 °C), and T_{max} (401 °C) indicating that the sulfonyl bridge is imparting a slightly increased thermal stablility into the thermoset network.

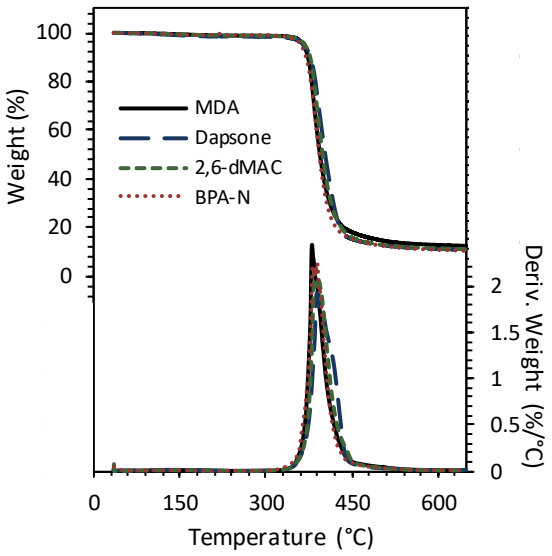

Figure A3. TGA thermograms and their respective 1st derivatives of the cured epoxy-amine thermosetting systems in N_2.

Table A4

Thermogravimetric properties for all the cured epoxy-amine thermosetting systems in N_2

Dianiline	***IDT*** **(°C)**	$T_{50\%}$ **(°C)**	T_{max} **(°C)**	**Char Content (%)**
MDA	365 ± 1	394 ± 1	384 ± 2	11.7 ± 0.8
2,5-dMAC	367 ± 1	398 ± 1	386 ± 4	11.2 ± 0.7
2,6-dMAC	368 ± 1	398 ± 1	388 ± 4	10.1 ± 1.0
2-MAC	367 ± 1	398 ± 1	386 ± 2	11.2 ± 0.8
2-MeOAC	364 ± 2	394 ± 2	382 ± 2	11.4 ± 0.4
3-MAC	359 ± 3	393 ± 1	382 ± 4	11.0 ± 1.9
BPA-N	361 ± 1	394 ± 1	389 ± 2	9.2 ± 1.2
Dapsone	373 ± 5	406 ± 3	395 ± 6	9.7 ± 1.1

The thermomechanical properties of the cured epoxy-aniline thermosets were measured to determine the effect of dianiline architecture on viscoelastic behavior. Figure A4 shows the DMA thermograms of storage moduli (E') and loss moduli (E'') as a function of temperature for the selected dianilines: MDA, Dapsone, 2,6-dMAC, and BPA-N. The summarized thermomechanical properties for all systems are provided in Table A5. As can be seen in Table A5, most cured epoxies containing a replacement dianiline had a higher glassy modulus than the MDA-containing cured epoxy system. The most notable increase occurs with the 2,5-dMAC-based cured resin, which has a 0.6 GPa higher average glassy E' at 25 °C than the MDA-containing cured epoxy system and a 0.8 GPa higher average glassy E' at 25 °C than the epoxy system cured with the other dimethyl species, 2,6-dMAC. Density increases often lead to increased glassy moduli [247]; however, the MDA thermoset has a higher density than all the other thermosets prepared. Increased hydrogen bonding for the dianilines with methoxy groups is a likely reason for the observed increases in glassy E' at 25 °C [61, 248]. The increased glassy E' at 25 °C for methyl substituted dianilines must be a result of increased energy to deform the sample. This would indicate that these substituents help prevent the sliding of adjacent molecules past each other.

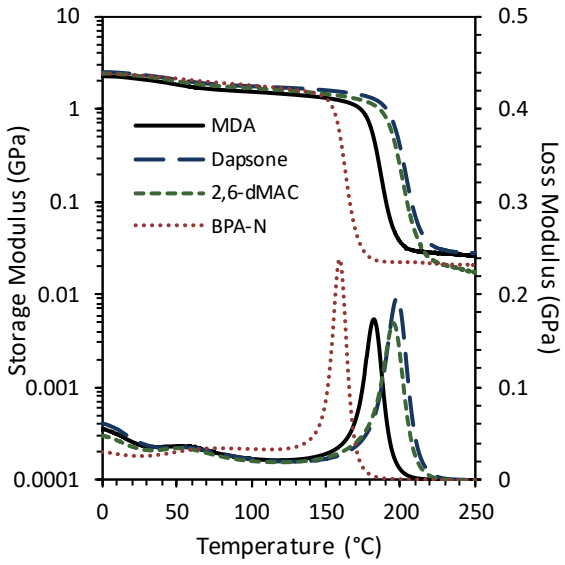

Figure A4. DMA thermograms of *E′* and *E″* of the epoxy-amine thermosets cured with dianilines.

Table A5

Thermomechanical properties for all epoxy-amine polymers with varying dianilines

Dianiline	***E′* @ 25°C (GPa)**	**Peak of *E″* (°C)**	**Peak of tan δ (°C)**	**M_C (g mol^{-1})**	**ρ @ 25°C (g cm^{-3})**
MDA	2.2 ± 0.1	182 ± 1	190 ± 1	419 ± 18	1.177 ± 0.002
2,5-dMAC	2.8 ± 0.2	179 ± 2	188 ± 1	430 ± 29	1.160 ± 0.005
2,6-dMAC	2.0 ± 0.4	196 ± 1	205 ± 1	429 ± 61	1.161 ± 0.001
2-MAC	2.0 ± 0.9	178 ± 1	187 ± 1	392 ± 3	1.166 ± 0.002
2-MeOAC	2.6 ± 0.2	167 ± 1	175 ± 1	400 ± 32	1.170 ± 0.002
3-MAC	2.5 ± 0.4	164 ± 1	173 ± 1	465 ± 1	1.162 ± 0.003
BPA-N	2.5 ± 0.1	159 ± 1	166 ± 1	600 ± 40	1.165 ± 0.001
Dapsone	2.4 ± 0.1	198 ± 1	207 ± 1	534 ± 63	1.117 ± 0.010

The T_gs of all cured resins acquired via DSC agreed with those acquired via DMA (Table A5). The average T_g of the epoxy system cured with MDA is 182 °C. The cured resins containing methoxy bearing dianilines are shown to have lower T_gs than MDA. For

example, the 2-MeOAC cured epoxy system has an average T_g of 167 °C, 15 °C lower than that of the system containing MDA, due to the methoxy moiety *ortho* to the amine, which allow for a higher degree of rotational freedom of the polymer backbone during heating [61, 85, 249, 250]. Also, the cured epoxy resin containing BPA-N has a significantly lower T_g (159 °C) than that of both polymers containing MDA and 2-MeOAC, likely due to the non-linear structure of the dianiline. While only single methoxy moieties *ortho* to the amines are shown to cause a significant reduction in T_g, methyl substituents are generally shown to be less detrimental to T_g. The only methyl bearing dianiline that is shown to reduce the T_g of the cured polymer system is 3-MAC, which is most likely attributed to the non-linearity of the dianiline. The cured epoxy resins containing 2,5-dMAC and 2-MAC have directly comparable T_gs (179 °C and 178 °C, respectively) to that of MDA (182 °C), and thus, these *ortho* and *meta* methyl groups have no effect on T_g. Interestingly, the cured epoxy resin containing 2,6-dMAC is shown to have an average T_g of 196 °C, approximately 14 °C higher than that of MDA. 2,6-dMAC has a similar structure to that of 2,5-dMAC; however, the difference is that the both methyl moieties are *ortho* to the amines, whereas in 2,5-dMAC, they are not. This placement of the methyl moieties increases the steric rigidity of the cured epoxy system and limits the movement of the polymer chains; thus, causing an increase in T_g. Furthermore, Dapsone also exhibits a higher T_g (198 °C) than MDA for the resulting cured epoxy system, likely due to the rigid sulfonyl spacer bridge, which restricts the movement of polymer chains and increases T_g.

All cured epoxy-amine thermosets exhibit comparable M_c values due to their similar extents of cure, with small differences being attributed to slight variations of

dianiline molecular weight. Three samples had significantly higher M_c values, indicating lower crosslink densities. These thermosets were those containing 3-MAC, BPA-N, or Dapsone. The lower crosslink density for the thermosets containing 3-MAC and BPA-N are likely due to lack of linearity that likely create a softer, rubbery polymer. Additionally, this lack of linearity results in greater frequency of intramolecular cyclization during cure, thereby effectively decreasing the crosslink density [243, 251]. The sulfonyl bridge in Dapsone likely has different rubbery behavior than alkyl and aromatic groups, resulting in reduced rubbery moduli.

Tan δ behavior trends were the same as for E''s, although the tan δ peaks occurred at 8-10 °C higher than the E'' peaks. This relatively small differences in tan δ and E'' peak temperatures indicate that the glass transition is very narrow and sharp for all of these thermosets [243, 252]. Figure A5 shows the tan δ thermograms for the selected cured epoxy systems containing dianilines: MDA, Dapsone, 2,6-dMAC, and BPA-N. The tan δ thermograms for all other dianilines are available in Appendix A.5.

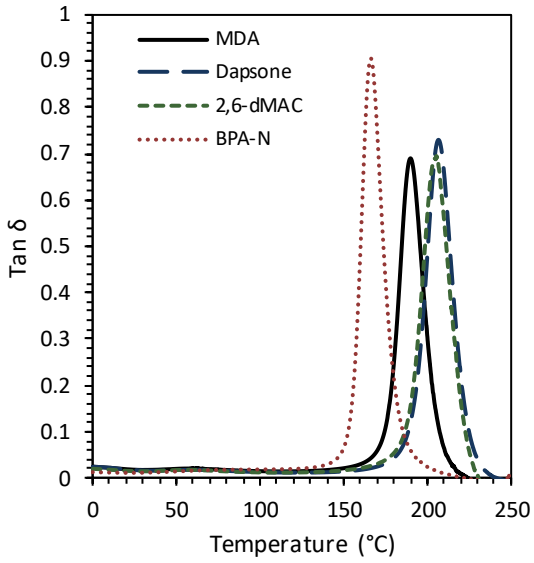

Figure A5. Tan δ thermograms of the epoxy-amine thermosets cured with dianilines.

The maximum value of the tan δ thermogram can be used as an insight into the extent of polymer chain segmental mobility [253]. All cured thermosets, except for BPA-N, exhibited nearly identical maximum values of tan δ, indicating similar chain mobility. BPA-N exhibits an increase in segmental mobility likely due to the lower crosslink density, as a result of its high M_c relative to all other dianilines, of the resulting cured thermoset.

A.4 Conclusions

A strategically selected set of substituted dianilines were prepared to develop structure-property-toxicity relationships by evaluating the effect of molecular structure on overall polymer performance and toxicity. Dianilines were synthesized to reduce toxicity and carcinogenic characteristics of the uncured resin while maintaining thermal and mechanical integrity of the resulting polymeric material. Structure-property relationships show that methoxy groups reduce the glass transition temperature while methyl groups

only slightly affect glass transition and, in some cases, cause an increase in thermal resistance. Structure-toxicity relationships indicate that multiple substituents on the aromatic ring (e.g., BPA-N) are necessary to significantly reduce the toxicity of the dianiline; however, this would likely result in reductions of cured polymer properties, which, depending on end goal applications, might not be of great concern.

A.5 Supporting Information

A.5.1 Dianiline synthesis.

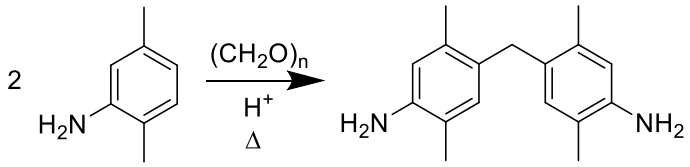

Figure A6. Synthesis of 4,4’-methylenebis(2,5-dimethylaniline).

2,5-dimethylaniline (3 g, 24.8 mmol), paraformaldehyde (0.186 g, 6.29 mmol), and 14 mL DI water were added to a round-bottom flask equipped with a magnetic stir bar. The reactants were mixed vigorously as 9 mL HCl (37 wt%) was slowly added. The reaction was then heated to 90 °C for 4 hours. The reaction mixture was cooled to 0 °C and was slowly neutralized to pH 10 with NaOH pellets. The mixture was extracted with CH2Cl2, and the organic extract was dried using MgSO4 and subsequently concentrated. The resulting solid was filtered and chromatographed to afford 4,4’-methylenebis(2,5-dimethylaniline) as an off-white solid. MP = 143 °C.

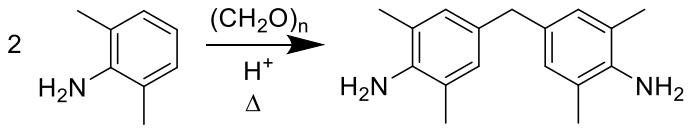

Figure A7. Synthesis of 4,4’-methylenebis(2,6-dimethylaniline).

2,6-dimethylaniline (3 g, 24.8 mmol), paraformaldehyde (0.186 g, 6.29 mmol), and 14 mL DI water were added to a round-bottom flask equipped with a magnetic stir bar. The reactants were mixed vigorously as 9 mL HCl (37 wt%) was slowly added. The reaction was then heated to 90 °C for 4 hours. The reaction mixture was cooled to 0 °C and was slowly neutralized to pH 10 with NaOH pellets. The mixture was extracted with CH2Cl2, and the organic extract was dried using MgSO4 and subsequently concentrated. The resulting solid was filtered and chromatographed to afford 4,4’-methylenebis(2,6-dimethylaniline) (42.5% yield) as an off-white solid. MP = 122 °C.

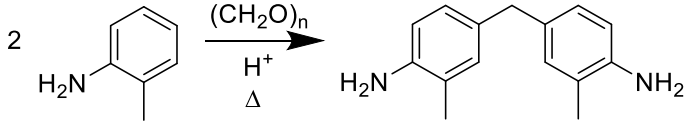

Figure A8. Synthesis of 4,4’-methylenebis(2-methylaniline).

In a 1 L round bottom flask, 2-methylaniline (40.0 g, 373.3 mmol), DI water (200 mL), HCl (37%, 130 mL), and paraformaldehyde (2.8 g, 93.2 mmol) were combined. The reaction was heated to 90 °C for 4 hr. The reaction mixture was cooled to 0 °C and was slowly neutralized to pH 10 with NaOH pellets. The mixture was extracted with CH2Cl2, and the organic extract was dried using MgSO4 and subsequently concentrated. The

resulting solid was filtered and chromatographed to afford 4,4'-methylenebis(2-methylaniline) (48.3% yield) as an off-white solid. MP = 160 °C.

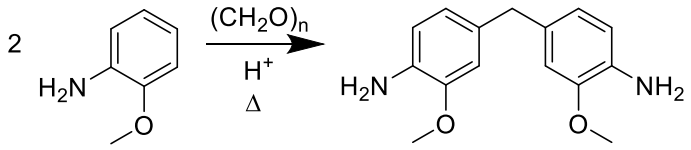

Figure A9. Synthesis of 4,4'-methylenebis(2-methoxyaniline).

In a 1 L round bottom flask, 2-methoxyaniline (40.0 g, 324.8 mmol), DI water (200 mL), HCl (37%, 130 mL) and paraformaldehyde (2.43 g, 80.9 mmol) were combined. The reaction was heated to 90 °C for 4 hr. The reaction mixture was cooled to 0 °C and was slowly neutralized to pH 10 with NaOH pellets. The mixture was extracted with CH2Cl2, and the organic extract was dried using MgSO4 and subsequently concentrated. The resulting oil was distilled under vacuum at 200 °C and the residual oil was chromatographed to afford 4,4'-methylenebis(2-methoxyaniline) (24.8% yield) as an off-white solid. MP = 102 °C.

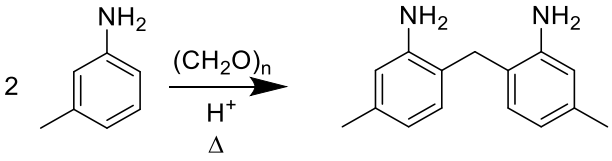

Figure A10. Synthesis of 6,6'-methylenebis(3-methylaniline).

In a 1 L round bottom flask, 3-methylaniline (40.0 g, 373.3 mmol), DI water (200 mL), HCl (37%, 130 mL) and paraformaldehyde (2.43 g, 80.9 mmol) were combined. The

reaction was heated to 90 °C for 4 hr. The reaction mixture was cooled to 0 °C and was slowly neutralized to pH 10 with NaOH pellets. The mixture was extracted with CH2Cl2, and the organic extract was dried using MgSO4 and subsequently concentrated. The resulting oil was distilled under vacuum at 200 °C and the residual oil was chromatographed to afford 6,6'-methylenebis(3-methylaniline) (25.6% yield) as an off white solid. MP = 124 °C.

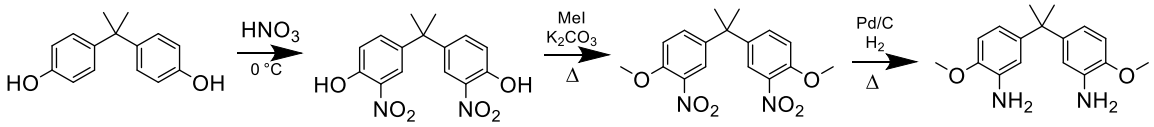

Figure A11. Synthesis of 5,5'-isopropylenebis(2-methoxyaniline).

In a 500 mL round bottom flask, bisphenol A (50.0 g, 219.0 mmol) and CH2Cl2 (70 mL) were combined at 0 °C. HNO3 (70%, 71 mL, 780.0 mmol) was added dropwise over 3 hr. The reaction was slowly neutralized with saturated aqueous NaHCO3. The mixture was extracted with CH2Cl2, and the organic extract was dried using MgSO4 and subsequently concentrated. The resulting oil was diluted with MeOH to give a yellow solid that was filtered and washed with MeOH to afford 4,4'-(propane-2,2-diyl)bis(2-nitrophenol) (59.5% yield).

In a 250 mL round bottom flask, 4,4'-(propane-2,2-diyl)bis(2-nitrophenol) (20.0g, 62.8 mmol), DMF (80 mL), and K2CO3 (47.0 g, 340.1 mmol) were combined. MeI (36.0 g, 253.6 mmol) was added slowly over 10 min, reaction foamed. The reaction was heated to 70 °C for 8 hr. The mixture was diluted with water and extracted with ethyl acetate, and the organic extract was dried using MgSO4 and concentrated. The resulting oil was

filtered over a short pad of silica gel via elution with 60% EtOAc:Hexanes to afford 4,4'-(propane-2,2-diyl)bis(1-methoxy-2-nitrobenzene) (52% yield) as a yellow solid.

In a 250 mL hydrogenating jar 4,4'-(propane-2,2-diyl)bis(1-methoxy-2-nitrobenzene) (25.0 g, 72.2 mmol), 1,4-dioxane and Pd/C (10% wet) (1.3 g) were combined. The reaction mixture was pressurized with 4 bars of H2 then evacuated. This procedure was repeated twice and then pressurized with 4 bars of H2 and heated to 55 °C with shaking. Heating was removed once the mixture came to temperature. There was an exotherm, external cooling was applied, as needed, to keep the temperature below 95 °C. The mixture was shaken for 1 hour after the exotherm had stopped and the temperature dropped to ~30 °C. The reaction mixture was filtered over a short pad of celite and washed with MeOH. The filtrate was concentrated and chromatographed to give 5,5'-(propane-2,2-diyl)bis(2-methoxyaniline) (73.5%) as an off white solid. MP = 104 °C.

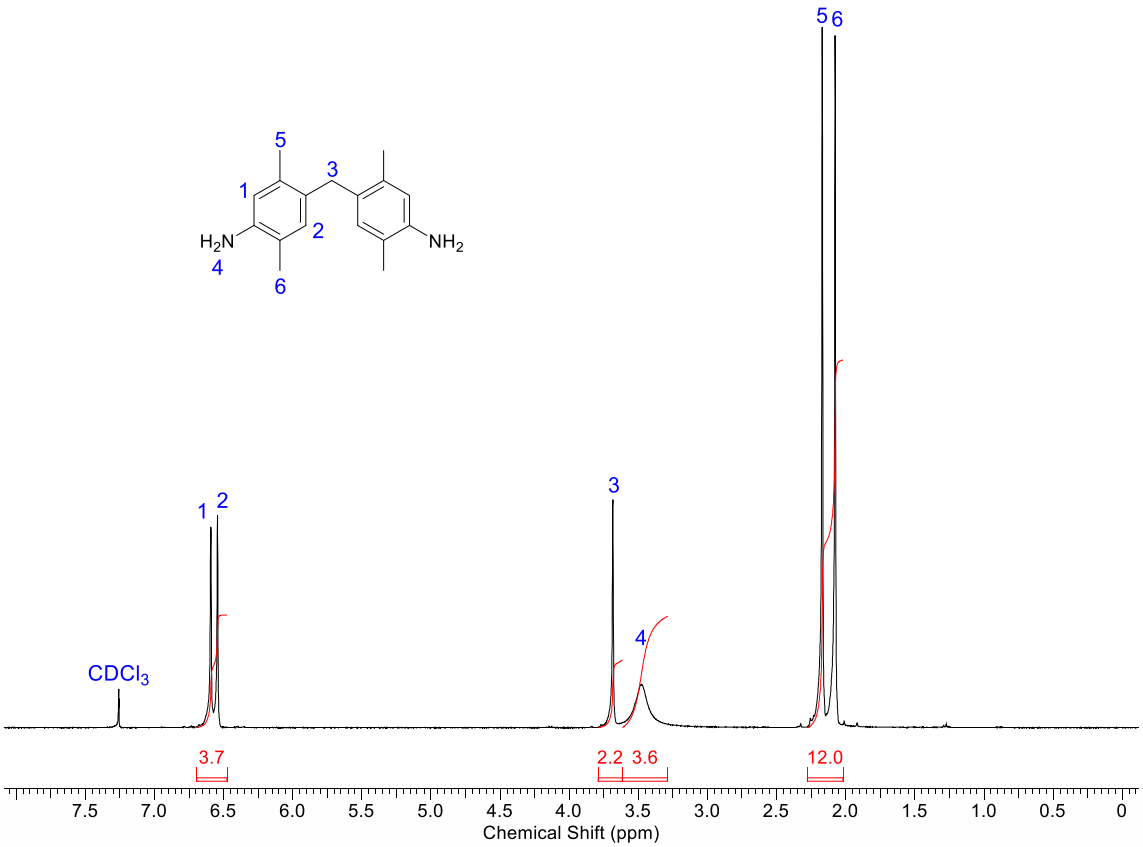

Figure A12. ^{1}H-NMR spectrum of 4,4'-methylenebis(2,5-dimethylaniline) (2,5-dMAC) with peak assignments.

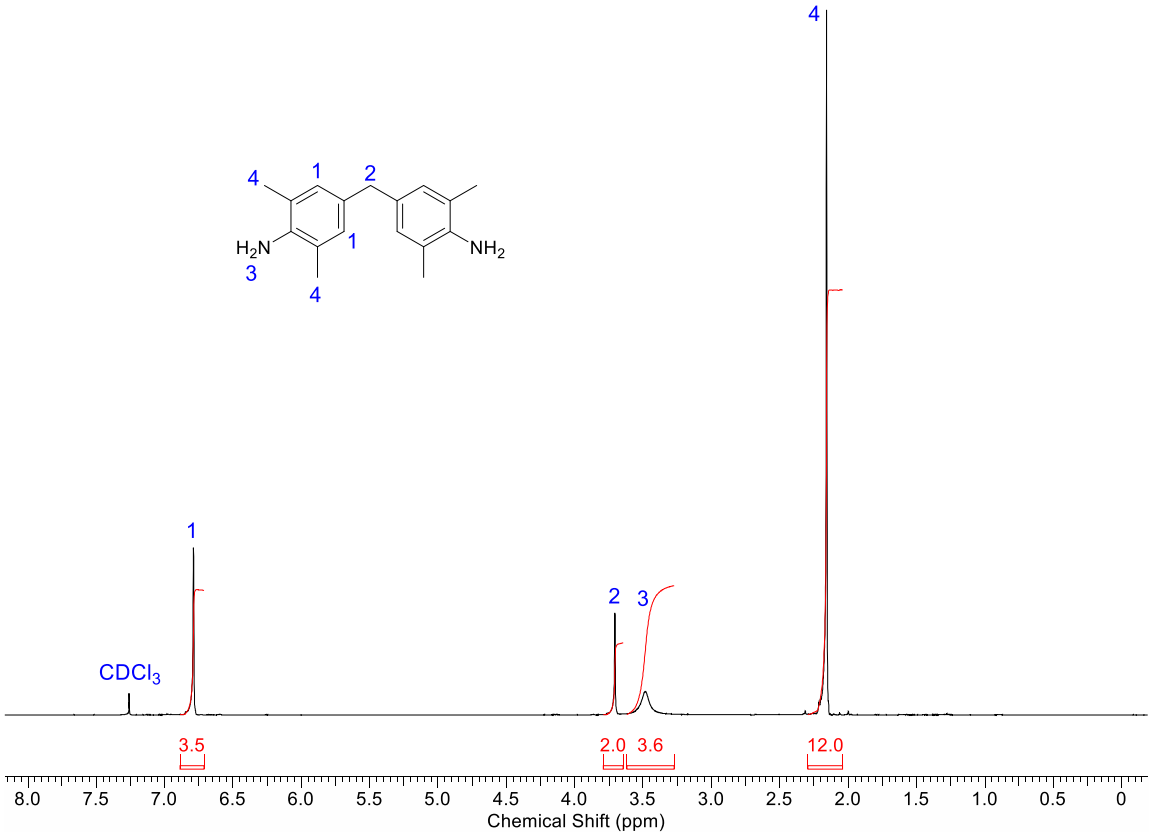

Figure A13. ^{1}H-NMR spectrum of 4,4'-methylenebis(2,6-dimethylaniline) (2,6-dMAC) with peak assignments.

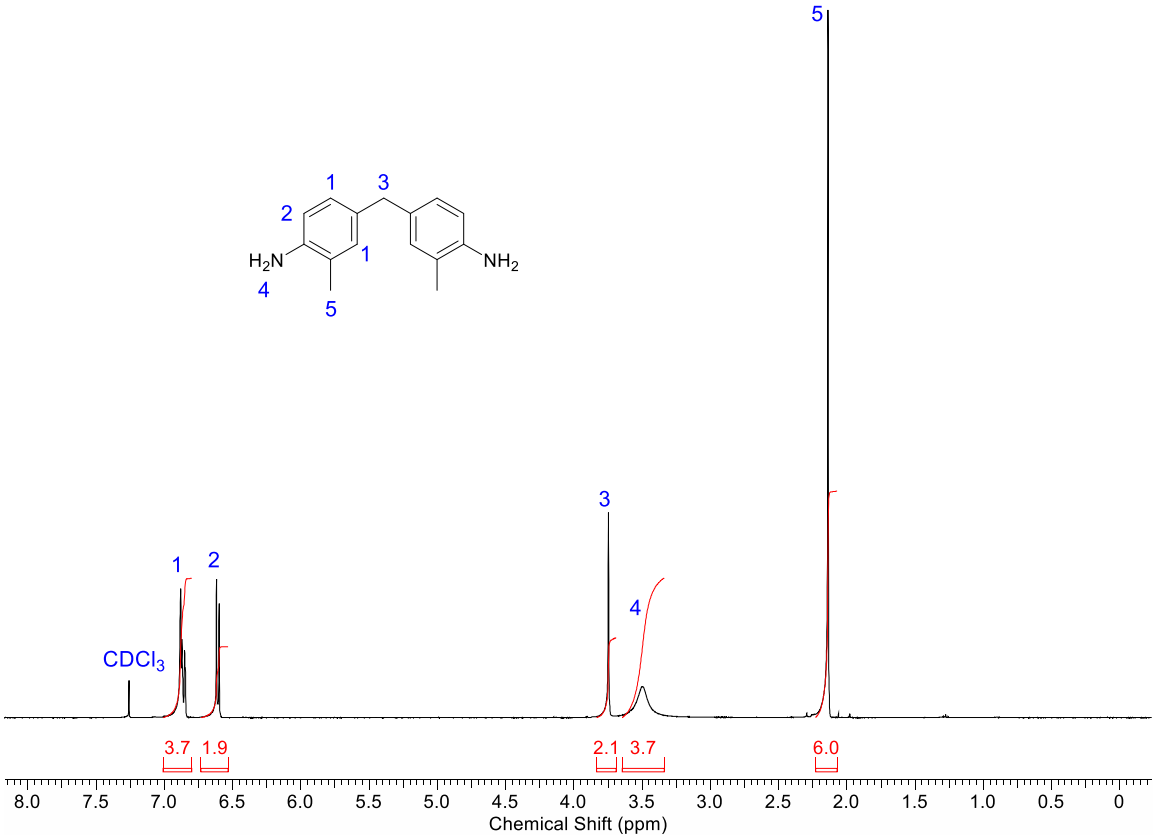

Figure A14. ^{1}H-NMR spectrum of 4,4'-methylenebis(2-methylaniline) (2-MAC) with peak assignments.

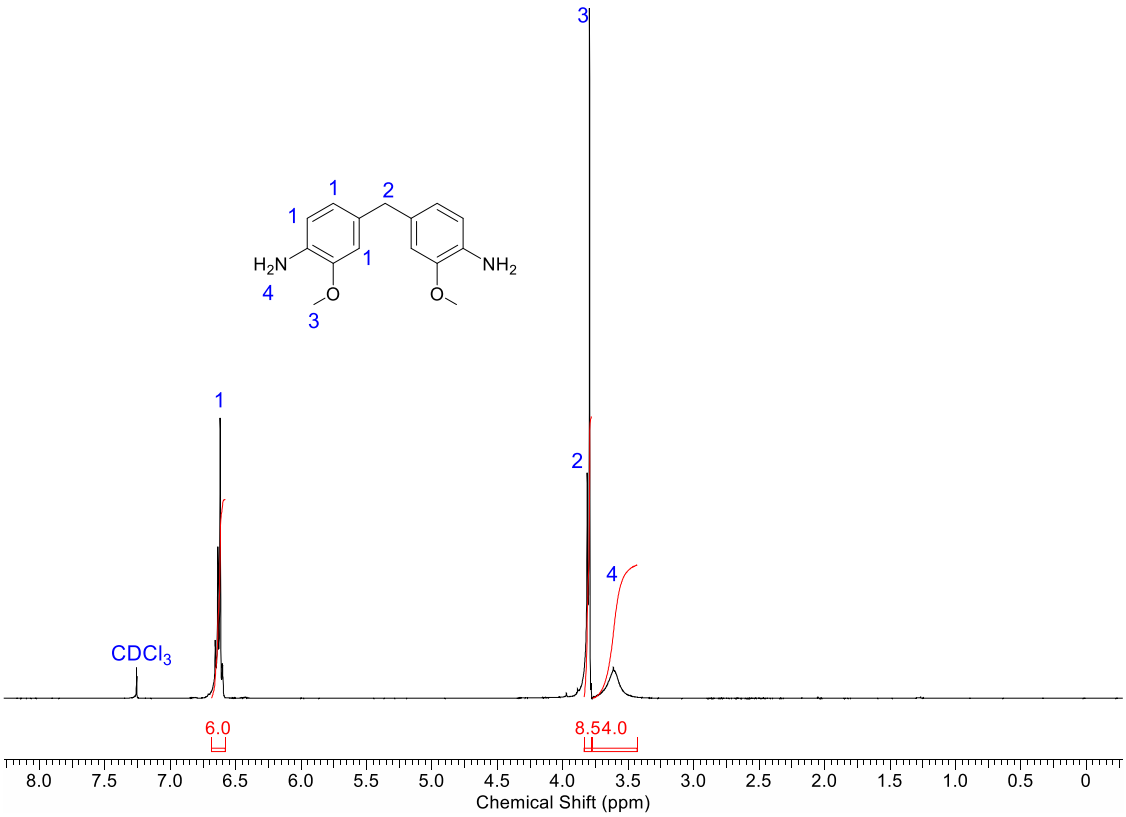

Figure A15. ^{1}H-NMR spectrum of 4,4'-methylenebis(2-methoxyaniline) (2-MeOAC) with peak assignments.

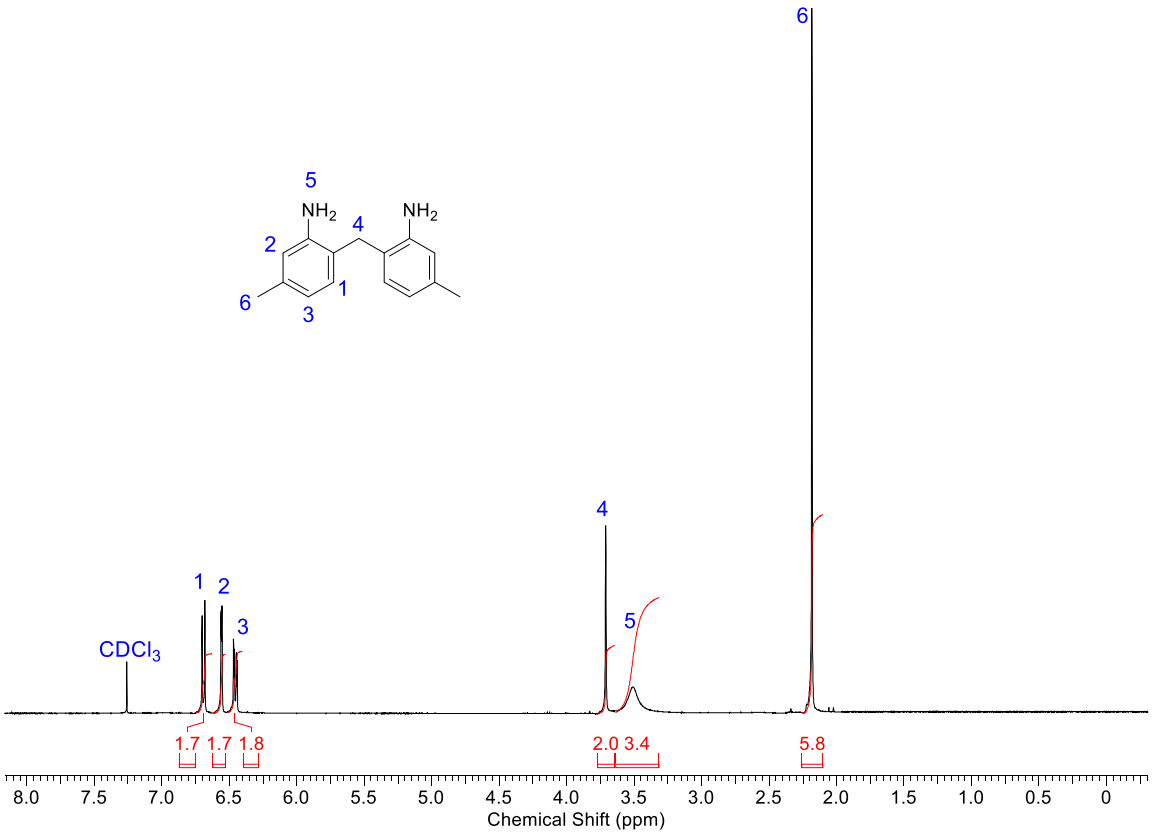

Figure A16. ^{1}H-NMR spectrum of 6,6'-methylenebis(3-methylaniline) (3-MAC) with peak assignments.

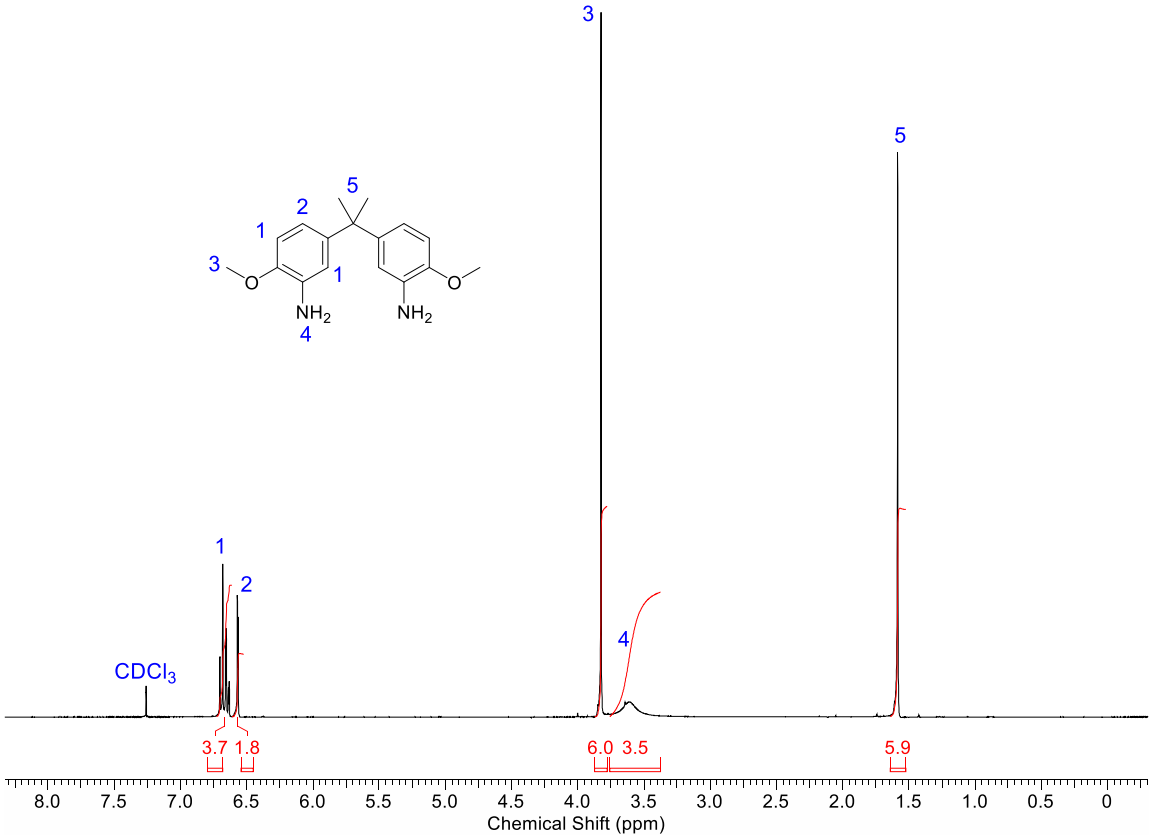

Figure A17. ^{1}H-NMR spectrum of 5,5'-isopropylenebis(2-methoxyaniline) (BPA-N) with peak assignments.

A.5.2 Cured polymer properties.

Table A6

T_g values for all epoxy-amine polymers with varying dianilines according to DSC measurements

Dianiline	**T_g (°C)**
MDA	180.5 ± 3.5
2,5-dMAC	178.5 ± 0.7
2,6-dMAC	196.0 ± 4.2
2-MAC	178.8 ± 0.3
2-MeOAC	165.0 ± 4.2
3-MAC	164.0 ± 2.8
BPA Nitrate	159.5 ± 2.1
Dapsone	197.5 ± 0.7

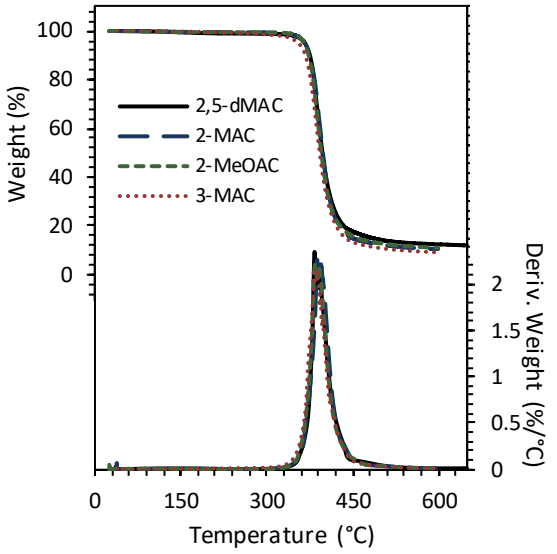

Figure A18. TGA thermograms and their respective 1st derivatives of epoxy-amine thermosets cured with dianilines.

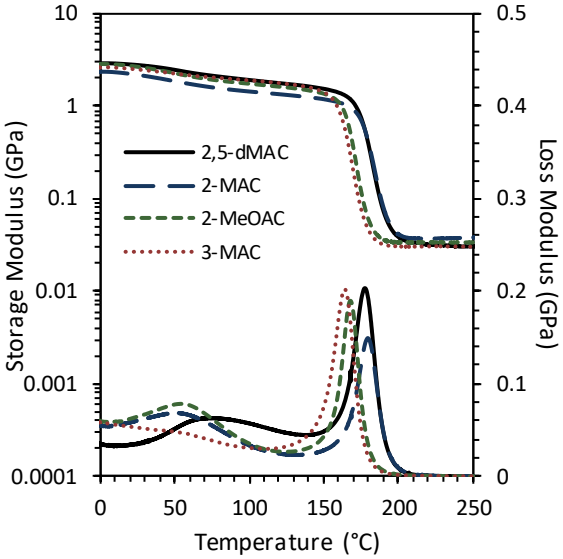

Figure A19. DMA thermograms of *E′* and *E″* of the epoxy-amine thermosets cured with dianilines.

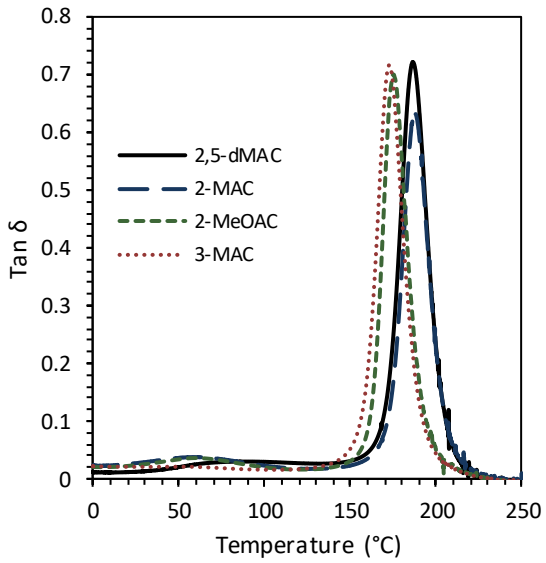

Figure A20. Tan δ of the epoxy-amine thermosets cured with dianilines.

Table A7

Additional thermomechanical properties for all epoxy-amine polymers with varying dianilines

Dianiline	**Rubbery *E′* (MPa)**	**Rubbery *T* (°C)**
MDA	34.7 ± 0.9	222 ± 8
2,5-dMAC	33.2 ± 2.0	217 ± 4
2,6-dMAC	34.7 ± 4.7	236 ± 4
2-MAC	36.5 ± 0.5	218 ± 3
2-MeOAC	34.7 ± 2.6	202 ± 3
3-MAC	30.0 ± 0.3	209 ± 4
BPA-N	23.7 ± 2.1	214 ± 11
Dapsone	28.1 ± 2.7	260 ± 10

Appendix B

Supporting Information for Chapter 3

Text and figures are reproduced and adapted with permission from A.W. Bassett, C.M. Breyta, A.E. Honnig, J.H. Reilly, K.R. Sweet, J.J. La Scala, and J.F. Stanzione III, "Synthesis and characterization of molecularly hybrid bisphenols derived from lignin and CNSL: Application in thermosetting resins," *European Polymer Journal*, 2019, 111, 95-103, reference [36].

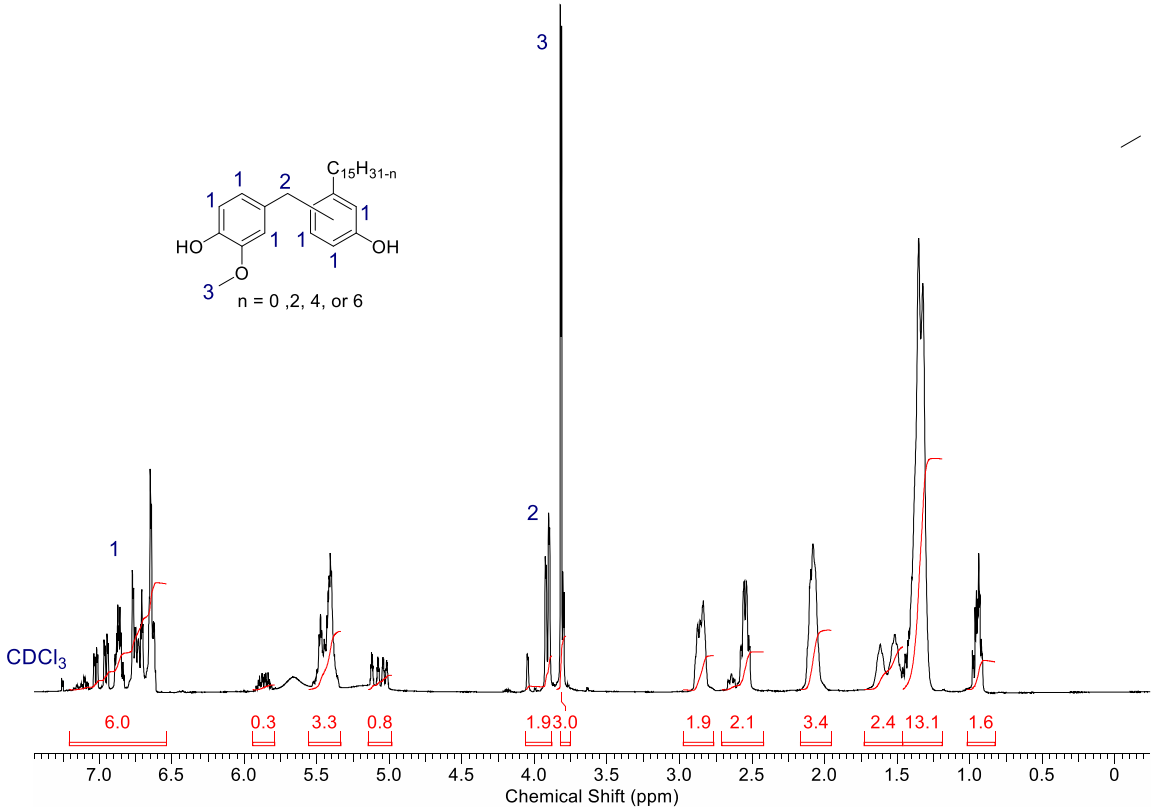

Figure B1. ^{1}H-NMR spectrum of VAC with peak assignments. Unassigned peaks are associated with the alkyl chain.

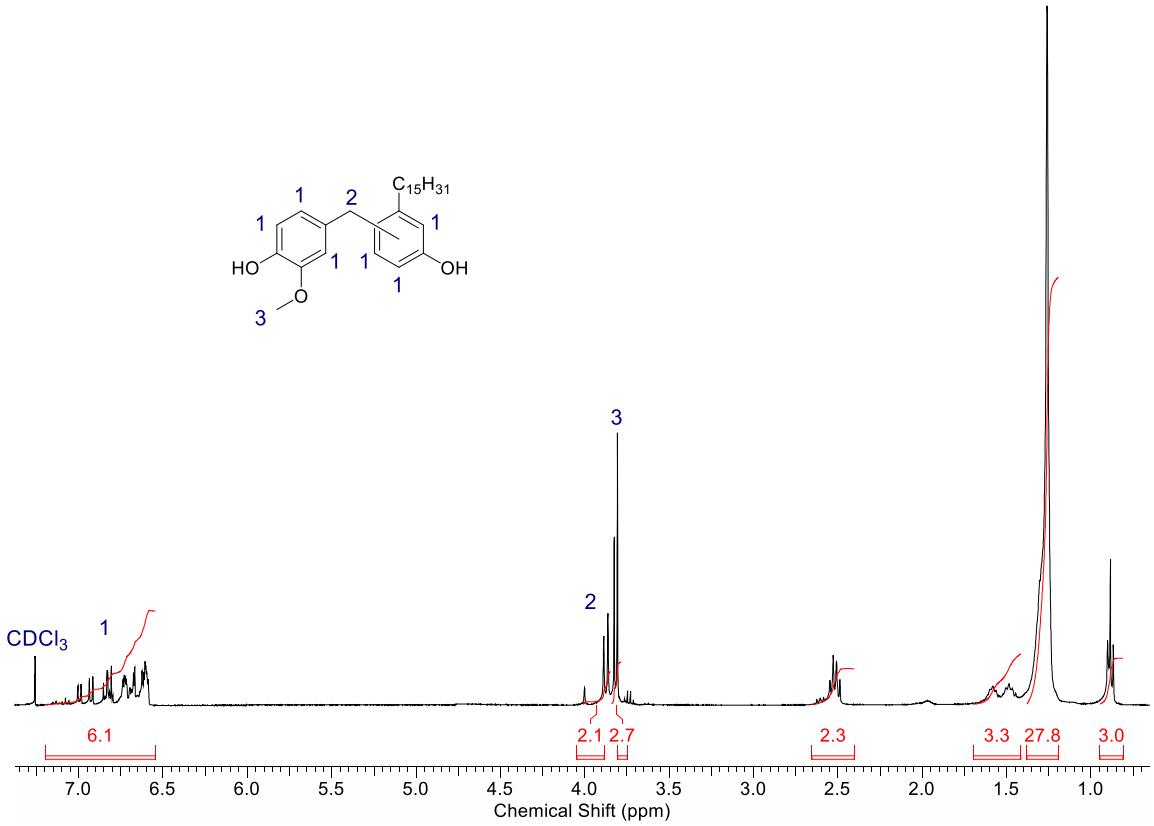

Figure B2. ^{1}H-NMR spectrum of VAHC with peak assignments. Unassigned peaks are associated with the alkyl chain. *VAHC:* ^{1}H-NMR ($CDCl_3$): δ 0.9 (3 H, t), 1.3 (28 H, s), 1.5 (3 H, m), 2.5 (2 H, m), 3.8 (3 H, s), 3.9-4.0 (2 H, s), 6.6-7.0 (6 H, m).

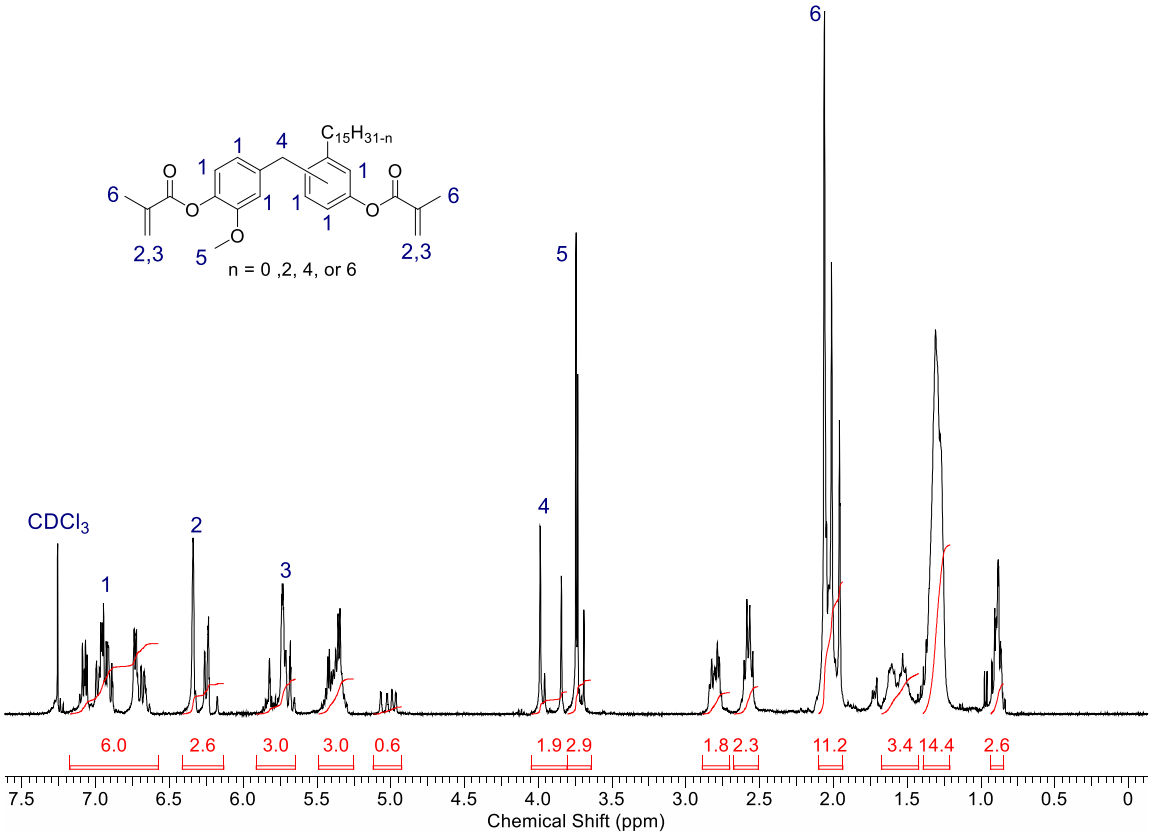

Figure B3. [1]H-NMR spectrum of VACDM with peak assignments. Unassigned peaks are associated with the alkyl chain.

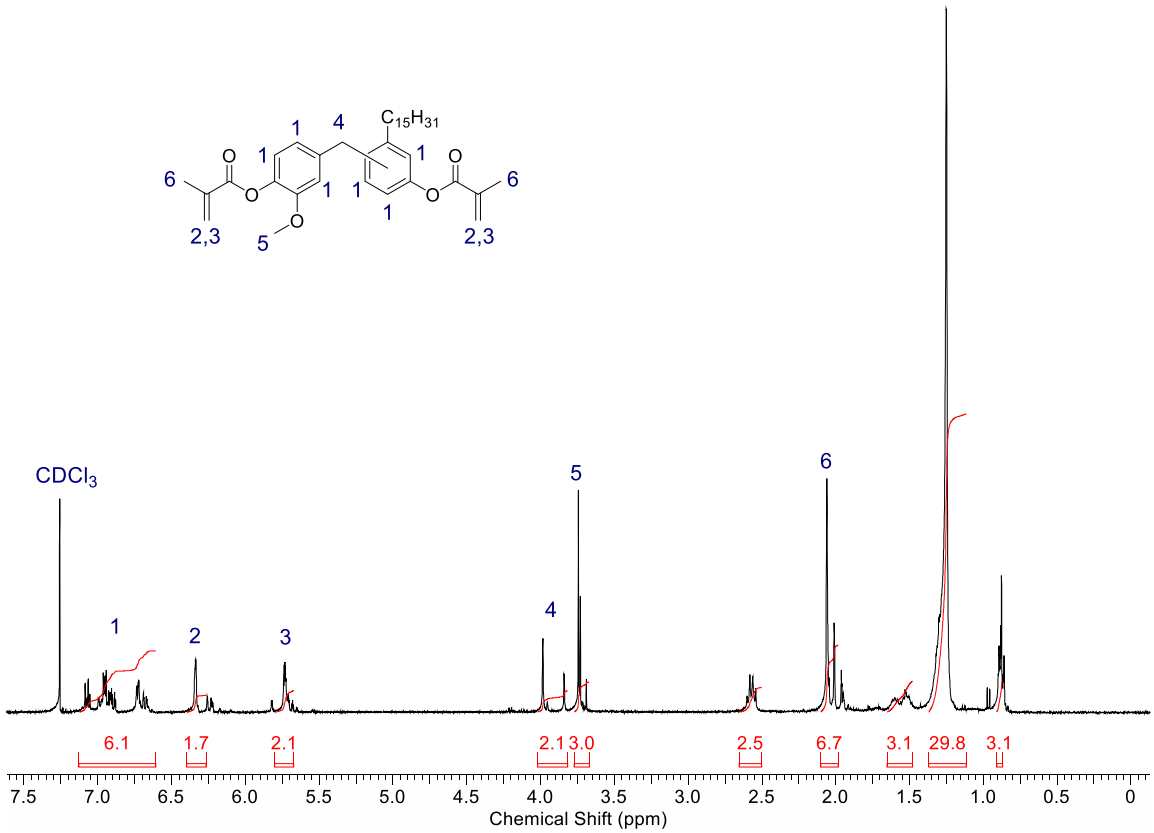

Figure B4. ^{1}H-NMR spectrum of VAHCDM with peak assignments. Unassigned peaks are associated with the alkyl chain. *VAHCDM:* ^{1}H-NMR ($CDCl_3$): δ 0.9 (3 H, t), 1.3 (29 H, s), 1.5 (3 H, m), 2.0-2.1 (6 H, s), 2.5 (2 H, m), 3.7 (3 H, s), 3.9-4.0 (2 H, s), 5.7 (2 H, m), 6.3 (2 H, m), 6.6-7.0 (6 H, m).

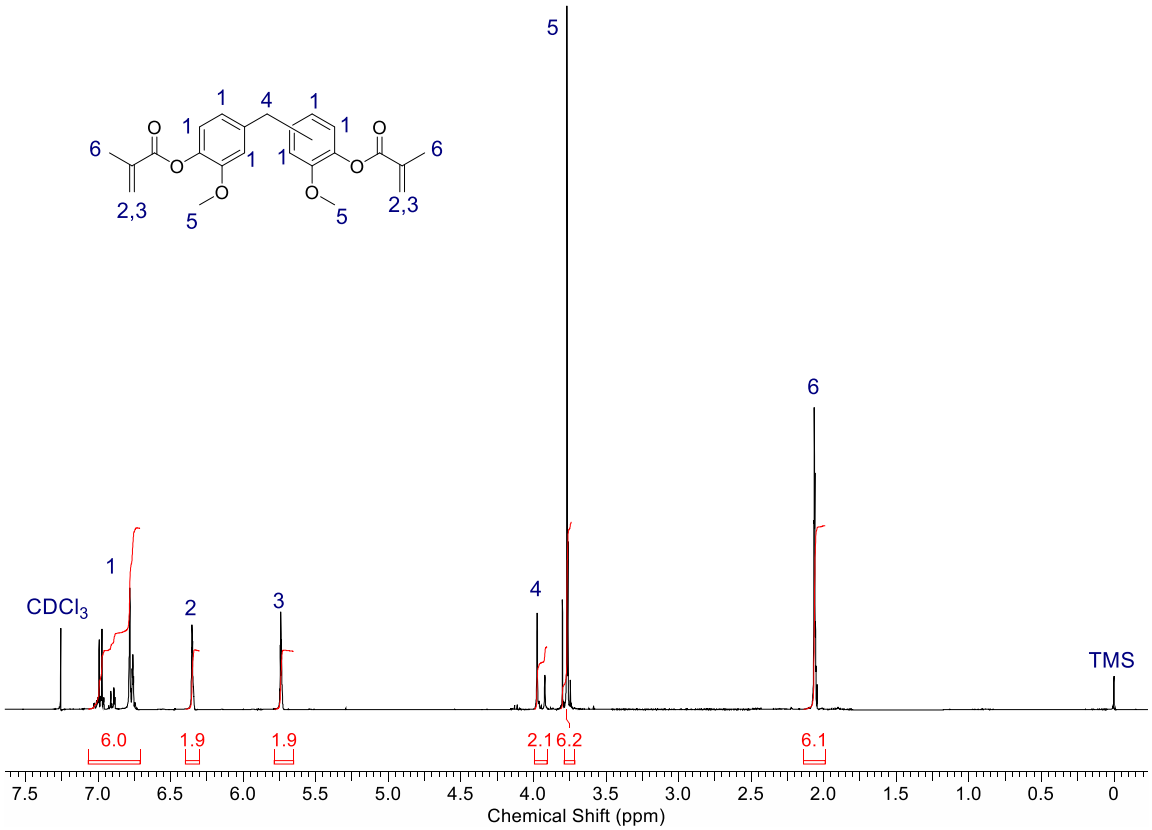

Figure B5. ^{1}H-NMR spectrum of BGDM with peak assignments. *BGDM:* ^{1}H-NMR ($CDCl_3$): δ 2.1 (6 H, s), 3.8 (6 H, s), 3.9-4.0 (2 H, s), 5.7 (2 H, m), 6.4 (2 H, m), 6.8-7.0 (6 H, m).

Table B1

The individual and overall extents of cure after cure at 90 °C

System	Methacrylate Conversion (%)	Styrene Conversion (%)	Overall Extent of Cure (%)
VE828 35 wt% Styrene	48	90	72
BPADM 35 wt% Styrene	56	85	70
VACDM 35 wt% Styrene	-	-	-
VAHCDM 35 wt% Styrene	91	90	90

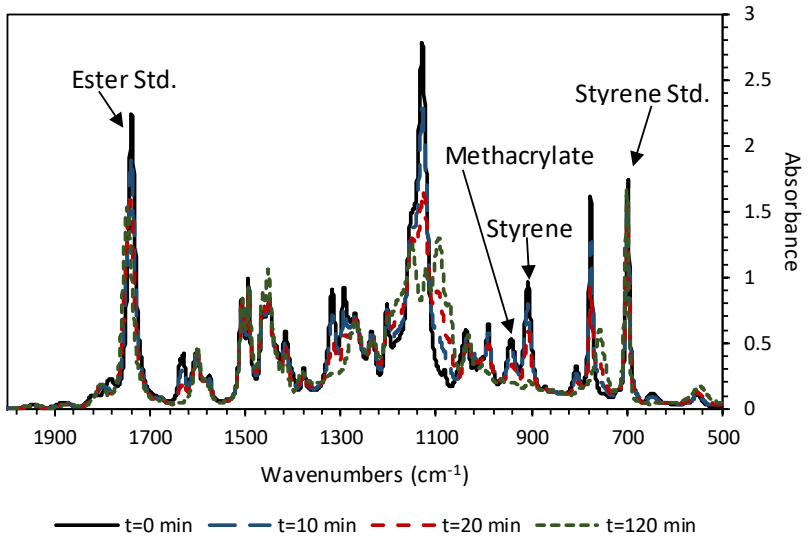

Figure B6. Mid-IR spectra of VAHCDM 35 wt% Styrene resin as a function of cure time at 90 °C.

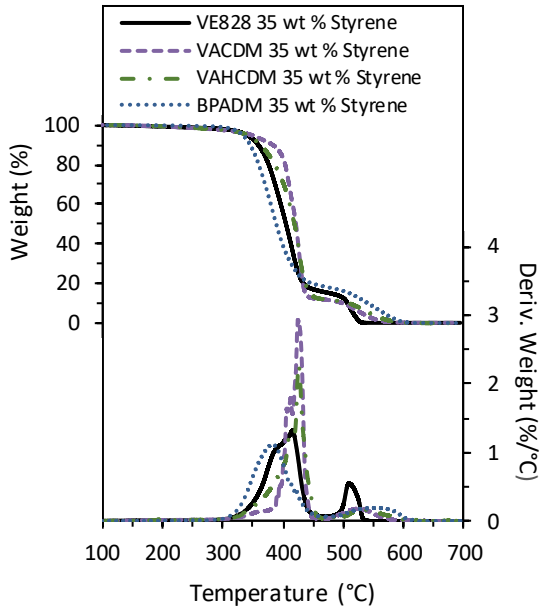

Figure B7. TGA thermograms and their respective 1st derivatives of cured resins in an oxidative environment.

Table B2

Thermogravimetric properties of cured resins in an oxidative environment

System	IDT (°C)	$T_{50\%}$ (°C)	T_{max} (°C)	Char Content (%)
VE828 35 wt% Styrene	342 ± 2	404 ± 1	414 ± 2	0.02 ± 0.03
BPADM 35 wt% Styrene	332 ± 2	383 ± 6	377 ± 6	0.07 ± 0.06
VACDM 35 wt% Styrene	346 ± 2	421 ± 1	425 ± 1	0.06 ± 0.05
VAHCDM 35 wt% Styrene	341 ± 2	418 ± 1	425 ± 1	0.02 ± 0.03

Appendix C

Supporting Information for Chapter 4

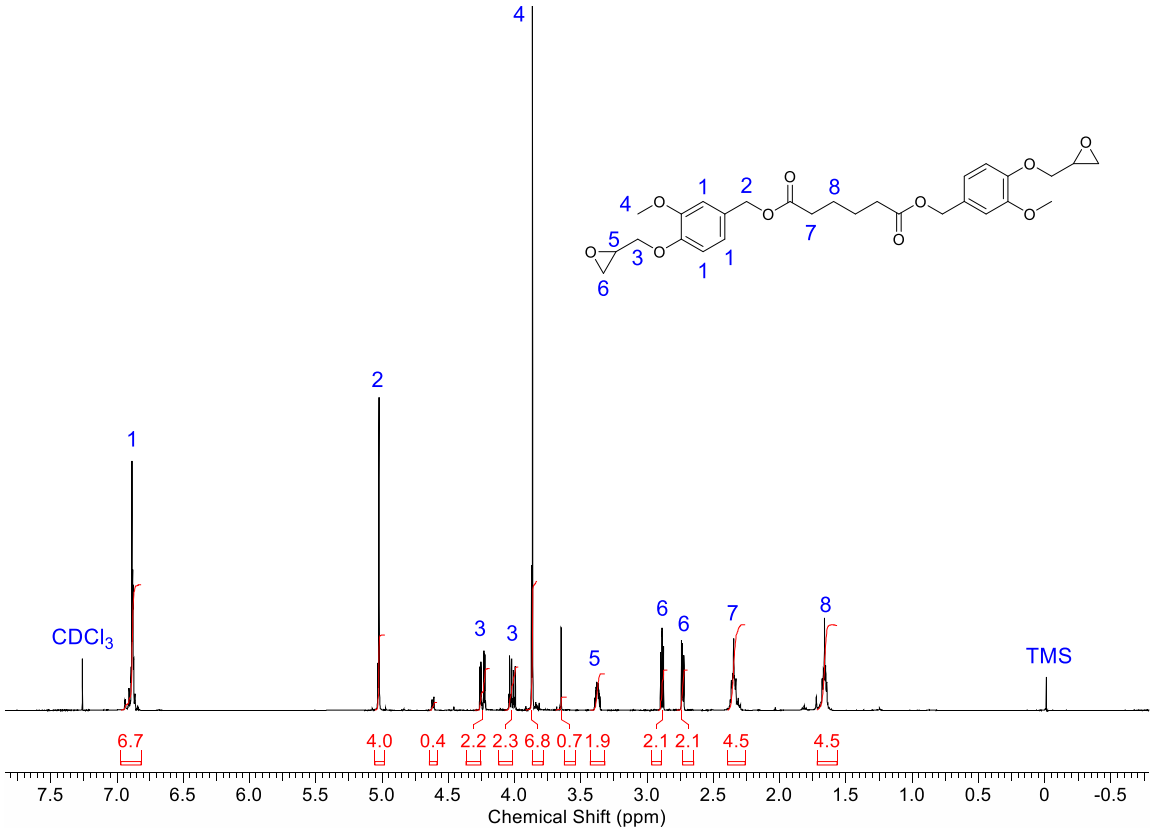

Figure C1. ^{1}H-NMR spectrum of diglycidyl ether of bis-vanillyl alcohol adipate (DGEBVA-Ad) with peak assignments and integrations.

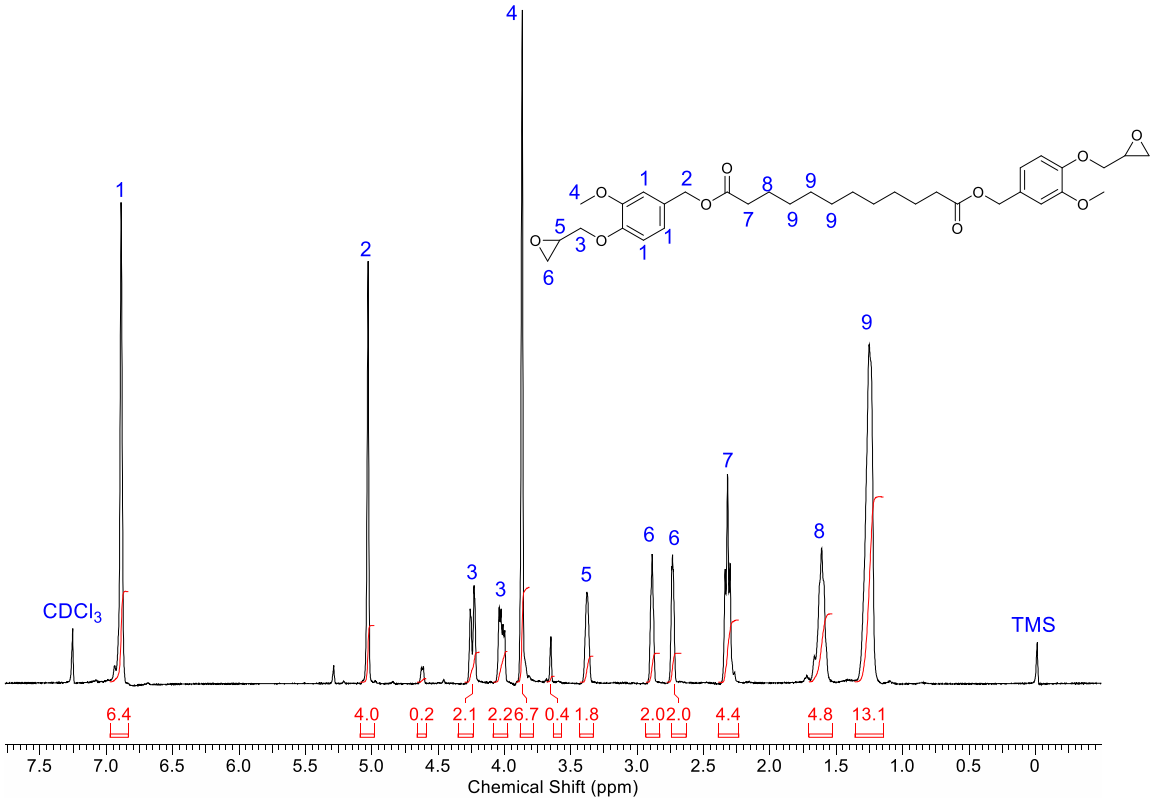

Figure C2. [1]H-NMR spectrum of diglycidyl ether of bis-vanillyl alcohol C12 (DGEBVA-C12) with peak assignments and integrations.

Table C1

Thermomechanical results for all ester-spaced, aromatic diglycidyl ether samples cured with Epikure W

Sample	**Rubbery E′ (MPa)**	**Rubbery T (°C)**
DGEBVA-Ad	1.8 ± 0.6	132 ± 2
DGEBVA-C12	9.5 ± 0.5	54 ± 4
DGEBVA-C18	2.7 ± 0.4	59 ± 2

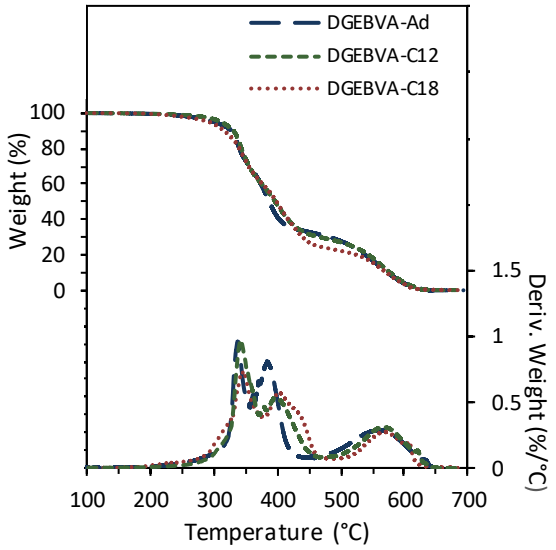

Figure C3. TGA thermograms (in air) of all ester-spaced, aromatic diglycidyl ethers cured with Epikure W.

Table C2

Thermogravimetric properties for all ester-spaced, aromatic diglycidyl ether samples cured with Epikure W in air

Sample	**IDT (°C)**	**$T_{50\%}$ (°C)**	**T_{max} (°C)**	**Char Content (%)**
DGEBVA-Ad	302 ± 7	384 ± 4	334 ± 3	0.11 ± 0.05
DGEBVA-C12	311 ± 5	396 ± 1	342 ± 1	0.20 ± 0.05
DGEBVA-C18	295 ± 3	398 ± 2	343 ± 2	0.15 ± 0.05

Appendix D

Supporting Information for Chapter 5

Text and figures are reproduced and adapted with permission from A.W. Bassett, K.R. Sweet, R.M. O'Dea, A.E. Honnig, C.M. Breyta, J.H. Reilly, J.J. La Scala, T.H. Epps III, and J.F. Stanzione III, "Dual-functional, Aromatic, Epoxy-Methacrylate Monomers from Bio-based Feedstocks and Their Respective Epoxy-functional Thermoplastics," *Journal of Polymer Science*, 2020, 58 (5), 673-682, reference [108].

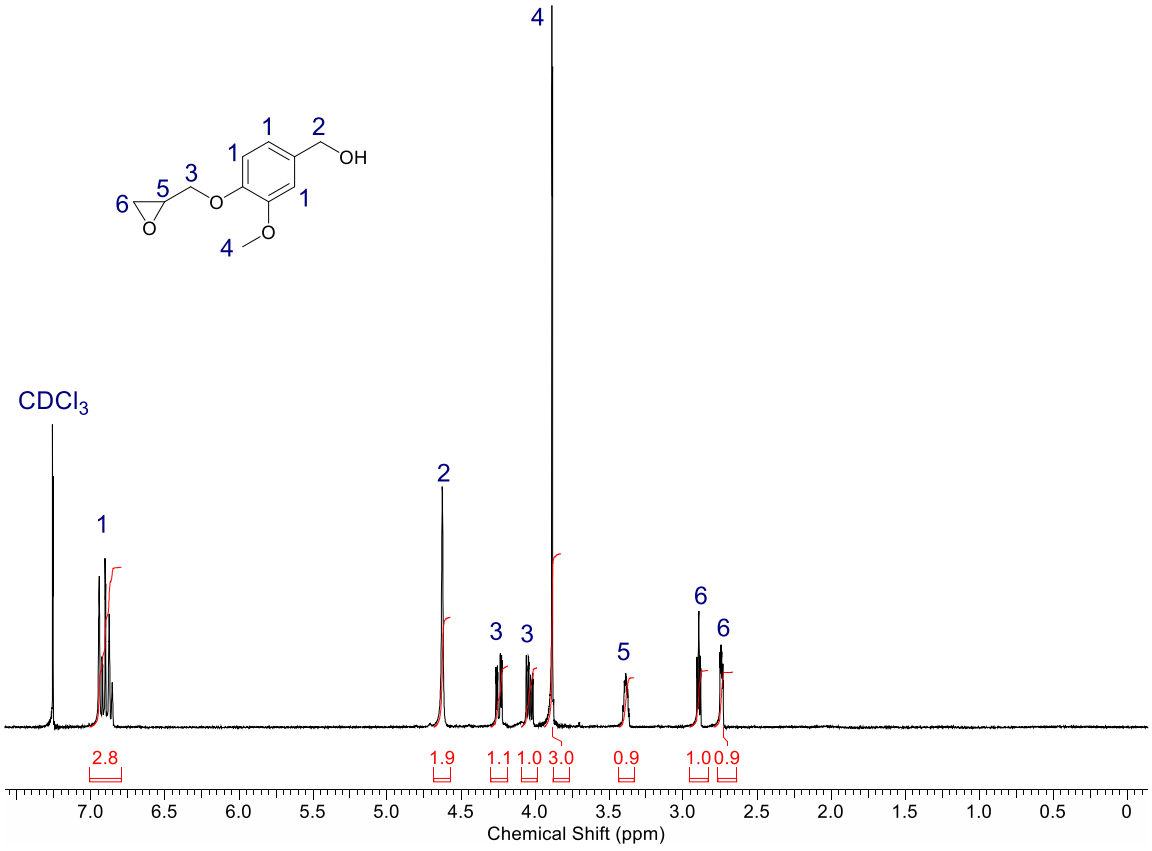

Figure D1. ^{1}H-NMR (proton nuclear magnetic resonance) spectrum of monoglycidyl ether of vanillyl alcohol (MGEVA) with peak assignments and integrations.

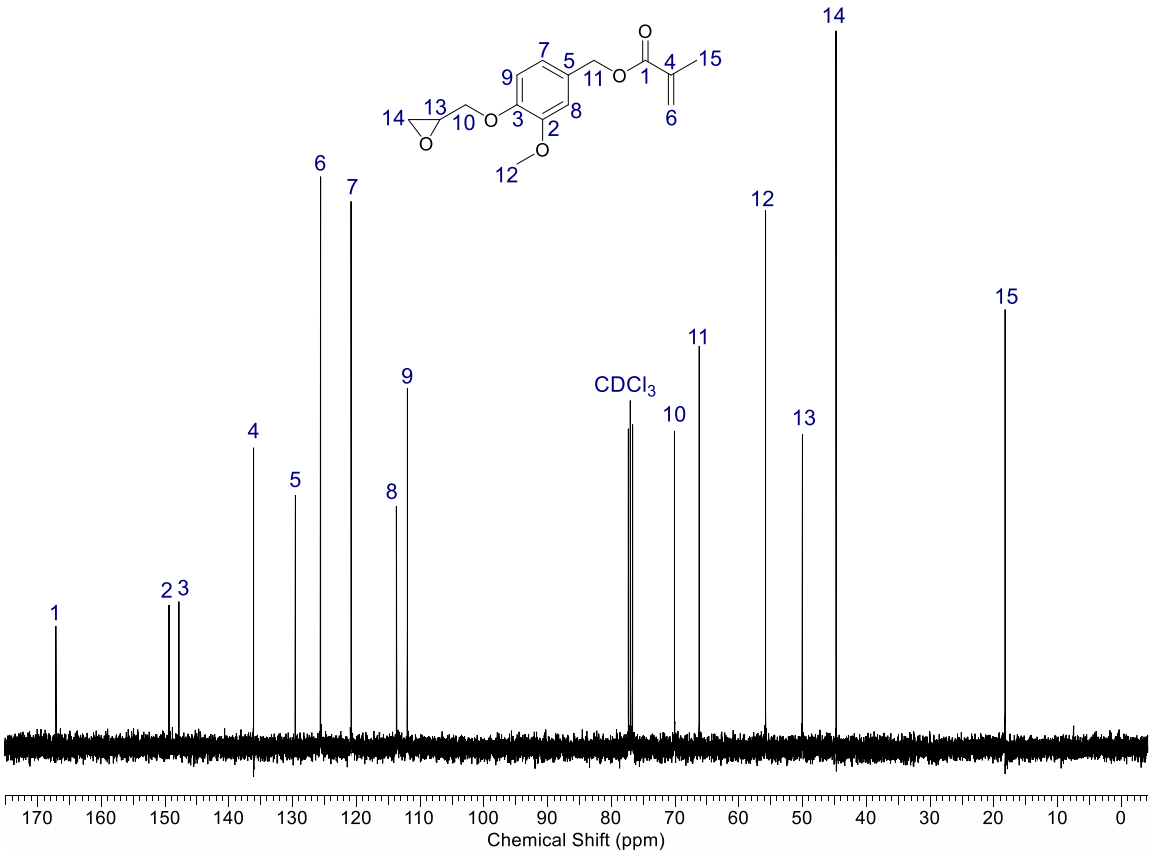

Figure D2. ^{13}C-NMR (carbon nuclear magnetic resonance) spectrum of vanillyl alcohol epoxy-methacrylate (VAEM) with peak assignments.

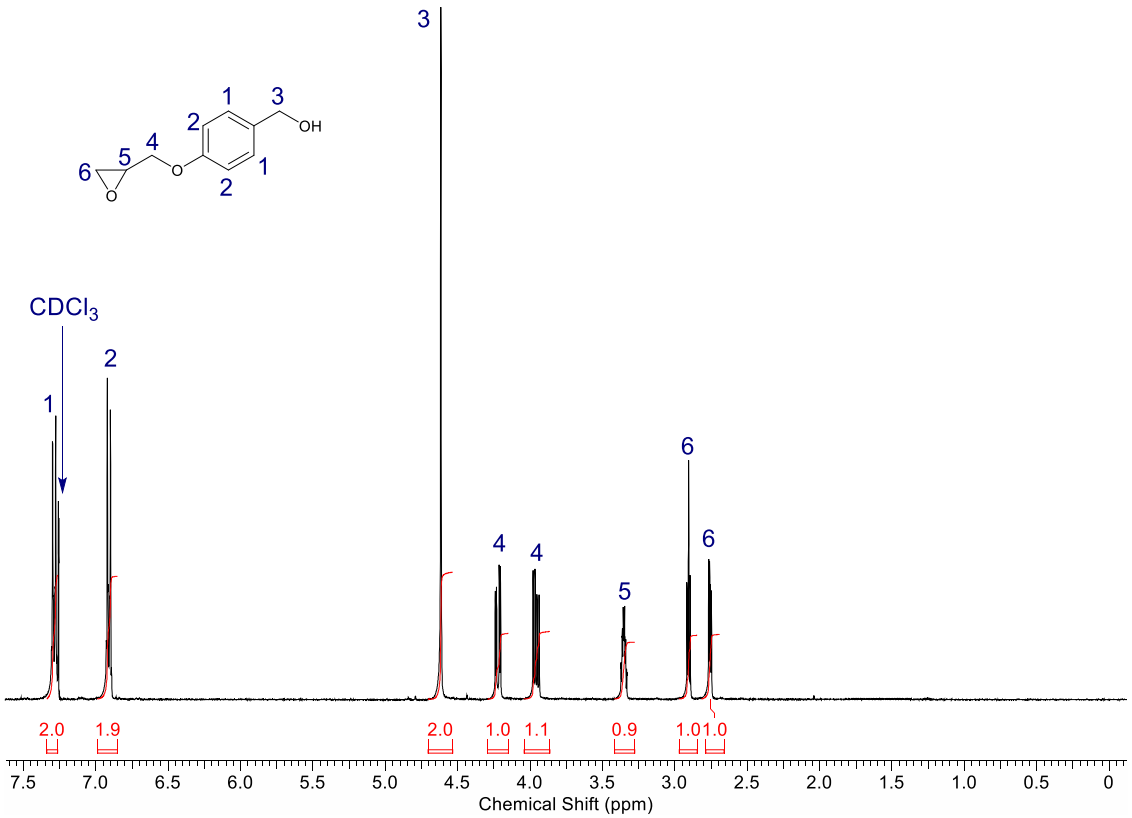

Figure D3. ^{1}H-NMR spectrum of monoglycidyl ether of gastrodigenin (MGEGD) with peak assignments and integrations.

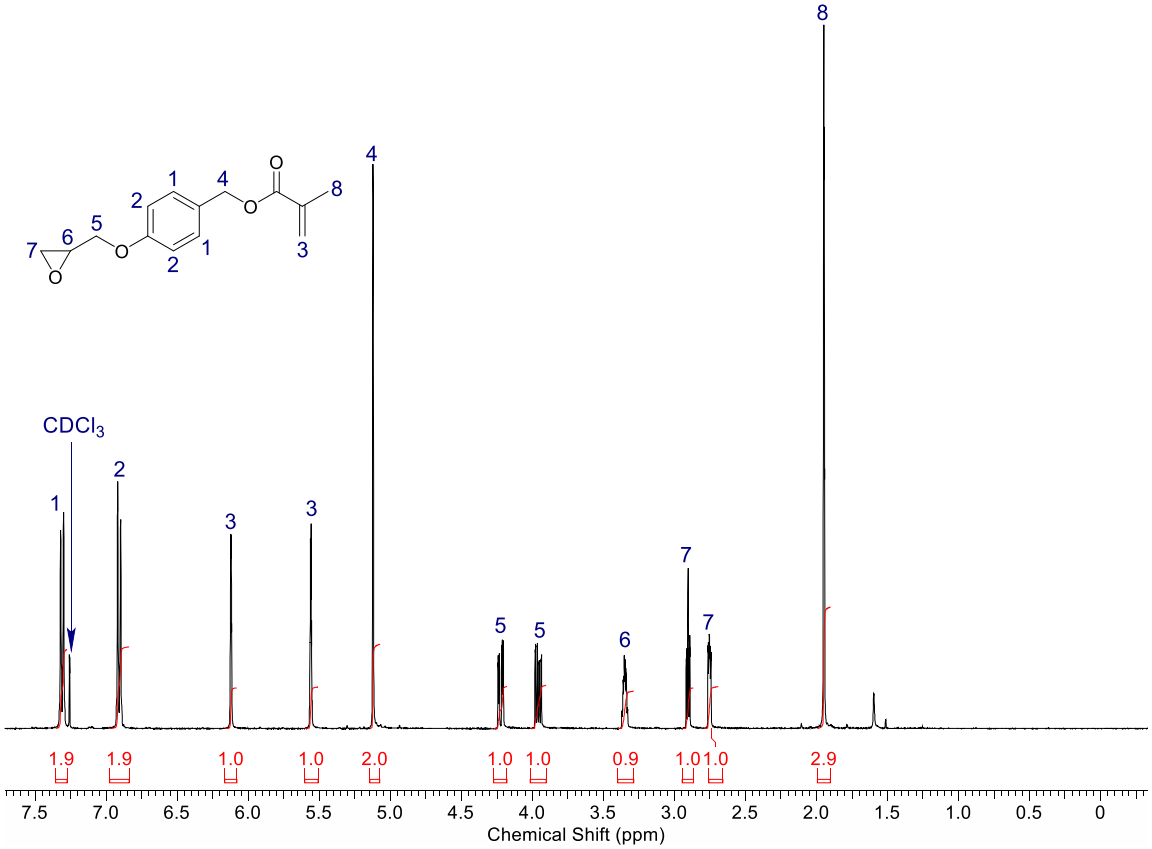

Figure D4. ^{1}H-NMR spectrum of gastrodigenin epoxy-methacrylate (GDEM) with peak assignments and integrations.

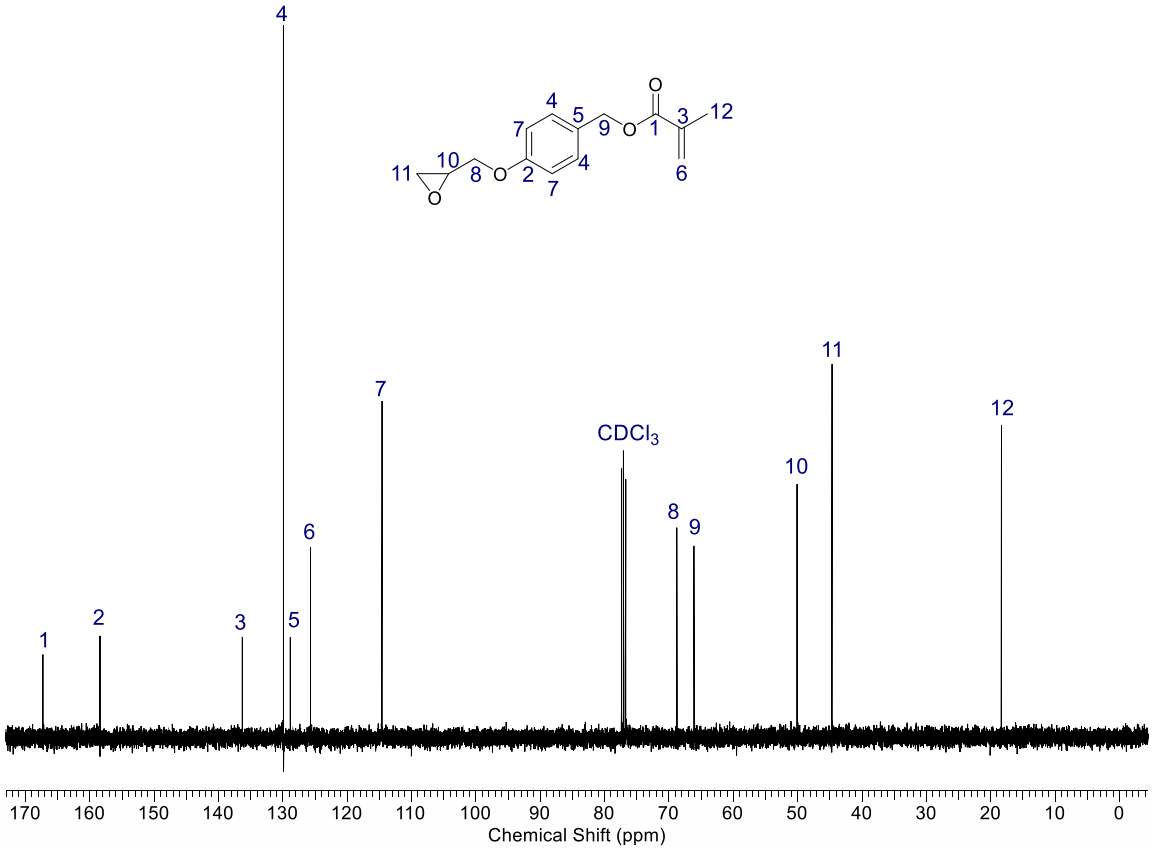

Figure D5. ^{13}C-NMR spectrum of GDEM with peak assignments.

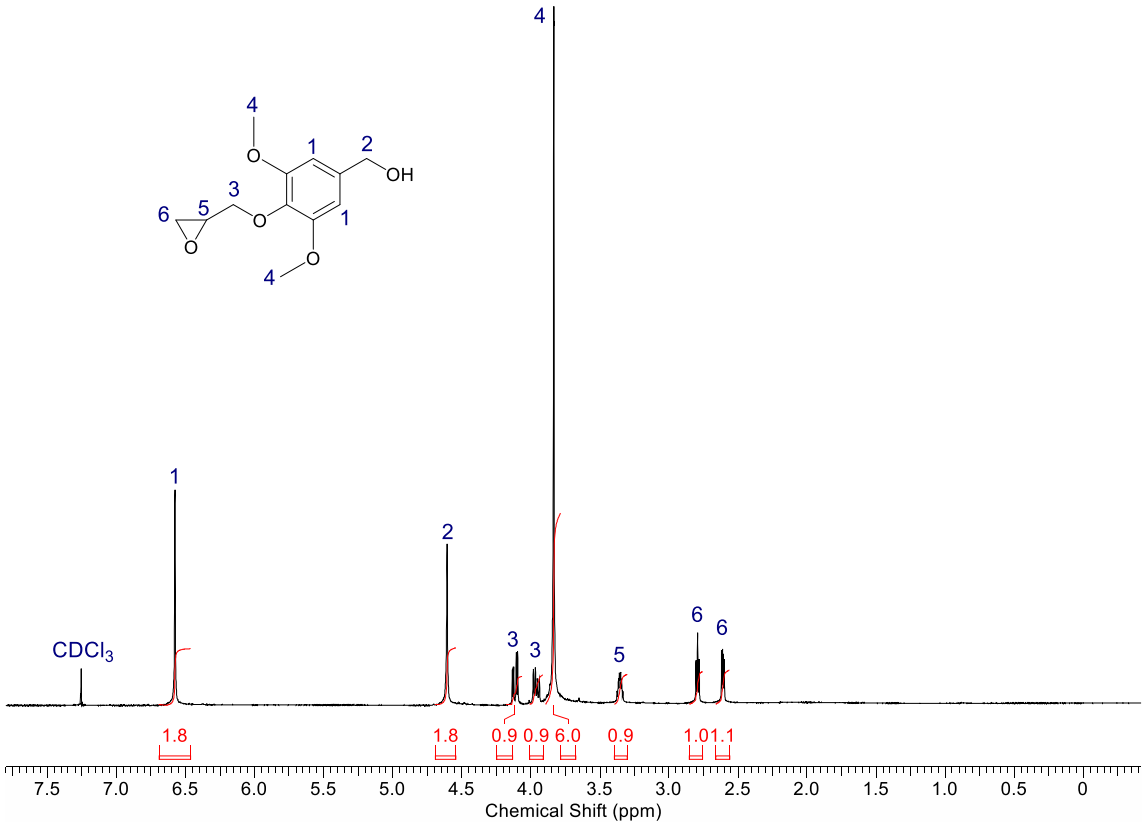

Figure D6. ^{1}H-NMR spectrum of monoglycidyl ether of syringyl alcohol (MGESA) with peak assignments and integrations.

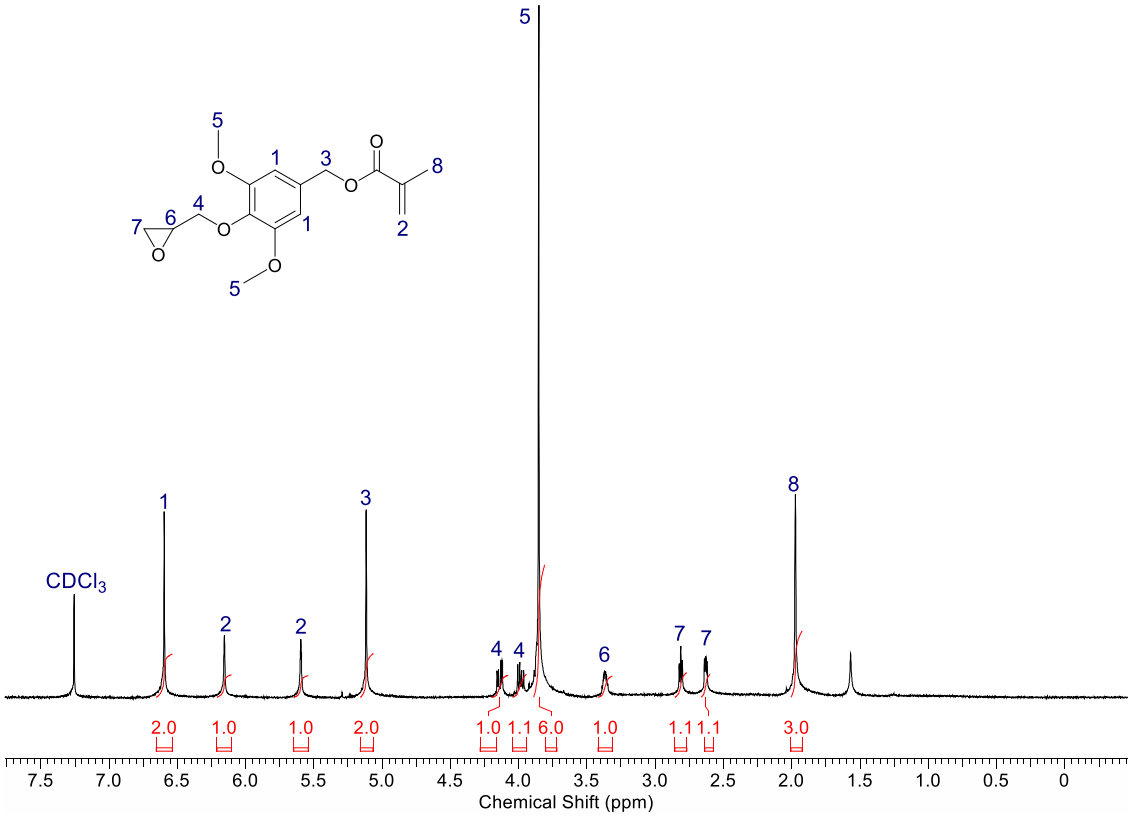

Figure D7. ^{1}H-NMR spectrum of syringyl alcohol epoxy-methacrylate (SAEM) with peak assignments and integrations.

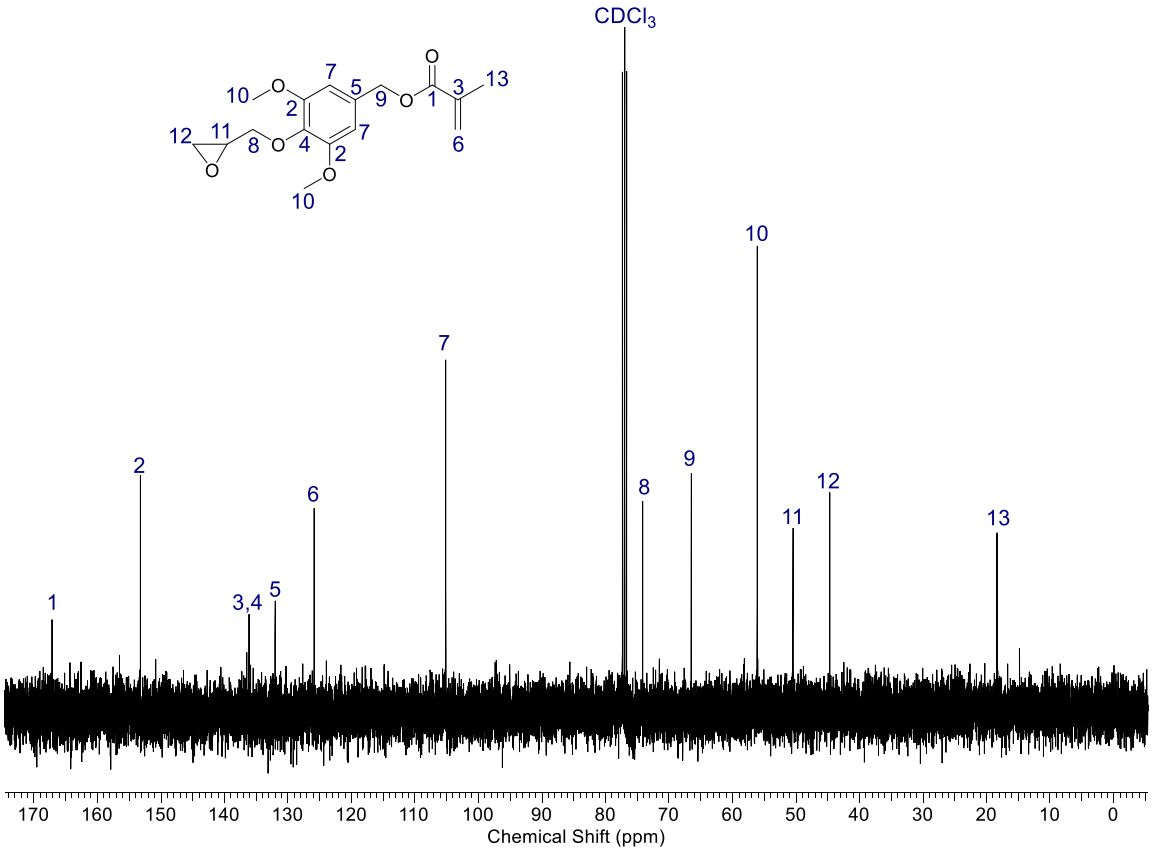

Figure D8. ^{13}C-NMR spectrum of SAEM with peak assignments.

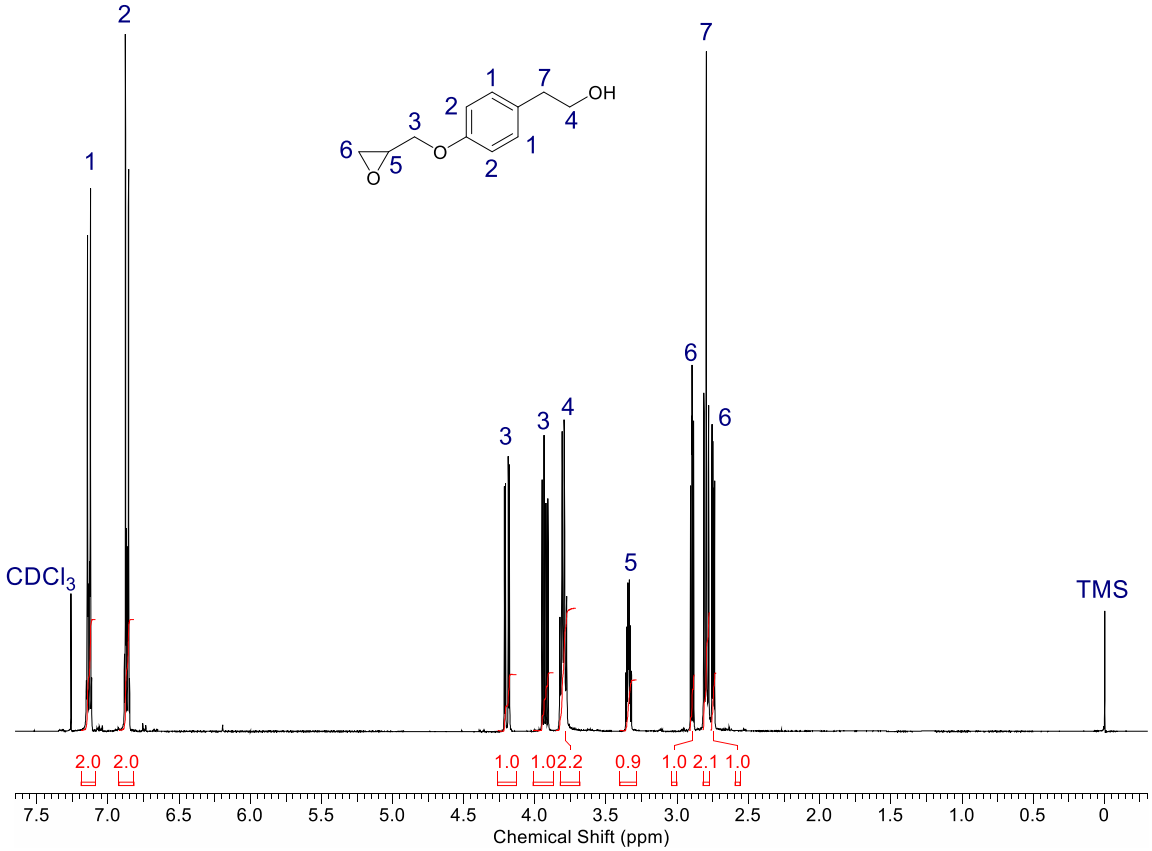

Figure D9. ^{1}H-NMR spectrum of monoglycidyl ether of tyrosol (MGET) with peak assignments and integrations.

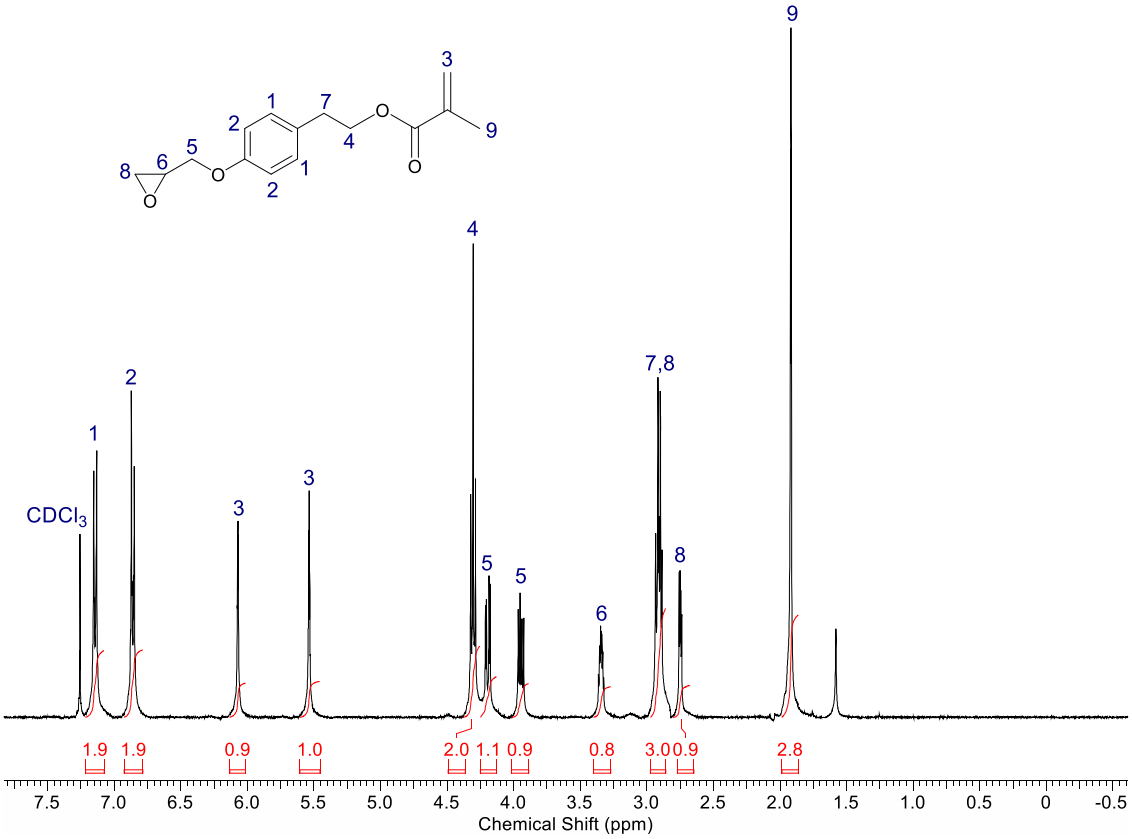

Figure D10. ^{1}H-NMR spectrum of tyrosol epoxy-methacrylate (TEM) with peak assignments and integrations.

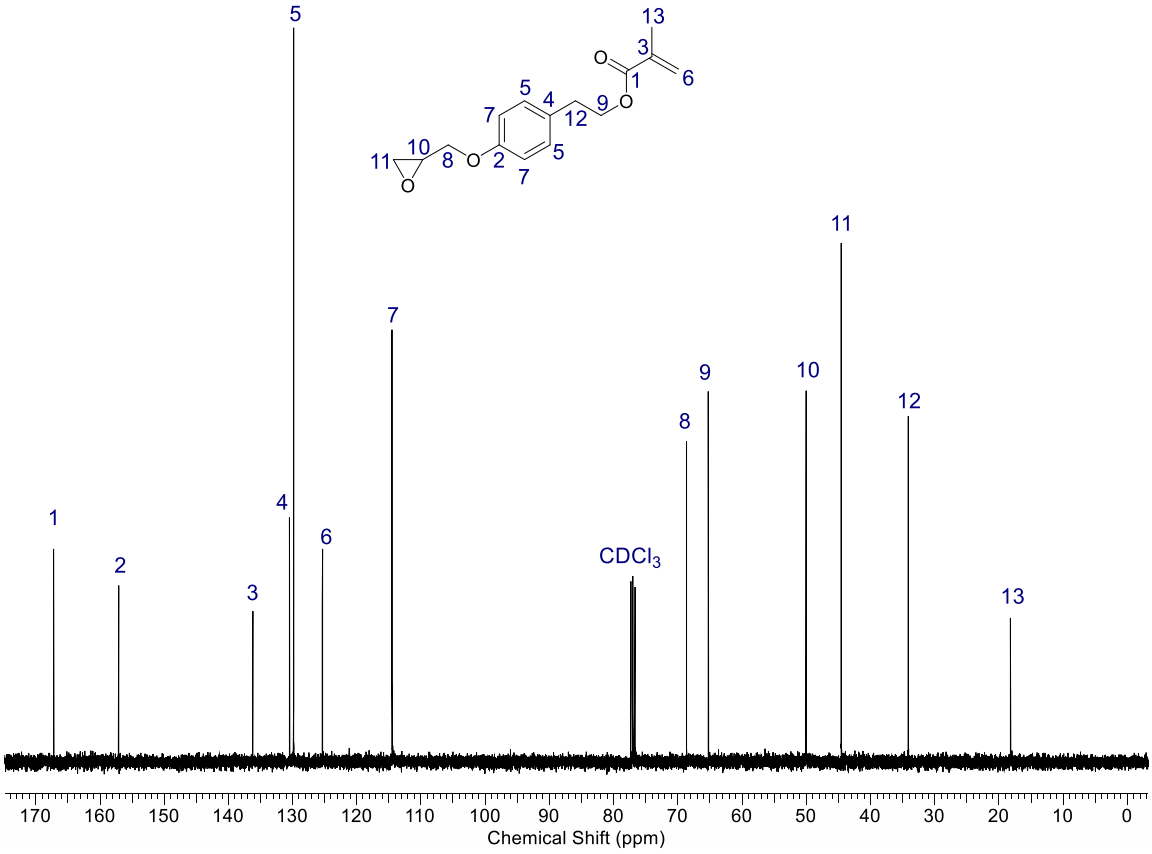

Figure D11. ^{13}C-NMR spectrum of TEM with peak assignments.

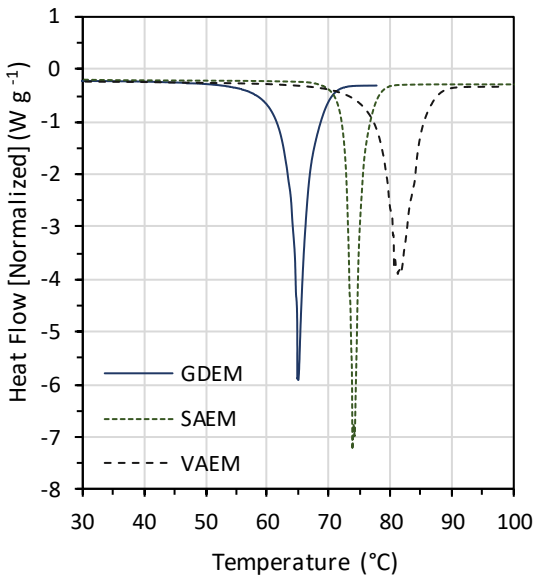

Figure D12. Differential scanning calorimetry (DSC) thermograms of VAEM, SAEM, and GDEM.

Table D1

DSC results, including T_m and Enthalpy of melting, for VAEM, SAEM, and GDEM

Monomer	**T_m (°C)**	**Enthalpy of Melting (kJ mol^{-1})**
VAEM	81	35.77
SAEM	73	33.46
GDEM	65	32.38

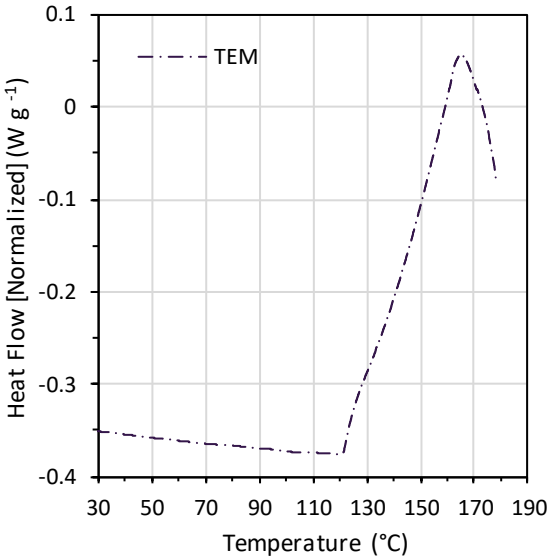

Figure D13. DSC trace of TEM.

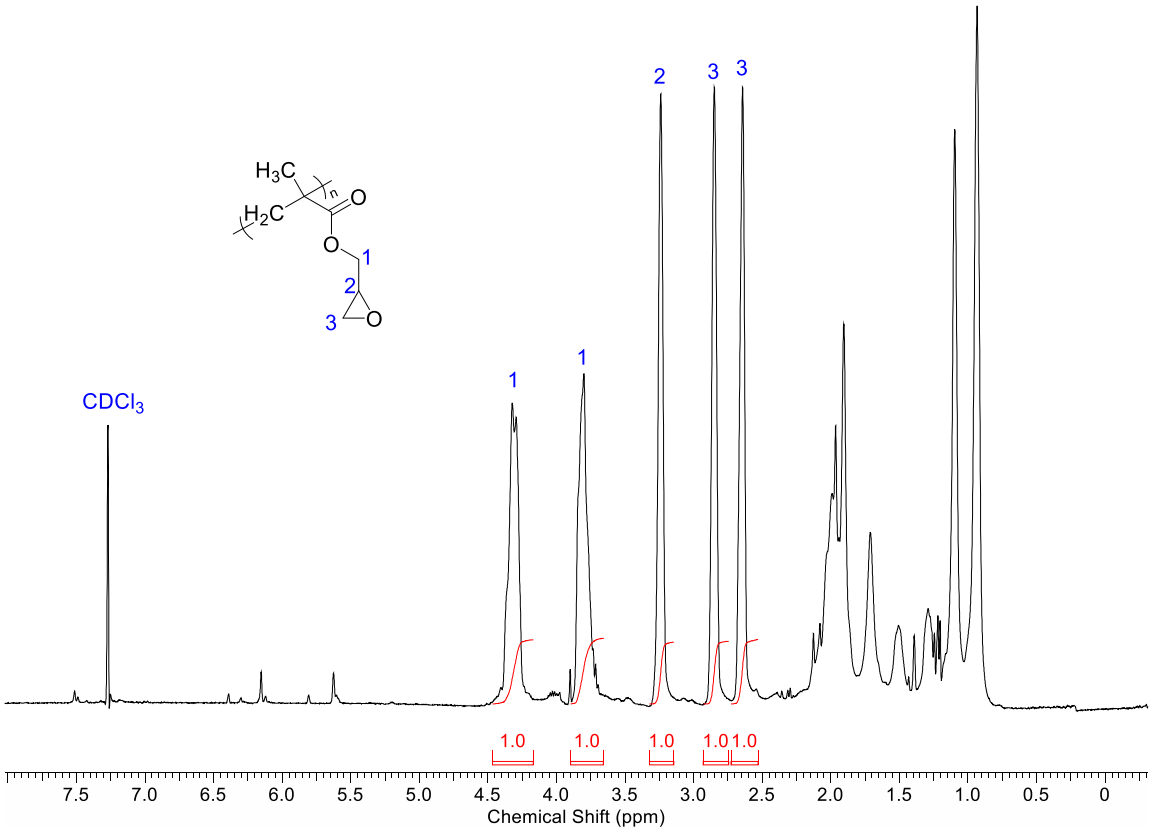

Figure D14. ^{1}H NMR spectrum with partial peak assignments and associated integrations for poly(glycidyl methacrylate) (poly(GMA)).

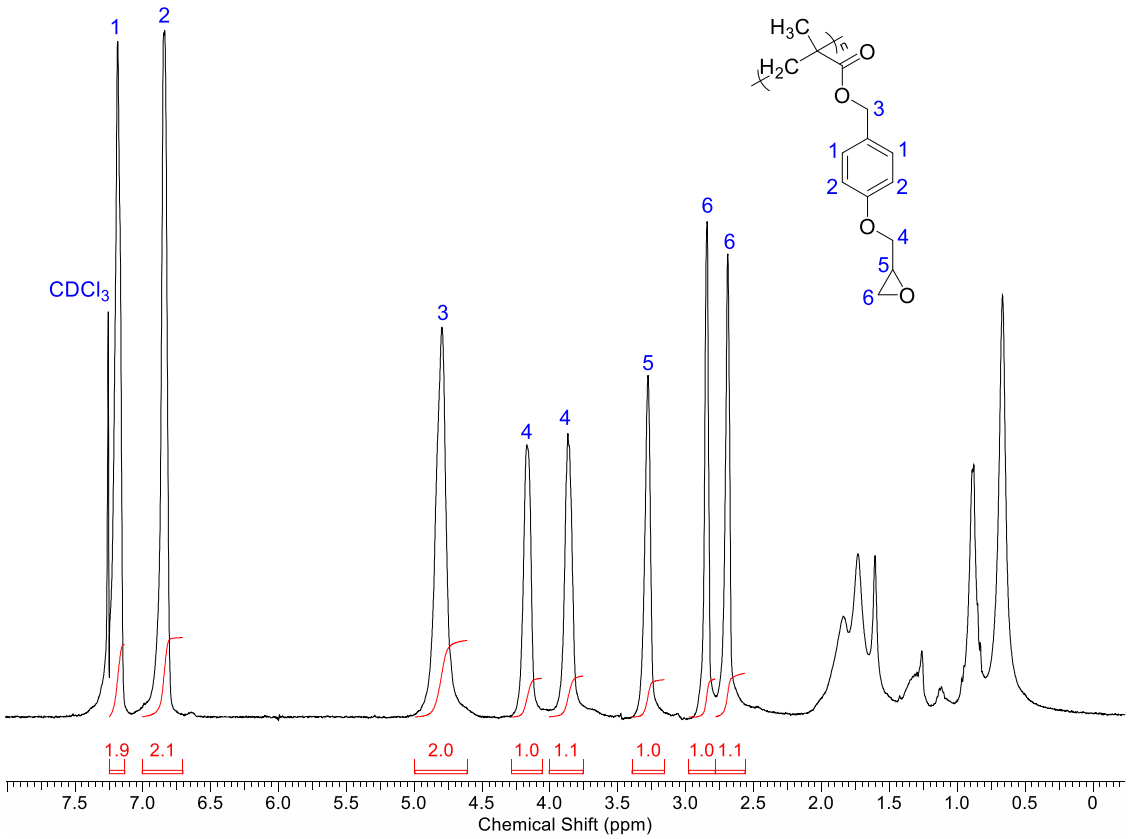

Figure D15. ^{1}H NMR spectrum with partial peak assignments and associated integrations for poly(GDEM).

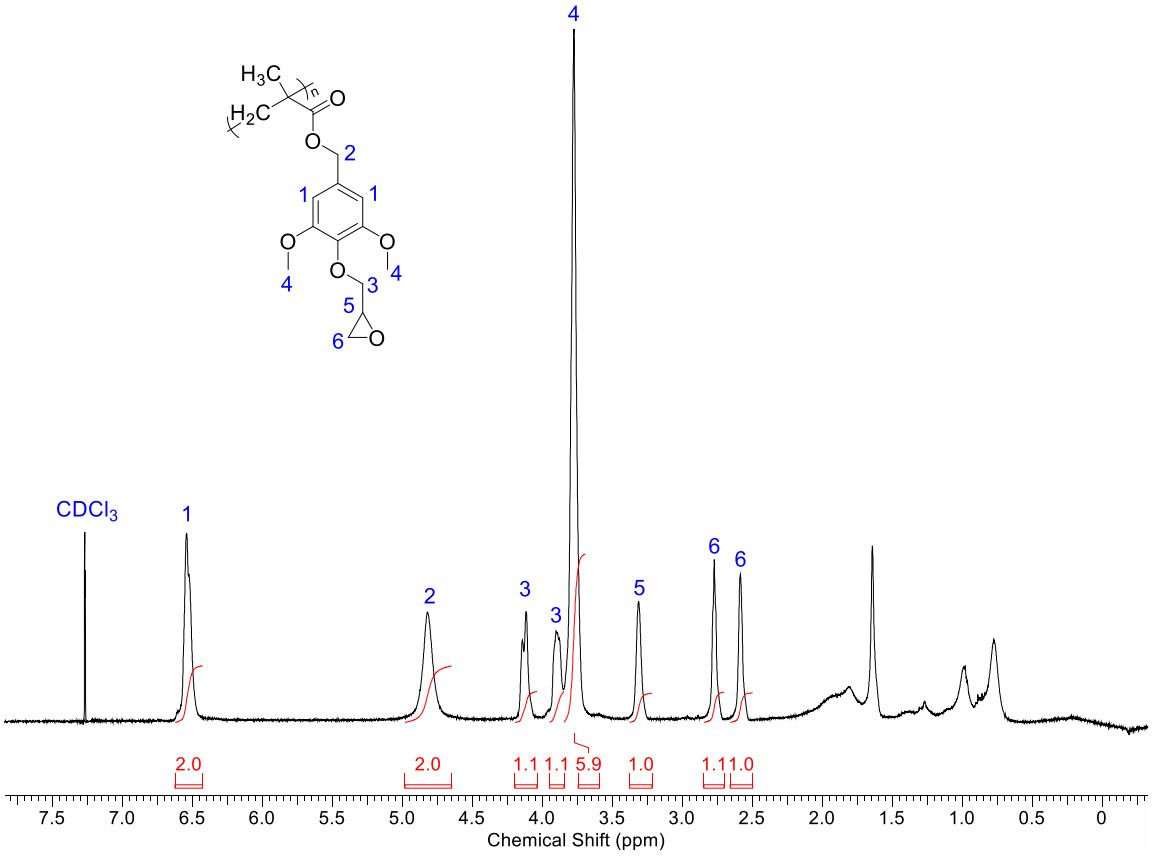

Figure D16. ^{1}H NMR spectrum with partial peak assignments and associated integrations for poly(SAEM).

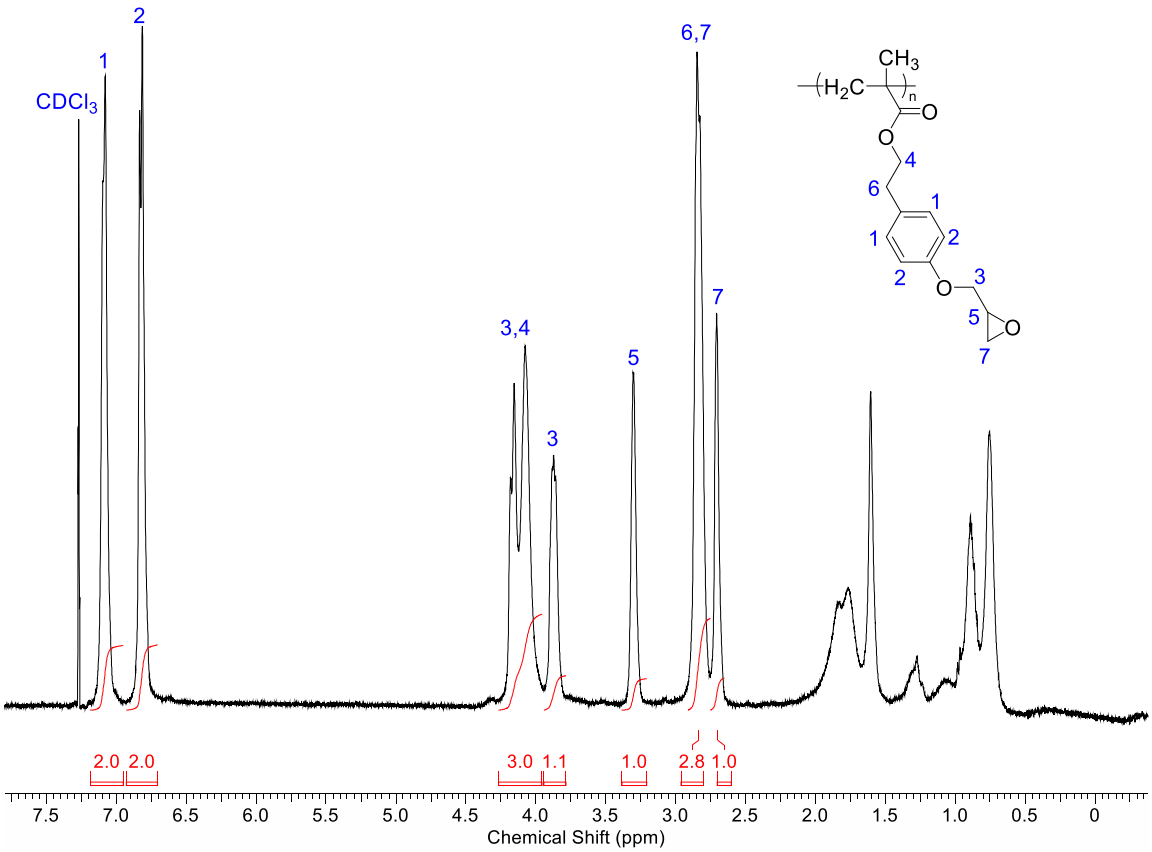

Figure D17. ^{1}H NMR spectrum with partial peak assignments and associated integrations for poly(TEM).

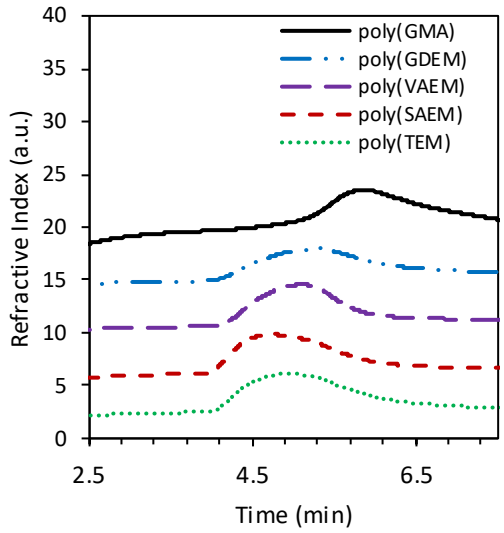

Figure D18. Advance Polymer Chromatography (APC) chromatograms of the thermoplastic polymers. Vertically offset for clarity.

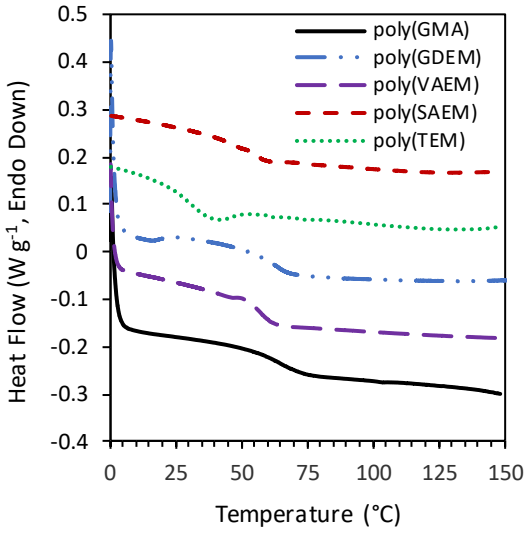

Figure D19. DSC thermograms of the thermoplastic polymers. Vertically offset for clarity.

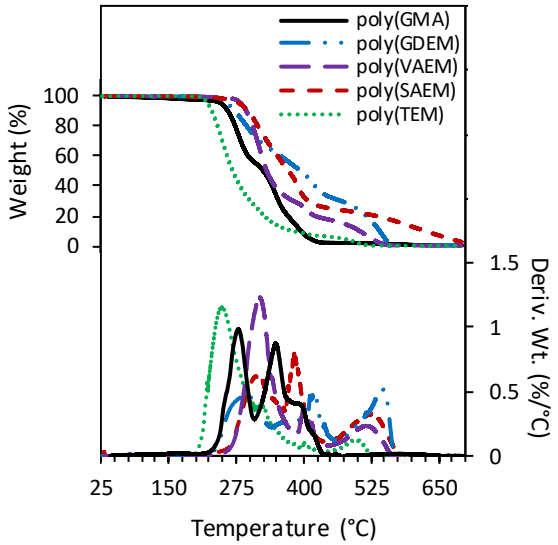

Figure D20. Thermogravimetric analysis (TGA) thermograms and the first derivatives of the thermoplastic polymers in an oxidative environment (air).

Table D2

Thermogravimetric properties of the epoxy-functional homopolymers in N_2

Sample	IDT (°C)	$T_{50\%}$ (°C)	T_{max} (°C)	Char Content (%)
poly(GMA)	248 ± 1	309 ± 1	287 ± 1	0.4 ± 0.2
poly(GDEM)	260 ± 1	398 ± 5	294 ± 1	0.3 ± 0.3
poly(VAEM)	287 ± 3	335 ± 5	320 ± 2	0.4 ± 0.1
poly(SAEM)	282 ± 1	379 ± 4	383 ± 1	0.1 ± 0.1
poly(TEM)	223 ± 1	268 ± 1	248 ± 1	0.3 ± 0.1

Table D3

Film thicknesses before and after washing and re-annealing. Measurements prior to washing are less certain due to increased surface roughness relative to the washed and re-annealed films. Reflectance curves were fit assuming a refractive index of 1.52 for all films to obtain approximate thicknesses

Sample	**Thickness Before Washing (nm)**	**Thickness After Washing (nm)**
poly(GMA)	~40	22.4 ± 1.36
poly(SAEM)	24.12 ± 0.04	28.82 ± 0.06
poly(VAEM)	~40	32.59 ± 1.91
poly(GDEM)	44.32 ± 1.39	41.54 ± 0.42

Appendix E

Supporting Information for Chapter 6

Text and figures are reproduced and adapted with permission from A.W. Bassett, A.E. Honnig, C.M. Breyta, I.C. Dunn, J.J. La Scala, and J.F. Stanzione III, "Vanillin-based Resin for Additive Manufacturing," *In preparation*, reference [26].

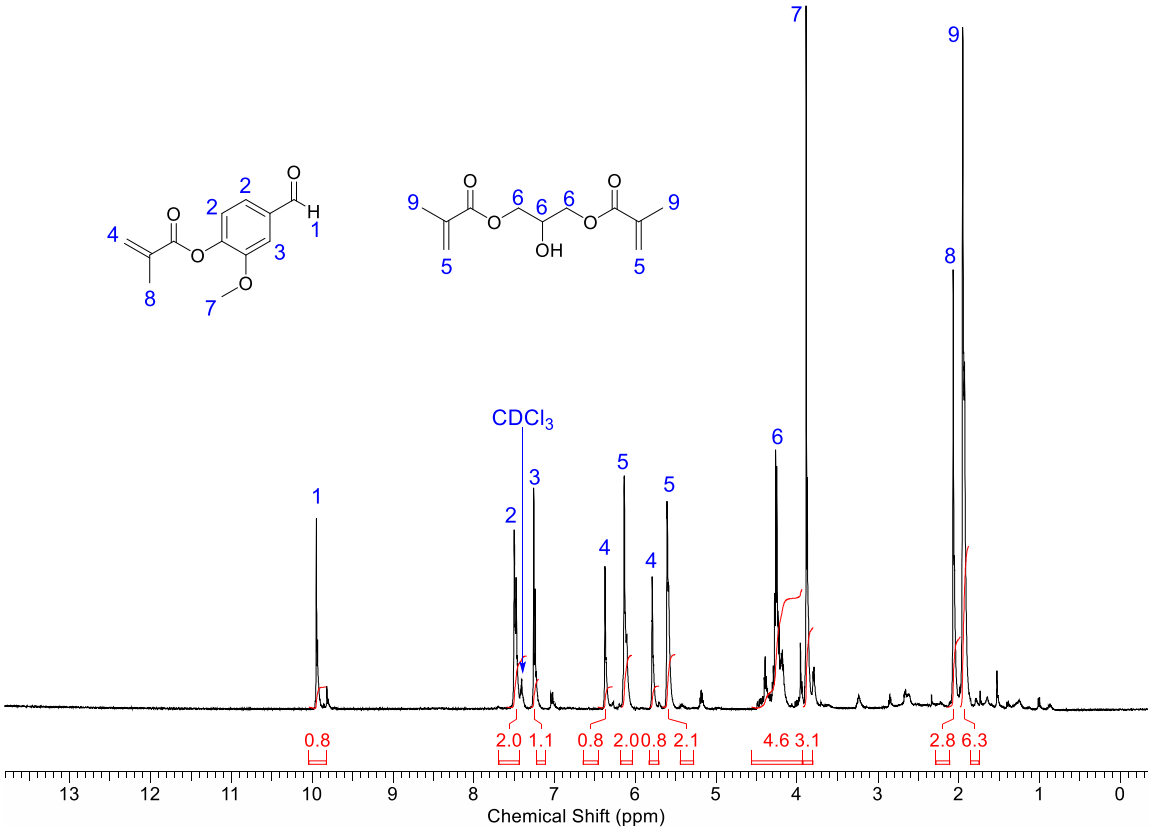

Figure E1. ^{1}H-NMR spectrum of 1P2S MV-GMA resin.

Table E1

Additional viscoelastic properties of 1P2S MV-GMA AM and 1P2S MV-GMA AM-FC

Sample	Rubbery E′ (MPa)	Rubbery T (°C)
1P2S MV-GMA AM	4.7 ± 2.7	238 ± 2
1P2S MV-GMA AM-FC	12.0 ± 5.2	242 ± 3

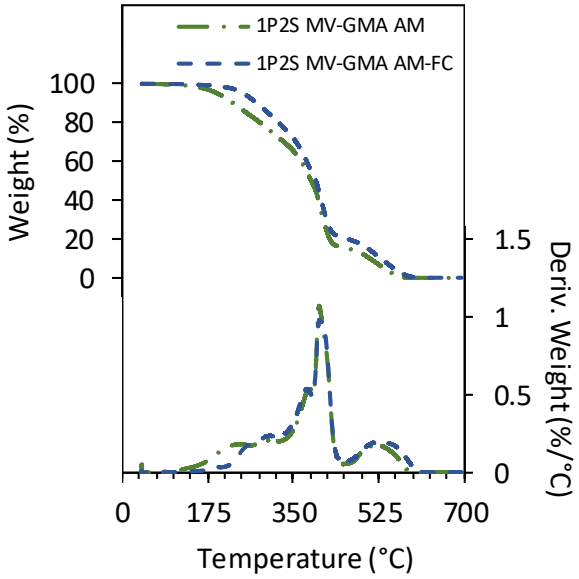

Figure E2. TGA thermograms and the respective 1st derivatives of the 1P2S MV-GMA AM and form cured samples in air.

Table E2

Thermogravimetric properties for the 1P2S MV-GMA AM and FC in air

System	IDT (°C)	$T_{50\%}$ (°C)	T_{max} (°C)	Char Content (%)
1P2S MV-GMA AM	198 ± 7	389 ± 2	402 ± 1	0.2 ± 0.1
1P2S MV-GMA AM-FC	245 ± 4	395 ± 1	403 ± 1	0.3 ± 0.1

Appendix F

Supporting Information for Chapter 7

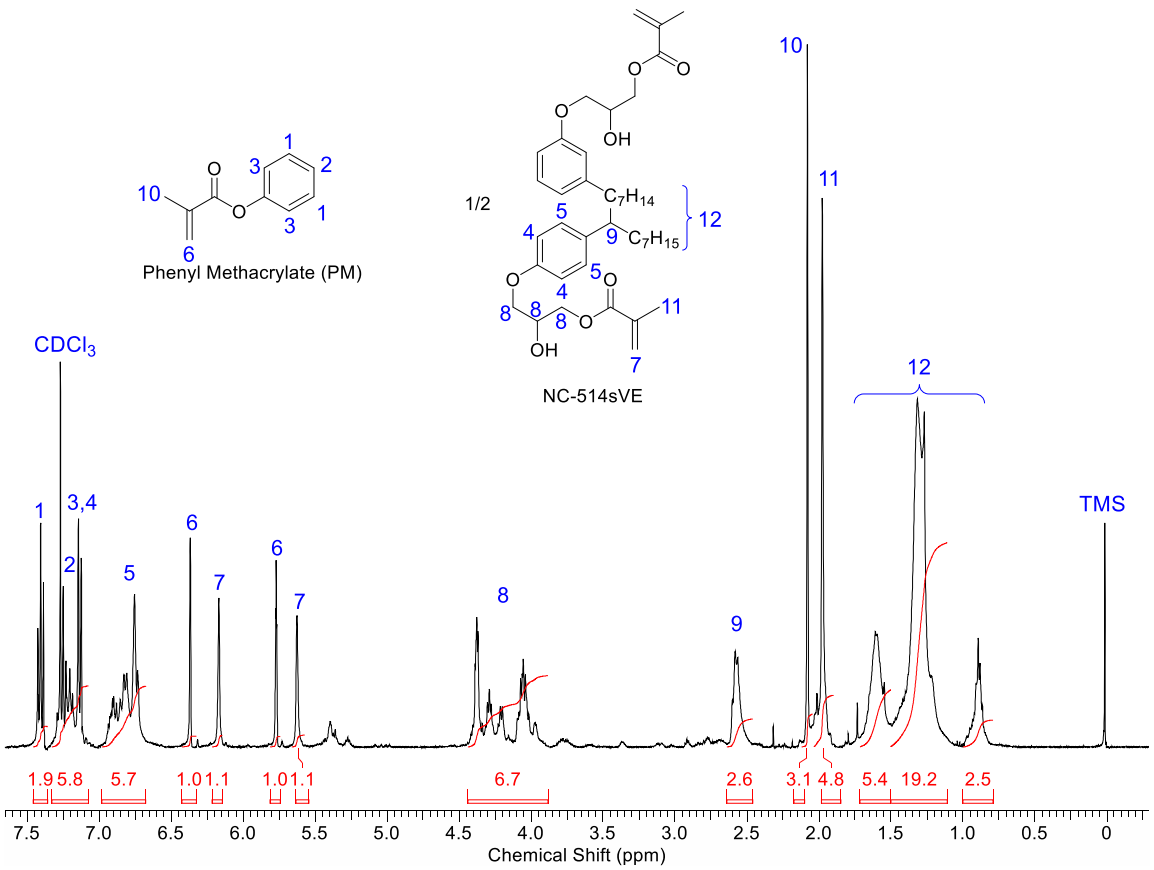

Figure F1. ^{1}H-NMR spectrum of the 1P2S PM-NC514sVE resin.

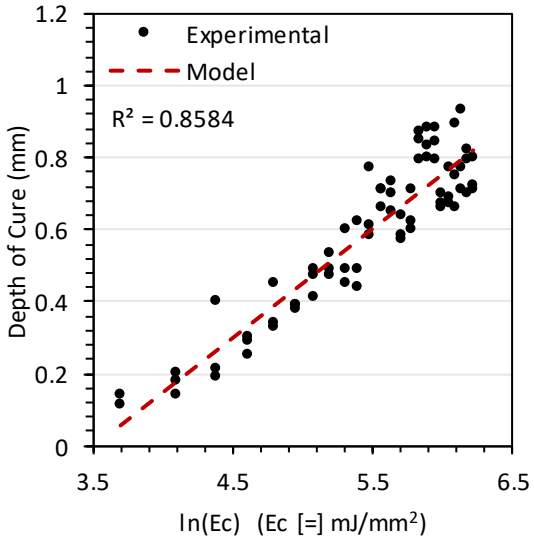

Figure F2. Working curve for 1P2S PM-NC514sVE 0% IM resin.

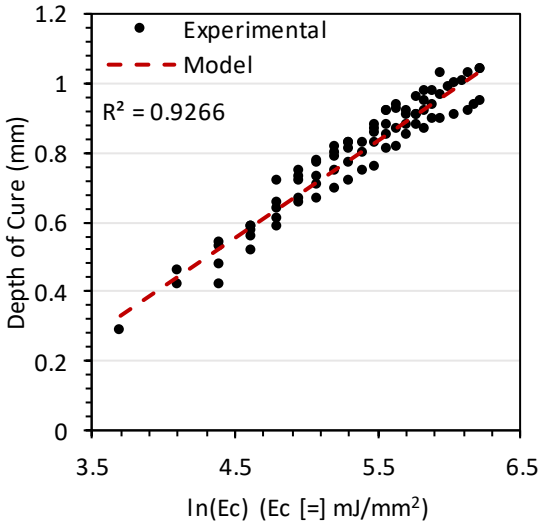

Figure F3. Working curve for 1P2S PM-NC514sVE 10% IM resin.

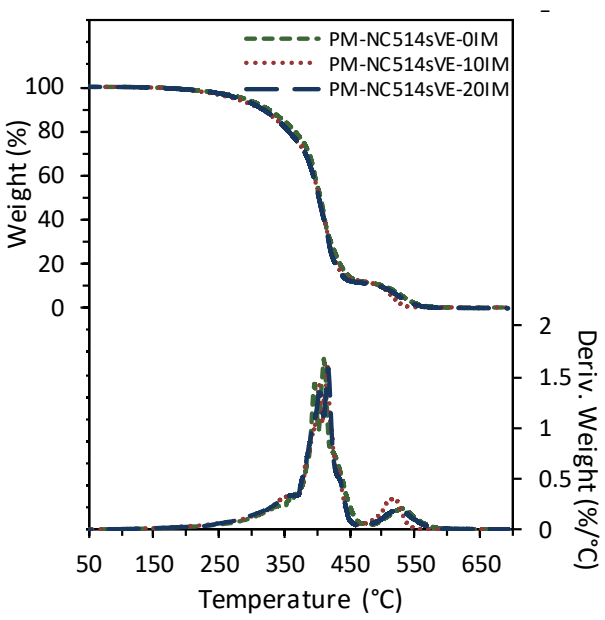

Figure F4. TGA thermograms and respective 1st derivatives of 1P2S PM-NC514sVE with varying IM weight percent in air.

Table F1

Thermogravimetric data for 1P2S PM-NC514sVE cured resins with varying IM weight percent in air

Sample	IDT (°C)	$T_{50\%}$ (°C)	T_{max} (°C)	Char Content (%)
1P2S PM NC514sVE 0% IM	284 ± 2	405 ± 1	411 ± 1	0.2 ± 0.2
1P2S PM NC514sVE 10% IM	269 ± 4	404 ± 1	415 ± 1	0.3 ± 0.1
1P2S PM NC514sVE 20% IM	280 ± 2	404 ± 1	416 ± 2	0.1 ± 0.1

Table F2

Additional thermomechanical results for 1P2S PM-NC514sVE cured resins with varying IM weight percent

Sample	**Rubbery E′ (MPa)**	**Rubbery T (°C)**
1P2S PM NC514sVE 0% IM	3.6 ± 0.5	111.9 ± 2.3
1P2S PM NC514sVE 10% IM	21.4 ± 2.9	131.5 ± 5.7
1P2S PM NC514sVE 20% IM	33.0 ± 3.8	165.5 ± 5.8

Appendix G

Supporting Information for Chapter 8

Text and figures are reproduced and adapted with permission from A.W. Bassett, A.E. Honnig, J.J La Scala, and J.F. Stanzione III, "Network Toughening of Additively Manufactured, High Glass Transition Temperature Materials via Sequentially Cured, Interpenetrating Polymers," *In preparation*, reference [199].

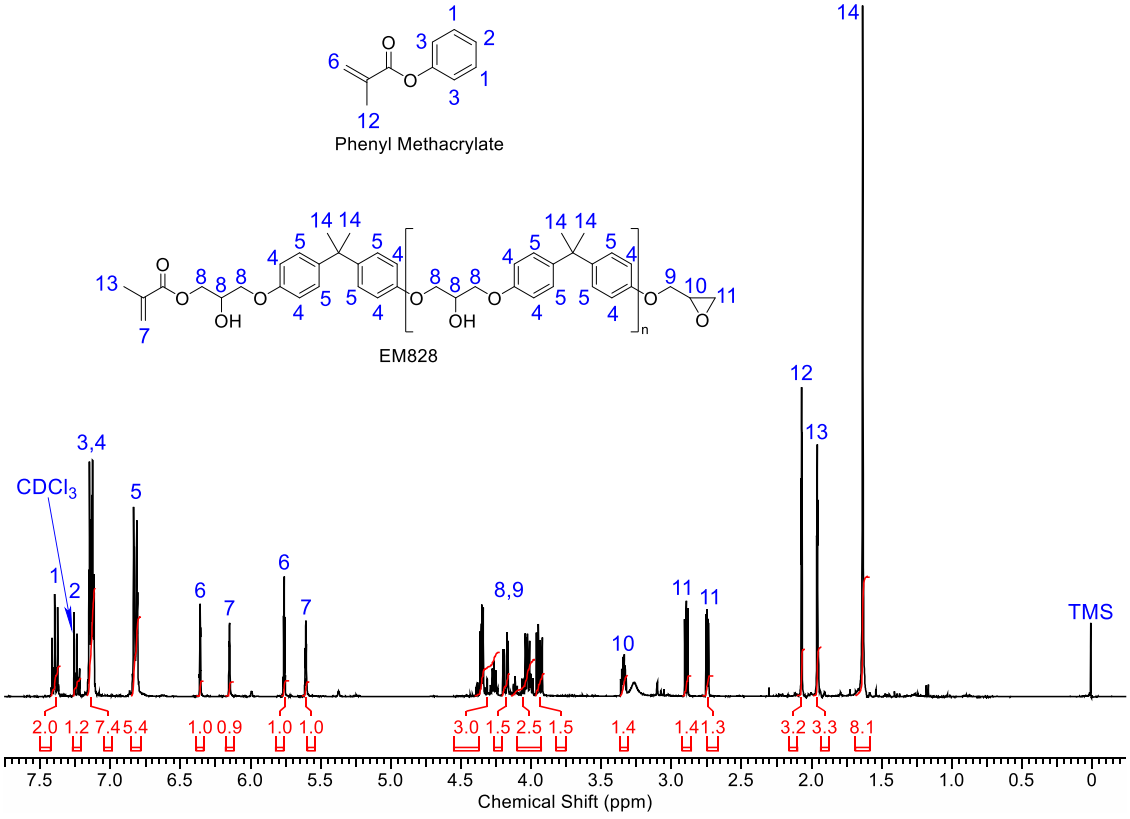

Figure G1. ^{1}H-NMR spectrum of the PM-EM828 resin.

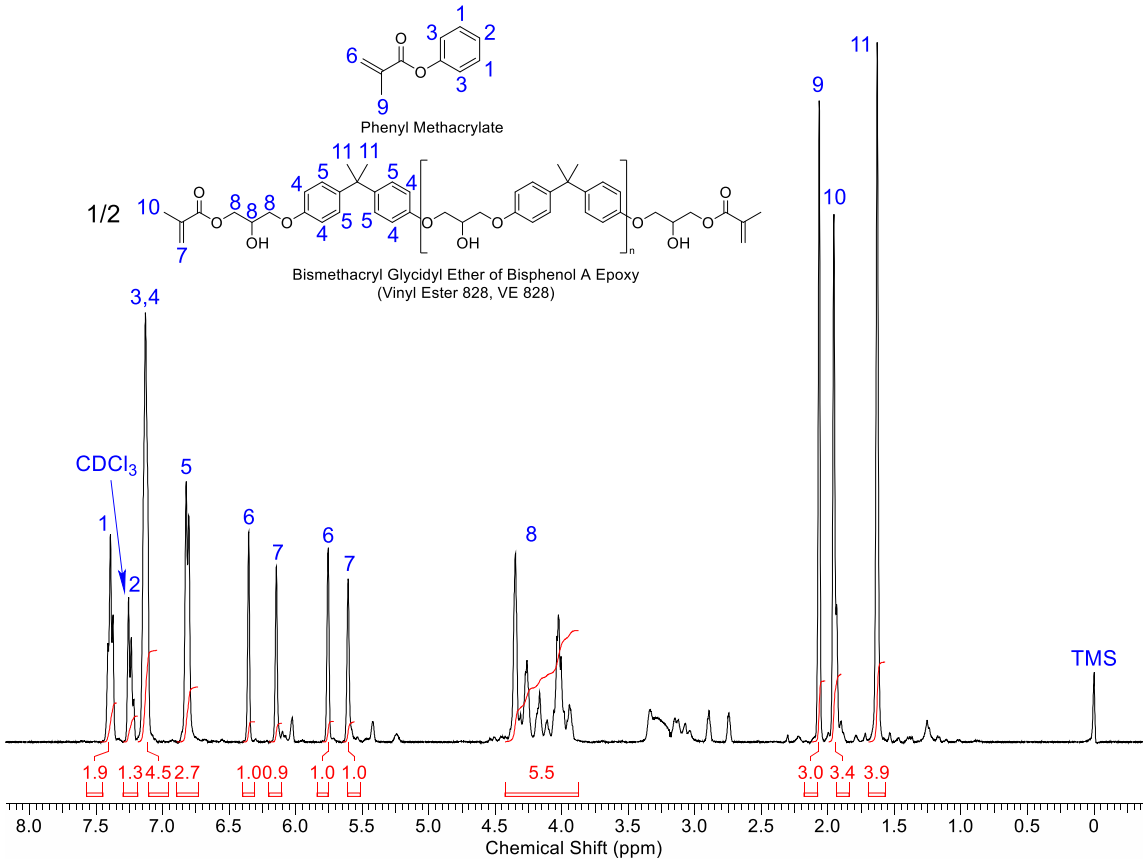

Figure G2. ^{1}H-NMR spectrum of the PM-VE828 resin.

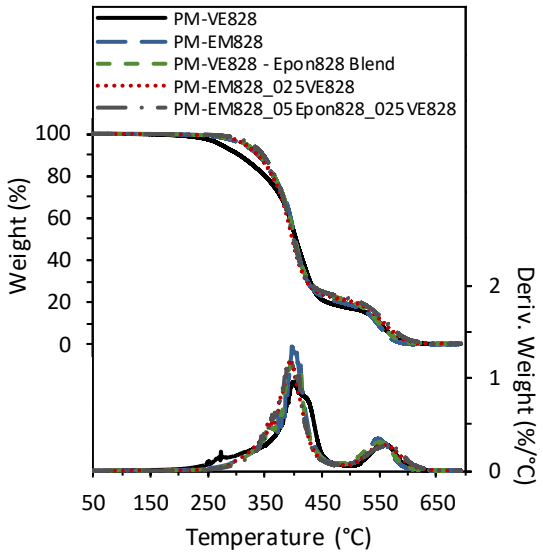

Figure G3. TGA thermograms and the respective 1st derivatives of all thermosets in air.

Table G1

Thermogravimetric properties of all thermosets in air

Sample	IDT (°C)	$T_{50\%}$ (°C)	T_{max} (°C)	Char Content (%)
PM-VE828	271 ± 3	404 ± 1	397 ± 3	0.18 ± 0.01
PM-EM828	316 ± 3	403 ± 1	399 ± 4	0.17 ± 0.10
PM-VE828 - Epon828 Blend	315 ± 2	402 ± 1	396 ± 1	0.27 ± 0.07
PM-EM828_025VE	315 ± 1	398 ± 1	394 ± 1	0.34 ± 0.01
PM-EM828_05Epon828_025VE828	324 ± 4	400 ± 1	397 ± 2	0.50 ± 0.06

Table G2

Additional viscoelastic properties of all thermosets

Sample	Rubbery E′ (MPa)	Rubbery T (°C)
PM-VE828	36.1 ± 1.9	176 ± 4
PM-EM828	26.4 ± 4.8	161 ± 9
PM-VE828 - Epon828 Blend	15.1 ± 1.8	179 ± 5
PM-EM828_025VE828	28.9 ± 4.9	180 ± 5
PM-EM828_05Epon828_025VE828	28.6 ± 1.3	178 ± 3

Appendix H

List of Acronyms, Abbreviations, and Symbols

3D printing	Three-dimensional printing
AM	Additive manufacturing
APC	Advanced polymer chromatography
CS	Cold spray
Đ	Dispersity
DMA	Dynamic mechanical analysis
DSC	Differential scanning calorimetry
E'	Storage modulus
E''	Loss modulus
FTIR	Fourier transform infrared
G_{1C}	Critical strain energy release rate
IDT	Initial decomposition temperature at 5% weight loss
IPN	Interpenetrating polymer network
K_{1C}	Critical-stress-intensity factor
M_c	Molecular weight between crosslinks
M_n	Number average molecular weight
M_w	Weight average molecular weight
Mid-IR	Mid-infrared
N_2	Nitrogen
Near-IR	Near-infrared
NMR	Nuclear magnetic resonance
PRE	Photoreactive extrusion

SEC	Size exclusion chromatography
SLA	Stereolithography
T_g	Glass transition temperature
T_m	Melting temperature
Tan δ	Tan delta
TGA	Thermogravimetric analysis
UV/Vis	Ultra-violet/Visible light
ρ	Density

Appendix I

Copyright Permissions

Chapter 3 Text, Figures, & Tables

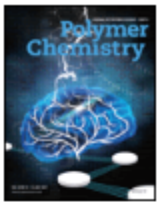

Thank you for your order!

Dear Mr. Alexander Bassett,

Thank you for placing your order through Copyright Clearance Center's RightsLink® service.

Order Summary

Licensee:	Alexander Bassett
Order Date:	Jan 29, 2020
Order Number:	4758211274746
Publication:	Journal of Polymer Science
Title:	Dual-functional, aromatic, epoxy-methacrylate monomers from bio-based feedstocks and their respective epoxy-functional thermoplastics
Type of Use:	Dissertation/Thesis
Order Total:	0.00 USD

View or print complete details of your order and the publisher's terms and conditions.

Sincerely,

Copyright Clearance Center

Tel: +1-855-239-3415 / +1-978-646-2777
customercare@copyright.com
https://myaccount.copyright.com

Copyright Clearance Center RightsLink®

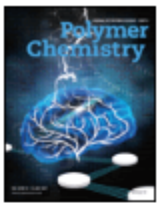

Thank you for your order!

Dear Mr. Alexander Bassett,

Thank you for placing your order through Copyright Clearance Center's RightsLink® service.

Order Summary

Licensee:	Alexander Bassett
Order Date:	Jan 29, 2020
Order Number:	4758211427950
Publication:	Journal of Polymer Science
Title:	Dual-functional, aromatic, epoxy-methacrylate monomers from bio-based feedstocks and their respective epoxy-functional thermoplastics
Type of Use:	Dissertation/Thesis
Order Total:	0.00 USD

View or print complete details of your order and the publisher's terms and conditions.

Sincerely,

Copyright Clearance Center

Tel: +1-855-239-3415 / +1-978-646-2777
customercare@copyright.com
https://myaccount.copyright.com

Copyright Clearance Center RightsLink®

Thank you for your order!

Dear Mr. Alexander Bassett,

Thank you for placing your order through Copyright Clearance Center's RightsLink® service.

Order Summary

Licensee:	Alexander Bassett
Order Date:	Jan 29, 2020
Order Number:	4758210558580
Publication:	Journal of Applied Polymer Science
Title:	Alternative monomers for 4,4′-methylenedianiline in thermosetting epoxy resins
Type of Use:	Dissertation/Thesis
Order Total:	0.00 USD

View or print complete details of your order and the publisher's terms and conditions.

Sincerely,

Copyright Clearance Center

Tel: +1-855-239-3415 / +1-978-646-2777
customercare@copyright.com
https://myaccount.copyright.com

Copyright Clearance Center RightsLink®

Thank you for your order!

Dear Mr. Alexander Bassett,

Thank you for placing your order through Copyright Clearance Center's RightsLink® service.

Order Summary

Licensee:	Alexander Bassett
Order Date:	Jan 29, 2020
Order Number:	4758210990372
Publication:	Journal of Applied Polymer Science
Title:	Alternative monomers for 4,4'-methylenedianiline in thermosetting epoxy resins
Type of Use:	Dissertation/Thesis
Order Total:	0.00 USD

View or print complete details of your order and the publisher's terms and conditions.

Sincerely,

Copyright Clearance Center

Tel: +1-855-239-3415 / +1-978-646-2777
customercare@copyright.com
https://myaccount.copyright.com

Copyright Clearance Center RightsLink®